A ROLE FOR ΔFOSB IN THE REGULATION OF PARKIN IN BRAIN REGIONS CONTAINING DIFFERENTIALLY SUSCEPTIBLE DOPAMINERGIC NEURONS

By

Joseph Robert Patterson

A DISSERTATION

Submitted to
Michigan State University
in partial fulfillment of the requirements
for the degree of

Genetics-Doctor of Philosophy

2016

ABSTRACT

A ROLE FOR ΔFOSB IN THE REGULATION OF PARKIN IN BRAIN REGIONS CONTAINING DIFFERENTIALLY SUSCEPTIBLE DOPAMINERGIC NEURONS

By

Joseph Robert Patterson

The hallmark pathologies of Parkinson disease (PD) are the formation of Lewy bodies and the progressive loss of nigrostriatal dopamine (NSDA) neurons. In mice, the NSDA neurons are preferentially damaged through exposure to the neurotoxicant 1-methyl-4-phenyl-1,2,3,6-tetrahydropyridine (MPTP). Another population of DA neurons that are initially damaged by MPTP, but are able to recover are the tuberoinfundibular DA (TIDA) neurons. Parkin is a product of the *PARK2* gene, which is linked to autosomal recessive or juvenile PD. Parkin has multiple functions in neurons and is predicted to protect against the neurotoxic effects of MPTP. Potential transcription factors of parkin were identified using TFSEARCH, PROMO, and Patch 1.0, and refined to 11 based the transcription factor being identified in all three programs, being known to be found in the brain, and known to respond to a type of stress that MPTP could cause. The candidate transcription factors were examined at 6 h after MPTP in regions containing the cell bodies of TIDA and NSDA neurons. From these candidates, only FosB and ΔFosB have expression patterns that mirror parkin.

Further examination of the temporal expression and cellular localization of FosB and ΔFosB after acute neurotoxicant administration were examined.

Regions containing the cell bodies of the TIDA (arcuate nucleus; ARC) and NSDA (substantia nigra; SN) neurons were dissected and processed for Western blot analysis. The results reveal that expression of FosB and ΔFosB correlates with parkin, increasing in the ARC and not in the SN. Furthermore, total FosB protein was localized to nuclei of NSDA and TIDA neurons, and expression of each FosB and ΔFosB examined in cytoplasmic and nuclear fractions derived from the ARC and SN. Though the number of DA neurons expressing total FosB does not change at 6 h post-MPTP, ΔFosB does increase in the nuclear fraction from the ARC.

AAV-mediated expression vectors were used to increase ΔFosB in the NSDA and TIDA neurons, in both cases, parkin increased about 2-fold. The dominant negative protein ΔJunD, which lacks a DNA binding domain, predominantly dimerizes with the FosBs and inhibits their ability to act as transcription factors was injected into the ARC. The AAV-ΔJunD virus blocked the increase of parkin after MPTP in the TIDA neurons. Taken together, the results support the role of FosB and ΔFosB as transcription factors of parkin, since they are predicted to bind the *Park2* promoter, their expression correlates with the differential expression of parkin, increases prior to parkin, are present in nuclei of TIDA neurons, ΔFosB is sufficient to drive parkin expression, and ΔJunD blocks the increase of parkin in the ARC in response to MPTP.

ACKNOWLEDGEMENTS

Walt Disney once said "Around here, however, we don’t look backwards for very long. We keep moving forward, opening new doors, and doing new things, because we're curious and curiosity keeps leading us down new paths". I feel this quote best sums up not only how to approach graduate school and science, but life. It is important to recognize what has happened and learn from it, but unless you "keep moving forward", you will never get anywhere.

In the completion of this dissertation, there are many people that have played some role that need to be acknowledged. First off, I have to thank my advisers, Dr. Keith Lookingland and Dr. John Goudreau. Keith, I want to thank you for the opportunity to grow as a scientist and the independence to develop and explore my own ideas. John, I would like to thank you for always suggesting new avenues to explore, as well as introducing me to researchers in the field.

I want to thank my current and former labmates Dr. Matthew Benskey, Dr. Chelsea Tiernan, Dr. Tyrell Simkins, Dr. Hae-young Hawong, Teri Lansdell, and Brittany Winner. You have all made the time in the lab interesting. I also want to thank the rotating graduate students I have worked with, especially Laura Harding, for her contribution to the Nrf2 aspects of this dissertation. I must also thank all of the undergraduate

students that I have worked with, especially Elizabeth Kim, who aided in quantification of data, as well as solution making, and animal care.

I want to thank Dr. AJ Robison and his lab for the use of their viral vectors and their invaluable knowledge concerning FosB and ΔFosB. I also want to thank my committee members, Dr. Christina Chan and Dr. Monique Floer for their insight on the project. I also want to acknowledge the Genetics Program and its director Dr. Cathy Ernst. They have helped fund my studies through teaching assistantships. Special thanks to Dr. Jennifer Schisa, my undergraduate research and MS research advisor, work in your lab is what started me down this path.

Most of all I want to thank my family, as they are the ones that tolerated me throughout it all. To my wife Cassie, I want to thank you for putting up with the long hours, late nights, and my ramblings throughout the last few years. Your love and support is what got me through. To my son Jordan, you brighten my day and inspire me to be better. I want to thank my parents, Robert and Nancy, for their support throughout school. I also want to thank my in-laws for keeping Cassie and Jordan company while I was busy, as well as Tuesday night dinners. Finally I want to acknowledge my dog Echo, who kept me company while I was writing my dissertation.

TABLE OF CONTENTS

LIST OF TABLES

LIST OF FIGURES

KEY TO ABBREVIATIONS

3V	Third ventricle
AAV	Adeno-associated virus
AMPA	α-amino-3-hydroxy-5-methyl-4-isoxazolepropionic acid
ANOVA	Analysis of Variance
AP-1	Activator protein 1
ARC	Arcuate nucleus
ARE	Antioxidant response element
ATF4	Activating transcription factor 4
BCA	Bicinchoninic acid
BDNF	Brain derived neurotrophic factor
BSA	Bovine serum albumin
°C	Degrees Celsius
Ca^{2+}	Calcium
Caltech	California Institute of Technology
CaMKII	Calmodulin kinase II
CamKIV	Calmodulin kinase IV
cAMP	Cyclic adenosine monophosphate
CCCP	Carbonyl cyanide 3-chlorophenyl hydrazone
ChIP	Chromatin immunoprecipitation
ChIP-Seq	Chromatin immunoprecipitation sequencing

CREB	cAMP response element binding protein
CTCF	CCCTC-binding factor
Cul3	Cullin3
Cy3	Cyanine 3
d	Day(s)
D1	Dopamine receptor D1
D2	Dopamine receptor D2
DA	Dopamine
DAT	Dopamine transporter
DCF-DA	2', 7'-dichlorofluorescine diacetate
DDC	Dopa decarboxylase
ddH_2O	Double-distilled dihydrogen monoxide (water)
DMEM	Dulbecco's modified eagle medium
DNA	Deoxyribonucleic acid
DOPA	3, 4-Dihydroxyphenylalanine
DOPAC	3, 4-Dihydroxyphenylacetic acid
DOPAL	3, 4-Dihydroxyphenylacetaldehyde
EDTA	Ethylenediaminetetraacetic acid
EGTA	Ethylene glycol-bis(β-aminoethyl ether)-N,N,N',N'-tetraacetic acid
eIF2α	Eukaryotic initiation factor 2α
ENCODE	Encyclopedia of DNA elements
ER	Endoplasmic reticulum

GADD43	Growth arrest and DNA damage inducible protein 34
GAPDH	Glyceraldehyde 3-phosphate dehydrogenase
GFAP	Glial fibrillary acidic protein
GTP	Guanosine triphosphate
h	Hour(s)
H3	Histone protein 3
HAT	Histone acetyltransferase
HPLC	High pressure liquid chromatography
i.p.	Intraperitoneal
IBR	In-between RING
kb	Kilobase
KCl	Potassium chloride
kDa	Kilodalton
Keap1	Kelch-like ECH-associate protein 1
kg	Kilogram
KO	Knock-out
LAT	L-amino acid transporter
L-DOPA	Levodopa
LICR	Ludwig Institute for Cancer Research
LRRK2	Leucine-rich repeat kinase 2
LyF-1	Lymphoid transcription factor 1
MAO-B	Monoamine oxidase B

Mb	Megabase
ME	Median eminance
MEL cells	Murine erthroleukemia cells
MeOH	Methanol
mg	Miligram
MgCl2	Magnesium chloride
min	Minute(s)
miRNA	Micro ribonucleic acid
ml	Milliliter
mM	Millimolar
mm	Millimeter
MN9D	Murine mesencephalon-derived dopaminergic neuronal cell line 9D
MPP+	1-methyl-4-phenylpyridinium
MPTP	1-methyl-4-phenyl-1,2,3,6-tetrahydropyridine
mRNA	Messenger ribonucleic acid
MSN	Medium spiny neuron
MyoD	Myogeneic differentiation
NAc	Nucleus accumbens
NaCl	Sodium chloride
NAD+/NADH	Nicotinamide adenine dinucleotide
NaOH	Sodium hydroxide
NeuN	Neuronal nuclei

ng	Nanogram
NGS	Normal goat serum
NMDA	N-methyl-D-aspartate
Nrf1	Nuclear factor (erythroid-derived 2)-like 1
NRF1	Nuclear respiratory factor 1
Nrf2	Nuclear factor (erythroid-derived 2)-like 2
NSDA	Nigrostriatal dopamine
Pacrg	Park2 co-regulated gene
PARIS	Parkin interacting substrate
PBS	Phosphate buffered saline
PD	Parkinson disease
PERK	PKR-like ER localized eIF2α kinase
pg	Picogram
PGC-1α	Peroxisome proliferator-activated receptor gamma coactivator 1α
PINK1	PTEN-induced putative kinase 1
PKA	Protein kinase A
PMA	Phorbol 12-myristate 13-acetate
PSU	Pennsylvania State University
REP	Repressor element of parkin
RING	Really interesting new gene
RIPA buffer	Radioimmunoprecipitation assay buffer
ROS	Reactive oxygen species

RTPCR	Real-time polymerase chain reaction
s	Second(s)
s.c.	Subcutaneous
SDS	Sodium dodecyl sulfate
SEM	Standard error of the mean
Ser	Serine
SIRT2	Sirtin 2
SN	Substantia nigra
SNCA	α-synuclein
SOS	Sodium octyl sulfate
SRF	Serum response factor
SRY	Sex determining region on chromosome Y
ST	Striatum
SYDH	Stanford/Yale
TCF11	Transcription factor 11
TDF	Testis determining factor
TGX	Tris-glycine extended
TH	Tyrosine hydroxylase
TIDA	Tuberoinfundibular dopamine
TPA	12-O-tetradecanoylphorbol-12-acetate
TRE	TPA-response element
Tris-HCl	Tris-hydrochloric acid

tRNA	Transfer ribonuclei acid
Ubl	Ubiquitin-like
UCSC	University of California Santa Cruz
µg	Microgram
µM	Micromolar
uORF	Upstream open reading frame
UPR	Unfolded protein response
UPS	Ubiquitin proteasome system
USF	Upstream stimulating factor
V	Volts
VMAT	Vesicular monoamine transporter
VTA	Ventral tegmental area
WT	Wild-type

Chapter 1: General Introduction

Parkinson Disease

Parkinson disease (PD) is the second most prevalent neurodegenerative disease and is characterized by the degeneration of the nigrostriatial (NS) dopamine (DA) neurons and the formation of Lewy bodies or intraneuronal protein aggregates (Nuytemans et al., 2010). The loss of the NSDA neurons leads to the classic motor symptoms of PD, which are resting tremor, bradykinesia, rigidity, and postural instability (Jankovic, 2008; Fahn, 2003). Additionally, other there are non-motor symptoms associated with PD, such as depression, hyposmia, anhedonia, gastrointestinal issues, sleep disorder, cognitive impairment and neuropsychiatric symptoms (Sveinbjorndottir, 2016).

The first clinical description of PD was in Dr. James Parkinson's 1817 "An Essay on the Shaking Palsy". Dr. Parkinson described the symptoms as "involuntary tremulous motion, with lessened muscular power, in parts not in action even when supported; with propensity to bend the trunk forward, and to pass from a walking to a running pace". This description from Dr. Parkinson best describes the resting tremor and postural instability associated with PD. Though Parkinson was the first to clinically describe the disease, mention of its symptoms can be found throughout history. Symptoms of PD, mostly the tremors, were alluded to in two books of the

Old Testament and once in the New Testament, described by Leonardo da Vinci, referred to as "the palsy" by William Shakespeare, and mentioned in ancient medical texts, such as Charaka Samhita from India, the Akkadian Diagnostic Handbook from Mesopotamia, and De Tremore, Palpitatione, Convulsione et Rigore by Galen of Pergamon (Raudino, 2012).

NSDA Neurons and PD

Cell bodies of the NSDA neurons are located in the substantia nigra pars compacta (SNpc) and axons project to and terminate in the striatum (ST) (**Figures 1.1 and 1.2**). DA synthesis within DA neurons starts with the transport of dietary tyrosine into the neurons via the large neutral amino acid transporter (LAT) (Fernstrom and Fernstrom, 2007). Tyrosine hydroxylase (TH), the rate-limiting enzyme in DA synthesis, adds a hydroxyl group to tyrosine, converting it to 3,4-dihydroxyphenylalanine (DOPA) (Levitt et al., 1965). A carboxyl group is then removed by DOPA decarboxylase (DDC), producing DA, which is packaged into synaptic vesicles via the vesicular monoamine transporter (VMAT) (Weihe et al., 1994; Lovenberg et al., 1962) (**Figure 1.3**). An action potential causes synaptic vesicles within the pre-synaptic axon terminal to release DA into the synaptic cleft.

The NSDA neurons synapse on the medium spiny neurons (post-synaptic), which possess D1 or D2-like DA receptors. Both D1 and D2 receptors are G-

protein coupled receptors. DA binding to the receptor leads to the exchange of GTP for a GDP in the α subunit of the trimeric G-protein. The released α subunit acts on adenylate cyclase, either stimulatory or inhibitory based on the whether the subunit expressed in the cells is a α_s or α_i subunit respectively. Inhibition of adenylate cyclase results in a decrease in cyclic adenosine monophosphate (cAMP), where stimulation increases cAMP (Kebabian and Greengard, 1971). This regulation of cAMP modifies the activity of protein kinase A, of which cAMP is a co-factor. Protein kinase A can phosphorylate TH, increasing its activity and DA synthesis (Kim et al., 1993).

In addition to post-synaptic DA receptors, NSDA neurons have pre-synaptic D2 autoreceptors, which released DA can act on and repress DA synthesis in a negative feedback loop. DA not interacting with DA receptors can be scavenged using the DA transporter (DAT), which is used to re-uptake DA into the terminals of the pre-synaptic neurons (Shimada et al., 1991). The recaptured DA, as with newly synthesized DA, can be either packaged into synaptic vesicles or metabolized. Monoamine oxidase B (MAO-B) found bound to the outer membrane of mitochondria will deaminate DA, producing 3, 4-dihydroxyphenylacetaldehyde (DOPAL) (Hafer et al., 1987; O'Carroll et al., 1983). The aldehyde on DOPAL is oxidized by aldehyde dehydrogenase, forming 3, 4-dihydroxyphenylacetic acid (DOPAC), which can exit the axons via simple diffusion (Marchitti et al., 2007) (**Figure 1.3**).

The role of the NSDA neurons terminating in the ST is in the regulation of the basal ganglia and motor control. The basal ganglia are comprised of interconnected nuclei that connect to the motor cortex and function to coordinate movement. The circuitry of the direct pathway involves D1 receptor expressing medium spiny neurons, which send inhibitory signals to the globus pallidus interna and substantia nigra pars reticulata. The globus pallidus interna and substantia nigra pars reticulata send inhibitory signals to the thalamus, which sends excitatory signals to the motor cortex. The motor cortex, in turn, sends inhibitory signals to the brain stem, spinal cord and subthalamic nucleus. The inhibitory signals from the motor cortex to the subthalamic nucleus sends excitatory signals to the globus pallidus interna and subtantia nigra pars reticulata. The circuitry of the indirect pathway involves the D2 receptor expressing medium spiny neurons, which send inhibitory signals to the globus pallidus externa, which in turn sends inhibitory signals to the subthalamic nucleus, globus pallidus interna and substantia nigra pars reticulata.

Increased DA release from the NSDA neurons terminating near medium spiny neurons interacts with D1 and D2 receptors. Medium spiny neurons with D1 receptors are activated by DA, which inhibits neurons in the globus pallidus interna and substantia nigra pars reticulata that normally inhibit thalamic neurons. This allows neurons in the thalamus to send excitatory signals to the motor cortex. Medium spiny neurons with D2 receptors are

inhibited by DA, which blocks the inhibition of neurons in the globus pallidus externa, allowing the globus pallidus externa neurons to inhibit neurons in the subthalamic nucleus, globus pallidus interna and subtantia nigra pars reticulata. This allows neurons in the thalamus to send excitatory signals to the motor cortex. The loss of the NSDA neurons leads to the decrease of DA acting on both types of medium spiny neurons, and thus has the inverse effect as DA release, decreasing the signal sent to the motor cortex, causing the motor symptoms associated with PD.

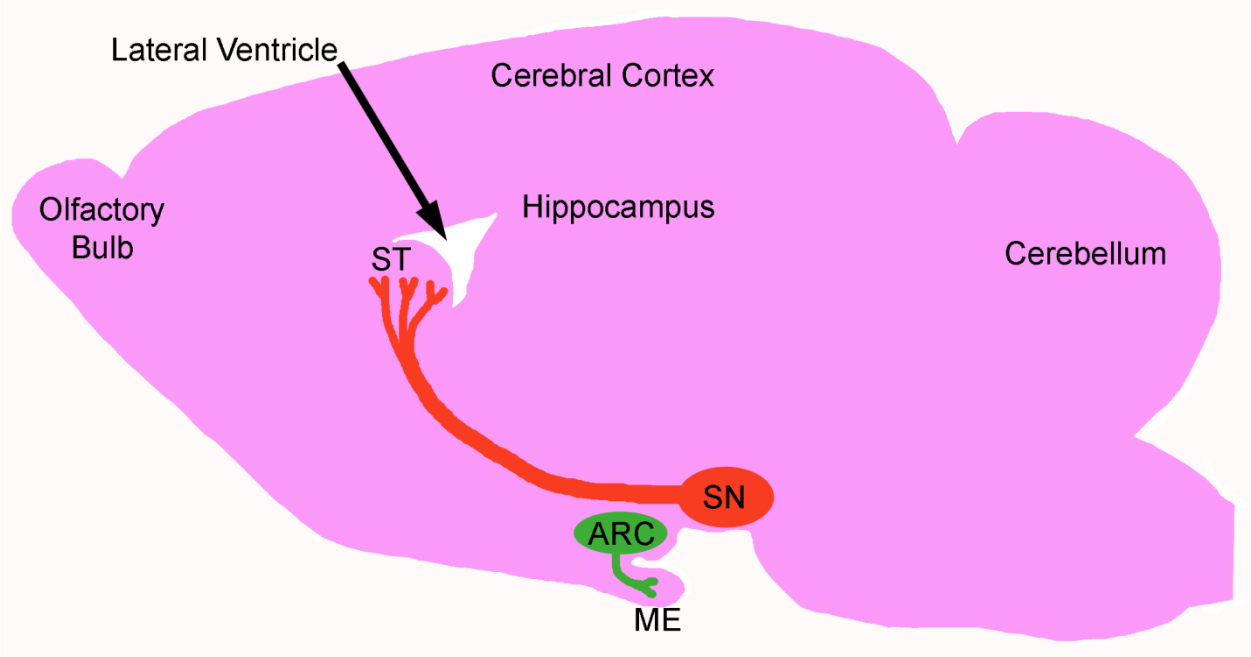

Figure 1.1 Location of NSDA and TIDA neuronal pathways. The NSDA neurons (red) have cell bodies in the SN and project rostral to the ST. The TIDA (green) neurons are housed entirely in the MBH, with cell bodies in the ARC and axon terminals in the ME. Also shown as references, are the locations of the lateral ventricle, olfactory bulb, cerebral cortex, hippocampus, and cerebellum.

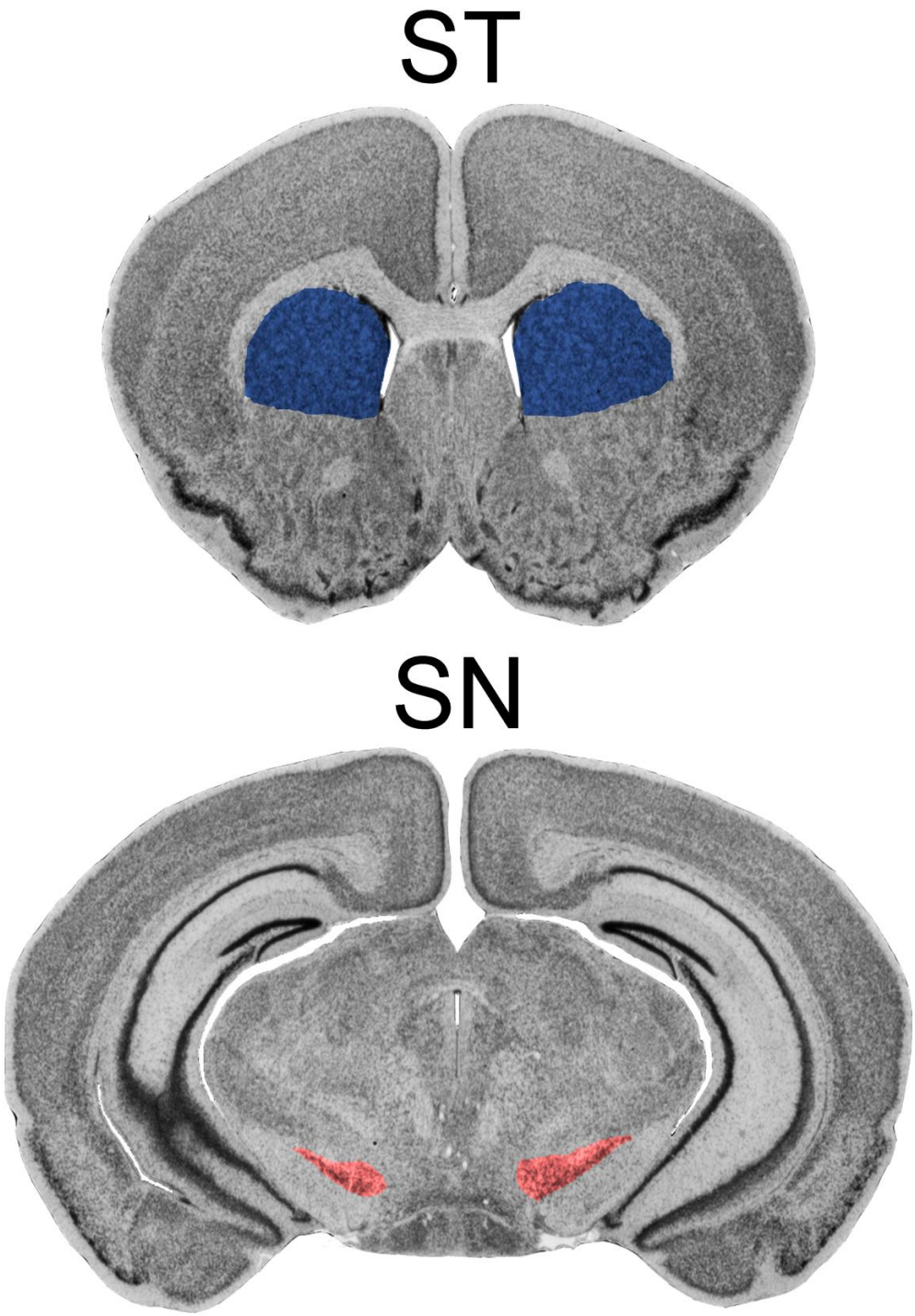

Figure 1.2 Coronal sections containing ST and SN. The ST (blue) is located in a section rostral to the SN (red). Coronal sections are modified from the mouse brain library (www.mbl.org).

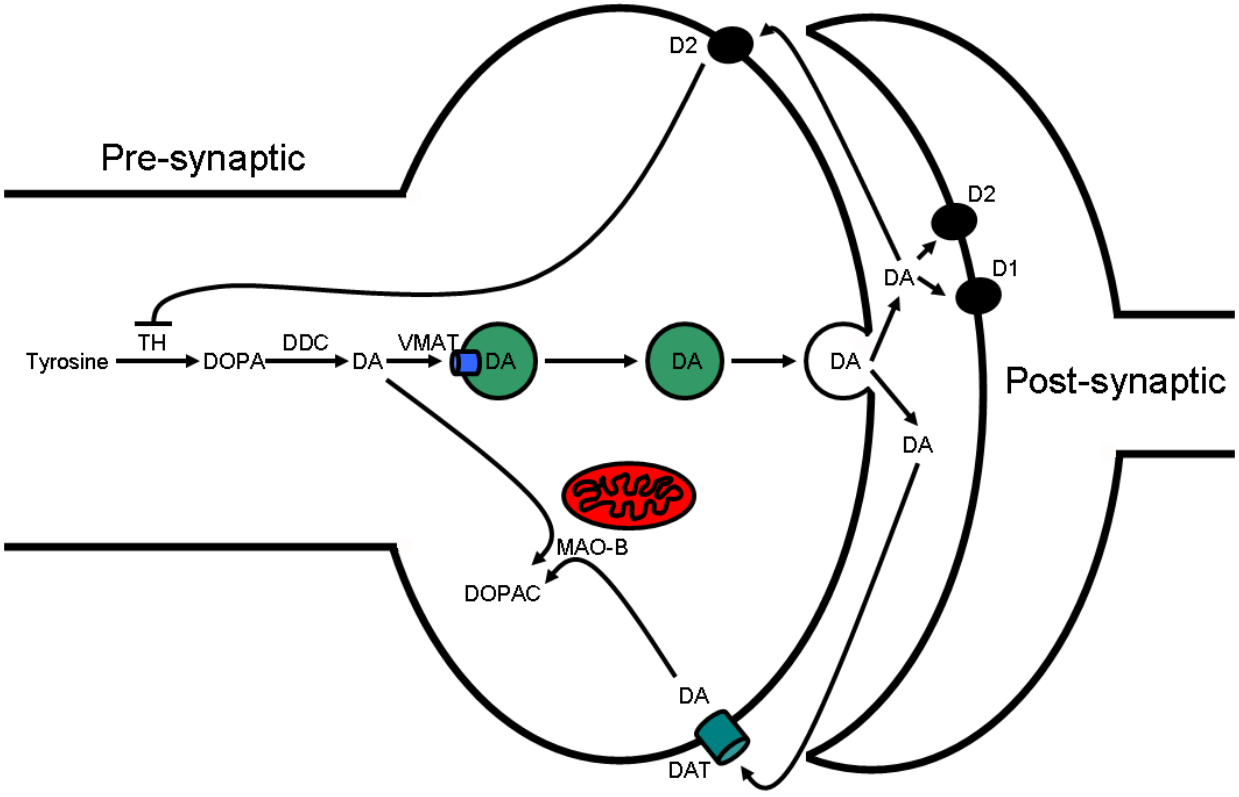

Figure 1.3 Schematic diagram of a NSDA axon terminal. TH adds a hydroxyl group to tyrosine, converting it to DOPA. DOPA has a carboxyl group removed by DDC, converting it to DA. DA is packaged into synaptic vesicles by VMAT. DA can then be released into the synapse. Once in the synapse, DA can contact D1 or D2 receptors on the post-synaptic neurons (post-synaptic neurons possess either D1 or D2, not both as depicted in the simplified figure), or the D2 receptor on the pre-synaptic axon terminal. DA binding to the D2 receptor leads to the inhibition of TH. DA in the synapse can also re-enter the axon through DAT. DA scavenged by DAT or not packaged into vesicles, can be broken down into DOPAC by MAO-B.

Etiology of PD

Though the exact cause of PD is unknown, there are both genetic and environmental factors shown to be associated with the disease. There are 19 loci that have been identified based on family histories and genome wide association studies as Parkinson disease related or *Park* loci. The most commonly studied are parkin (*Park2*), α-synuclein (*SNCA, or Park1, and Park4*), leucine-rich repeat kinase 2 (*LRRK2* or *Park8*), *PTEN*-induced putative kinase 1 (*PINK1* or *Park6*) and *DJ-1* (*Park6*) (Nuytemans et al., 2010). Parkin is an E3 ubiquitin ligase that tags misfolded proteins for degradation, but this protein has other functions than just within the ubiquitin proteasome system (UPS) as discussed below (see Parkin). Individuals with parkin mutations have been found to have a loss of NSDA neurons, noradrenergic neurons in the locus coeruleus, and variable Lewy pathology. The α-synuclein protein has been suggested to normally function in vesicle trafficking, and oligomers of α-synuclein are a key component of Lewy body aggregates associated with PD (Cookson, 2012; Cookson, 2009). The mechanism by which LRRK2 leads to PD is not known, however, some mutations in the gene affect kinase activity (MacLeod et al., 2006; Klein and Westenberger, 2012). PINK1 on defective or damaged mitochondria can phosphorylate parkin, leading to the ubiquitylation of mitochondrial proteins such as mitofusin and voltage-dependent anion channel 1. This process labels mitochondria for degradation through mitophagy (Poole et al., 2008,

2010; Geisler et al., 2010). DJ-1 is predicted to function as an oxidative stress sensor via conserved cysteine residues (Wilson, 2011; Waak et al., 2009). Along with parkin, these genes account for six of the nineteen *Park* loci (Klein and Westenberger, 2012; Hardy, 2010; Nuytemans et al., 2010).

Less is known about the link between PD and the other *Park* loci. *Park3*, *Park10*, *Park12*, and *Park16* do not have exact gene names and *Park10* is recognized as a risk locus, rather than having a Mendelian inheritance pattern (Hernandez et al., 2016; Mitsui and Tsuji, 2014, Klein and Westenberger, 2012; Hardy, 2010). The loci with confirmed genes can be grouped into categories. *UCH-L1 (Park5)* and *FOXO7 (Park15)* are involved in the UPS, *PLA2G6 (Park14)* is involved in lipid metabolism, *ATP13A2 (Park9)* and *VPS35 (Park7)* with lysosome function, *HTRA2 (Park13)* is associated with mitochondria, *GIGYF2* (*Park11*) is predicted to function in the regulation of tyrosine kinase receptor signaling, *EIF4G1 (Park18)* with translation, and *DNAJC16* (*Park19*) encodes a heatshock protein (Hernandez et al., 2016; Mitsui and Tsuji, 2014, Klein and Westenberger, 2012; Hardy, 2010). With the exception of *Park10* and *Park16* which do not follow a known inheritance pattern, and *Park12* which follows an X-linked pattern, the other *Park* loci follow either autosomal dominant (*Park1, Park3, Park4, Park5, Park8, Park11, Park13, Park17,* and *Park18*) or autosomal recessive (*Park2, Park6, Park7, Park9, Park14, Park15,* and *Park19*) Mendelian inheritance patterns (Hernandez et al., 2016). These monogenic forms of PD

are responsible for approximately 30% of familial and less than 6% of sporadic PD (Kumar et al., 2011).

In addition to monogenic forms of parkinsonism, there are risk loci that can factor into polygenic parkinsonism. Examples of risk loci identified via GWAS are *MAPT* which is associated with microtubules, *GBA* which is associated with the lysosome, *ATXN3* which is associated with the UPS, *ATXN2* which does not have a known function, *NUCKS1* which is involved in mitosis, *SIPA1L2* which is involved in the Ras signaling pathway, *TMEM163* which is predicted to function in the recruitment of cations to vesicles, *STK39* which is a serine/threonine kinase involved in stress response, *MCCC1* which is a subunit of 3-methylcrotonyl-CoA carboxylase, *TMEM175* which is a component of potassium channels in lysosomes, *SCARB2* which is involved in membrane transport to lysosomes, *HLA-DQB1* which is a component of a histocompatibility complex, *GPNMB* which is a transmembrane glycoprotein, *FGF20* which is a fibroblast growth factor, *INPP5F* which is a specific phosphatase, *MIR4697* which encodes a miRNA (microRNA), *CCDC62* which is a coactivator for nuclear receptors, *GCH1* which is an enzyme in tetrahydrobiopterin synthesis, *VPS13C* which plays a role in vesicle trafficking, *STX1B* which is predicted to play a role in synaptic vesicle exocytosis, *SREBF* which is a transcription factor involved in sterol syntheis, *RIT2* which is involved in the mitogen activated protein kinase pathway, and *DDRGK1* which plays a role in endoplasmic reticulum stress

(Hernandez et al., 2016; Mitsui and Tsuji, 2014; Hardy, 2010). Some short nucleotide polymorphisms in *SNCA* and *LRRK2* are also associated with risk in the context of polygenic PD, in addition to those involved in monogenic PD (Hernandez et al., 2016).

Both monogenic and polygenic factors have a role in the risk of developing PD, as well as the age of onset. Rare mutations in monogenic genes that are highly penetrant, such as those in *Park2* are more likely to cause PD at an early age (Escott-Price et al., 2015). This compares to polygenic causes of PD, where common variants of multiple risk loci cause the disease. In this case there tends to be a lower occurrence of the disease and a later age of onset. The caveat however is that with increased common variants of risk loci, the prevalence of the disease can increase as well as the potential for an earlier age of onset (Escott-Price et al., 2015).

In addition to genetic risk factors, there are environmental risk factors that mostly revolve around rural living and farming. In addition to rural living itself, other aspects such as drinking well water and consequential exposure to manganese, herbicides such as paraquat and pesticides such as rotenone have all been suspected (Bellou et al., 2016; Pezzoli et al., 2013; Mortimer et al., 2012; Noyce et al., 2012; Van der Mark et al., 2012; Brown et al., 2006). In the early 1980s heroin addicts in San Francisco who used a synthetic opiate desmethylprodine exhibited Parkinsonian symptoms, more specifically the inability to initiate movement. These symptoms were found

to be caused by a by-product produced in the production of desmethylprodine, called 1-methyl-4-phenyl-1,2,3,6-tetrahydropyradine (MPTP). Exposure to MPTP in primates results in the selective degeneration of the NSDA neurons, but with no Lewy body pathology (Dauer and Przedborski, 2003; Langston et al., 1999; Ballard et al., 1985).

MPTP

The selectivity of MPTP for DA neurons is based on the mechanism of action of the drug. MPTP is highly lipophilic and readily crosses the blood brain barrier. MPTP is metabolized in glial cells by monoamine oxidase-B into 1-methyl-4-phenylpyridinium (MPP^+) (Markley et al., 1984; Dauer and Przedborski, 2003). This toxic metabolite is selectively taken up into the DA neurons through DAT, which normally functions in the re-uptake of released DA from the synapse (Chan et al., 1991; Dauer and Przedborski, 2003) (**Figure 1.4**). MPP^+ has many adverse effects on the neurons including the uptake via the VMAT and displacement of stored DA from the synaptic vesicles (potentially leading to accumulation of toxic DA metabolites), inhibition of mitochondrial Complex I, and interactions with cytosolic enzymes, each of which can cause oxidative stress (Chan et al., 1991; Liu et al., 1992; Dauer and Przedborski, 2003). In some MPTP dosing paradigms, indicators of oxidative stress are present, such as lipid peroxidation and increased superoxide dismutase (Hung and Lee, 1998). Oxidative stress

could also be related to other effects of MPTP, such as microtubule destabilization (Cartelli et al., 2013; Cappelletti et al., 2005). *In vitro*, MPP^+ has also been shown to act as a proteasome inhibitor (Lansdell, et al., submitted).

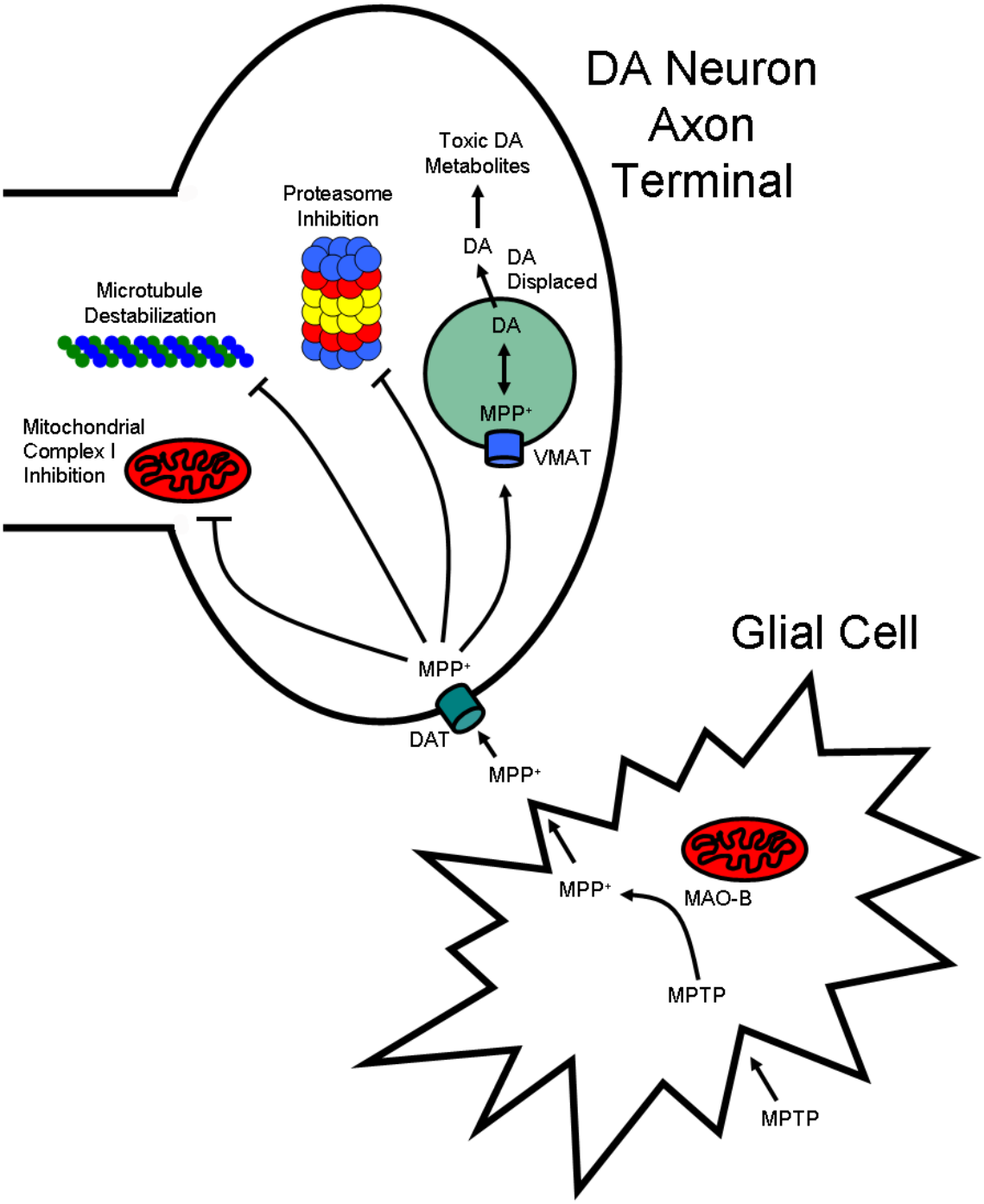

Figure 1.4 Mechanism of action of MPTP. MPTP readily crosses the blood-brain barrier and is converted to MPP^+ by mitochondrial MAO-B in glial cells. MPP^+ released from glial cells enter DA neurons through DAT. In DA neurons, MPP^+ can enter into synaptic vesicles via VMAT and displace stored DA, resulting in generation of toxic DA metabolites. MPP^+ *in vitro* can directly inhibit the proteasome, destabilize microtubules and inhibit mitochondrial Complex I.

In mice, acute MPTP (single subcutaneous injection of 20 mg/kg) decreases stored DA in the axon terminal regions of the NSDA, MLDA, and TIDA neurons. DA in the NSDA neurons does not recover, whereas DA in the TIDA neurons fully recovers by 24 h after MPTP (Behrouz et al., 2007). The cell bodies of the TIDA neurons are located in the arcuate nucleus (ARC) of the mediobasal hypothalamus (**Figure 1.5**). The axons of TIDA neurons are short relative to those of NSDA neurons and do not extend out of the mediobasal hypothalamus, instead the axons project basally and terminate outside the blood-brain barrier in the median eminence (ME) (**Figure 1.5**). TIDA neurons are also unaffected in PD (Matzuk et al., 1985). Recovery of the TIDA neurons is not only dependent on *de novo* protein synthesis, but also increased expression of parkin, which occurs in the TIDA but not the NSDA neurons (Benskey et al., 2012; 2015).

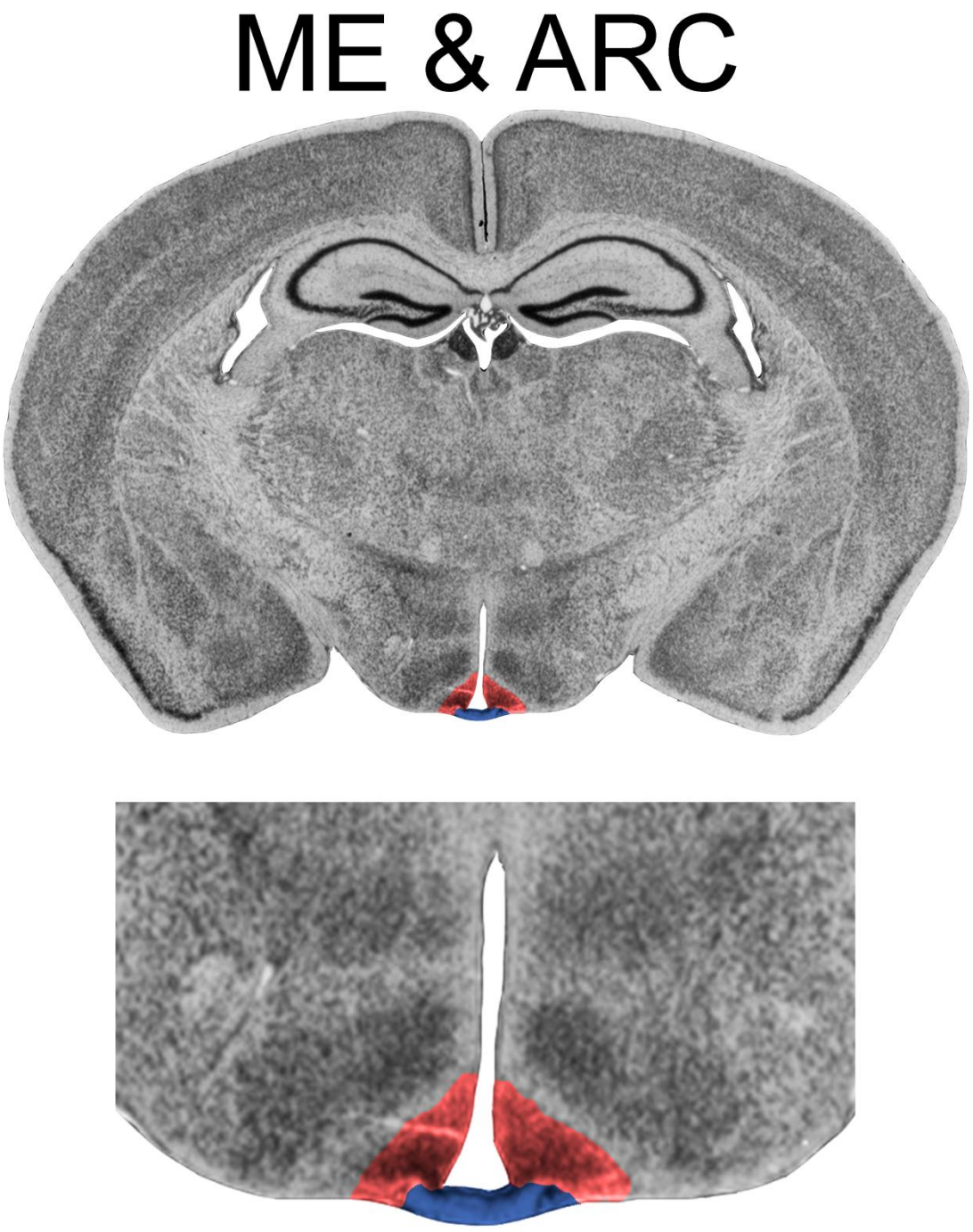

Figure 1.5 Coronal sections containing ME and ARC. Within the MBH the ME (blue) is located directly below the third ventricle and the ARC (red) is flanking the third ventricle. Coronal sections are modified from the mouse brain library (www.mbl.org).

Parkin

Parkin is an enzyme containing 465 amino acids in humans and 464 amino acids in mice (Kitada et al., 1998; Li and Gehring, 2015). Both human and mouse parkin have a ubiquitin like domain (Ubl), linker region, three really interesting new gene (RING0, RING1, and RING2) domains, a repressor element of parkin (REP) and an in-between RING domain (IBR) (Wenzel et al., 2011; Hristova et al., 2009; Zhang et al., 2000; Li and Gehring, 2015) (Figure 1.6). These domains allow parkin to function as an E3 ubiquitin ligase (Zhang et al., 2000; Li and Gehring, 2015). In the UPS, an E1 activating enzyme binds ubiquitin in an ATP dependent reaction and in turn, transfers the ubiquitin to the E2 conjugating enzyme. A misfolded protein substrate bound to an E3 ubiquitin ligase interacts with the E2 conjugating enzyme, which transfers the ubiquitin to the substrate. This process is repeated, forming a polyubiquitin chain. The ubiquitinated substrate can then be transferred to the proteasome to be degraded (Pickart, 2001; Li and Gehring, 2015). In the context of parkin, each domain aids in the function of parkin as an E3 ubiquitin ligase.

The Ubl domain interacts with Rpn10, a regulatory subunit of the 26S proteasome, and is predicted to aid in the binding of parkin to the proteasome (Sakata et al., 2003; Wilkinson et al., 2000). In the context of the UPS, the RING1 domain of parkin interacts with the E2 conjugating enzyme and RING2 contains a catalytic cysteine involved in ubiquitin

transfer to the substrate (Zhang et al., 2000). RING0 can interact with 14-3-3 chaperone proteins, which leads to the inhibition of the ubiquitin ligase activity of parkin (Hristova et al., 2009; Sato et al., 2006). REP located between the IBR and RING2 domains can interact with RING1 to block the E2 conjugating enzyme from binding (Trempe et al., 2013).

In addition to its role as an E3 ubiquitin ligase, parkin has other functions. The RING1, linker, and RING2 domains can bind to microtubules and aid in their assembly and stability (Yang et al., 2005; Ren et al., 2003,2009). Parkin can affect proteasome activity, where in the ST of mice deficient in parkin, there is decreased proteasome activity as compared to wild-type (WT) mice (Lansdell, et al., submitted).

Parkin can regulate mitochondrial dynamics, including degradation, fusion, fission, and biogenesis. PINK1 is constitutively expressed and subsequently degraded in the mitochondrial matrix. When mitochondria are damaged, depolarization of the membrane leads to PINK1 localization to the outer mitochondrial membrane. PINK1 recruits parkin which ubiquitinates proteins of the mitochondrial membrane and leads to the formation of a mitophagosome that fuses with a lysosome to degrade the mitochondria (Clark et al., 2006; Park et al., 2006, 2009; Poole et al., 2008; Vives-Bauza et al., 2010; Pickrell et al., 2015; Li and Gehring, 2015; Lutz et al., 2009; Narendra et al., 2008). In fission and fusion, key proteins involved in each process, such as dynamin-related protein 1, mitofusin 2, and optic atrophy 1,

are substrates of parkin. However, parkin functions more prominently in fission, where overexpression of parkin leads to elongated mitochondria and the loss of parkin leads to increased fusion (Poole et al., 2008; Buhlman et al., 2014; Chen et al., 2005; Ziviani et al., 2010; Li and Gehring, 2015).

The regulation of mitochondrial biogenesis by parkin is via peroxisome proliferator-activated receptor-γ coactivator 1α (PGC-1α). PGC-1α is a regulator of mitochondrial biogenesis that is transcriptionally repressed by parkin-interacting substrate (PARIS) (Shin et al., 2011). The E3 ubiquitin ligase activity of parkin degrades PARIS, resulting in increased expression of PGC-1α and its coactivator nuclear respiratory factor 1 (NRF1), which together stimulate mitochondrial biogenesis (Russell et al., 2004; Wu et al., 1999). Finally, parkin has been shown to be a transcription factor of presenilin-1 and presenilin-2, two proteins involved in Alzheimer disease (Duplan et al., 2013). Parkin as a transcription factor uses the RING1-IBR-RING2 domains and has a consensus sequence or GCCGGAG (Duplan et al., 2013).

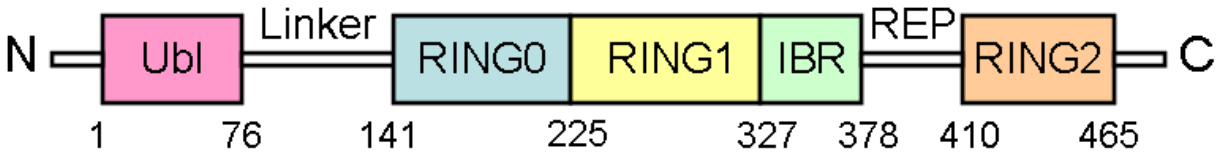

Figure 1.6 Schematic depicting the structure of the parkin protein. Shown is the human parkin protein with 465 amino acids. The location of the Ubl, linker region, RING0, RING1, IBR, REP, and RING2 domains are shown, with length in amino acids of each domain indicated by the numbers below.

Parkin and MPTP

Recovery of DA stores in axon terminals of the TIDA neurons is dependent on parkin and over-expression of parkin in the NSDA neurons rescues the loss of TH after acute MPTP exposure (Benskey et al., 2015). Comparing regions containing TIDA and NSDA neuronal axon terminals, at 4 h post-MPTP, there are high levels of MPP^+ in both the ST and ME, but by 24 h MPP^+ is cleared from these tissues (Benskey et al., 2012). After a single 20 mg/kg subcutaneous injection of MPTP, parkin mRNA in TIDA neuronal cell bodies in the ARC increases almost 3-fold 8 h post-injection, and parkin protein almost 2.5 fold within 36 h (Benskey et al., 2012). In contrast, in NSDA neuronal cell bodies in the SN parkin mRNA expression remains unchanged 8 h post-MPTP and parkin protein decreases by 36 h post exposure (Benskey et al., 2012). In the context of chronic MPTP (mice treated every 3.5 days for 35 days with MPTP were allowed to recover 21 days), parkin in the ARC remains elevated over the 21-day recovery period (Benskey et al., 2013). These results indicate that differential susceptibility of central DA neurons to acute neurotoxicant exposure is correlated with *de novo* synthesis of parkin.

In comparing the effects of MPTP and known functions of parkin, it is evident that parkin has the potential to counteract the effects of MPTP. MPTP can cause depletion of DA vesicular storage and impaired expression of TH, both of which parkin has been shown to counteract (Benskey et al., 2015).

MPTP causes the destabilization of microtubules, which parkin can counteract through stabilization and assembly of microtubules (Cartelli et al., 2013; Yang et al., 2005; Ren et al., 2003, 2009). MPTP inhibits mitochondrial Complex I and damages mitochondria, whereas parkin has a significant role in mitochondrial fission, fusion, degradation, and biogenesis (Li and Gehring, 2015; Shin et al., 2011). It is apparent then that parkin is a neuroprotective protein that is central to the differential susceptibility between the TIDA and NSDA neurons to acute neurotoxic insult. Through the identification of regulators of parkin, such as transcription factors, the underlying cause of the differential expression of parkin may be discovered, as well as the pathways involved, thereby providing potential avenues for the development of therapeutic neuroprotective strategies for the treatment of PD.

Summary

Regional differences in parkin expression after MPTP correspond with the recovery of DA neurons. i.e. parkin increases in the ARC and the TIDA neurons recover, whereas parkin does not increase in the SN and the NSDA neurons do not recover (Benskey et al., 2012). These changes in parkin expression occur within the context of acute MPTP exposure, but chronic neurotoxicant exposure has similar regional effects demonstrating a prolonged increase in parkin expression up to 3 weeks after cessation of MPTP treatment (Benskey et al., 2013).

Differential regulation of parkin expression could potentially be due to differences in transcription factor regulation of the parkin promoter between TIDA and NSDA neurons. By finding candidate transcription factors, followed by the regional, temporal, and sub-cellular expression after MPTP, parkin transcription factors can identified. Expression of these transcription factors can then be altered via adeno-associated virus (AAV) expression vectors, where expression of transcriptional activators are expected to increase parkin expression and transcriptional repressors decrease parkin expression.

Central Hypothesis: Differential regulation of parkin expression in response to neurotoxic insult is due to unique expression patterns of transcription factors in the DA neurons as predicted by their susceptibility to acute MPTP administration.

Specific Aim 1. Identification of candidate transcription factors of parkin.

Hypothesis: Through predictive transcription factor binding software, candidate transcription factors of parkin can be identified.

Specific Aim 2. Characterization of candidate transcription factors of parkin.

Hypothesis: Characterization of regional differences in temporal expression patterns and sub-cellular localization of candidate

transcription factors in the ARC and SN will be able to narrow down the list of candidate transcription factors.

Specific Aim 3. Manipulation of expression of transcription factors and their subsequent effects on parkin expression.

Hypothesis: Through the overexpression of proteins consistent with the expectations of a parkin promoter transcriptional activator, parkin expression is predicted to increase. Additionally, by preventing expression or function of parkin promoter transcriptional activators, subsequent increased parkin expression in the ARC after MPTP should be blocked.

Chapter 2: Methods

Animals

C57BL/6J male WT mice were obtained from The Jackson Laboratory, Bar Harbor, ME. Mice were housed 3-5 to a cage in a room with a 12 h light/dark cycle (lights on 0700 h) and provided food and water *ad libitum*. All animal use was performed with approval from the Michigan State University Institutional Animal Care and Use Committee (AUF 10/14-183-00).

Drug Treatment

MPTP (Sigma Aldrich #M0896 or Santa Cruz Biotechnology Inc. sc-206178) was dissolved in 0.9% saline and diluted to 2.0 mg/ml based on the free base of MPTP. Animals were randomly assigned to treatment groups and were injected with MPTP (20 mg/kg; s.c.) or vehicle (0.9% saline, 10 ml/kg; s.c.).

Brain Removal and Median Eminence Dissection

At designated times after MPTP injection, mice were killed by decapitation with a guillotine. Scissors were used cut the skin midline along the top of the head, starting at the base of the skull and ending rostral to the eyes. One blade of the scissors were inserted into the spinal column and the other blade used to make two bilateral cuts. The frontal bone of the skull was cut

between the eyes. The skull was then cut along the sagittal suture, starting at the neck and proceeding rostral to the frontal bone cut. Forceps were used to peel open the skull, then the brain was carefully lifted back to expose and the optic nerves were cut. The brain was then teased out onto a wet piece of filter paper on a chilled Petri dish.

The brain was positioned to expose the ventral side and a water bottle was used to gently clean the brain as well as to better expose the third ventricle. One blade of the iridectomy scissors was inserted into the third ventricle and two cuts were made lateral of the median eminence (ME) (Figure 2.1, Panels B-C). The boundaries of the median eminence were defined by the noticeable vasculature present in the tissue. The ME was lifted with forceps and a third cut was made near the optic chiasm to detach the tissue (Figure 2.1, Panels D-E). The ME was then placed into buffer, differing based on the analytical endpoint of the experiment. A water bottle was used to again clean the brain and open the third ventricle, before the brain could be further processed, differing based on the analytical endpoint of the experiment as described below.

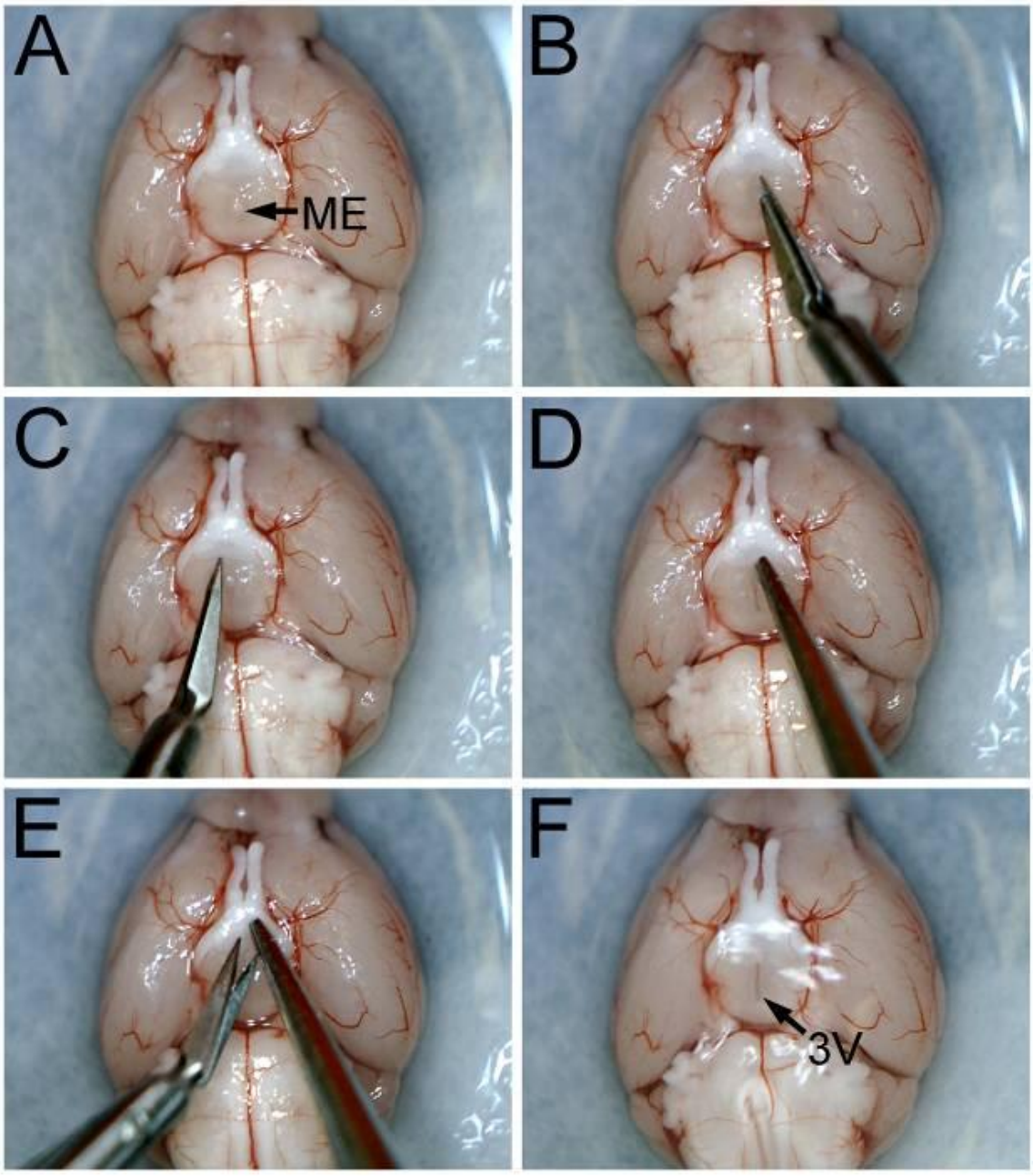

Figure 2.1 Removal of the median eminence (ME). (A) The brain before dissection, arrow points to the ME. Typically vascularization of the ME can be visualized and is used to demarcate the ME. (B) Scissors were inserted into the third ventricle (3V) and the right side of the ME was cut. (C) Scissors were reinserted into the third ventricle and the left side of the ME was cut. (D) Forceps were used to grasp and lift the ME, further exposing the third ventricle. (E) While still holding the ME, the scissors were used to cut the ME near the optic chiasm. The ME was then removed and placed in buffer. (F) The ventral surface of the brain showing the remaining mediobasal hypothalamus and 3V after removal of the ME.

Tissue Preparation for Conventional Western Blots

Brains were frozen on dry ice, wrapped in aluminum foil and stored at -80 °C until further processed. A cryostat set at approximately -10 °C was used to cut 500 µm coronal sections through the brain from rostral to caudal. Coronal sections containing the striatum (ST), arcuate nucleus (ARC) and substantia nigra (SN) were collected on glass slides (**Figure 2.2**). Three sections were taken through the ST, starting just prior to where the corpus callosum joins the right and left hemispheres and ending prior to the anterior commissure connecting the hemispheres. Two sections were taken through the ARC, starting caudal of the optic chiasm where the third ventricle is present and the optic tracts begin to ascend into the brain. One section was taken through the SN, the section was taken when the hippocampus had descended halfway down the brain and the SN was just starting to be visible. Between collecting these sections, the brain was sectioned at 100 to 200 µm so as to not miss the defined landmarks.

Within the coronal sections, ST, ARC, and SN brain regions were individually microdissected using micropunching tools. For the ST, a modified 18 gauge needle punching tool (1 mm inner diameter) was used to bilaterally dissect the ST just below and lateral to the corpus callosum (**Figure 2.2, Top Panel**). For the ARC, an 18 gauge needle punching tool was used to take a single punch from each section containing the ARC (**Figure 2.2, Middle Panel**). The punch was centered along the third ventricle and

was taken half to a third of the way up the third ventricle dorsal to the ventral surface of the hypothalamus. For the SN, a 21 gauge oval needle punching tool (500 µm inner diameter) was used to take bilateral punches from the darker area of the midbrain representative of the SN (**Figure 2.2, Bottom Panel**). These punches were dorsal relative to the darker areas and contained some of the area above.

Tissue punches were transferred into RIPA buffer (20 mM Tris-HCl (pH 7.5), 150 mM NaCl, 1mM Na_2EDTA, 1 mM EGTA, 1% NP-40, 1% sodium deoxycholate, 1X Halt™ protease and 1X Halt™ phosphatase inhibitor). Samples were lysed by sonication and centrifuged at 10,000 x g for 10 min. Supernatant fractions containing soluble proteins were collected and kept at -80 °C until used for Western blots. Aliquots of each sample were used for BCA assays to load equal protein in each well for Western blots.

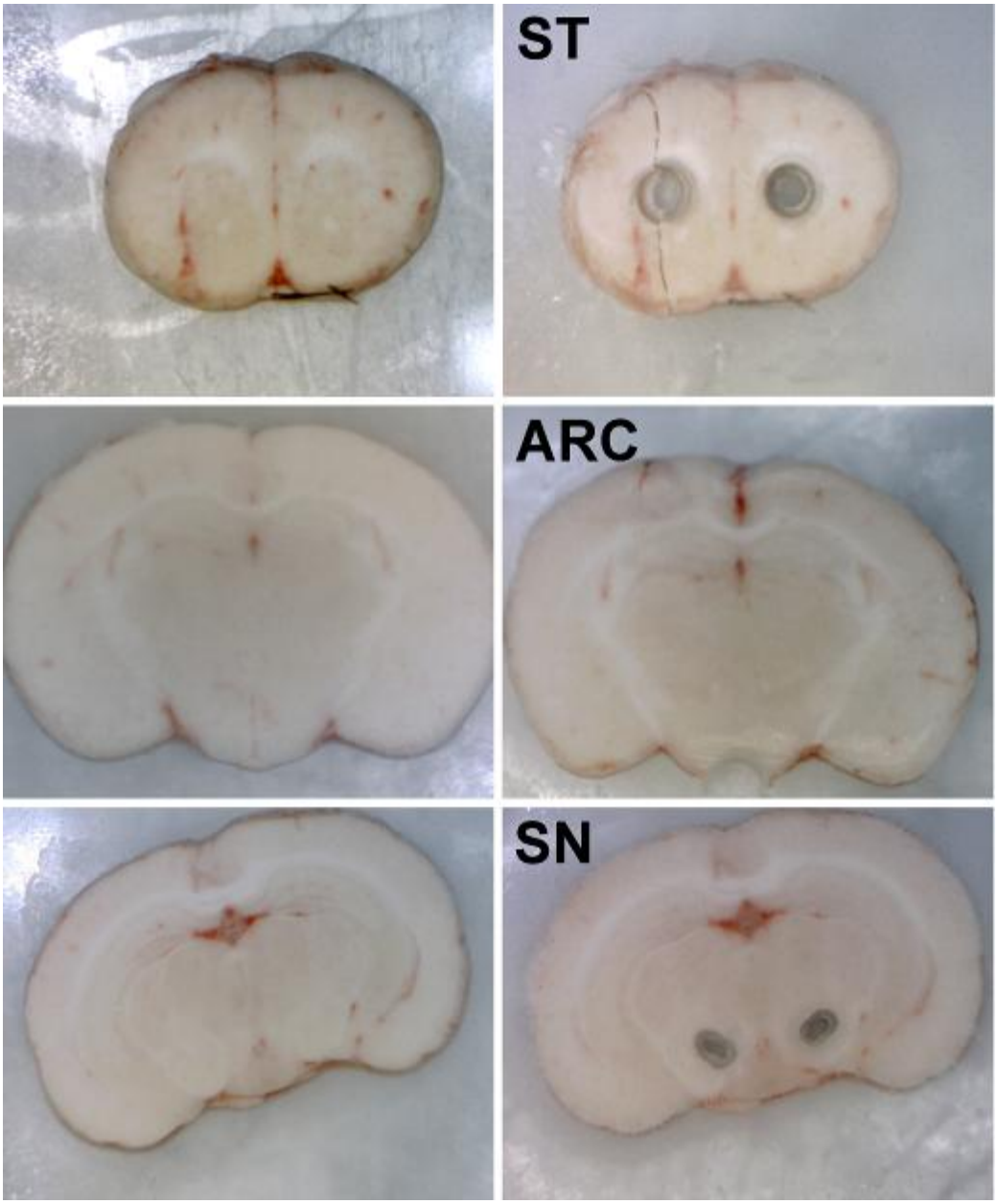

Figure 2.2 Microdissection of the ST, ARC, and SN. Top panels show a 500 µm section containing the ST. Middle panels show a 500 µm section containing the ARC. Bottom panels show a 500 µm section containing the SN. Left panels show the sections before brain regions were removed and right panels show the sections after brain regions were removed.

BCA Assay for Western Blots

BCA reagents were mixed at a 50:1 (bicinchoninic acid:copper sulfate) ratio. An aliquot from the samples were diluted in water (2 µl sample in 48 µl ddH_2O). A serial dilution of BSA (250, 125, 62.5, 31.25, 15.62, 7.81 and 0 ng) were used for the standards. To each tube, 0.5 ml of mixed BCA reagents were added. Tubes were incubated for 15 min in a 60 °C water bath and scanned with a Tecan Infinite M1000 Pro Microplate Reader to determine protein concentration.

Western Blot Analyses

Protein from each sample was run on a 4-20% TGX gel (Bio-Rad), and transferred to a PVDF membrane. Membranes were activated in methanol, blocked in either 5% BSA or milk, and incubated with primary antibodies overnight at 4 °C (Table 2.1). Membranes were washed and incubated at RT with the appropriate secondary antibody (Table 2.2). Membranes were washed and exposed using either a SuperSignal™ West Femto (Thermo Scientific #34095) or SuperSignal™ West Pico (Thermo Scientific #34077) substrate kit with the Li-Cor Fc Odyssey Infrared Imaging System. The process was repeated for the housekeeping protein GAPDH or β-actin, which was used to normalize each protein of interest. Band densitometry was performed using Li-Cor Image Studio Lite (version 5.0).

Bands for the protein of interest and loading control had a box drawn around them, and the signal measured. Sample signals were normalized by membrane using the formula: Signal $X_1 = (X_1/Y_1)/\Sigma(X_n/Y_n)$ where X_1 is the signal from the protein of interest, Y_1 is the loading control signal, and $\Sigma(X_n/Y_n)$ is the sum of each protein of interest to loading control ratio on the membrane. Using the above formula multiple membranes were compared. After statistics were performed, fold change was calculated by dividing the treatment over the vehicle (for the treatment group) and vehicle divided by vehicle (for the control group). Error was propagated using the formula: error propagated = fold change $\bullet \sqrt{[(SEM_1/MEAN_1)^2 + (SEM_2/MEAN_2)^2)]}$.

Table 2.1 List of primary antibodies used. Antibody, the blocking buffer it was diluted with, animal it was raised in, company it was purchased from, and working dilution are shown.

Primary Antibody	Blocking Buffer	Source	Company	Dilution
ATF4	4% BSA in PBST	Rabbit	Cell Signaling #11815	1:500
c-Fos	4% BSA in PBST	Rabbit	Cell Signaling #4384	1:500
c-Jun	4% BSA in PBST	Rabbit	Millipore #09-754	1:500
CREB	4% BSA in PBST	Rabbit	Cell Signaling #9197	1:500
CREB-P (ser133)	4% BSA in PBST	Rabbit	Cell Signaling #9198	1:500
DAT	4% BSA in PBST	Rat	Millipore #MAB369	1:500
eIF2α	4% BSA in PBST	Rabbit	Cell Signaling #5324	1:500
eIF2α-P (ser51)	4% BSA in PBST	Rabbit	Cell Signaling #3597	1:500
FosB	4% BSA in PBST	Rabbit	Cell Signaling #2251	1:500
GAPDH	4% Milk in PBST	Mouse	Sigma Aldrich #G8795	1:500
Histone H3	4% BSA in PBST	Rabbit	Cell Signaling #4499	1:500
JunD	4% BSA in PBST	Rabbit	Cell Signaling #5000	1:500
NRF1	4% BSA in PBST	Rabbit	Cell Signaling #12381	1:500
NRF1/TCF11	4% BSA in PBST	Rabbit	Cell Signaling #8052	1:500
NRF2	4% BSA in PBST	Rabbit	Abcam #AB137550	1:500
Parkin	4% Milk in PBST	Mouse	Cell Signaling #4221	1:500
Parkin	4% BSA in PBST	Rabbit	Cell Signaling #2132	1:500
SRF	4% BSA in PBST	Rabbit	Cell Signaling #5147	1:500
SRF-P (ser103)	4% BSA in PBST	Rabbit	Cell Signaling #4261	1:500
SRY	4% Milk in PBST	Mouse	Abcam #AB22166	1:500
TH	4% BSA in PBST	Rabbit	Millipore #AB152	1:500
TH-P (ser40)	4% BSA in PBST	Rabbit	Cell Signaling #2791	1:500
VMAT2	4% BSA in PBST	Rabbit	Millipore #AB1767	1:500
β-actin	4% Milk in PBST	Mouse	Cell Signaling #3700	1:500

Table 2.2 List of secondary antibodies used. Antibody, the blocking buffer it was diluted with, animal it was raised in, company it was purchased from, and working dilution are shown.

Secondary Antibody	Blocking Buffer	Source	Company	Dilution
Goat anti-rabbit	4% BSA in PBST	Goat	Cell Signaling #7074	1:2000
Goat anti-rat	4% BSA in PBST	Goat	Cell Signaling #7077	1:2000
Horse anti-mouse	4% Milk in PBST	Horse	Cell Signaling #7076	1:2000

Nuclear and Cytoplasmic Fraction Isolation

Nuclear extractions were performed based on methods reported by Karunakaran and Ravindranath (2009) and Korner et al. (1989). After the ME was removed, fresh brains were placed in cold PBS, and sectioned with a razor blade using a Zivic brain matrix (**Figure 2.3**). Sections containing the ST (1 mm), ARC (2 mm) and SN (1 mm) were collected and the regions were individually microdissected from fresh tissue, similar to in **Figure 2.2**. The ST tissue was placed into tissue buffer for later neurochemical analysis and the ARC and SN were placed into PBS (pH 7.4) in a 0.5 ml microcentrifuge tube. Tubes were briefly centrifuged (2,000g for 30 s), PBS decanted, and 30 µl of weak lysis buffer (10 mM HEPES (pH 7.9), 1.5 mM $MgCl_2$, 10 mM KCl, 0.5 mM dithiothreitol, 1X Halt™ protease and 1X Halt™ phosphatase inhibitor cocktails) added to each tube. Four gentle strokes with a Kimble™ Kontes™ Pellet Pestle™ with chlorotrifluoroethylene tip was used to homogenize the tissue. Samples were incubated on ice in weak lysis buffer for 5 min and centrifuged at 10,000 g for 10 min at 4 °C. Supernatant collected (cytoplasmic fraction) and 20 µl of a strong lysis buffer (20 mM HEPES (pH 7.9) 0.84 M NaCl, 1.5 mM MgCl2, 0.4 mM EDTA, 0.5 mM dithiothreitol, 1X Halt™ protease and 1X Halt™ phosphatase inhibitor cocktails) added to the pellet. Pellet was re-suspended, incubated on ice for 30 min (vortexing every 10 min), and centrifuged at 10,000 g for 10 min at 4°C. Supernatant was collected (nuclear fraction), a BCA assay used to

measure protein concentration in both the cytoplasmic and nuclear fractions, and equal amounts of protein used for Western blotting.

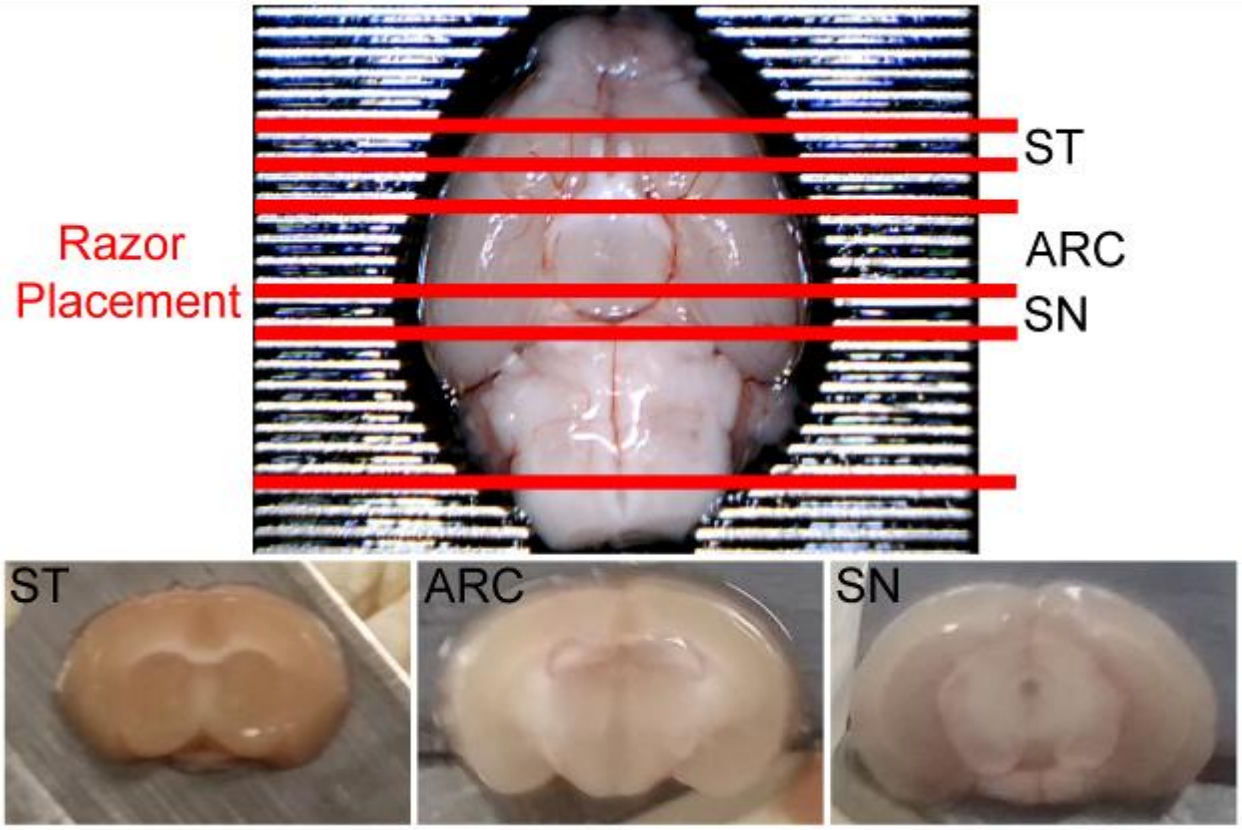

Figure 2.3 Fresh brain sectioning for nuclear and cytoplasmic fraction isolation. Brains were positioned ventral side up in a Zivic brain matrix. Razor blade positions are denoted with red lines, slots are 500 µm apart. The first razor blade was placed in a caudal portion of the brain as a backstop, followed by the most rostal blade. Two large bumps can be seen, one on each side of the optic nerves, the first slot in the matrix that intersects these was selected as the position of the most rostral blade. The third blade placed was just caudal of the optic chiasm, followed by the fourth blade four slots caudal, and fifth blade six slots caudal. The final blade was placed two slots caudal of the most rostral blade. All but the most caudal razor were removed and the three indicated sections (ST, ARC, and SN) were collected and brain regions dissected the same as with frozen sections.

Immunofluorescent Staining and Quantification

Mice were anesthetized with a lethal dose of ketamine:xylazine (24.4 mg/kg:3.6 mg/kg; i.p.) and were considered unresponsive via pedal reflex/toe pinch test. Animals were suspended on a mesh grate at an approximately 30° angle, and a superficial incision made across the belly (enough to cut the skin but not damage internal organs). Two lateral incisions were made through the diaphragm and ribs. A hemostat was attached to the xiphoid cartilage at the base of the ribs and used to retract the ribs and expose the heart. A needle connected to a peristaltic pump was inserted into the left ventricle and the right atrium was cut. Mice were transcardially perfused with 0.9% saline, followed by 4% paraformaldehyde in 0.1M phosphate buffer (pH 7.4). Perfused brains were removed and transferred to vials of 4% parafomaldehyde for 24 h at 4 °C.

Fixed brains were placed in 20% sucrose-phosphate buffer until fully infiltrated for cryoprotection. Coronal sections (20 µm) through the ARC and SN were cut on a cryostat (-9 °C), and sections collected in five sets 100 µm apart in 0.05 M phosphate buffer (pH 7.4). Brain sections were washed in phosphate buffer with 0.1% Triton X100, then blocked in 5% NGS or 5% BSA. Sections were transferred into 1:1000 rabbit anti-FosB (SCBT #sc-48), 1:500 sheep anti-TH (Millipore #AB1542), 1:500 goat anti-GFAP (SCBT #sc-6170) or 1:500 rabbit anti-NeuN Cy3 conjugate (Millipore #ABN78C3) (**Table 2.1**). Sections were washed, incubated with 1:1000 F(ab')2 anti-rabbit Alexa

Fluor® 488 conjugate (Cell Signaling #4412), 1:1000 donkey anti-sheep Alexa Fluor® 594 conjugate (Thermo Scientific #A11016), or 1:1000 donkey anti-goat Alexa Fluor® 594 conjugate (Thermo Scientific #A11058), and mounted.

Staining order was crucial for double labeling. For FosB and TH double labeling, the order was block with BSA, sheep anti-TH, donkey anti-sheep, reblock with NGS, rabbit anti-FosB, and goat anti-rabbit. For FosB and GFAP double labeling, the order was block with BSA, goat anti-GFAP, donkey anti-goat, reblock with NGS, rabbit anti-FosB, and goat anti-rabbit. For FosB and NeuN double labeling, the order was block with NGS, rabbit anti-FosB, goat anti-rabbit, and then rabbit anti-NeuN. Slides were imaged with a Nikon TE2000-U inverted fluorescent microscope. ImageJ was used to quantify cells co-localized with or without FosB staining in sections located 100 µm apart (Abramoff et al., 2004). The percentage of the cells containing total FosB were calculated and averaged across animals within each treatment group. Final image plates were made in Adobe Photoshop CS2.

BCA Protein Assay for Neurochemistry

The pellets from the neurochemistry sample preparation were re-suspended in 50 µl of 1.0 N NaOH and were sonicated for 10 s, briefly vortexed, and centrifuged for 10 min at 10,000g. BCA reagents were mixed at a 50:1 (bicinchoninic acid:copper sulfate) ratio. Samples (25 µl) were

diluted in 25 µl 1 N NaOH and 500 mL of BCA solution was added). A serial dilution of BSA (250, 125, 62.5, 31.25, 15.62 and 0 ng) were used for the standards. Tubes were incubated for 15 min in a 60 °C water bath and scanned with a Tecan Infinite M1000 Pro Microplate Reader to determine protein concentration.

Neurochemical Analysis of DA and DOPAC in ST and ME

During sectioning, one 500 µm section containing the ST from each animal was dissected as described above and then transferred immediately into 50 µl cold tissue buffer (pH 2.5). Samples were briefly centrifuged (2,000g for 30 s), sonicated with three 1 s bursts. The proteins were pelleted by centrifugation for 1 min at 12,000g. The supernatant were transferred to a fresh tube and brought to a final volume using a beveled Hamilton syringe. The final volumes were based on the samples, a bilateral ST sample had 200 µl, unilateral ST sample had 100 µl, and ME had 50 µl. The samples were injected into the HPLC using a mobile phase of 0.03% SOS, 10% MeOH, pH 2.3 and detected using electrochemical detector with an oxidation potential of +0.4 V. Dopamine (DA) and 3,4-dihydroxyphenylacidic acid (DOPAC) content was quantified by comparison of peak heights of the standards to each sample, and then normalized to protein content (**Figure 2.4**).

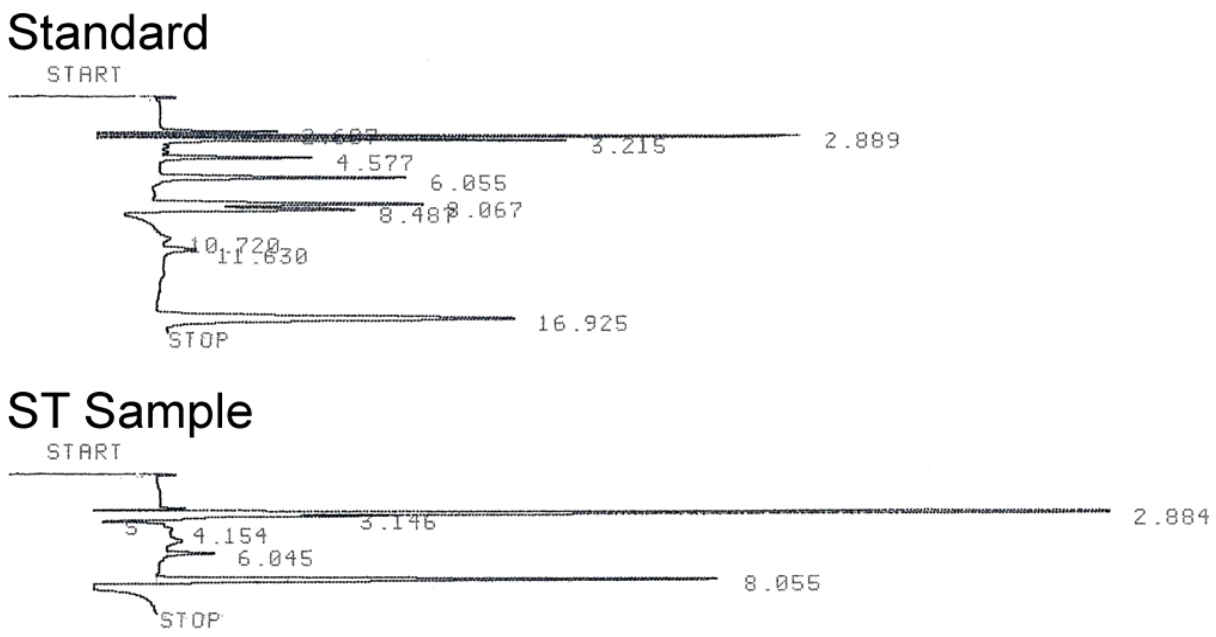

Figure 2.4 Example HPLC traces for neurochemistry. A standard containing different catacholamines of a known concentration was run at the beginning and end of each set of samples. Peaks for DA and DOPAC were hand measured for samples and compared to standards

Stereotaxic Surgeries

Mice were anesthetized with ketamine:xylazine (12.2 mg/kg:1.8 mg/kg; i.p.) and were considered unresponsive and ready for surgery via pedal reflex/toe pinch test. Animals were placed into the stereotaxic frame. The incisor bar was set at a height of 9.5 mm and both ear bars set at 15.0 mm, thereby placing the head at an approximately 15° angle. The scalp was swabbed three times with 70% ethanol followed by three times with Betadine to clean the surgical site. A sterile scalpel was used to make an incision along the rostrocaudal axis of the scalp, cutting the tissue from between the eyes to just rostral of the ears. The skin was retracted to expose the skull and the skull swabbed with a 1.5% hydrogen peroxide solution to remove the periosteum and highlight Bregma, or the intersection between the coronal and sagittal sutures.

A 30 gauge blunt Hamilton syringe was attached to a siliconized pulled glass micropipette (60-80 µm in diameter at the tip). The micropipette was filled with 2 µl of AAV-GFP, AAV-ΔFosB or AAV-ΔJunD serotype 2 expression vector. A Dremel drill was used to bore a small hole in the skull at the following needle insertion points. Unilateral SN injections of 500 nl were injected at 3.3 mm caudal, 1.6 mm and -1.6 mm lateral relative to Bregma and -4.6 mm ventral to the surface of the skull (**Figures 2.5 and 2.6**). Bilateral ARC injections of 250 nl were performed at a 10° angle at 2.4 mm caudal, 1.3 mm and -1.3 mm lateral relative to Bregma and 6.3 ventral to

the surface of the skull (Figures 2.7 and 2.8). AAV Injections were performed at a flow rate of 125 nl/min using an automated micropump (World Precision Instruments).

Following the injection, the needle was left in place for 5 min to prevent backflow. After the needle was removed, the hole in the skull was filled with sterile bone wax. A generic antibiotic ointment (mixture of polymyxin B sulfate, bacitracin and neomycin sulfate) was swabbed onto the tissue around the opening of the skull and the tissue was closed with surgical staples. Mice were injected with ketoprofen (50 mg/kg; s.c.) and transferred to cages on heating pads until completely awake. Mice were moved to a recovery room and their health monitored daily for four weeks, at which time they were used for experiments.

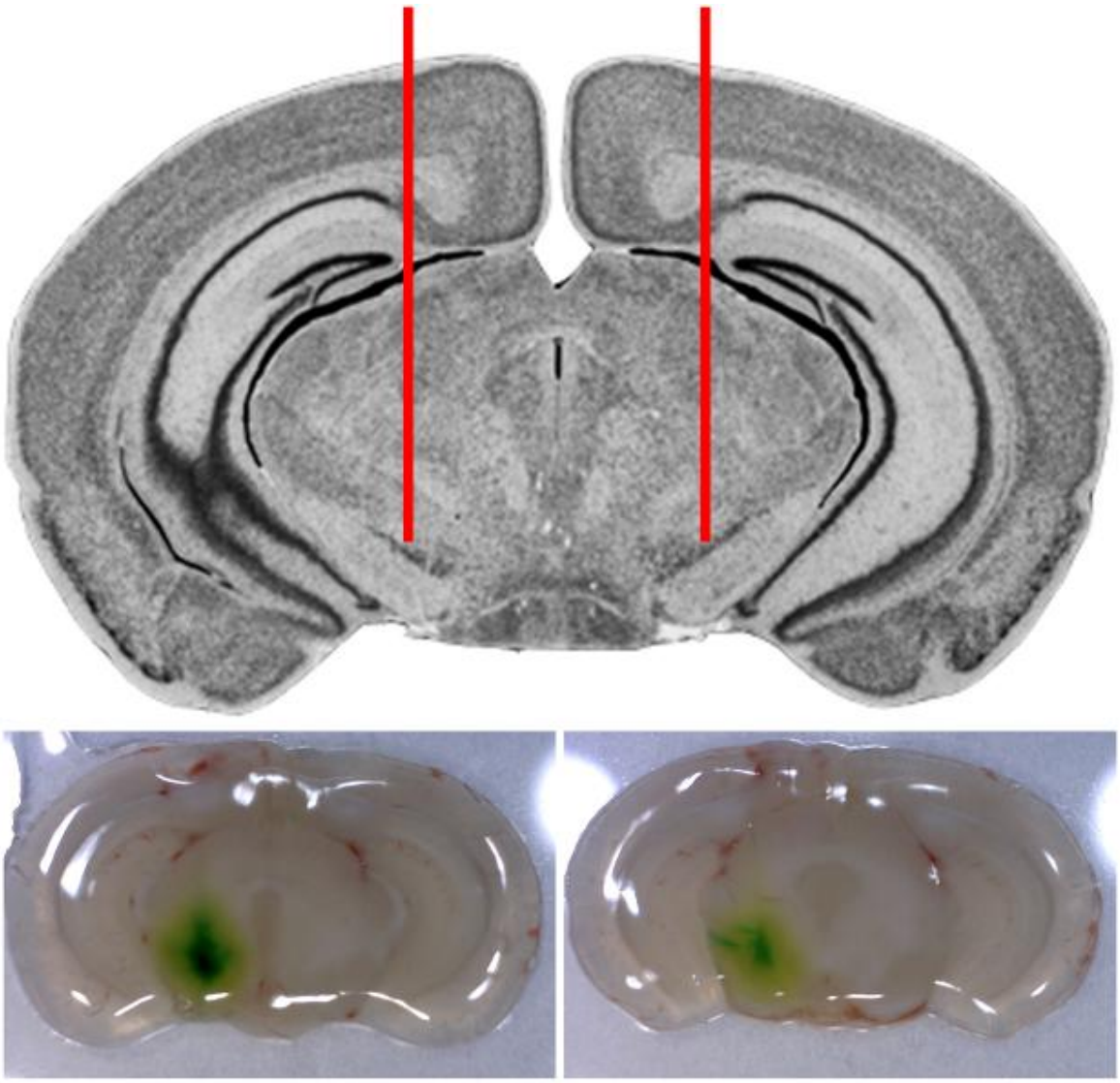

Figure 2.5 Optimization of stereotaxic AAV delivery into the SN. Bilateral injections of 500 nl was made at coordinates -3.3 mm caudal, 1.6 mm and -1.6 mm lateral relative to Bregma, and -4.6 mm ventral to the surface of the skull. (Top Panel) Needle positions are depicted as red lines on the coronal section above. (Bottom Panel) To optimize coordinates, green dye was injected unilaterally, the brain frozen, sectioned, and imaged. Coordinates were readjusted until green dye was delivered to the correct location. Two examples of sections with green dye in the correct location are shown.

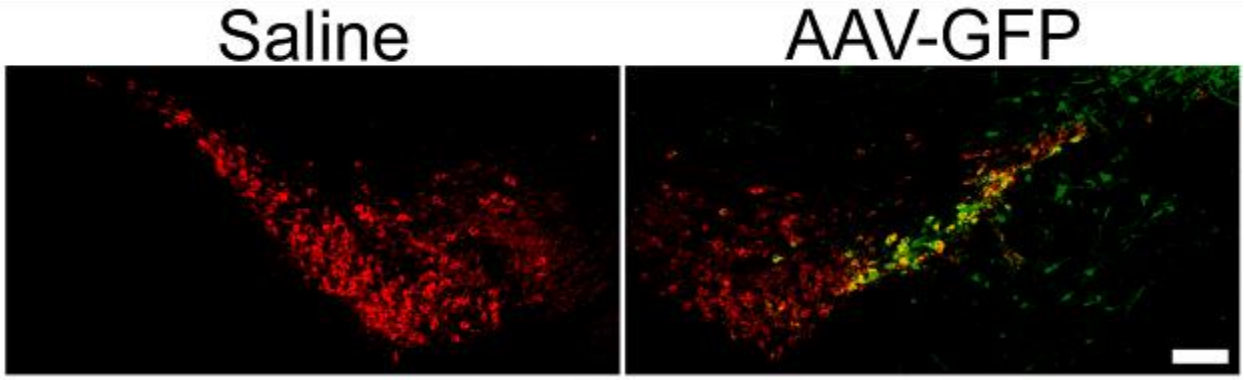

Figure 2.6 Representative images showing localization and spread of the AAV-GFP viral vector as compared to a saline sham control. DA neurons (TH-IR neurons, red) from a single brain are shown overlapping (yellow) with infected cells (green) localized to the SN, and not spreading into the ventral tegmental area. Scale bar is 100 μm.

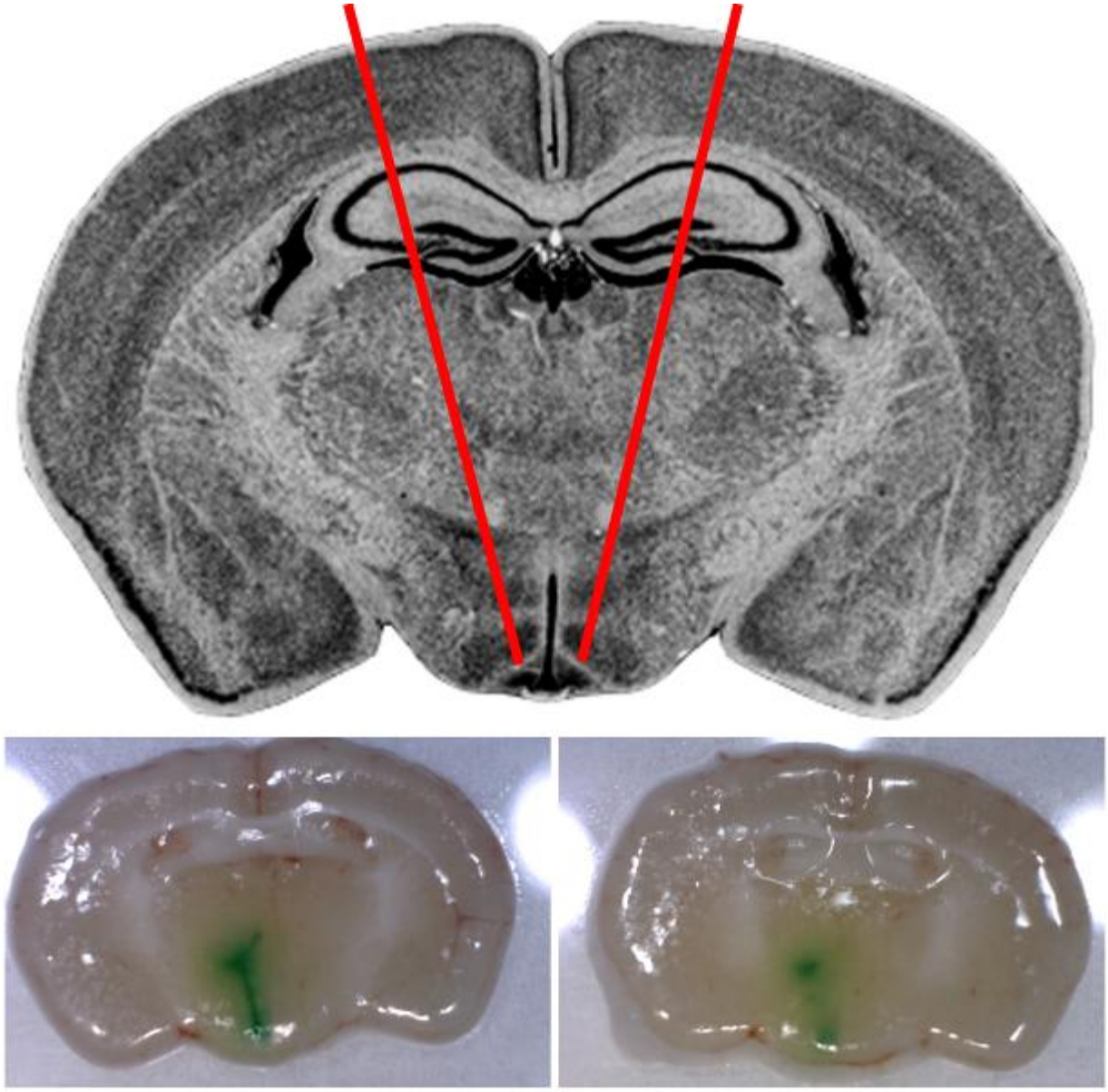

Figure 2.7 Optimization of AAV delivery to the ARC. Bilateral ARC injections of 250 nl were performed at a 10° angle at 2.4 mm caudal, 1.3 mm and -1.3 mm lateral relative to Bregma, and 6.3 mm ventral to the surface of the skull. (Top Panel) Needle positions are depicted as red lines on the coronal section above. (Bottom Panel) To optimize coordinates, green dye was injected unilaterally, the brain frozen, sectioned, and imaged. Coordinates were readjusted until green dye was delivered to the correct location. Two examples of sections with green dye in the correct location are shown.

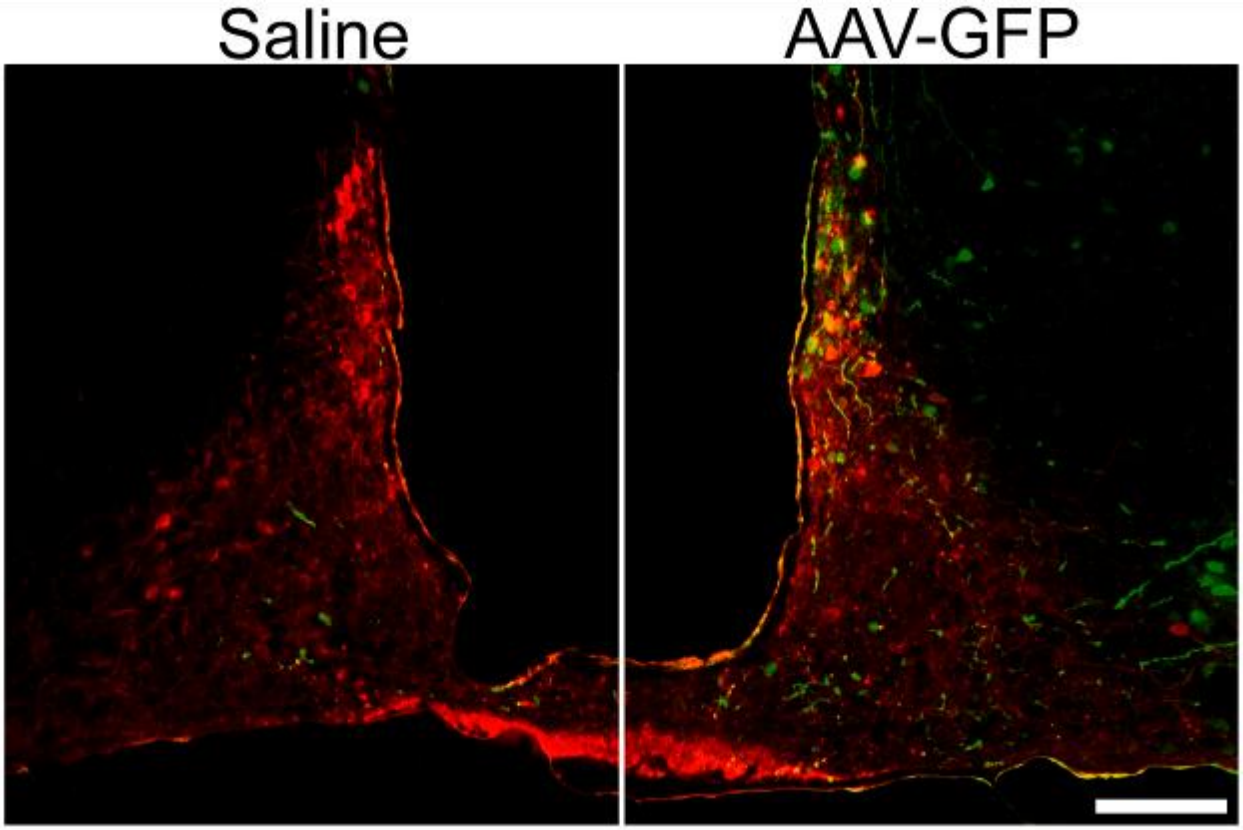

Figure 2.8 Representative images showing localization and spread of the AAV-GFP viral vector as compared to a saline sham control. DA neurons (TH-IR neurons, red) from a single brain are shown overlapping (yellow) with infected cells (green) Images are from the same brain section, with some virus crossing over to the saline side. Scale bar is 100 μm.

Cell Culture

MN9D cells (Choi et al., 1992) were cultured on poly-D-lysine (50 µg/ml) coated plates in DMEM media (Sigma D5648) supplemented with 0.37% sodium bicarbonate (Sigma S5761) 50 U/ml Penicillin/Streptomycin (Gibco 15070-063) and 10% Fetal Clone 3 (Hyclone SH30109.03). MN9D cells were differentiated through the addition of 1mM *n*-butyrate added to the media for 5-7 days (media and *n*-butyrate changed on day 3 and 5). Cells were treated with either MPP^+ (200 µM), tunicamycin (2 µg/ml), or PMA (50 µM) which were added to the media.

Cell Harvesting and Processing

Media was removed and PBS (pH 7.4) was used to gently wash the cells. Fresh PBS was added, a cell scraper was used to detach the cells and the cells suspended in 1 ml of PBS. Cells in PBS were collected in a microcentrifuge tube, an aliquot of 200 µl was taken for neurochemical analyses, a small aliquot of cells (20 µl) was taken to perform a cell viability assay, and the remaining 780 µl used for Western blots. For neurochemistry and Western blot samples, cells were pelleted by centrifugation (10 min at 10,000g), supernatant (PBS) was removed and replaced with either 100 µl RIPA buffer or 50 µl of tissue buffer. Cells were then processed the same as tissue, described above.

Cell Viability Assay

The aliquot of the cell suspension were taken from the 0 and 24 h (MPP^+, tunicamycin, and PMA) groups. Trypan blue (20 µl) was added to each aliquot and gently mixed. Aliquots were pipetted onto a hemocytometer and examined using a microscope with a 10X phase-contrast objective. White and blue cells in four quadrants of the hemocytometer were counted for each sample. White cells that did not absorb the trypan blue were counted as live cells, whereas blue cells that absorbed the dye were counted as dead cells. The number of white (living) cells was divided by the total of both the white and blue (total) cells for each sample.

DCF-DA Assay

Brains were removed, ME dissected, frozen and sectioned as described above. Two 500 µm sections containing the ARC, one 500 µm section containing the SN, and two 500 µm sections containing the ST (the first section for 2', 7'-dichlorofluorescin diacetate (DCF-DA) assay and second section taken for neurochemistry) were collected on glass slides and regions dissected as previously described. These brain regions were transferred immediately into PBS (pH 7.4) and kept at -80 °C until the DCF-DA assay. On the day of the DCF-DA assay, samples were briefly centrifuged (2,000g for 30 s), PBS removed and replaced with 400 µl of 10 µM DCF-DA. Samples were incubated for 1 h at 37 °C, DCF-DA removed and replaced with 350 µl

of lysis buffer (0.1% SDS in tris-HCl; pH 7.5). Samples were sonicated until the tissue punch was completely broken up. Samples were centrifuged at 6,000 g at 4 °C for 20 min. and the supernatant plated in a black well plate. Samples were plated in quadruplicate randomly in a 384 well plate. Relative fluorescent units at an excitation of 485 nm and emission of 520 nm were collected for each well.

Statistical Analysis

One-way analysis of variance (ANOVA) tests were used to detect differences between three or more groups, and two-sample t-tests or paired t-tests were used to detect differences between two groups. Sample sizes had a power greater than or equal to 0.80. A p value less than or equal to 0.05 was considered a significant difference. In experiments where an ANOVA was used and a significant difference was found, post hoc Tukey tests were used for comparisons between groups. Investigators conducting endpoint data collection were blinded to treatment group assignment.

Chapter 3: Examination of Potential Regulators of Parkin

Introduction

The differential regulation of parkin between brain regions in response to MPTP is likely due to transcriptional regulation of the *Park2* gene. The *Park2* gene is controlled by a bi-directional promoter, which also regulates expression of the parkin co-regulated gene (*Pacrg)* gene (Asakawa et al., 2001; West et al., 2004) (**Figure 3.1**). *Park2* and *Pacrg* are arranged head to head with approximately 200 bp between transcriptional start sites, 204 bp in humans and 203 bp in mice (Asakawa et al., 2001; West et al., 2003) (**Figure 3.2**). Hypermethylation of the region between the *Park2* and *Pacrg* transcriptional start sites causes a decrease in the expression of both parkin and PACRG in tumor cell lines, further supporting the importance of the bi-directional promoter for both genes (Agirre et al., 2006). Though hypermethylation has been shown in tumor cell lines to alter parkin expression, methylation of the *Park2* promoter does not contribute to the development of PD (Cai et al., 2011). In addition, inhibition of DNA methyltransferase has no effect on parkin transcription (Wang et al., 2013). Since parkin is expressed in both the TIDA and NSDA neurons, and there is no evidence to suggest methylation of the promoter has clinical implications, it is unlikely that methylation of the promoter is responsible for the differential expression of parkin, especially the increased expression in the

TIDA neurons following acute neurotoxicant exposure. Alternatively, the differential regulation of parkin could be due to histone modifications and/or the expression of transcription factors within the neurons.

Similar to other bi-directional promoters, the *Park2* promoter in both humans and mice does not have a TATA or CAAT box, and contains multiple CpG islands (Asakawa et al., 2001; Orekhova and Rubtsoz, 2011; UCSC Genome Browser). Previous work on the *Park2* promoter has identified key regions within the promoter sequence important for transcription factor binding. The region 0 to -72 bp upstream of the parkin transcriptional start site is sufficient to drive transcription of parkin, with the region -38 to -72 bp most important for the binding of transcription factors (West et al., 2003). This region contains a putative N-myc binding site, which has been shown to be a transcriptional repressor of parkin (West et al., 2004). The studies performed by West and others were based on a luciferase reporter in a neuroblastoma cell line and did not examine the promoter beyond -151 bp relative to the parkin transcriptional start site. In addition to the 34 bp region identified by West and others, another highly conserved region of the parkin promoter was identified. The region -155 to -178 bp upstream of the transcriptional start site of parkin is conserved among humans, mice, horses, and cattle (Bouman et al., 2011). This region contains a putative CREB/ATF/AP-1 binding site, and some cell culture models have indicated that ATF4 is a transcriptional activator of parkin (Bouman et al., 2011; Sun

et al., 2012). Taken together, this not only shows transcriptional regulation of parkin via transcription factors, but also suggests that the regions -38 to 72 bp and -155 to -178 bp may be crucial to the regulation of parkin. In order to predict which transcription factors may play a role in the differential regulation of parkin between brain regions, data concerning the *Park2* promoter was collected from ENCODE, PATCH, PROMO, and TFSearch.

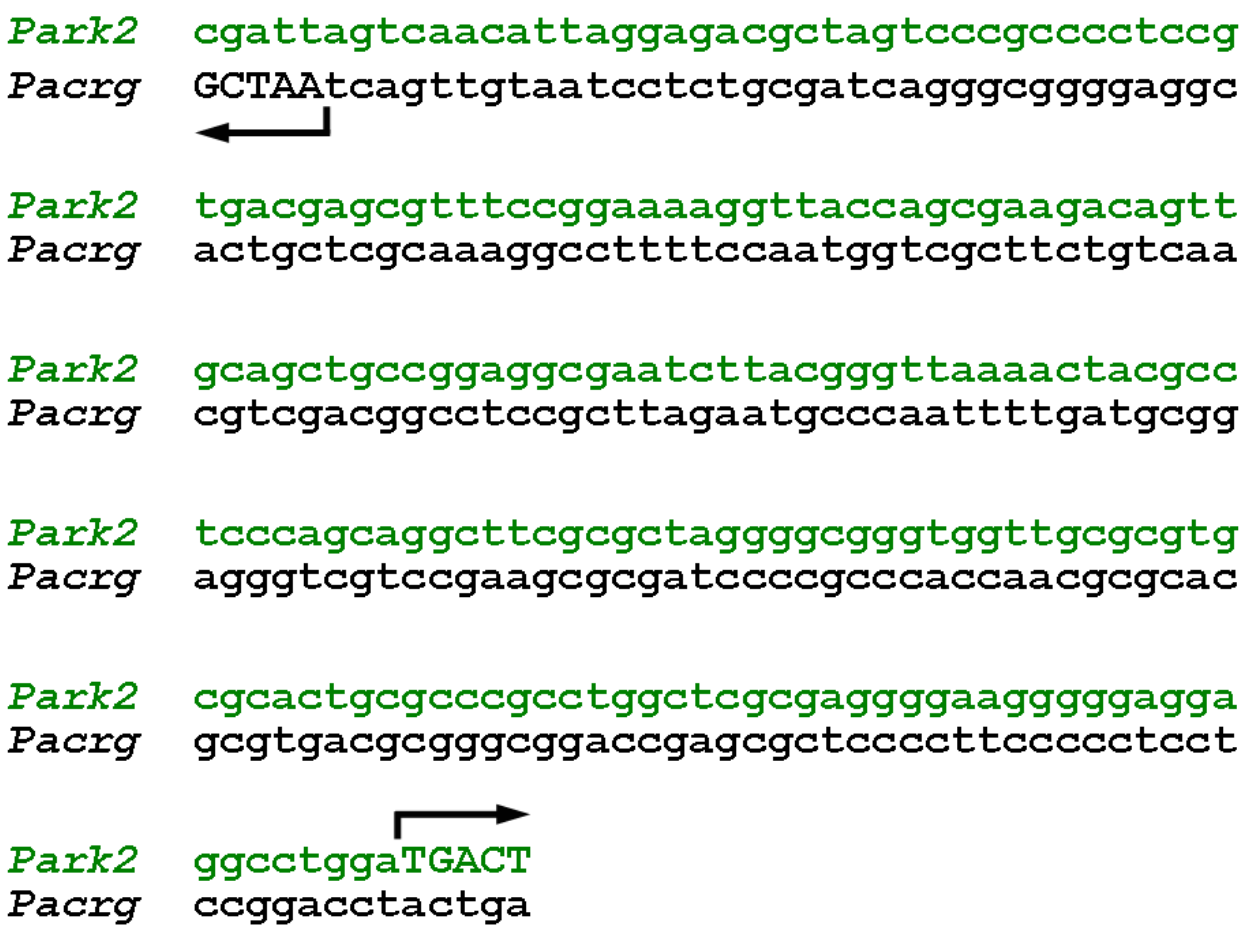

Figure 3.1 Coding strand sequences of the mouse bi-directional promoter of *Park2* (green) and *Pacrg* (black). *Park2* and *Pacrg* are oriented head to head, with both genes transcribed from different strands. Sequences were aligned and show the transcriptional start site and direction of transcription (arrows) as well as the first five transcribed bases of each gene (capital letters). Rows are 40 bases long.

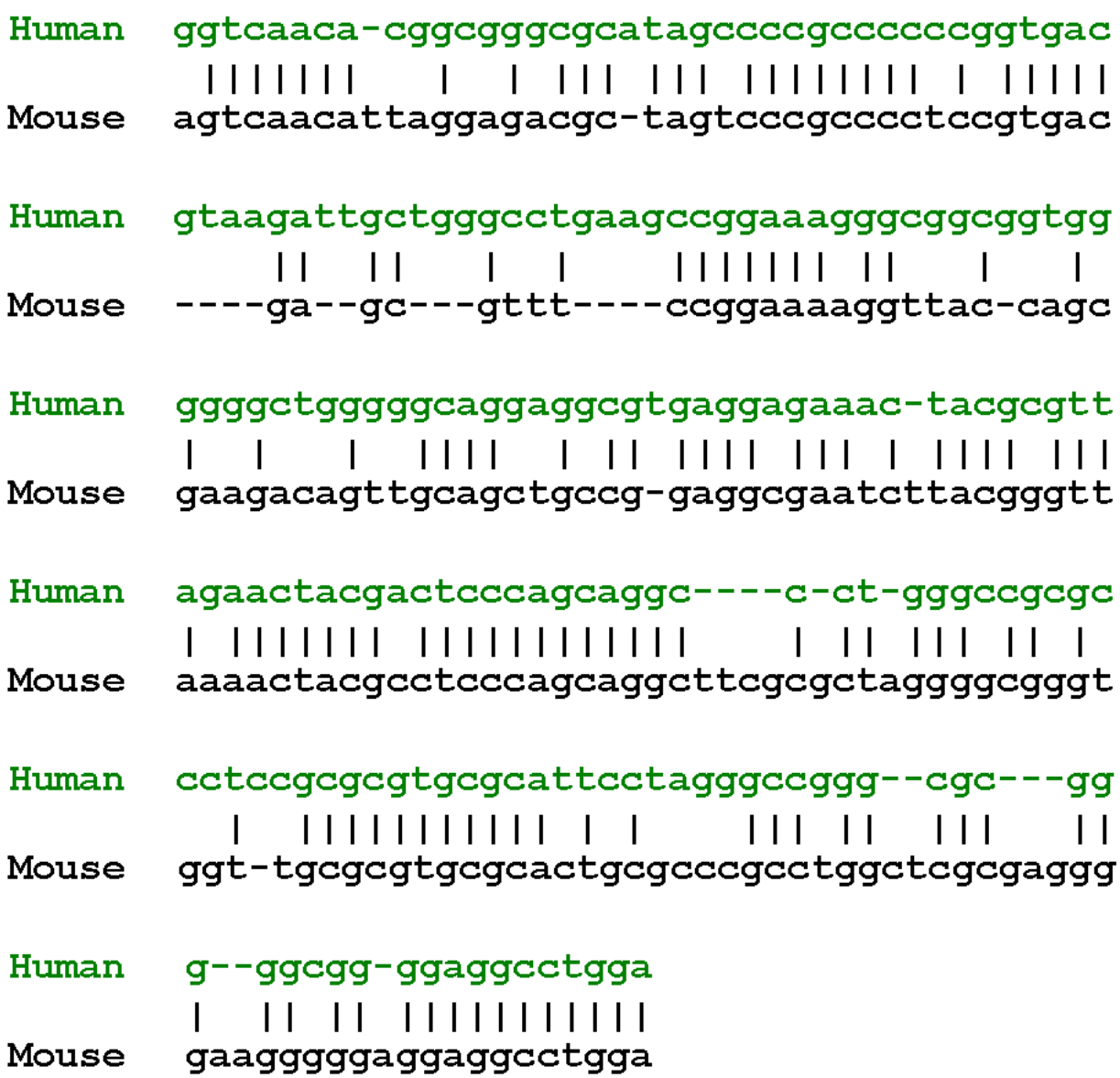

Figure 3.2 Coding strand sequences of the human *Park2* (green) and mouse *Park2* (black) promoters. Sequences were aligned, bases identical in each are indicated by lines, gaps in the sequence when aligned are indicated by dashes. Rows are 40 bases long.

DNA Methylation

Results

Data from ENCODE concerning CpG islands, DNaseI hypersensitivity, ChIP-seq data for histone modifications and transcription factors within the *Park2* promoter was collected from the Penn State University (PSU), California Institute of Technology (Caltech), University of Washington (UW), Ludwig Institute for Cancer Research (LICR), and Stanford/Yale (SYDH) groups and examined (Rosenbloom et al., 2015, 2013; Kent et al., 2002). The region between *Park2* and *Pacrg* is marked as having CpG islands, which begin in the transcribed region of *Pacrg* and continue well into the *Park2* region (**Figure 3.3**). The GC percent shown in ENCODE indicates areas within the promoter that range from high to low GC content, with the promoter overall having high GC content, with a few valleys towards the middle with low GC content (Rosenbloom et al., 2015, 2013; Kent et al., 2002). As a whole, the GC content of the mouse promoter is 64.0% and in humans is 72.5% (Rosenbloom et al., 2015, 2013; Kent et al., 2002). The high GC content and presence of CpG islands suggests methylation of the promoter may play a role in the regulation of parkin.

The possible role of nucleosome positioning and histone modification in the regulation of parkin was examined. DNaseI hypersensitivity from ENCODE collected from the PSU group shows the parkin promoter is highly DNaseI hypersensitive in GATA-1 erythroid progenitor cells (**Figure 3.4**).

From the UW group, the parkin promoter was shown to be highly DNaseI hypersensitive in murine erythroleukemia cells, ES-CJ7 cells, CD19 positive B-cells, mouse cerebrum, cerebellum, and whole brain (8 week and embryonic day 14.5) (Figure 3.5) (Rosenbloom et al., 2015, 2013; Kent et al., 2002). DNaseI cuts naked DNA, where histones interacting with DNA (also known as nucleosomes) protect DNA from DNaseI. Hypersensitivity to DNaseI suggests that nucleosomes are most likely not present in the promoter region.

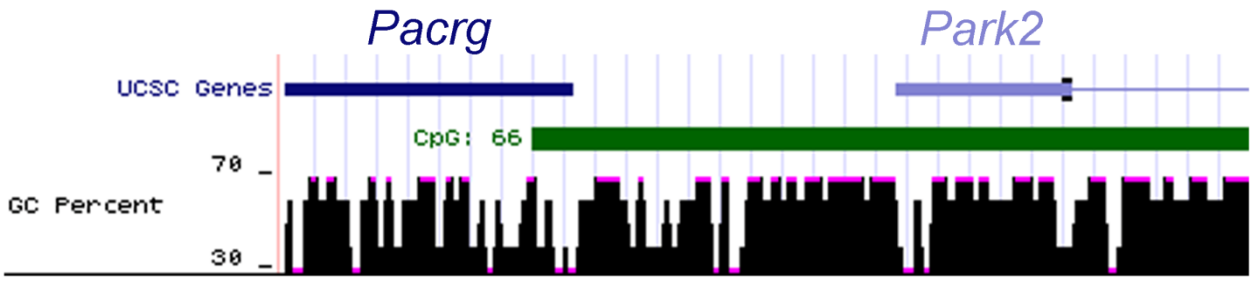

Figure 3.3 GC percentage and CpG islands of the mouse *Park2* promoter. Image is modified from ENCODE data from chromosome 17. The region between *Pacrg* (dark blue) and the *Park2* (light blue) genes is considered the promoter region. Location of CpG island rich regions within the sequence are denoted by the green bar. Percentage of guanine and cytosine in the sequence in clusters of five nucleotides are shown in black (Rosenbloom et al., 2015, 2013; Kent et al., 2002).

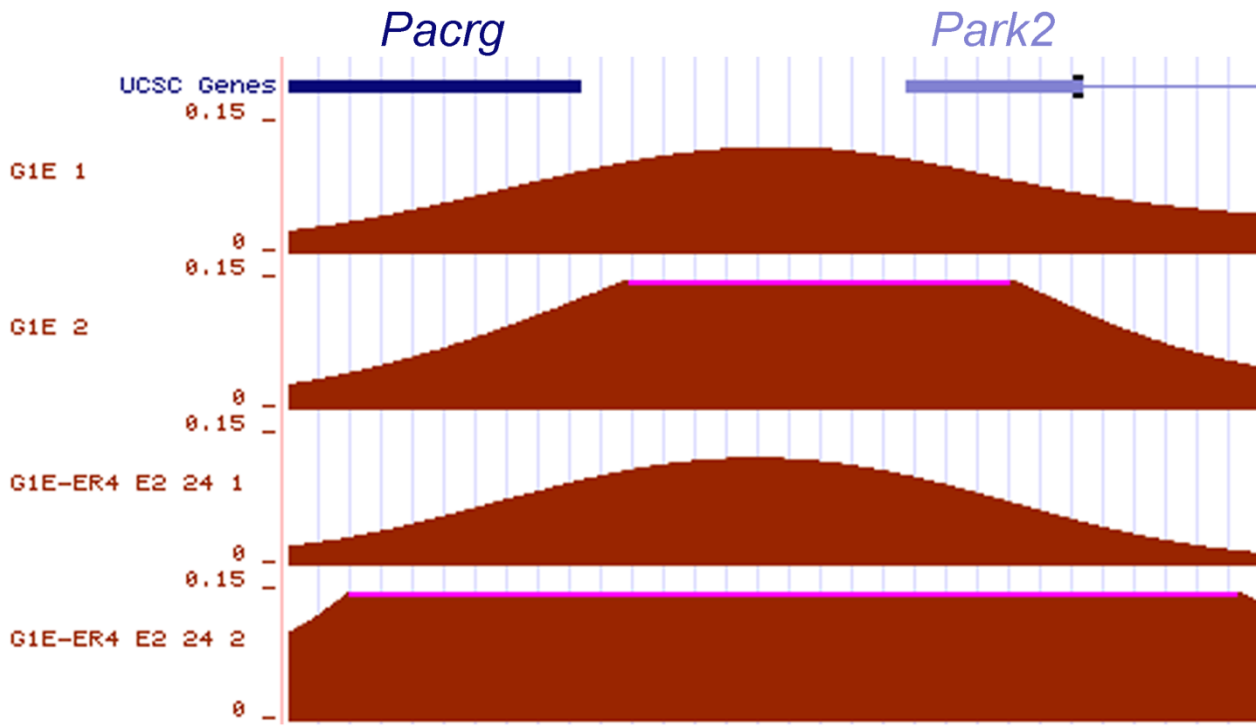

Figure 3.4 DNaseI hypersensitivity from the PSU group. Image is modified from ENCODE data from chromosome 17. The region between *Pacrg* (dark blue) and the *Park2* (light blue) genes is considered the promoter region. Location DNaseI hypersensitive regions within the sequence are shown in GATA-1 erythroid progenitor cells (Rosenbloom et al., 2015, 2013; Kent et al., 2002).

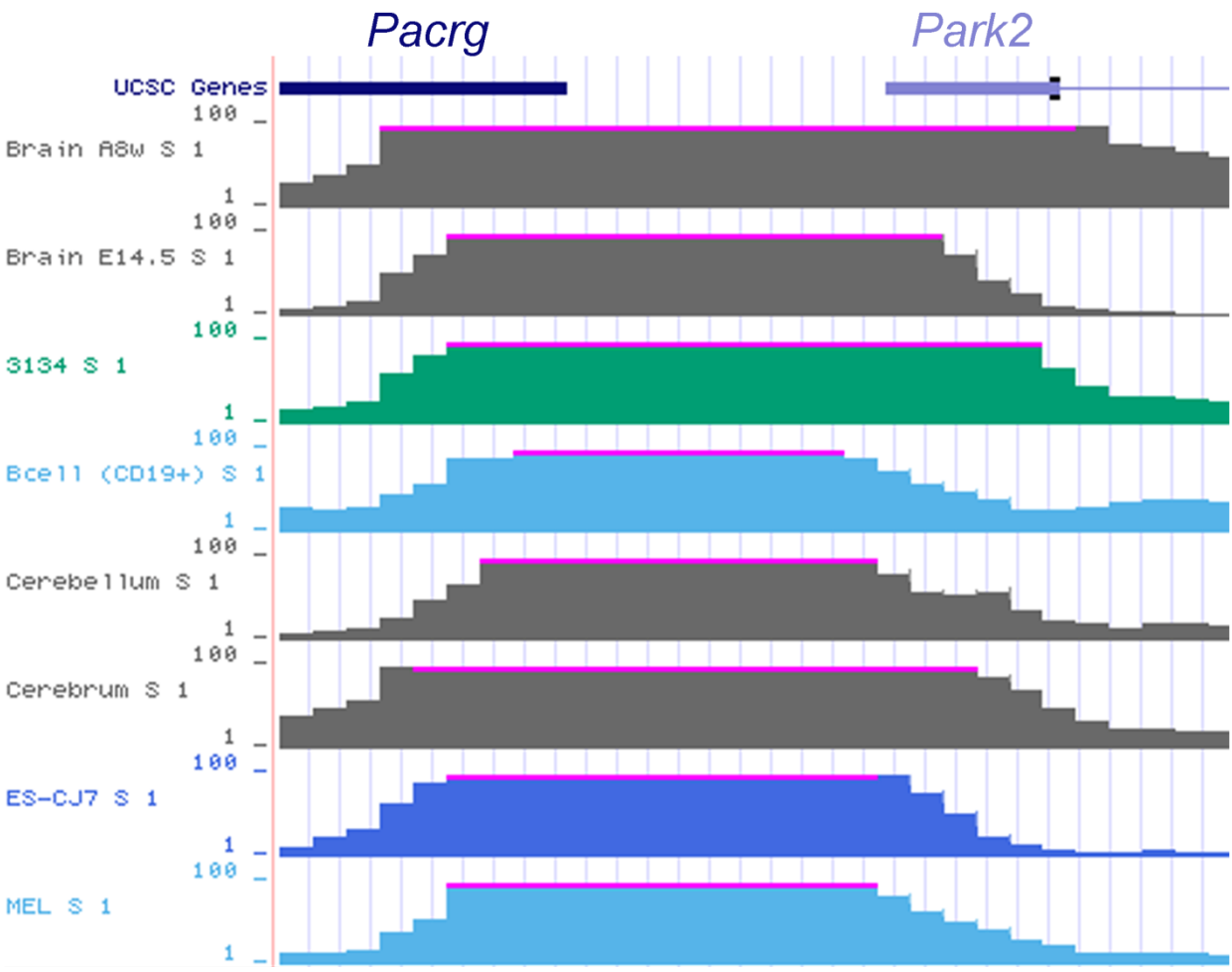

Figure 3.5 DNaseI hypersensitivity from the UW group. Image is modified from ENCODE data from chromosome 17. The region between *Pacrg* (dark blue) and the *Park2* (light blue) genes is considered the promoter region. Location DNaseI hypersensitive regions within the sequence are shown in whole brain, cerebrum, CD19 positive B-cells, 3131 cells, ES-CJ7 cells, and MEL cells (Rosenbloom et al., 2015, 2013; Kent et al., 2002).

Discussion

The bidirectional nature of the promoter, which controls both *Park2* and *Pacrg* suggests the promoter is key to the regulation of parkin expression. After exposure to MPTP, mRNA for both parkin and PACRG increase only in the ARC, further supporting the hypothesis that the common promoter regulates expression of both genes (Behrouz dissertation). Through the examination of the promoter, especially the potential epigenetic factors involved, what regulates parkin may be deduced. Along with transcription factors, the promoter has the potential to be regulated by methylation of the DNA, positioning and modification of the histones.

In terms of DNA methylation, the GC content of the promoter becomes important. Traditionally, the cytosines within DNA can be modified with the addition of a methyl group to the fifth carbon. As the guanine on one strand will pair with a cytosine on the other strand, the guanine is also representative of a potentially methylatable cytosine. Within the mouse promoter the GC content is 64.0% and in the human promoter it is 72.5%. The relatively high GC content of the promoter suggests the presence of CpG sites that have the potential to be methylated. Within the mouse promoter, ENCODE shows the entire promoter located within a CpG island that continues into the *Park2* gene (Rosenbloom et al., 2015, 2013; Kent et al., 2002). This suggests that DNA methylation may play a inhibitory role in the

regulation of parkin since DNA methylation is usually associated with low expression or silencing of a gene,.

Assuming this is true for parkin, a decrease in DNA methylation associated with increased parkin promoter activity would be expected in TIDA neurons, and maintained basal levels or possibly an increase would be expected in NSDA neurons. Specifically in the SN, MPTP has been show to alter the methylation of a few genes in a genome-wide study (Hu et al., 2015). In their study the found decreased methylation at 39 loci and increased methylation at 5 loci, including the start of the PD related gene *Uchl1* (Hu et al., 2015). Among all their hits, there was no mention of change in methylation of *Park2*, or any other PD related genes. This suggests another mechanism is probably responsible for the differential expression of parkin after MPTP. The basal methylation status of the promoter would also be predicted to be low in both TIDA and NSDA neurons, since parkin is normally expressed in both the ARC and SN.

Histones and Histone Modifications

Results

Concerning nucleosomes, modification of the histones can also have a role in gene regulation. Overall, ChIP-seq data did not show histone modifications present directly in the promoter, but rather at the beginning of the *Pacrg* and *Park2* genes. The Caltech group looked at H3K4me2 and

H3K4me3 in C2 cells. H3K4me2 is found near the beginning of the *Pacrg* gene, and H3K4me3 is found near the start of the *Park2* gene (**Figure 3.6**). From the SYDH group, H3K4me and H3K4me3 markings were examined in MEL cells, and only H3K4me3 appeared to be present at both the starts of the *Park2* and *Pacrg* genes, but not in the center of the promoter (**Figure 3.7**). The LICR group looked at H3K4me, H3K4me3, H3K27a, and H3K27me3 in the cerebellum; H3K4me (8 week and embryonic day 14.5), H3K4me3 (8 week and embryonic day 14.5), H3K9a (8 week), H3K27a (8 week and embryonic day 14.5), H3K27me3 (8 week), H3K36me3 (8 week), and H3K79me2 (8 week) in the liver; H3K4me (8 week and embryonic day 14.5), H3K4me3 (8 week and embryonic day 14.5), H3K9a (8 week), H3K27a (8 week and embryonic day 14.5), H3K27me3 (8 week), H3K36me3 (8 week), and H3K79me2 (8 week) in the heart; and H3K4me, H3K4me3, H3K9a, H3K27a, H3K27me3, H3K36me3, and H3K79me2 in MEL cells (**Figures 3.8-11**) (Rosenbloom et al., 2015, 2013; Kent et al., 2002). All of the histone modification markers were located more towards the *Park2* gene and less within the promoter. The histone marks present were H3K4me3 and H3K27a in the cerebellum; H3K4me3, H3K9a and H3K27a in the heart (both 8 weeks and embryonic day 14.5); H3K4me3, H3K9a and H3K27a in the liver (both 8 weeks and embryonic day 14.5); and H3K4me3 and H3K9a in MEL cells (**Figures 3.8-11**). The PSU group looked at H3K4me3, H3K9me3, H3K27me3, and H3K36me3 in CH12 cells (**Figure 3.12**), H3K4me3,

H3K9me3, H3K27me3, and H3K36me3 in erythroblasts (**Figure 3.13**), and H3K4me, H3K4me3, H3K9me3, H3K27me3, and H3K36me3 in megakaryocytes (**Figure 3.14**). In all three cell types, only H3K4me3 appeared to be present, and more towards the *Park2* gene than the promoter (**Figures 3.12-14**) (Rosenbloom et al., 2015, 2013; Kent et al., 2002).

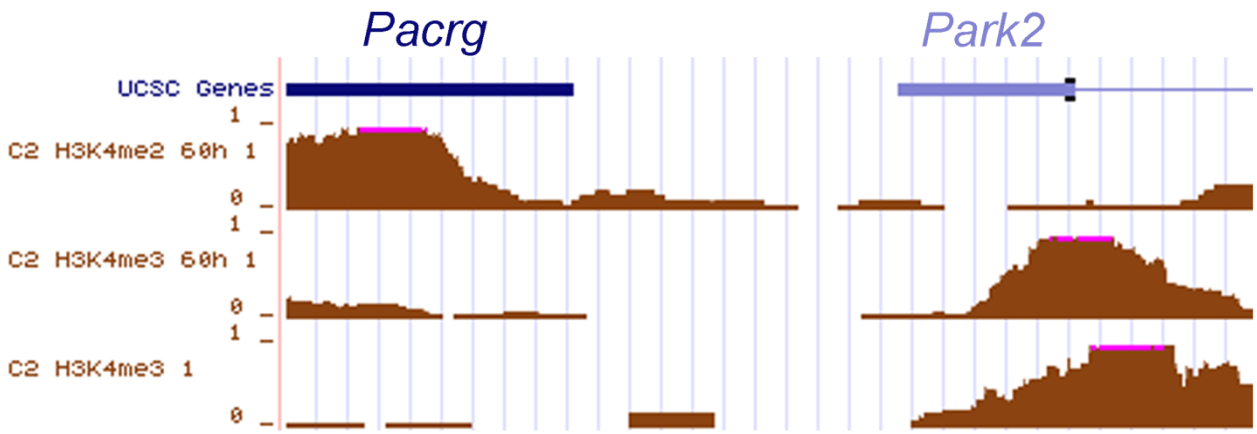

Figure 3.6 Histone modification marks from the Caltech group. Image is modified from ENCODE data from chromosome 17. The region between *Pacrg* (dark blue) and the *Park2* (light blue) genes is considered the promoter region. Location of histone marks within the region are shown in C2 cells (Rosenbloom et al., 2015, 2013; Kent et al., 2002).

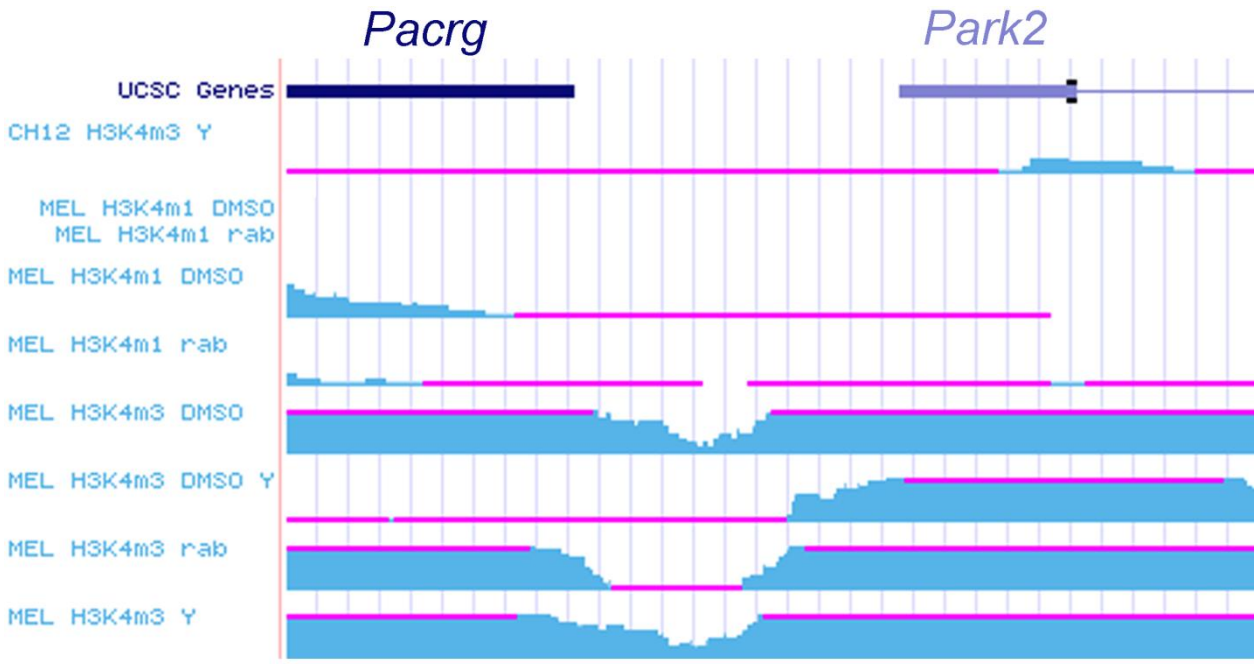

Figure 3.7 Histone modification marks from the SYDH group. Image is modified from ENCODE data from chromosome 17. The region between *Pacrg* (dark blue) and the *Park2* (light blue) genes is considered the promoter region. Location of histone marks within the region are shown in CH12 and MEL cells (Rosenbloom et al., 2015, 2013; Kent et al., 2002).

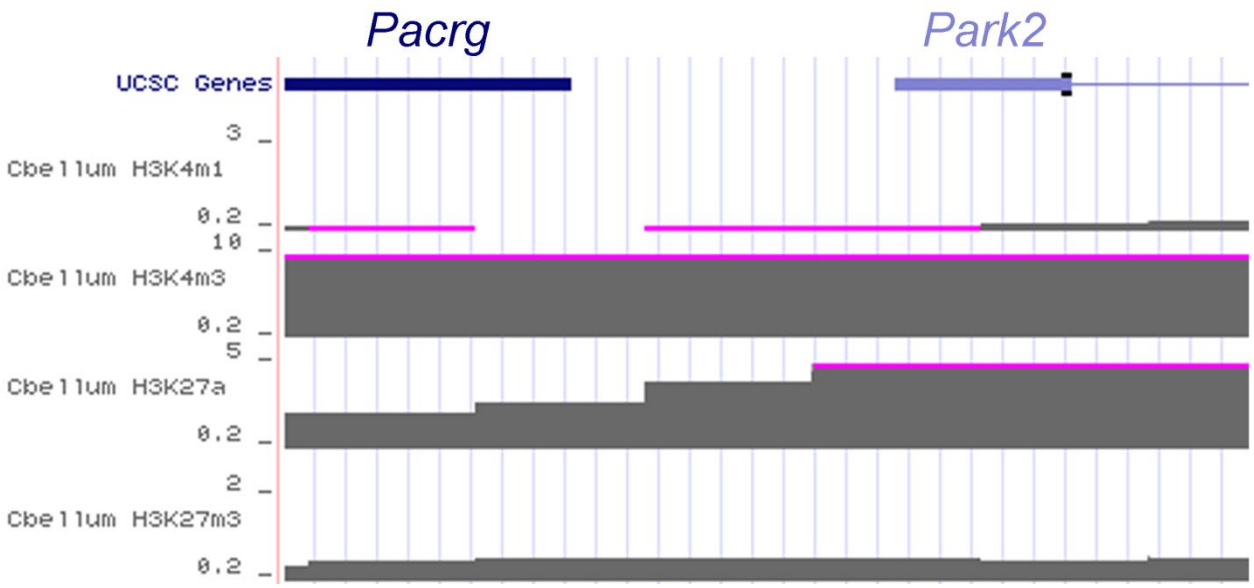

Figure 3.8 Histone modification marks from the LICR group in the cerebellum. Image is modified from ENCODE data from chromosome 17. The region between *Pacrg* (dark blue) and the *Park2* (light blue) genes is considered the promoter region. Location of histone marks within the region are shown in cerebellum tissue (Rosenbloom et al., 2015, 2013; Kent et al., 2002).

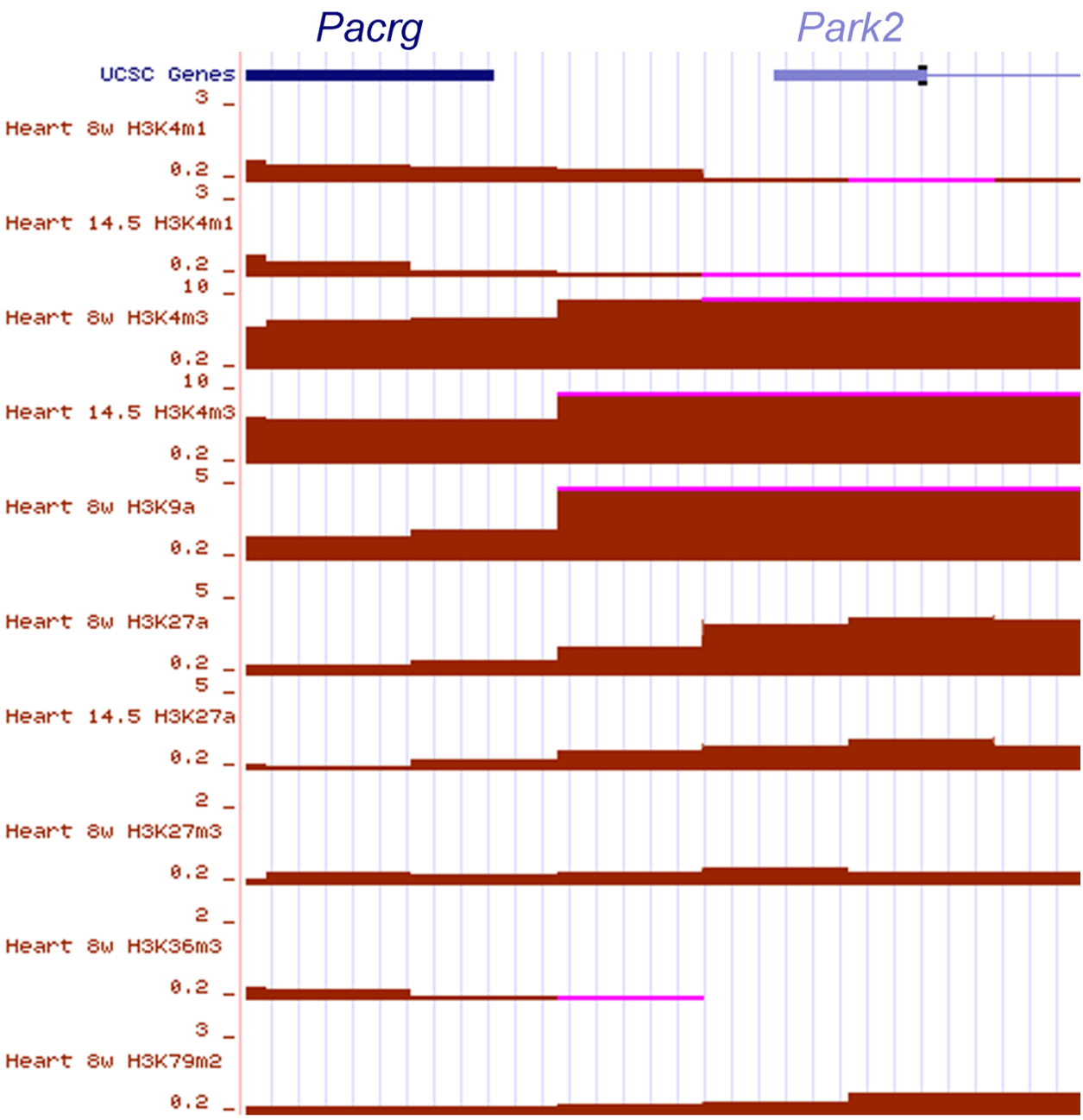

Figure 3.9 Histone modification marks from the LICR group in the heart. Image is modified from ENCODE data from chromosome 17. The region between *Pacrg* (dark blue) and the *Park2* (light blue) genes is considered the promoter region. Location of histone marks within the region are shown in heart tissue (Rosenbloom et al., 2015, 2013; Kent et al., 2002).

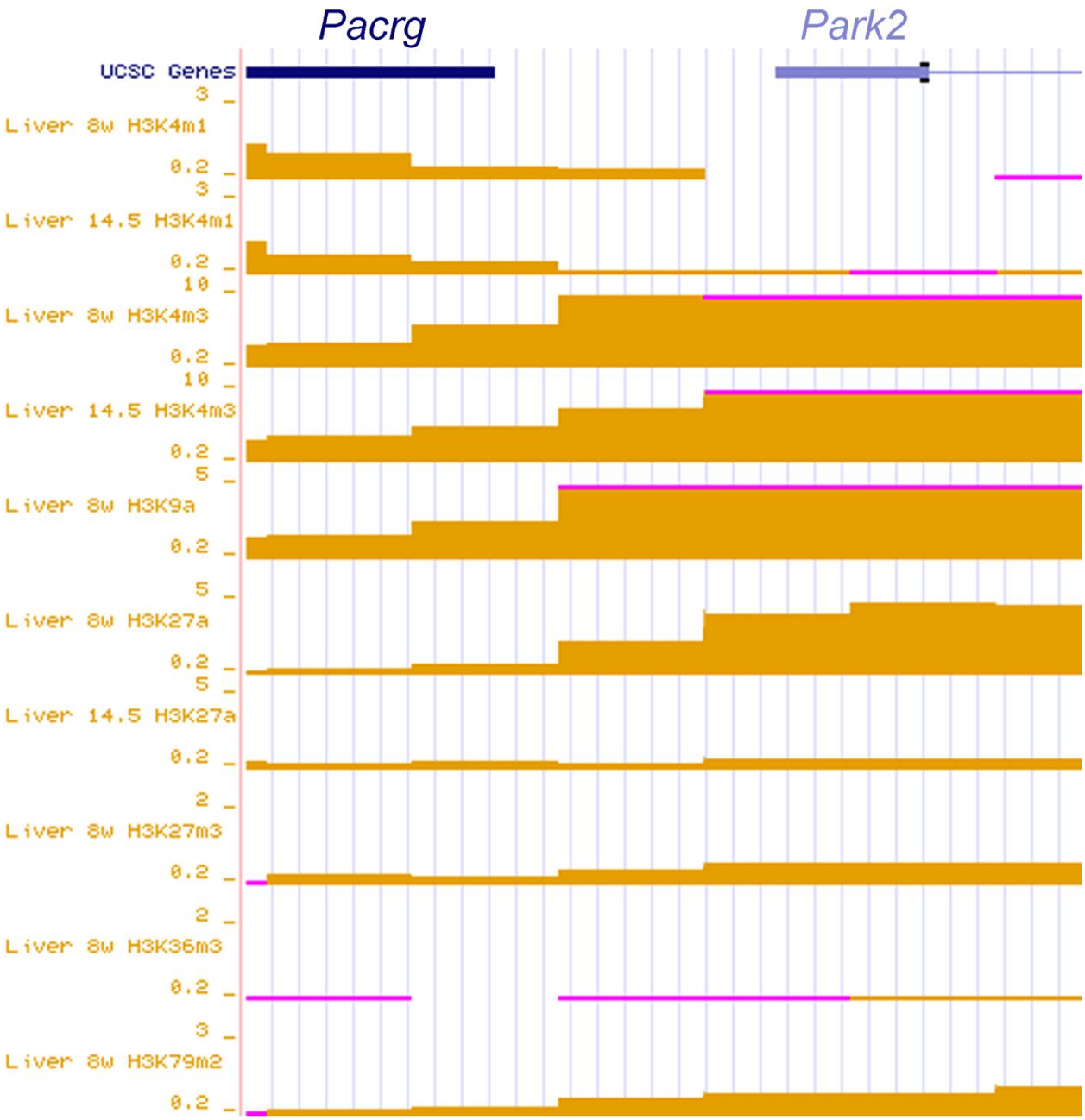

Figure 3.10 Histone modification marks from the LICR group in the liver. Image is modified from ENCODE data from chromosome 17. The region between *Pacrg* (dark blue) and the *Park2* (light blue) genes is considered the promoter region. Location of histone marks within the region are shown in liver tissue (Rosenbloom et al., 2015, 2013; Kent et al., 2002).

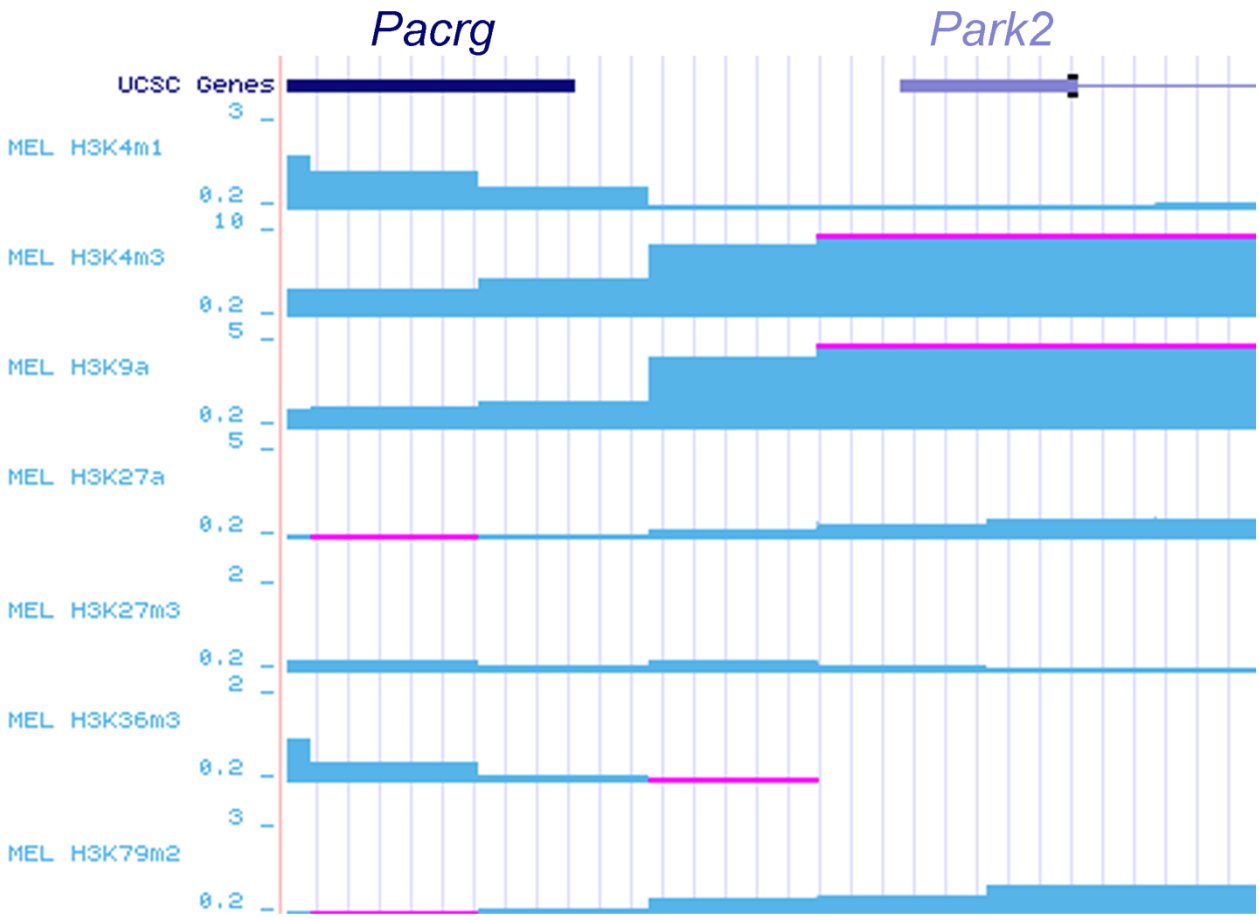

Figure 3.11 Histone modification marks from the LICR group in MEL cells. Image is modified from ENCODE data from chromosome 17. The region between *Pacrg* (dark blue) and the *Park2* (light blue) genes is considered the promoter region. Location of histone marks within the region are shown in MEL cells (Rosenbloom et al., 2015, 2013; Kent et al., 2002).

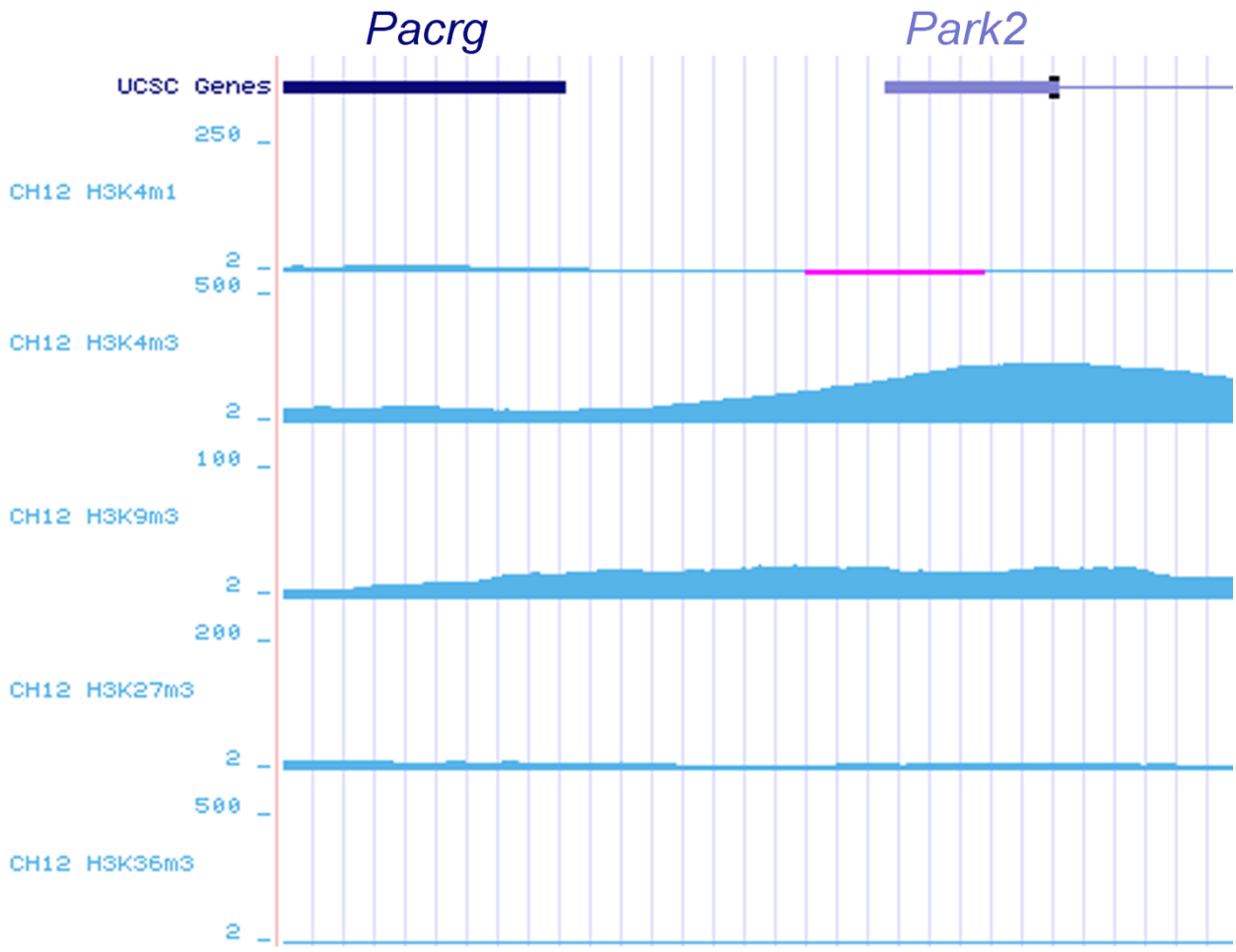

Figure 3.12 Histone modification marks from the PSU group in CH12 cells. Image is modified from ENCODE data from chromosome 17. The region between *Pacrg* (dark blue) and the *Park2* (light blue) genes is considered the promoter region. Location of histone marks within the region are shown in CH12 cells (Rosenbloom et al., 2015, 2013; Kent et al., 2002).

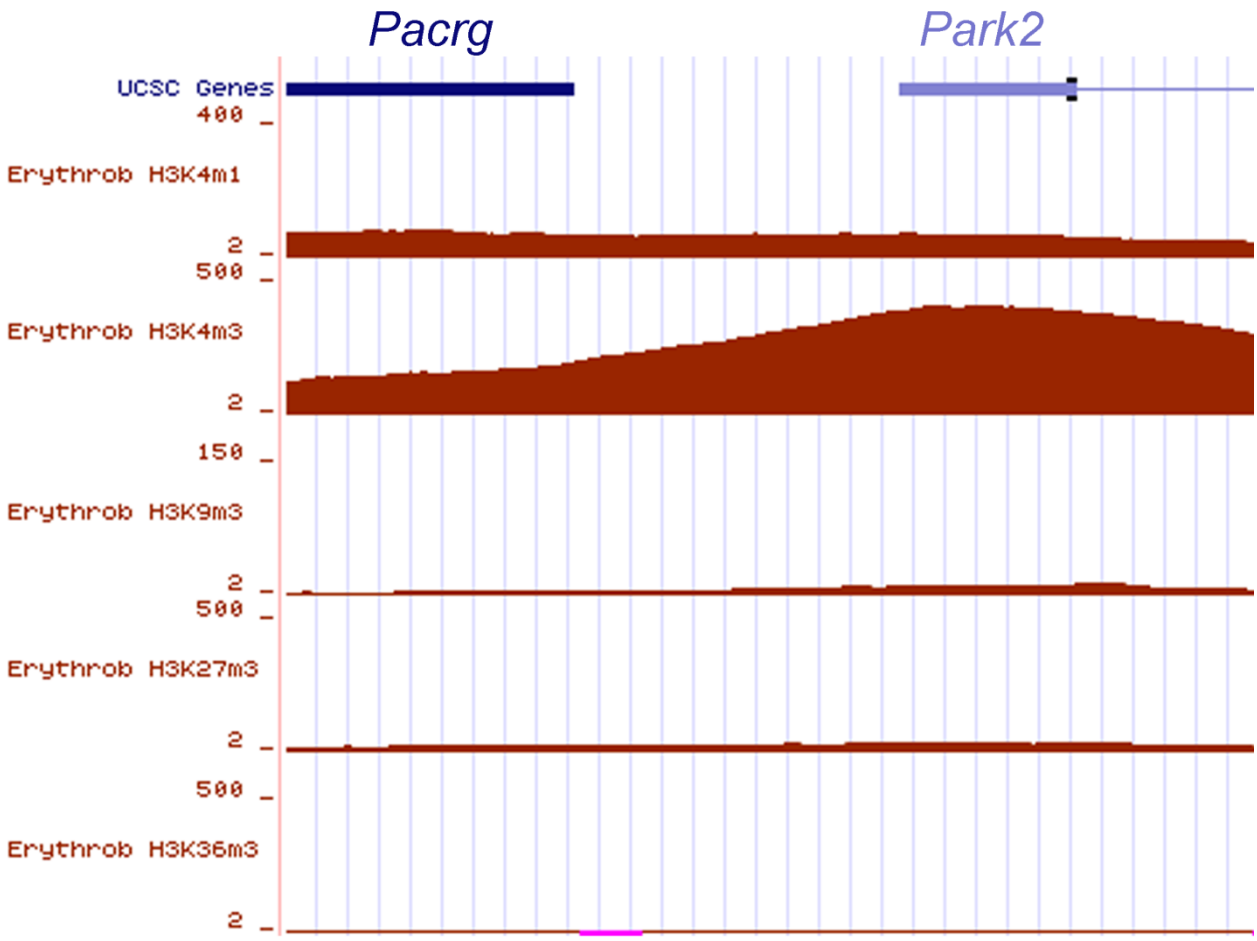

Figure 3.13 Histone modification marks from the PSU group in erythroblasts. Image is modified from ENCODE data from chromosome 17. The region between *Pacrg* (dark blue) and the *Park2* (light blue) genes is considered the promoter region. Location of histone marks within the region are shown in erythroblasts (Rosenbloom et al., 2015, 2013; Kent et al., 2002).

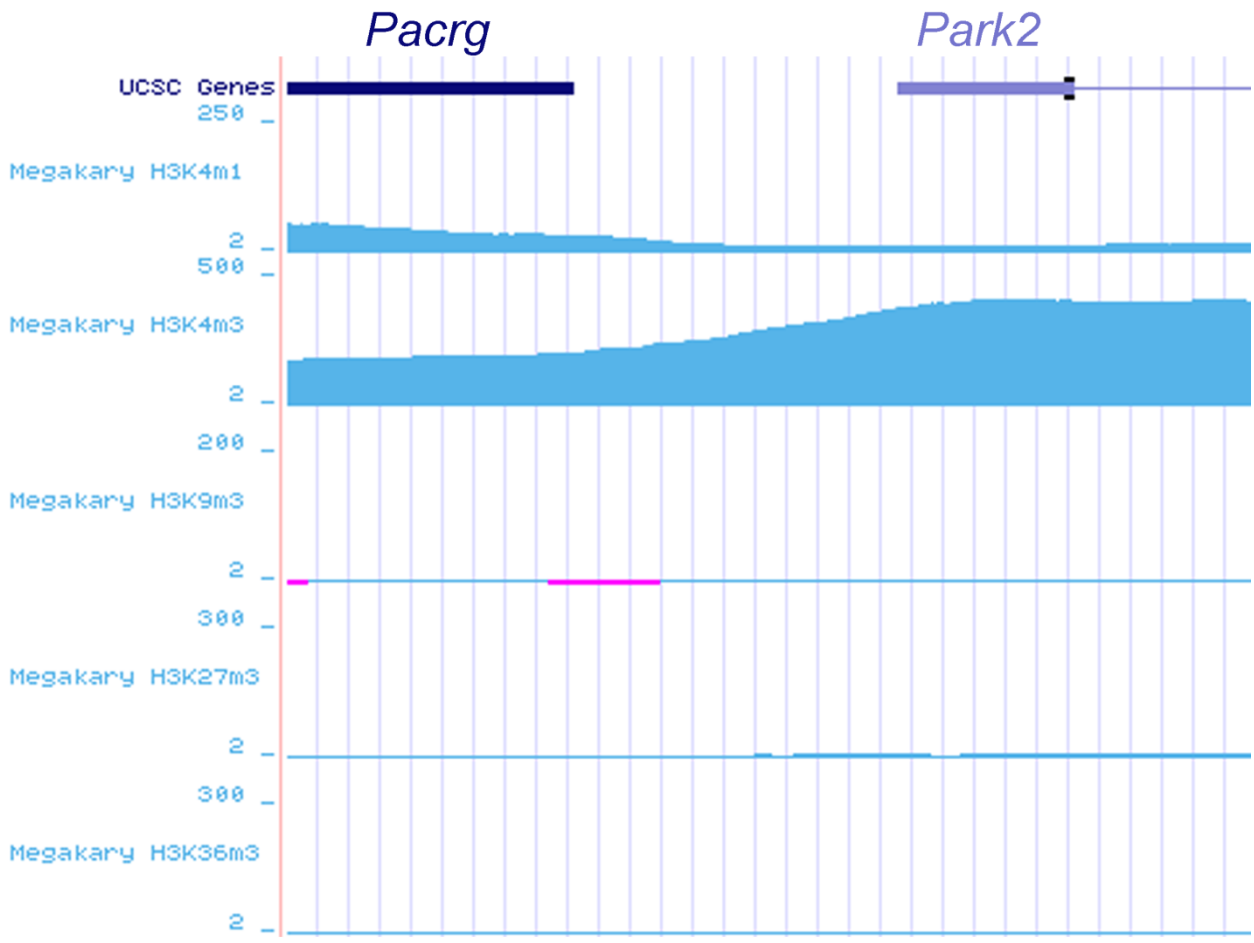

Figure 3.14 Histone modification marks from the PSU group in megakaryocytes. Image is modified from ENCODE data from chromosome 17. The region between *Pacrg* (dark blue) and the *Park2* (light blue) genes is considered the promoter region. Location of histone marks within the region are shown in megakaryocytes (Rosenbloom et al., 2015, 2013; Kent et al., 2002).

Discussion

Similar to DNA methylation, modification and localization of histones could play a role in the regulation of parkin. Data from ENCODE shows the parkin promoter is DNaseI hypersensitive in different cell lines, cerebrum, cerebellum, and whole brain. DNaseI hypersensitivity suggests the absence or presence of few nucleosomes within the promoter, as nucleosomes would be expected to protect the DNA. Without nucleosomes blocking access to the parkin promoter, it should be free to be influenced by transcription factors.

Examining the reported position of nucleosomes directly, ENCODE shows H3K4 tri-methylation and H3K9 acetylation in cell lines, cerebellum, heart and liver (Rosenbloom et al., 2015, 2013; Kent et al., 2002). These histone marks are shown to be present within the promoter and/or the start of *Park2*. Reported histone marks shown to be absent were H3K4 mono and di-methylation, H3K9 tri-methylation, H3K27 acetylation, H3K27 tri-methylation, H3K36 tri-methylation, and H3K79 di-methylation. The presence of H3K4 tri-methylation and H3K9 acetylation associated with *Park2* and its promoter, are both indicative of a promoter of an active or potentially active gene (Karmodiya et al., 2012; Bannister and Kouzarides, 2011; Shahbazian and Grunstein 2007; Martin and Zhang 2005).

Taken together, epigenetic factors may have some influence on the promoter, but probably not a determining factor in the differential regulation after neurotoxicant exposure. Since parkin is normally expressed in both the

ARC and SN, it is unlikely a repressive mechanism such as DNA methylation is being removed to increase parkin expression in the ARC in response to toxicant exposure. The presence of already permissive histone modifications also suggests that there is no hindrance to parkin expression, so an increase in another factor would be expected to cause toxicant-induced differential expression of parkin.

Transcription Factors

Results

UCSC Genome Browser and ENCODE

Examination of the available transcription factor binding data from ENCODE, suggests a few transcription factors that may regulate parkin. From the Caltech group, myogenin and MyoD are shown to interact with the promoter region (**Figure 3.15**). From data from the LICR group, RNA polymerase 2 and CTCF was shown to bind to the promoter in the cerebellum, heart, liver, and MEL cells; and p300 was shown to only bind in tissue from the heart (**Figure 3.16**). From data from the PSU group, GATA-1, Tal1, and FlI1 were not shown to interact with the promoter in erythroblasts, GATA-1 erythroid progenitor cells, or megakaryocytes (**Figure 3.17**). From data from the SYDH group, CTCF, GATA-1, c-Jun, and p300 did not appear to strongly bind in CH12 or MEL cells, where RNA polymerase 2 bound in

both CH12 and MEL cells (**Figure 3.18**) (Rosenbloom et al., 2015, 2013; Kent et al., 2002).

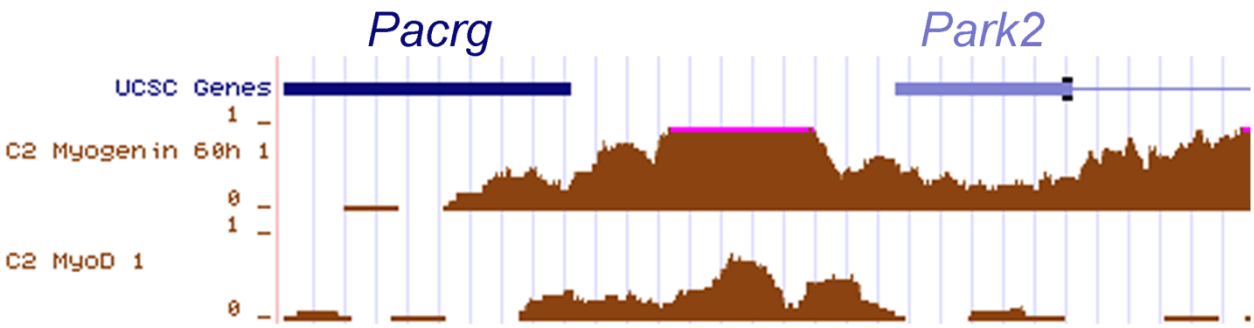

Figure 3.15 Known transcription factor binding via ChIP-seq data from the Caltech group. Image is modified from ENCODE data from chromosome 17. The region between *Pacrg* (dark blue) and the *Park2* (light blue) genes is considered the promoter region. Locations of transcription factor binding within the region are shown for C2 cells (Rosenbloom et al., 2015, 2013; Kent et al., 2002).

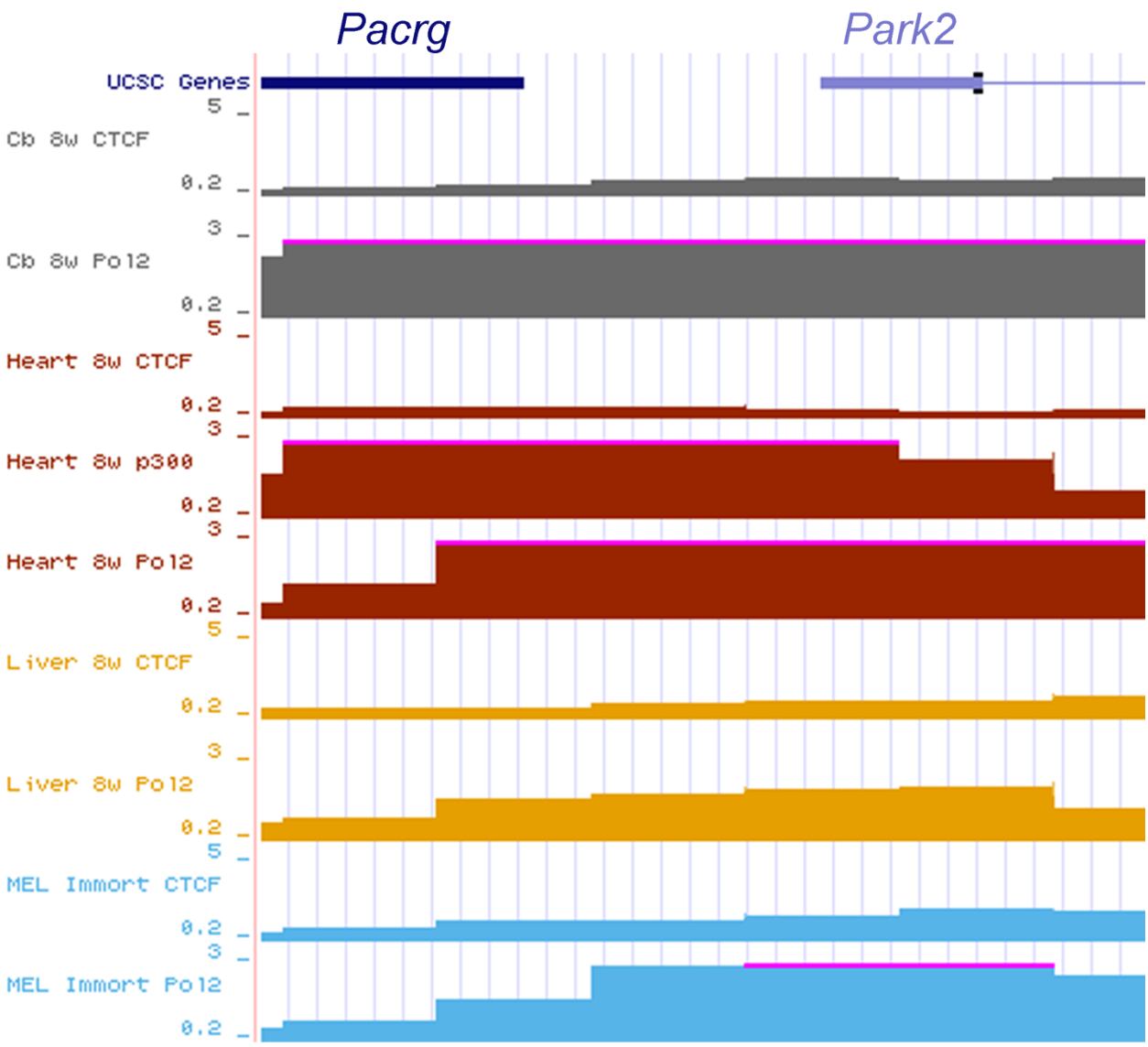

Figure 3.16 Known transcription factor binding via ChIP-seq data from the LICR group. Image is modified from ENCODE data from chromosome 17. The region between *Pacrg* (dark blue) and the *Park2* (light blue) genes is considered the promoter region. Locations of transcription factor binding within the region are shown for MEL cells, cerebellum, heart, and liver tissue (Rosenbloom et al., 2015, 2013; Kent et al., 2002).

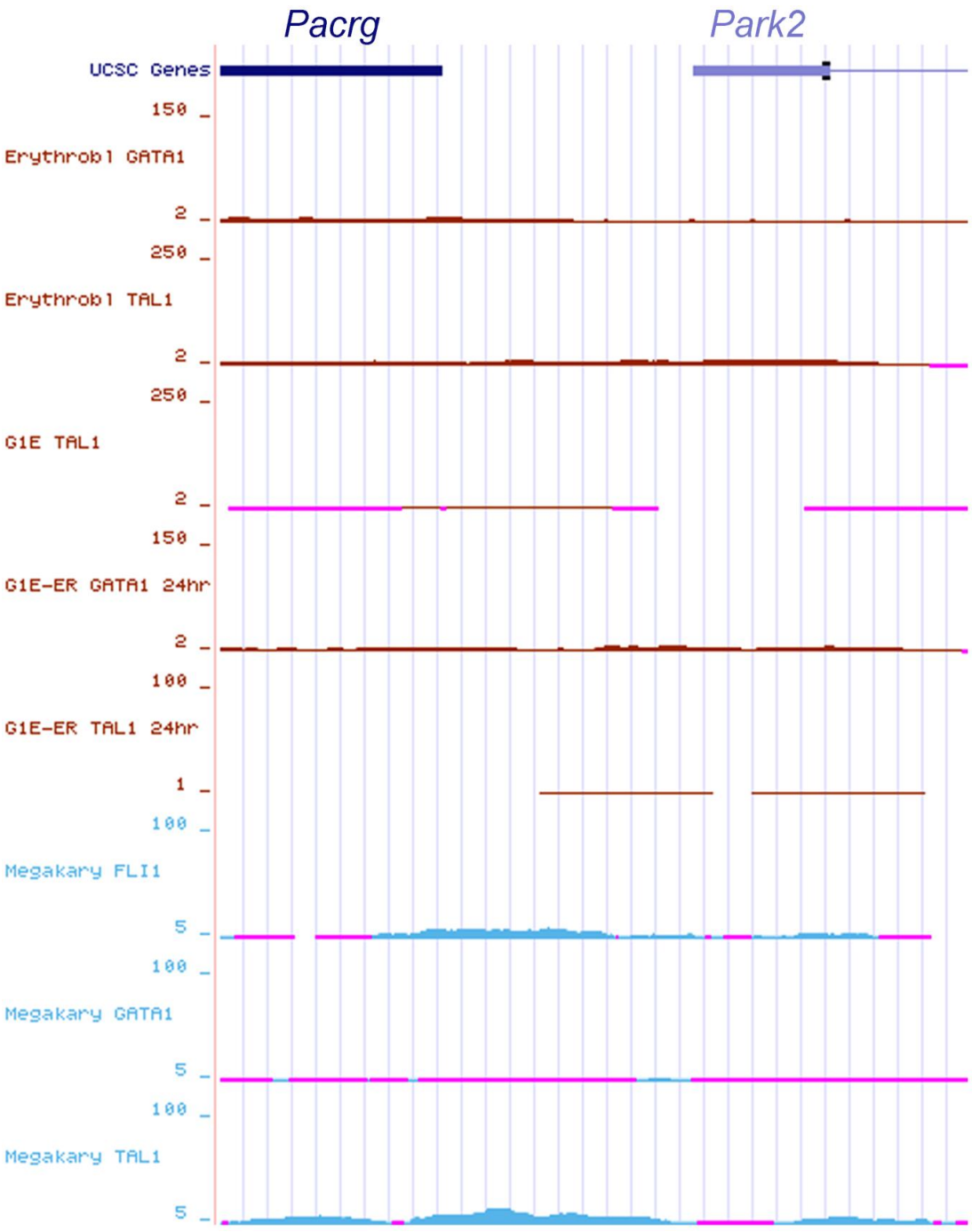

Figure 3.17 Known transcription factor binding via ChIP-seq data from the PSU group. Image is modified from ENCODE data from chromosome 17. The region between *Pacrg* (dark blue) and the *Park2* (light blue) genes is considered the promoter region. Locations of transcription factor binding within the region are shown for erythroblasts, GATA-1 erythroid progenitor cells, and megakaryocytes (Rosenbloom et al., 2015, 2013; Kent et al., 2002).

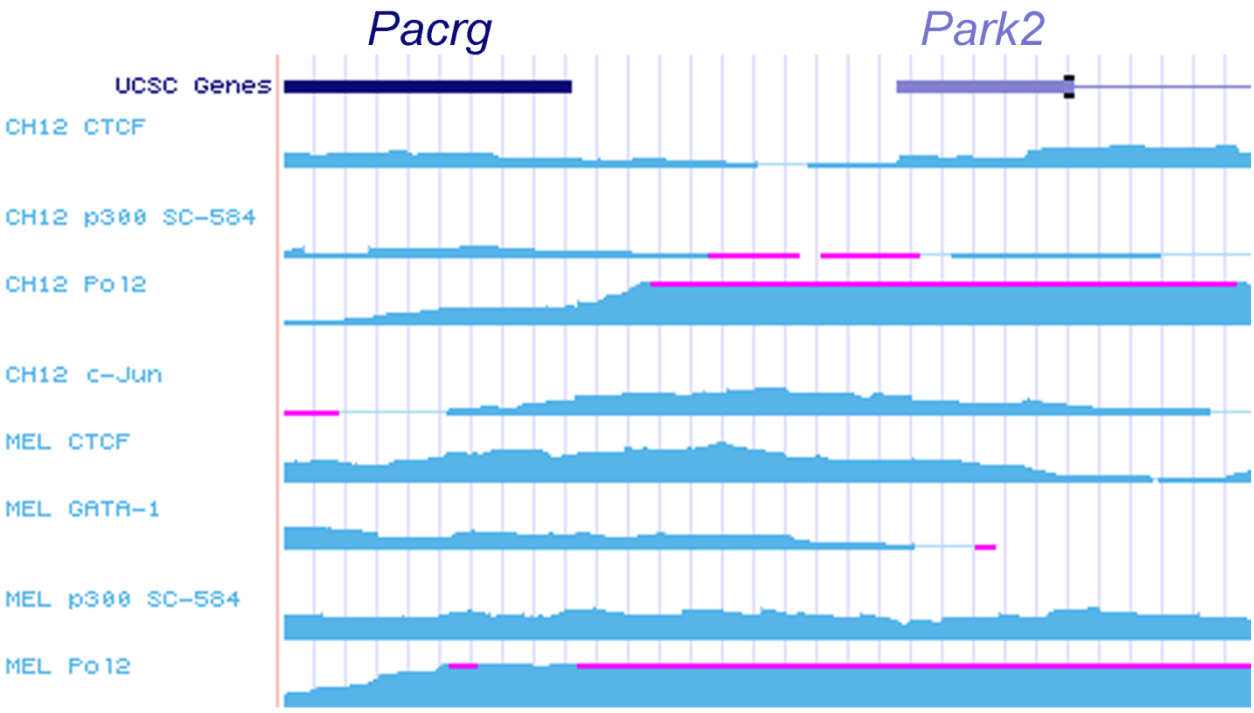

Figure 3.18 Known transcription factor binding via ChIP-seq data from the SYDH group. Image is modified from ENCODE data from chromosome 17. The region between *Pacrg* (dark blue) and the *Park2* (light blue) genes is considered the promoter region. Locations of transcription factor binding within the region are shown for CH12 and MEL cells (Rosenbloom et al., 2015, 2013; Kent et al., 2002).

PATCH1.0

Data from the program PATCH 1.0, predicting the binding of transcription factors to the promoter region, shows 98 potential transcription factors varying in predicted binding scores, from the mouse promoter region (Matys et al., 2003) (Table 3.1). PATCH 1.0 is a pattern-based program for predicting transcription factor binding sites based on similarity to a consensus binding site. Transcription factors identified were constrained to those found in vertebrates only and the program default settings were used, with a mismatch penalty of 100, maximum number of mismatches of 2, and the lower score boundary set at 85.0. Transcription factors identified by Patch 1.0 were AhR, AP-2, AP-2alphaA, AP-2alphaB, AP-4, AR, ARIX, Arnt, C/EBP, C/EBPbeta, CACCC binding factor, c-Ets-2, c-Fos, c-Jun, c-Myb, CNBP, CREB, CREBbeta, CRE-BP1, CTCF, E12, E2F, E2F-1, E2F-4, E47, EBP-80, ETF, f(alpha)-f(epsilon), FXR, GammaCAC1, GammaCAC2, GATA-1, GR, Gsh-1, HEB, HIF-1, hnRNP K, HrpF, IL-6, INSAF, IPF1, IRE-ABP, ISGF-3, Isl-1, LBP-1, LUN-1, LXR-alpha, LXR-beta, LyF-1, MAZ, MAZi, MTF-1, MyoD, Myogenin, NF-1, NFAT-1, NF-ATc, NF-ATp, NF-ATx, NF-E, NF-Y, NRF-1, Pax-2, Pax-5, Pax-8, PPAR-alpha, PPAR-gamma, PR B, Pu box, RE-BP, RXR-alpha, RXR-beta, SMAD-3, SMAD-4, Sp1, Sp3, Sp4, SRF, SRY, STAT1, STAT3, STAT5A, STAT5B, STAT6, T3R-alpha, T3R-alpha1, T3R-beta1, Tal-1, USF, USF-1, USF-2, v-Jun, WT1, XF1, XF2, XPF-1, XrpFl, and ZAP.

Table 3.1 Putative transcription factors of the mouse parkin promoter identified by PATCH 1.0. Transcription factors along with their respective highest binding score are shown.

Transcription Factor	Highest Score	Transcription Factor	Highest Score
AhR	100.0	MAZ	85.7
AP-2	85.7	MAZi	85.7
AP-2alphaA	85.7	MTF-1	100.0
AP-2alphaB	85.7	MyoD	100.0
AP-4	100.0	Myogenin	87.5
AR	100.0	NF-1	85.7
ARIX	100.0	NFAT-1	100.0
Arnt	100.0	NF-ATc	100.0
C/EBP	100.0	NF-ATp	100.0
C/EBPbeta	100.0	NF-ATx	100.0
CACCC-BF	100.0	NF-E	100.0
c-Ets-2	100.0	NF-Y	100.0
c-Fos	100.0	NRF-1	100.0
c-Jun	100.0	Pax-2	100.0
c-Myb	100.0	Pax-5	100.0
CNBP	85.7	Pax-8	100.0
CREB	100.0	PPAR-alpha	100.0
CREBbeta	100.0	PPAR-gamma	100.0
CRE-BP1	100.0	PR B	85.7
CTCF	100.0	Pu box	100.0
E12	100.0	RE-BP	100.0
E2F	85.7	RXR-alpha	100.0
E2F-1	85.7	RXR-beta	100.0
E2F-4	85.7	SMAD-3	100.0
E47	87.5	SMAD-4	100.0
EBP-80	100.0	Sp1	100.0
ETF	85.7	Sp3	100.0
f(alpha)-f(epsilon)	87.5	SP4	100.0
FXR	100.0	SRF	100.0
GammaCAC1	100.0	SRY	85.7
GammaCAC2	100.0	STAT1	100.0
GATA-1	100.0	STAT3	87.5
GR	85.7	STAT5A	100.0
Gsh-1	87.5	STAT5B	100.0
HEB	100.0	STAT6	100.0

Table 3.1 Cont'd.

Transcription Factor	Highest Score	Transcription Factor	Highest Score
HIF-1	85.7	T3R-alpha	100.0
hnRNP K	85.7	T3R-alpha1	100.0
HrpF	100.0	T3R-beta1	100.0
IL-6	100.0	Tal-1	87.5
INSAF	87.5	USF	100.0
IPF1	100.0	USF-1	100.0
IRE-ABP	85.7	USF-2	100.0
ISGF-3	100.0	v-Jun	85.7
Isl-1	100.0	WT1	87.5
LBP-1	100.0	XF1	100.0
LUN-1	100.0	XF2	100.0
LXR-alpha	100.0	XPF-1	100.0
LXR-beta	100.0	XrpFI	100.0
LyF-1	100.0	ZAP	100.0

TFSearch

Data from the program TFSearch, predicting the binding of transcription factors to the promoter region, shows 22 potential transcription factors predicted to bind the mouse promoter region (Table 3.3). As with Patch 1.0, TFSearch is a pattern based program for predicting transcription factor binding sites based on similarity to a consensus binding site. Transcription factors were identified using program default settings, with a lower limit of an 85.0% binding prediction score. Transcription factors identified by TFSearch were AP-1, c-Ets, c-Myc, CRE-BP, E2F, Evi-1, GATA-1, GATA-2, GATA-3, HSF2, IK-2, Lyf-1, MyoD, MZF1, NF-E2, Nkx-2, p300, Sox-5, Sp1, SRY, STATx, and USF.

Table 3.2 Putative transcription factors of the mouse parkin promoter identified by TFSearch. Transcription factors along with their respective highest binding score are shown.

Transcription Factor	Highest Score
AP-1	88.7
c-Ets	87.3
c-Myc	89.1
CRE-BP	87.5
E2F	86.2
Evi-1	90.7
GATA-1	91.8
GATA-2	91.7
GATA-3	92.5
HSF2	85.9
Ik-2	91.7
Lyf-1	85.7
MyoD	88.4
MZF1	91.1
NF-E2	86.4
Nkx-2	97.7
p300	85.1
Sox-5	85.6
Sp1	87.7
SRY	100.0
STATx	90.4
USF	88.8

PROMO

Data from the program PROMO, predicting the binding of transcription factors to the promoter region, shows 193 potential transcription factors predicted to bind the mouse promoter region (Messeguer et al., 2002; Farre et al., 2003) (Table 3.4). PROMO is a matrix based program for predicting transcription factor binding sites. Unlike Patch 1.0 and TFSearch, PROMO assigns a dissimilarity score based on a position weight matrix for each transcription factor. A position weight matrix is based around the consensus binding sequence and accounts for common variations at different bases. Transcription factors were identified using program default settings, with an upper limit of 15.0% dissimilarity to the consensus transcription factor binding sequence. Transcription factors identified by PROMO were ABI4, Adf-1, AhR, AhR:Arnt, AIRE, ALF1B, Alfin1, ANT, Antp, AP-2, AP2-alphaA, AP-4, Arnt, ATF3, BR-C Z2, BR-C Z3, BTEB3, BTEB4, C/EBP, C/EBPalpha, C/EBPbeta, C/EBPbeta(p20), C/EBPdelta, CAC-binding protein, Cdx-1, c-Ets-1, c-Ets-1 54, c-Fos, c-Jun, c-Myb, COE1, COE2, CP2, c-Rel, CREMtau, CREMtau1, CREMtau2, Crx, Cutl1, D1, DBP, DEF:GLO, DEF:GLOLSQUA, DP-1, DRF1.1, DRF1.3, DSXF, DSXM, E12, E2F, E2F-1, E2F-1:DP-1, E2F-5, E47, E4F1, E74A, Egr-1, EllaE-A, Elf-1, Elk-1, ENKTF-1, ETF, Eve, f(alpha)-f(epsilon), FACB, FOXN2, FOXO3a, GAL4, GCF, GKLF, GR-alpha, GT-1, HELIOS, HES-1, HMG 1(Y), HNF-1A, HNF-1B, HNF-3, HNF-3beta, HOXA3, HSF1 (long), HSF1 (short), IA-1, IPF1, IRF-1, IRF-3, Isl-1, JunB, JunD, Kr,

Lf-A1, LVc, LyF-1, MATalpha2, Max-1, MAZ, MCM1, MF3, MNB1a, MYB2, MYBAS1, Myf-3, Myf-5, MyoD, myogenin, MZF-1, Ncx, NF-1, NF-1/L, NF-AT1, NF-AT2, NF-AT3, NF-ATI, NF-E4, Nkx2-1, NRF-1, Nrf2:MafK, p300, p53, Pax-2, Pax2a, Pax-5, Pax-6, Pax-9a, Pax-9b, PBF, POU1F1a, PR A, PR B, Prd, PUR alpha, PUR beta, R2, RC2, RelA, RFX1, Sp1, Sp3, Spz1, STAT1beta, STAT3, STAT4, STAT5A, StuAp, SUT1, T11, TAF, T-Ag, TCF-2, TRMI, Ubx, unc-86, USF, USF1, USF-1, USF2b, VDR, Vpr, VSF-1, WTI I, YY1, ZF5, Zic1, Zic2, and Zic3. From the 193 potential transcription factors, 164 are not repeated in the list, where AhR (2 times), C/EBPalpha (4 times), C/EBPbeta (3 times), c-Ets-1 (2 times), c-Fos (3 times), c-Jun (3 times), c-Myb (2 times), E2F-1 (2 times), Elf-1 (2 times), HNF-3beta (2 times), IPF1 (2 times), MyoD (3 times), NF-1 (2 times), NF-AT1 (2 times), Pax-5 (2 times), Sp1 (6 times), Sp3 (2 times), and USF2b (2 times) are repeated. These repeats depict predicted binding of transcription factors of different species to the promoter, for example, c-Fos is repeated three times, suggesting c-Fos of mouse, human, and rat origin can recognize and interact with the given sequence.

Table 3.3 Putative transcription factors of the mouse parkin promoter identified by PROMO. Transcription factors along with their lowest dissimilarity score are shown.

Transcription Factor	Lowest Dissimilarity Score	Transcription Factor	Lowest Dissimilarity Score
ABI4	3.5	IA-1	14.8
Adf-1	2.7	IPF1	3.0
AhR	0.8	IRF-1	7.9
AhR:Arnt	9.3	IRF-3	1.2
AIRE	11.9	Isl-1	7.0
ALF1B	5.4	JunB	2.9
Alfin1	9.1	JunD	8.6
ANT	14.1	Kr	13.7
Antp	2.2	LF-A1	9.7
AP-2	1.2	LVc	0.0
AP-2alphaA	0.0	LyF-1	5.6
AP-4	3.7	MATalpha2	2.0
Arnt	7.2	Max-1	0.0
ATF3	9.9	MAZ	14.3
BR-C Z2	9.2	MCM1	12.7
BR-C Z3	14.6	MF3	8.0
BTEB3	1.2	MNB1a	1.5
BTEB4	1.0	MYB2	0.0
C/EBP	0.0	MYBAS1	1.2
C/EBPalpha	0.0	Myf-3	0.0
C/EBPbeta	0.6	Myf-5	9.5
C/EBPbeta(p20)	14.0	MyoD	0.0
C/EBPdelta	0.0	myogenin	0.0
CAC-BP	4.6	MZF-1	0.1
Cdx-1	0.9	Ncx	0.0
c-Ets-1	5.7	NF-1	0.7
c-Ets-1 54	0.0	NF-1/L	14.5
c-Fos	5.7	NF-AT1	1.7
c-Jun	2.6	NF-AT2	4.9
c-Myb	3.5	NF-AT3	6.5
COE1	5.6	NF-ATI	1.1
COE2	4.7	NF-E4	9.2
CP2	5.5	Nkx2-1	1.4
c-Rel	3.0	NRF-1	0.0

Table 3.3 Cont'd.

Transcription Factor	Lowest Dissimilarity Score	Transcription Factor	Lowest Dissimilarity Score
CREMtau	0.0	Nrf2:MafK	9.3
CREMtau1	0.0	p300	0.0
CREMtau2	0.0	p53	3.9
Crx	1.9	Pax-2	0.3
Cutl1	9.5	Pax-2a	0.0
D1	11.3	Pax-5	2.7
DBP	7.1	Pax-6	0.0
DEF:GLO	9.4	Pax-9a	10.2
DEF:GLO:SQUA	0.0	Pax-9b	10.2
DP-1	11.6	PBF	0.0
DRF1.1	14.3	POU1F1a	6.7
DRF1.3	14.3	PR A	4.3
DSXF	14.5	PR B	4.3
DSXM	14.5	Prd	9.5
E12	9.4	PUR alpha	12.1
E2F	14.2	PUR beta	12.1
E2F-1	0.0	R2	4.8
E2F-1:DP-1	7.2	RC2	0.0
E2F-5	13.7	RelA	12.3
E47	4.3	RFX1	8.9
E4F1	1.9	Sp1	0.0
E74A	8.3	Sp3	1.0
Egr-1	8.0	Spz1	0.1
EIIaE-A	8.7	STAT1beta	12.7
Elf-1	1.9	STAT3	13.1
Elk-1	0.0	STAT4	1.5
ENKTF-1	12.6	STAT5A	0.0
ETF	0.6	StuAp	1.8
Eve	8.6	SUT1	11.6
f(α)-f(ε)	0.0	T11	5.9
FACB	0.0	TAF	8.0
FOXN2	13.9	T-Ag	3.1
FOXO3a	13.9	TCF-2	10.4
GAL4	6.0	TRMI	7.1
GCF	12.6	Ubx	1.2
GKLF	9.3	unc-86	5.8

Table 3.3 Cont'd.

Transcription Factor	Lowest Dissimilarity Score	Transcription Factor	Lowest Dissimilarity Score
GR-alpha	13.5	USF	8.2
GT-1	6.2	USF-1	5.6
HELIOS	1.4	USF2b	1.7
HES-1	0.0	VDR	0.0
HMG 1(Y)	2.7	Vpr	12.6
HNF-1A	4.5	VSF-1	12.7
HNF-1B	9.8	WTI I	10.5
HNF-3	11.3	YY1	0.0
HNF-3 beta	5.3	ZF5	0.0
HOXA3	2.5	Zic1	0.0
HSF1 (long)	14.3	Zic2	0.0
HSF1 (short)	14.3	Zic3	0.0

Discussion

In addition to the possible effects epigenetics may have, transcription factors could have a crucial role in the differential regulation of parkin. A myriad of potential transcription factors of parkin identified by PATCH 1.0, TFSearch, and PROMO could act as regulators of the parkin promoter. Comparing the predicted transcription factors from each site, PROMO had 128, PATCH 1.0 had 60, and TFSearch had 12 transcription factors unique to only that program (**Figure 3.19**). PROMO and PATCH 1.0 both had 24 transcription factors in common (NRF-1, E47, ETF, AP-2, AP-2alphaA, PR B, c-Myb, C/EBP, C/EBPbeta, Sp3, E12, Arnt, AhR, Pax-5, Isl-1, STAT3, NF-1, AP-4, MAZ, STAT5A, IPF1, Myogenin, Pax-2, and f(alpha)-f(epsilon)) (**Figure 3.19**). PROMO and TFsearch had 2 transcription factors in common (Nkx-2 and p300) (**Figure 3.19**). PATCH 1.0 and TFSearch had 2 transcription factors in common (GATA-1 and SRY) (**Figure 3.19**). Transcription factors were narrowed down to the 6 transcription factors are predicted by all 3 sites (AP-1, USF, Sp1, MyoD, E2F, and LyF-1) (**Figure 3.20**). Additional transcription factors of interest were selected from the three predictive binding programs based on the literature. Additional transcription factors of interest are SRY, NRF-1 and NRF-2 (**Figure 3.20**).

E2F is a family of transcription factors found in eukaryotes. The E2F family is composed of both transcriptional activators (E2F1, E2F2, E2F3a) and repressors (E2F3b, E2F4, E2F5, E2F6, E2F7, E2F8) (Muller and Helin,

2000). The role of E2F transcription factors is in cell cycle control, DNA repair and synthesis, and apoptosis. This suggests E2F would be most active during cell division or death (Liu and Greene, 2001; Muller and Helin, 2000). Since neurons do not divide once terminally differentiated from neural progenitor cells, E2F expression in neurons would be expected to be tied to apoptosis. E2F in this case would be promoting apoptosis, which is not observed with the TIDA neurons after MPTP, suggesting E2F is probably not increasing parkin expression (Liu and Greene, 2001). In addition, E2F1 expression via gene chip data has been previously shown to increase in the SN after MPTP, since E2F1 is traditionally a transcriptional activator and parkin does not increase in the SN, E2F1 is probably not acting on the *Park2* promoter (Behrouz dissertation).

LyF-1 (Lymphoid transcription Factor 1), also known as Ikaros, is a tumor suppressor protein commonly found in immune cells, such as B cells, T cells, NK cells, and granulocytes (Merkenschlager 2010, Kastner et al., 2013). Being as such, it is unlikely it is localized to neurons in the ARC or SN. In addition, there are no results for *in situ* hybridization of LyF-1 in the brain under normal conditions (Allen Brain Atlas).

MyoD (Myogeneic Differentiation) is a transcription factor that regulates muscle differentiation (Buckingham and Rigby, 2014). Since it is involved in muscle development, it is unlikely to be expressed in the brain. *In situ* hybridization results from the Allen Brain Atlas show no of MyoD in the

midbrain under normal conditions, and low levels present in the olfactory bulb and cerebellum. Though there is evidence that suggests MyoD has a role in motor and retinal neuron development, there is no evidence to suggest MyoD is present in nigrostriatal or tuberoinfundibular DA neurons of adult mice (Baguma-Nibasheka et al., 2016; Kablar 2004; Wang et al., 2003).

The NRF-1 indicated in the searches could refer to Nuclear Respiratory Factor 1 or Nuclear Factor Erythroid 2-Like 1. For purposes of clarification, Nuclear Respiratory Factor 1 will be abbreviated NRF1 and Nuclear Factor Erythroid 2-Like 1 abbreviated Nrf1. Nuclear Respiratory Factor 1 (NRF1) is a transcriptional activator of cytochrome C. Expression of NRF1 is induced by PGC-1, which is also a coactivator that works with NRF1 and regulates mitochondrial biogenesis (Wu et al., 1999). Parkin has also been shown to regulated PGC-1α through the degradation of its transcriptional repressor PARIS (Shin et al., 2011). NRF1 is also known to interact with the parkin promoter, as well as Pink1, DJ-1 and PAELR via ChIP-Seq experiments (Satoh et al., 2013). Nuclear Factor Erythroid 2-Like 1 (Nrf1) a known transcription factor of proteasome subunits. Inhibition or decreased activity of the proteasome allows the 120 kDa form of Nrf1 located in the endoplasmic reticulum, to be cleaved into a 65 kDa active form that localizes to the nucleus, and increases expression of proteasome subunits (Radhakrishnan et al., 2010, 2014). Nrf1 is also a basic leucine zipper

transcription factor, and has been shown to interact with members of the AP-1 family of transcription factors (Novotny et al., 1998). Both appear relevant to neurons and roles parkin is known to play in mitochondrial maintenance and the unfolded protein response (UPS).

Nuclear Factor Erythroid 2-Like 2 (Nrf2) is involved in the response of cells to oxidative stress, and has a role in the regulation of glutathione S-transferase and NAD(P)H:quinone oxidoreductase, as well as other antioxidant response proteins (Venugopal and Jaiswal, 1996; Hayes et al., 2000). As with Nrf1, Nrf2 can dimerize with activator protein-1 (AP-1) transcription factors (Novotny et al., 1998). MPP^+ is a mitochondrial Complex I inhibitor which can lead to the production of reactive oxygen species and can also displace DA from vesicles and produce toxic DA metabolites, including DA quinones (Hayes et al., 2000). Nrf2 in relation to antioxidant response proteins alone would be expected to be beneficial in response to MPP^+, although Nrf2 could have the additional benefits that parkin provides if it regulates parkin expression.

Specificity protein 1 (Sp1) is constitutively expressed in neurons, and post-translational modification and interactions between other transcription factors regulate the activity rather than the expression of Sp1 (Hung et al., 2006; Tan and Khachigian 2009; Miras-Portugal et al., 2015). MPTP and its metabolite MPP^+ however, have been shown to increase Sp1 expression (Chen et al., 2015). Caveats to this apparent discrepancy are that the mice

were treated for seven days via intraperitoneal injection and tissue was collected from the axon terminal region, where the presence of transcription factors would be in medium spiny neurons, rather than the DA neurons (Chen et al., 2015). In addition, Chen et al (2015) used primary human brain microvascular cells (a model for the blood brain barrier) and 25 μM MPP^+. These cells would not be expected to possess the dopamine transporter (DAT) to uptake MPP^+ and would most likely require a higher concentration of MPP^+ to illicit an effect (Chen et al., 2015). In addition, Sp1 has been predicted to act as a scaffold for other transcription factors, such as ATF3, STAT3, and c-Jun, linking Sp1 potentially to the AP-1 transcription factors (Kiryu-Seo et al., 2008).

Upstream stimulatory factor (USF) is a ubiquitously expressed transcription factor with a basic helix-loop-helix motif. The USF family is composed of USF1 and USF2, which can homo- or hetero-dimerize. The USF family plays a role in ultraviolet stress response, immune response, cell cycle, lipid metabolism, and has been shown to regulate some calcium dependant transcription factors in neurons (Corre and Galibert, 2005). USFs are ubiquitously expressed throughout the brain and other tissue making these potential regulators of parkin (Gregor et al., 1990; Sirito et al., 1992, 1994; Allen Brain Atlas).

Sex determining Region on chromosome Y (SRY) or Testis Determining Factor (TDF) is a transcription factor encoded by the *SRY* gene on the Y

chromosome. SRY is expressed for a short time in progenitor cells (pre-Sertoli cells), SRY directs these cells to become Sertoli cells, leading to the formation of the testis (Bradford et al., 2007). In addition to the expression of SRY during development of the testis, SRY is also present in the substantia nigra (SN) of adult male rodents (Dewing et al., 2006). Specifically, SRY is found in NSDA neurons expressing TH in the SN (Dewing et al., 2006). It has also been shown that SRY acts on the TH promoter (at a AP-1 site), and leads to the up-regulation of TH (Milsted et al., 2004). When SRY is knocked-down, there is no loss in neurons, but there are fewer neurons that express TH in the SN (Dewing et al., 2006). SRY has been shown to act as a repressor in some situations and shown to be present in NSDA neurons, as such, it could act as a repressor of parkin (Dewing et al., 2006; Rath et al., 2008). SRY mRNA has also been shown to be present in the ventral tegmental area, cortex, locus coeruleus and hypothalamus, and could act on both TH and parkin (Lee and Harley, 2012).

Activator Protein 1 (AP-1) is composed of homo or heterodimeric complexes that contains a combination of proteins from either the Jun, Fos, activating transcription factor (ATF), or Jun dimerization protein families (Hai and Curran, 1991). In mouse brain, FosB and ΔFosB expression increase in the ST following MPTP exposure, but remain unchanged in the SN (Pérez-Otaño et al., 1998; Potashkin et al., 2007). Expression of c-Fos and c-Jun in the SN are reported to increase in response to MPTP, however, these

changes require multiple doses or high doses of MPTP (Duchemin et al., 1992; Nishi, 1997; Chen et al., 2001;). In addition, ATF has been shown in cell culture (SH-SY5Y, HEK293T, PC12, and primary mouse cortical neurons) to be linked to parkin expression and endoplasmic reticulum (ER) stress, though there were no studies in animals to support the cell culture experiments (Bouman et al., 2011; Sun et al., 2013).

Taken together, the majority of the predicted transcription factors are related to the putative AP-1 binding site. This site is located approximately -160 bp upstream of the transcriptional start site of *Park2* and is conserved in *Homo sapiens*, *Mus musculus*, *Bos taurus*, and *Equus caballus* (Bouman et al., 2011). In addition to the AP-1 family of proteins that can bind to the site, SRY has been shown to bind AP-1 sites, as well as Nrf1 and Nrf2, which can dimerize with AP-1 proteins (Milsted et al., 2004; Novotny et al., 1998). For these reasons, the transcription factors that will be initially studied will be those that can interact with AP-1 sites, as well as NRF1, which has been shown via ChIP-Seq to interact with the *Park2* gene.

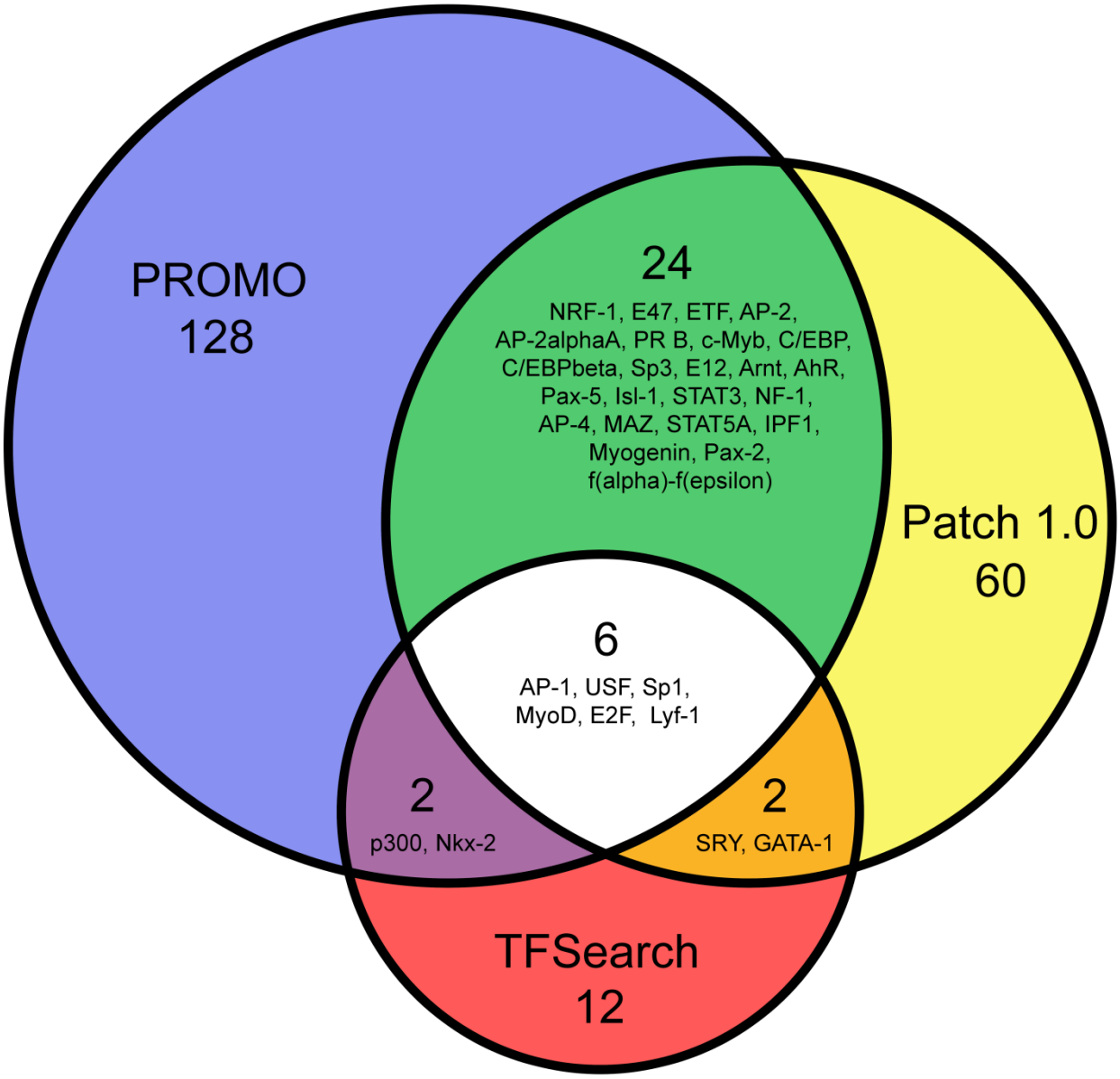

Figure 3.19 Putative transcription factors of parkin identified by one or more program. Venn diagram shows overlap within transcription factors identified from PROMO, Patch 1.0, and TFSearch.

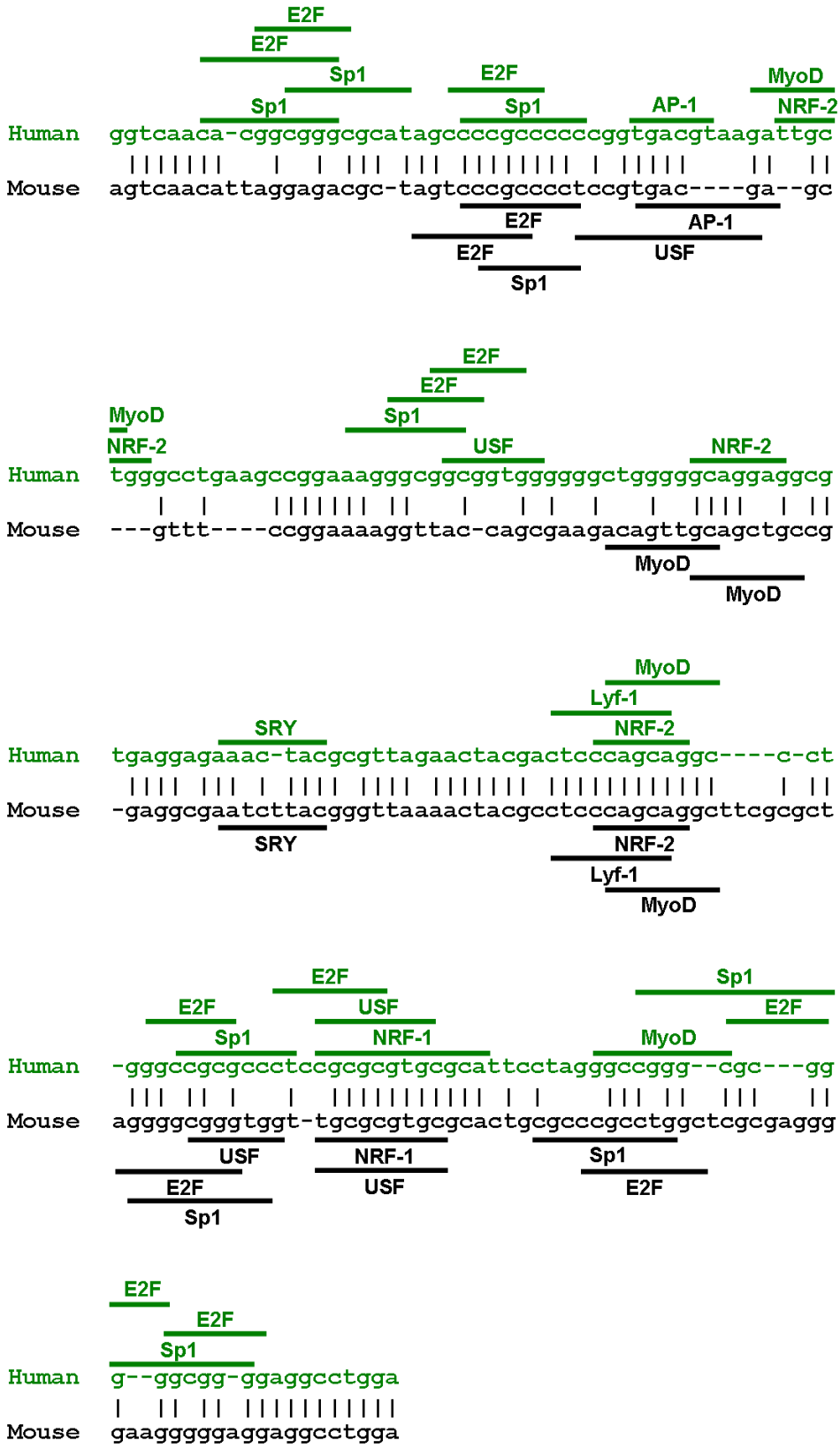

Figure 3.20 Predicted transcription binding sites on the mouse and human *Park2* promoters. Coding strand sequences of the human *Park2* (green) and

Figure 3.20 cont'd mouse *Park2* (black) promoters. Sequences were aligned, bases identical in each are indicated by lines, gaps in the sequence when aligned are indicated by dashes. Putative binding sites are color-coded by species and shown overlaying their respective sequences. Rows are 50 bases long.

Chapter 4: Assessment of Putative Transcription Factors of Parkin

Introduction

The differential expression of parkin between brain regions is in response to the metabolite of MPTP, MPP^+. This being the case, the effects of MPTP provides insight into what pathways may be activated following acute oxidative stress. MPP^+ is known to damage mitochondria, elicit oxidative stress via the production of reactive oxygen species (ROS), destabilize microtubules, directly inhibit the proteasome *in vitro*, and cause endoplasmic reticulum (ER) stress via the unfolded protein response (UPR) (Lansdell unpublished, Cartelli et al., 2013; Sun et al., 2013; Chan et al., 1991; Reinhart et al., 1987; Liu et al., 1992; Hung and Lee, 1997). Putative parkin transcription factors identified by both the literature and predictive software based on the sequence of *Park2* promoter, were selected to be examined based on if they were known to respond to a known effect of MPP^+.

ATF4, eIF2α and ER Stress

ATF4 and Nrf1 both are involved in pathways responding to ER stress and the UPR, with Nrf1 also related to proteasome dysfunction. ATF4, also known as CREB2, is a transcription factor that falls loosely into the CREB (cAMP Response Element Binding protein) family. As well as being in the CREB family, ATF4 also can dimerize with proteins in the AP-1 complex (Hai and

Curran, 1991). ATF4 has been shown to up-regulate parkin expression in cell culture including SH-SY5Y cells in response to the mitochondrial protein gradient uncoupler CCCP or ER stress inducer tunicamycin, and PC12 cells in response to ER stress inducer thapsigargin or MPP^+ (Sun et al., 2013; Bouman et al., 2011).

ER stress activates PERK (PKR-like ER localized eIF2α Kinase), which leads to the phosphorylation of eIF2α (Eukaryotic Initiation Factor 2α). Unphosphorylated eIF2α (along with GTP) binds a tRNA attached to methionine, this complex then interacts with other initiation factors to bind to the 40S (small) ribosomal subunit, this active complex then scans the mRNA for the start codon. The phosphorylated eIF2α, however, does not bind the tRNA-methionine, which means that it will not complex with the 40S subunit. The phosphorylation of eIF2α leads to the up-regulation of ATF4 via translational control involving a pair of uORFs (Upstream Open Reading Frames) (Vattem and Wek, 2004).

In an unstressed state when eIF2α is not phosphorylated, the active 40S complex scans the mRNA for the start codon in the first uORF, once found, the 60S (large) subunit binds and translation of uORF1 begins and ends. The 40S subunit continues to scan the mRNA and a new eIF2α-tRNA-methionine interacts with the 40S subunit. This re-initiates translation at the second uORF, which overlaps the ATF4 ORF. In a stressed state where eIF2α is phosphorylated, there is less eIF2α present to complex with tRNA-

methionine. After translation of the first uORF, the 40S subunit continues to scan the mRNA, but re-initiation takes longer because there is less eIF2α-tRNA-methionine. This delay leads to the 40S subunit missing the start codon in the second uORF, and instead finding the start codon in the ATF4 ORF (Vattem and Wek, 2004).

After it is translated, ATF4 leads to increased transcription of multiple genes, one of which is GADD34 (Growth Arrest and DNA Damage inducible protein 34) (Pons et al., 2007). GADD34 complexes with PP1 (Protein Phosphatase 1) to form a holoenzyme that dephosphorylates eIF2α, resulting in a feedback loop that shuts down the production of ATF4. After it has served its purpose, ATF4 can then be degraded (30-60 min half-life) (Pons et al., 2007).

Nrf1 and ER Stress

Like ATF4, Nrf1 is a basic leucine zipper transcription factor that must dimerize with another basic leucine zipper protein to function. Nrf1 is required for the production of proteasome subunits after proteasome inhibition (Radhakrishnan et al., 2010). Nrf1 starts as a 120 kDa protein localized to the ER lumen and under conditions of ER stress is retrotranlocated to the cytosol and bound by its N-terminus to the ER membrane. Under normal conditions, retrotranslocated Nrf1 is rapidly degraded by the proteasome. When the proteasome is inhibited, Nrf1 is

stabilized and can be cleaved by proteases (producing a 95 kDa protein) and translocated into the nucleus to up-regulate proteasome subunit genes (Radhakrishnan et al., 2014).

Nrf2 and Oxidative Stress

Nrf2 is related to Nrf1 and is involved in the response to oxidative stress. Nrf2 is involved in the regulation of glutathione S-transferase and NAD(P)H:quinone oxidoreductase, along with other antioxidant response proteins (Venugopal and Jaiswal, 1996; Hayes et al., 2000). Mice deficient in Nrf2 are more sensitive to MPTP (Chen et al,. 2009) and activation of Nrf2 in cell culture can protect against MPP^+ induced damage (Wruck et al., 2007). In the absence of oxidative stress, Nrf2 is bound to Keap1, which is an adapter for Cul3 E3 ligase complexes (Itoh et al., 1999; Kobayashi et al., 2004). When bound to Keap1, Nrf2 is rapidly ubiquitinated and subsequently degraded by the proteasome. In the presence of oxidative stress, key cysteines are oxidized, changing the conformation of Keap1 and thereby decreasing its affinity for Nrf2 (Taguchi et al., 2011). Loss of Keap1 binding allows Nrf2 to accumulate (Taguchi et al., 2011). Nrf2 is then phosphorylated by casein kinase 2 and this phosphorylated form can enter the nucleus and act as a transcription factor (Apopa et al., 2008). Both Nrf1 and Nrf2 recognize the Antioxidant Response Element (ARE) found in DNA sequences.

AP-1 Transcription Factors

Another set of transcription factors with basic leucine zipper motifs are the AP-1 family of transcription factor. AP-1 transcription factors recognize 12-O-tetradecanoylphorbol-13-acetate response elements (TRE) and TRE-like sites, which in some cases are contained within an antioxidant response element (ARE) (Xie et al., 1995). AP-1 transcription factors can form homo or heterodimeric complexes that contain a combination of proteins from either the Jun, Fos, ATF, or Jun dimerization protein families (Hai and Curran, 1991). Nrf1 and Nrf2 have also been show to be able to dimerize with AP-1 transcription factors (Novotny et al., 1998).

AP-1 transcription factors have previously been shown to respond to MPTP. Expression of c-Fos and c-Jun were reported to increase in the SN, and FosB/ΔFosB protein and mRNA expression increased in the ST following multiple or high doses of MPTP (Perez-Otano et al., 1998; Duchemin et al., 1992; Nishi, 1997; Chen et al., 2001). JunD is the binding partner that predominantly dimerizes with FosB. The dominant negative mutation of JunD, ΔJunD has been shown to reverse the effects of ΔFosB, as ΔJunD lacks a DNA binding domain and prevents dimers with a ΔJunD from interacting with DNA (Been et al., 2013; Berton et al., 2009; Struhl, 1988).

NRF1, Parkin and Mitochondrial Biogenesis

Not directly related to Nrf1 or Nrf2, but abbreviated the same is NRF1. NRF1 is a factor in mitochondrial biogenesis, more specifically is a transcriptional activator of cytochrome C, also known as mitochondrial Complex IV. Peroxisome proliferator-activated receptor-γ coactivator 1α (PGC-1α) is both a transcriptional activator of NRF1 and coactivator with the NRF1 protein to stimulate mitochondrial biogenesis (Russell et al., 2004; Wu et al., 1999). NRF1 also has direct links to parkin, where NRF1 has been shown via ChIP-Seq results to bind to the *Park2* promoter (Satoh et al., 2013). Parkin also regulates the expression of NRF1 through the degradation of the transcriptional repressor of PGC-1α, parkin-interacting substrate (PARIS) (Shin et al., 2011).

SRY and the TH Promoter

Sex determining Region on chromosome Y (SRY) is a transcription factor encoded by the *SRY* gene on the Y chromosome. SRY is the gene responsible for testis development. SRY interestingly has been found in the NSDA neurons of adult male rodents and to interact with an AP-1 site on the TH promoter (Dewing et al., 2006; Milsted et al., 2004). The loss of SRY also results in fewer TH expressing neurons in the SN of male rodents (Dewing et al., 2006). In addition to the SN, SRY has been found in the VTA, cortex, locus coeruleus and hypothalamus (Lee and Harley, 2012). This unusual

expression pattern and link to DA neurons makes SRY an interesting transcription factor to study.

Transcription Factor Regulation of the Parkin Promoter

All of these transcription factors have the potential to respond to the effects of MPP^+. In the examination of these transcription factors, certain criteria are expected of a transcription factor of parkin. A transcription factor of parkin should: 1) be up-regulated after MPTP in the ARC and not the SN (if a transcriptional activator), or be down-regulated in the ARC and not the SN (if a transcriptional repressor); 2) expression should change prior to an increase in parkin; 3) highly expressed for approximately as long as parkin is highly expressed (though this depends on if it is a early, intermediate or late responder); 4) present (and increase) in the nuclei of DA neurons and interact with the parkin promoter; 5) when expression is experimentally manipulated, there should be a corresponding effect on parkin expression.

Acute MPTP-induced Parkin Expression in the ARC

To initially examine these transcription factors, a 6 h time-point after MPTP administration was selected. Initial time-courses of parkin after MPTP shows parkin protein in the ARC increases by 12 h post-MPTP and is maintained at elevated levels at least until the 24 h time-point, and parkin mRNA is elevated at 8 h post-MPTP (Benskey et al., 2012). RNA polymerase

II elongation rates have been estimated to average between 1.3 and 4.3 kb per min., though have been shown to be as high as 50 kb per min. (Maiuri et al., 2011; Darzacq et al., 2007; Femino et al., 1998). Translation rates have been estimated at approximately 6 amino acids per sec (Ingolia et al., 2011; Bostrom et al., 1986). Since *Park2* is approximately 1.2 Mb and 464 amino acids, transcription is expected to range from 4.6 h (rate of 4.3 kb per min.) to 0.4 h (rate of 50 kb per min.), and about 1.3 min. for translation. This suggests that increased transcription of parkin probably starts somewhere between 3 and 7 h post-MPTP, this places 6 h post-MPTP in this window. The 6 h time-point also splits two previously examined time-points; 4 h were MPP^+ levels are high and 8 h where mRNA is elevated (Benskey et al., 2012). For all of the transcription factors examined, an increase in the ARC exclusively (or decrease in the SN exclusively) are sufficient for the transcription factor to be further studied.

ATF4

Results

Expression of ATF4 protein was unchanged at 6 h post-MPTP in both the ARC and SN. In the ARC, fold change for ATF4 protein in the saline control mice was 1.00 ± 0.09, and 0.85 ± 0.07 for 6 h post-MPTP treated mice (**Figure 4.1**). In the SN, fold change for ATF4 protein in the saline control mice was 1.00 ± 0.08, and 0.96 ± 0.10 for 6 h post-MPTP treated mice

(**Figure 4.2**). Upstream of ATF4, phosphorylated eIF2α was also unchanged in both the ARC and SN. In the ARC, fold change for phosphorylated eIF2α protein in the saline control mice was 1.00 ± 0.13, and 0.71 ± 0.23 for 6 h post-MPTP treated mice (**Figure 4.3**). In the SN, fold change for phosphorylated eIF2α protein in the saline control mice was 1.00 ± 0.16, and 1.27 ± 0.21 for 6 h post-MPTP treated mice (**Figure 4.4**).

Due to the lack of effect observed in mice, the dopaminergic neuronal MN9D cell line was used to further examine the effects of MPP^+ and ER stress. To induce ER stress tunicamycin was used to inhibit N-linked glycosylation and cause a UPR. In the vehicle control cells fold change for ATF4 was 1.00 ± 0.37 and 3.50 ± 0.33 at 12 h after the addition of MPP^+ (**Figure 4.5**). Parkin fold change in these cells was 1.00 ± 0.22 in the vehicle control cells and 1.14 ± 0.26 at 12 h after the addition of MPP^+ (**Figure 4.6**). The same vehicle controls were used for the tunicamycin treated cells. ATF4 in the tunicamycin treated cells was 9.73 ± 0.48 relative to the control, and parkin in the tunicamycin treated cells was 0.68 ± 0.15 (**Figures 4.7 and 4.8**).

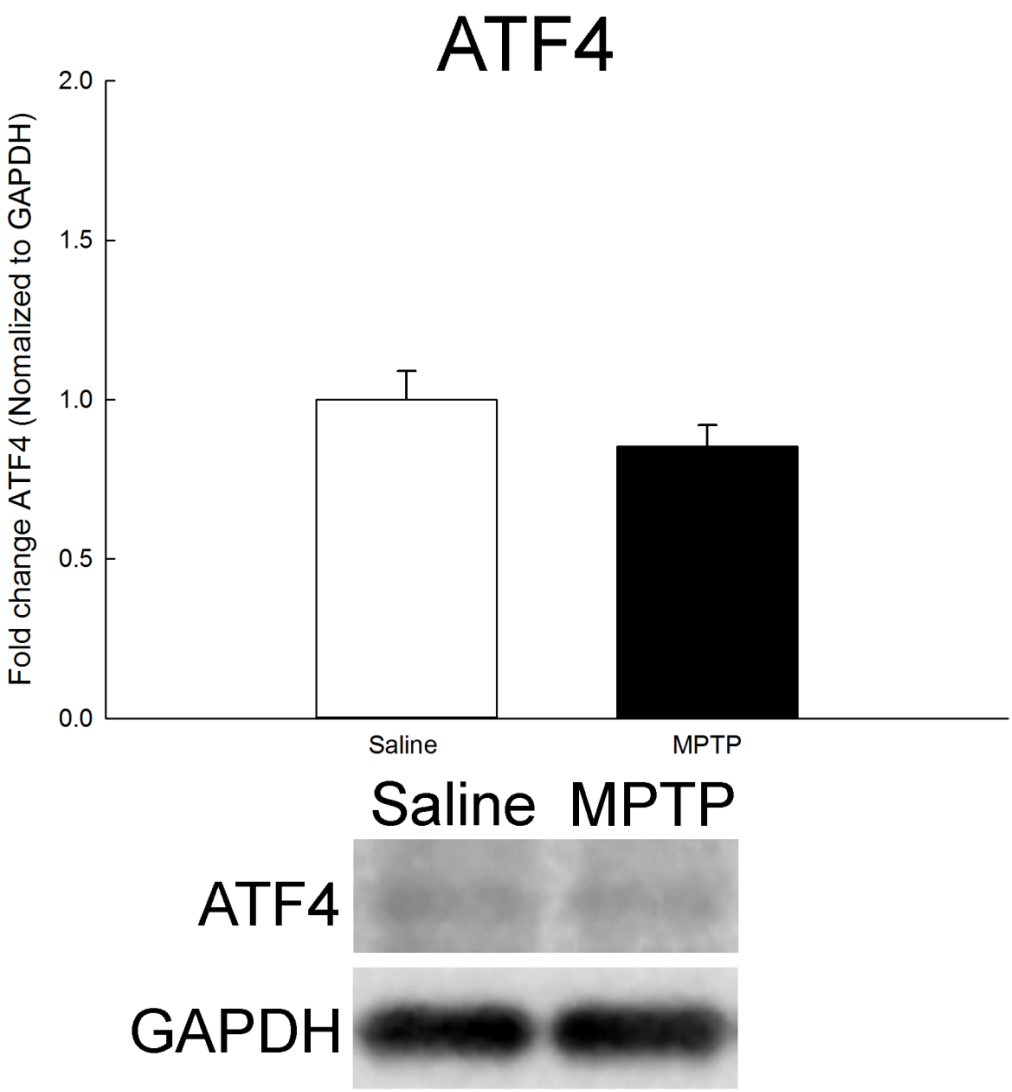

Figure 4.1 Comparison of the effects of MPTP on ATF4 in the ARC of mice. Male C57Bl/6J mice were treated with either saline (10 ml/kg; s.c.) or MPTP (20 mg/kg; s.c.) and killed by decapitation 6 h after injection (n=8/group). Brains were sectioned, ARC were microdissected, protein isolated and Western blots used to quantify ATF4 normalized to GAPDH. Columns indicate the group means, error bars represent +1 standard error of the mean.

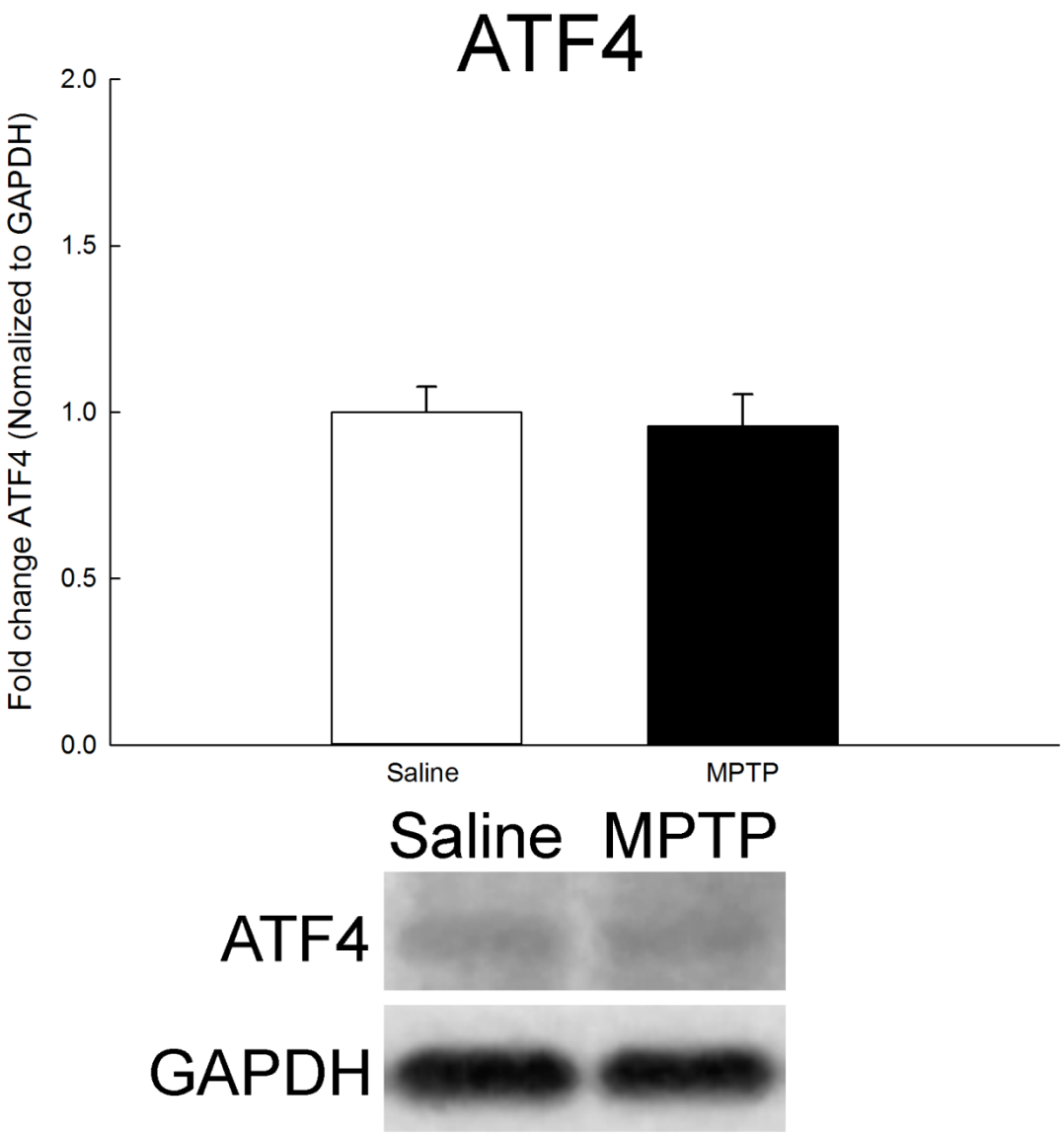

Figure 4.2 Comparison of the effects of MPTP on ATF4 in the SN of mice. Male C57Bl/6J mice were treated with either saline (10 ml/kg; s.c.) or MPTP (20 mg/kg; s.c.) and killed by decapitation 6 h after injection (n=8/group). Brains were sectioned, SN were microdissected, protein isolated and Western blots used to quantify ATF4 normalized to GAPDH. Columns indicate the group means, error bars represent +1 standard error of the mean.

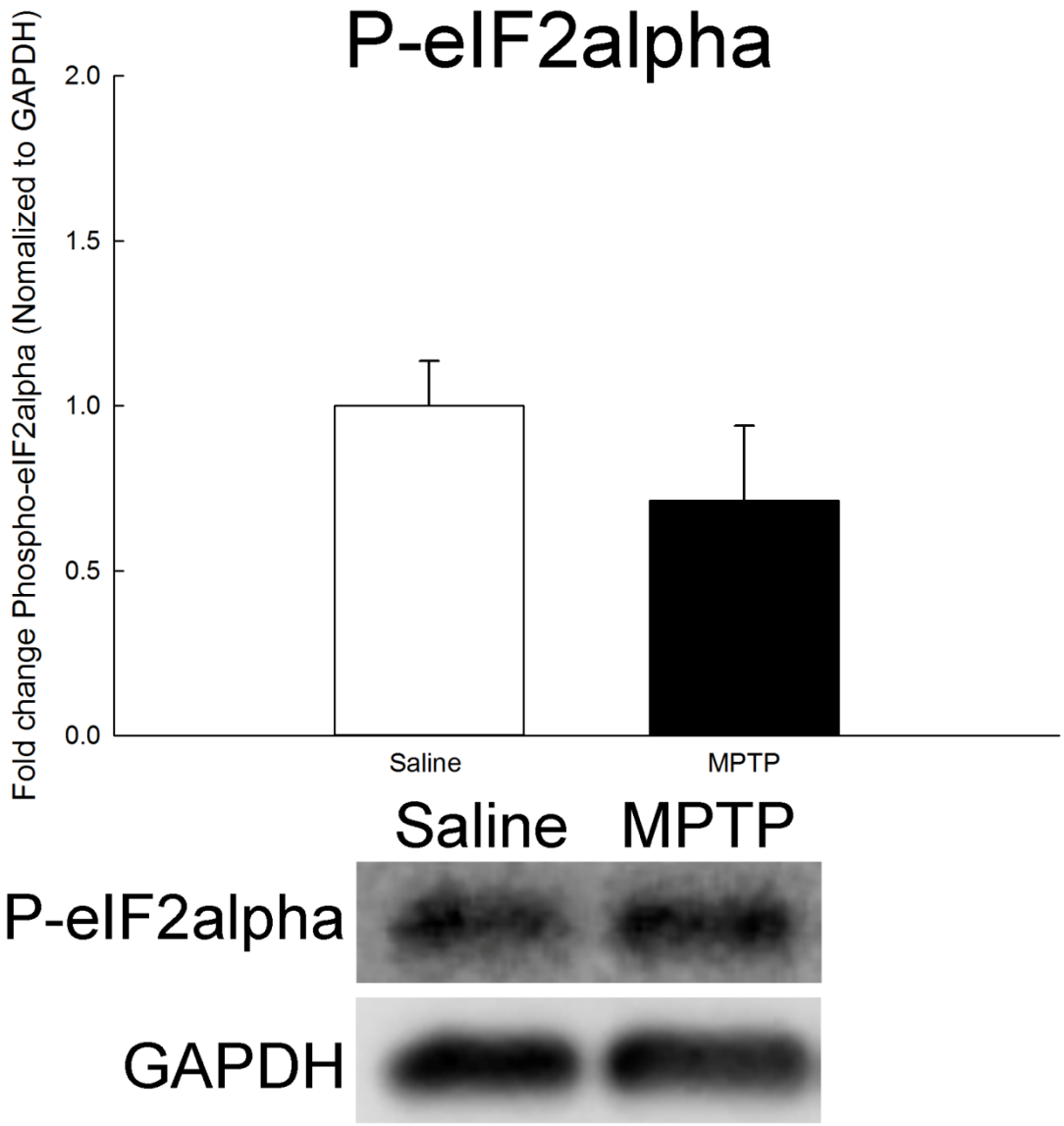

Figure 4.3 Comparison of the effects of MPTP on phosphorylated eIF2α in the ARC of mice. Male C57Bl/6J mice were treated with either saline (10 ml/kg; s.c.) or MPTP (20 mg/kg; s.c.) and killed by decapitation 6 h after injection (n=8/group). Brains were sectioned, ARC were microdissected, protein isolated and Western blots used to quantify phosphorylated eIF2α normalized to GAPDH. Columns indicate the group means, error bars represent +1 standard error of the mean.

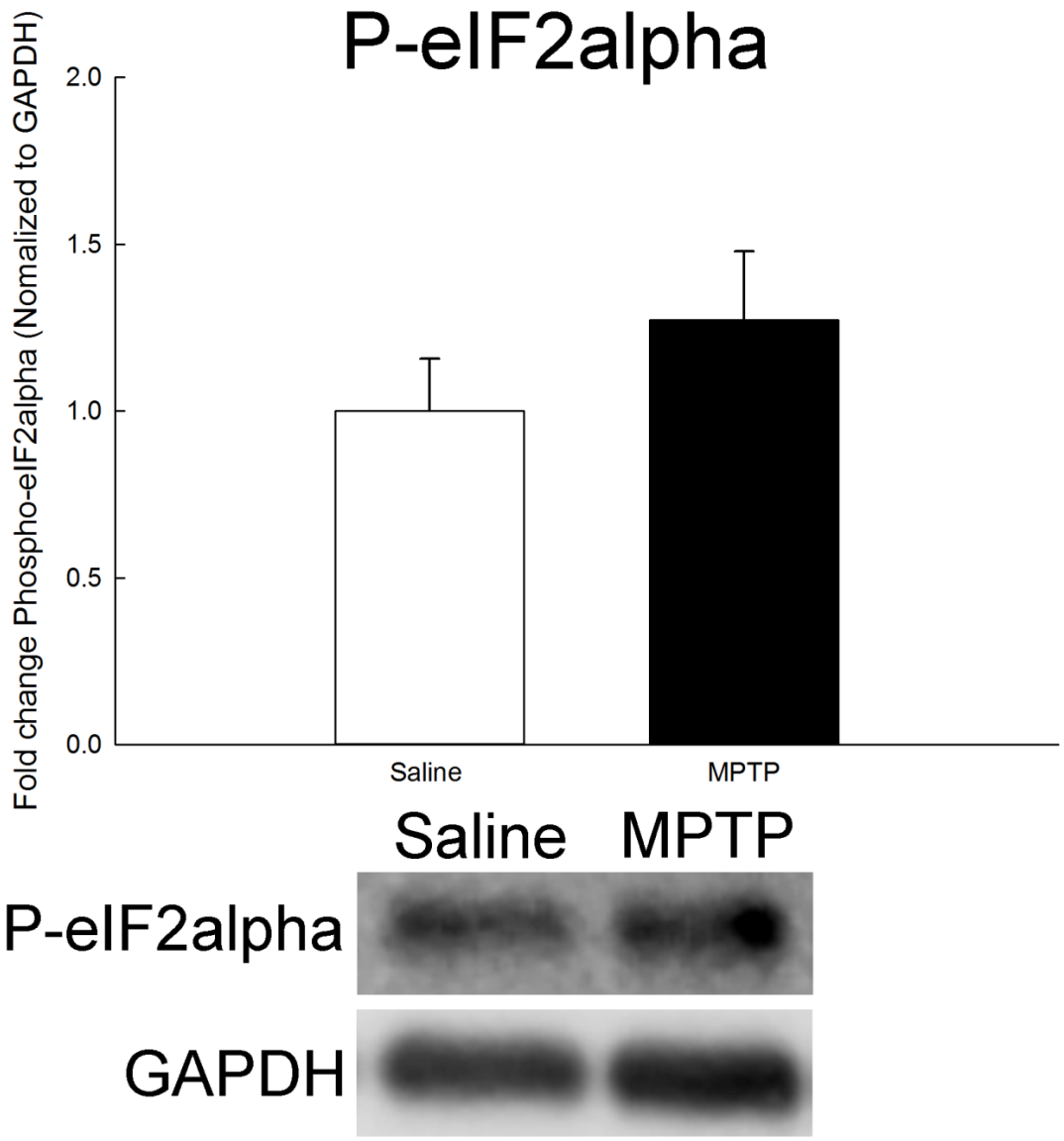

Figure 4.4 Comparison of the effects of MPTP on phosphorylated eIF2α in the SN of mice. Male C57Bl/6J mice were treated with either saline (10 ml/kg; s.c.) or MPTP (20 mg/kg; s.c.) and killed by decapitation 6 h after injection (n=8/group). Brains were sectioned, SN were microdissected, protein isolated and Western blots used to quantify phosphorylated eIF2α normalized to GAPDH. Columns indicate the group means, error bars represent +1 standard error of the mean.

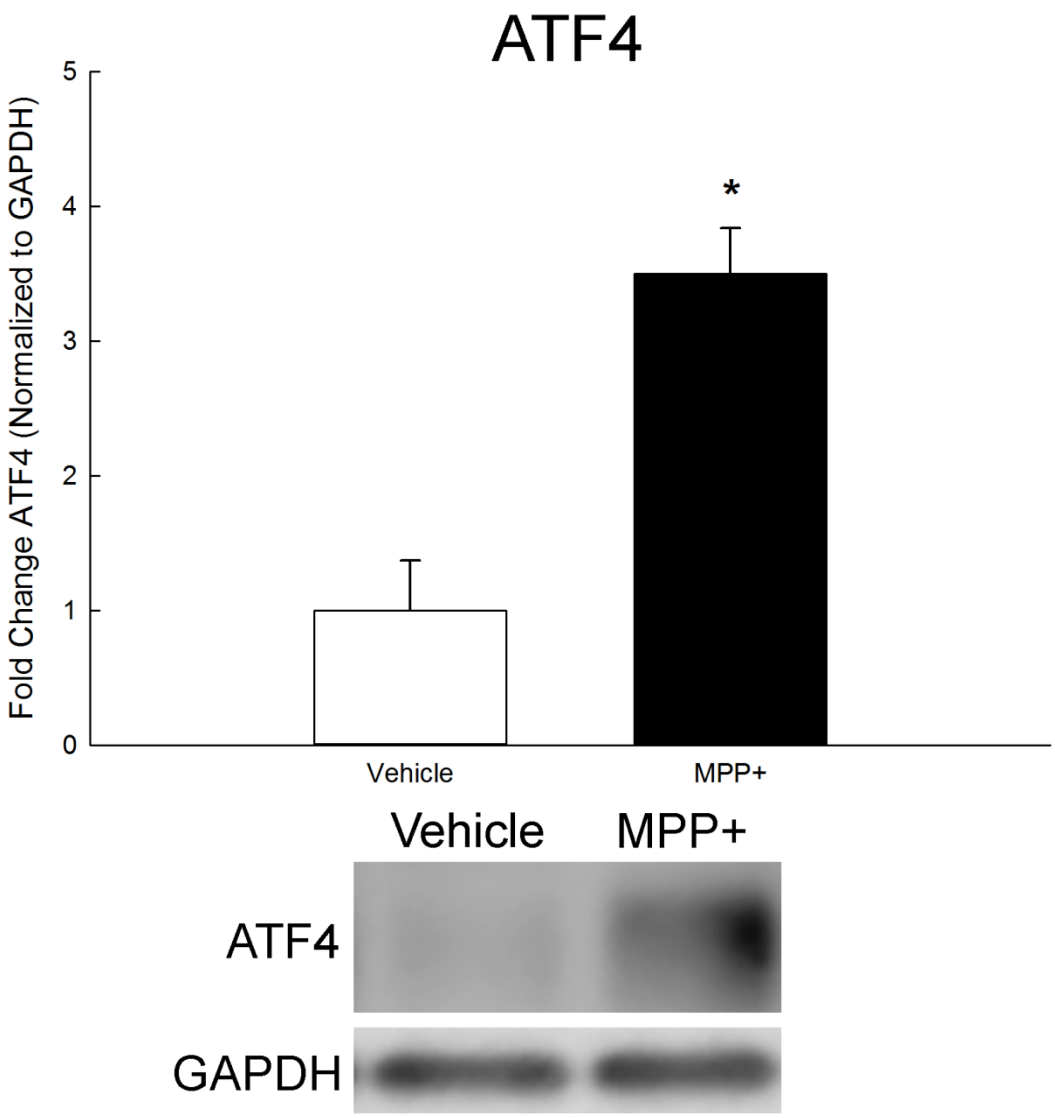

Figure 4.5 Comparison of the effects of MPP^+ on ATF4 in MN9D dopaminergic neuronal cell culture. MPP^+ was added to DMEM media to a concentration of 100 µM, cells were collected 12 hours later and processed for Western blots (n=3, with 3 technical repliates). Western blots were used to quantify ATF4 normalized to GAPDH. Columns indicate the group means, error bars represent +1 standard error of the mean, and significance ($p \leq 0.05$; t-test) is indicated with an asterisk.

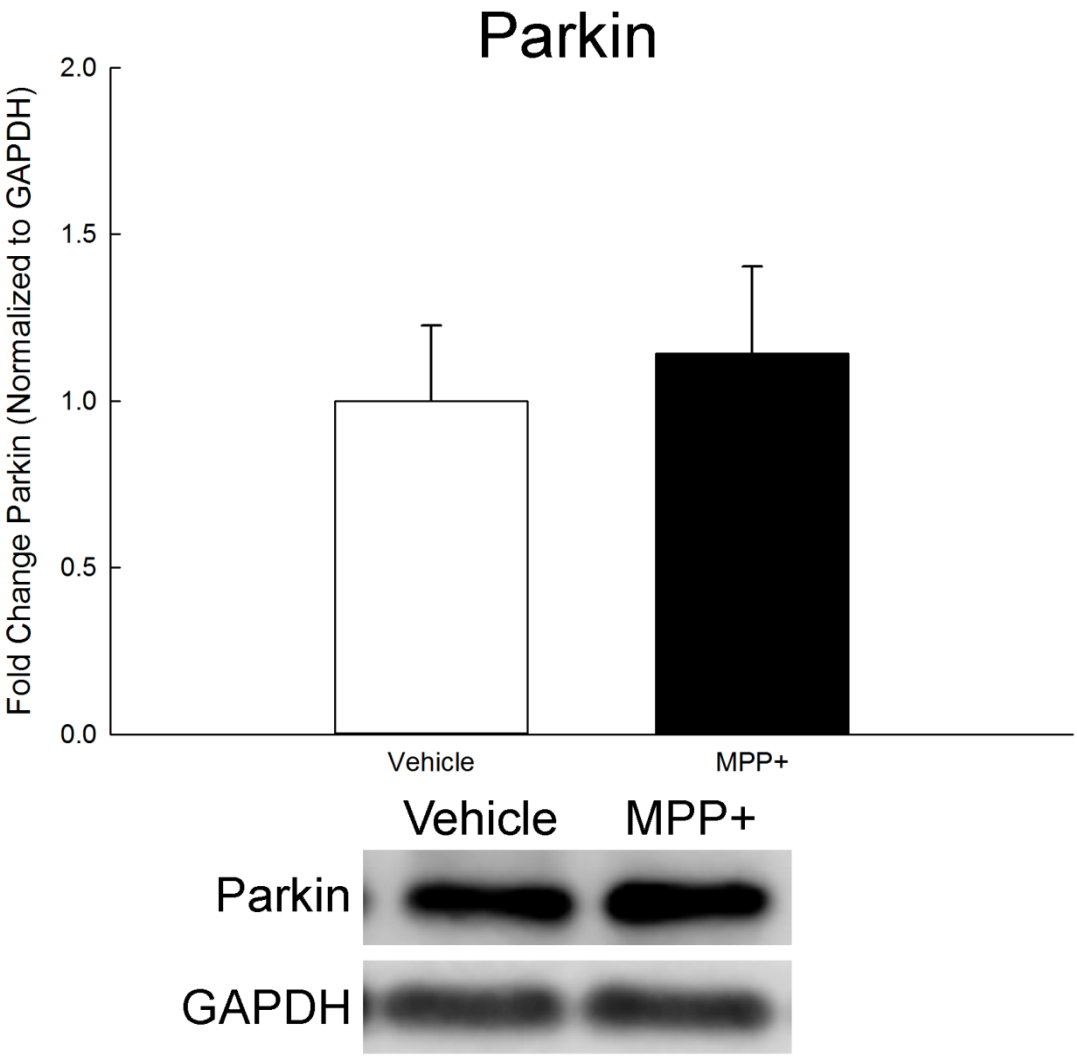

Figure 4.6 Comparison of the effects of MPP^+ on parkin in MN9D dopaminergic neuronal cell culture. MPP^+ was added to DMEM media to a concentration of 100 μM, cells were collected 12 hours later and processed for Western blots (n=3, with 3 technical repliates). Western blots were used to quantify parkin normalized to GAPDH. Columns indicate the group means, error bars represent +1 standard error of the mean.

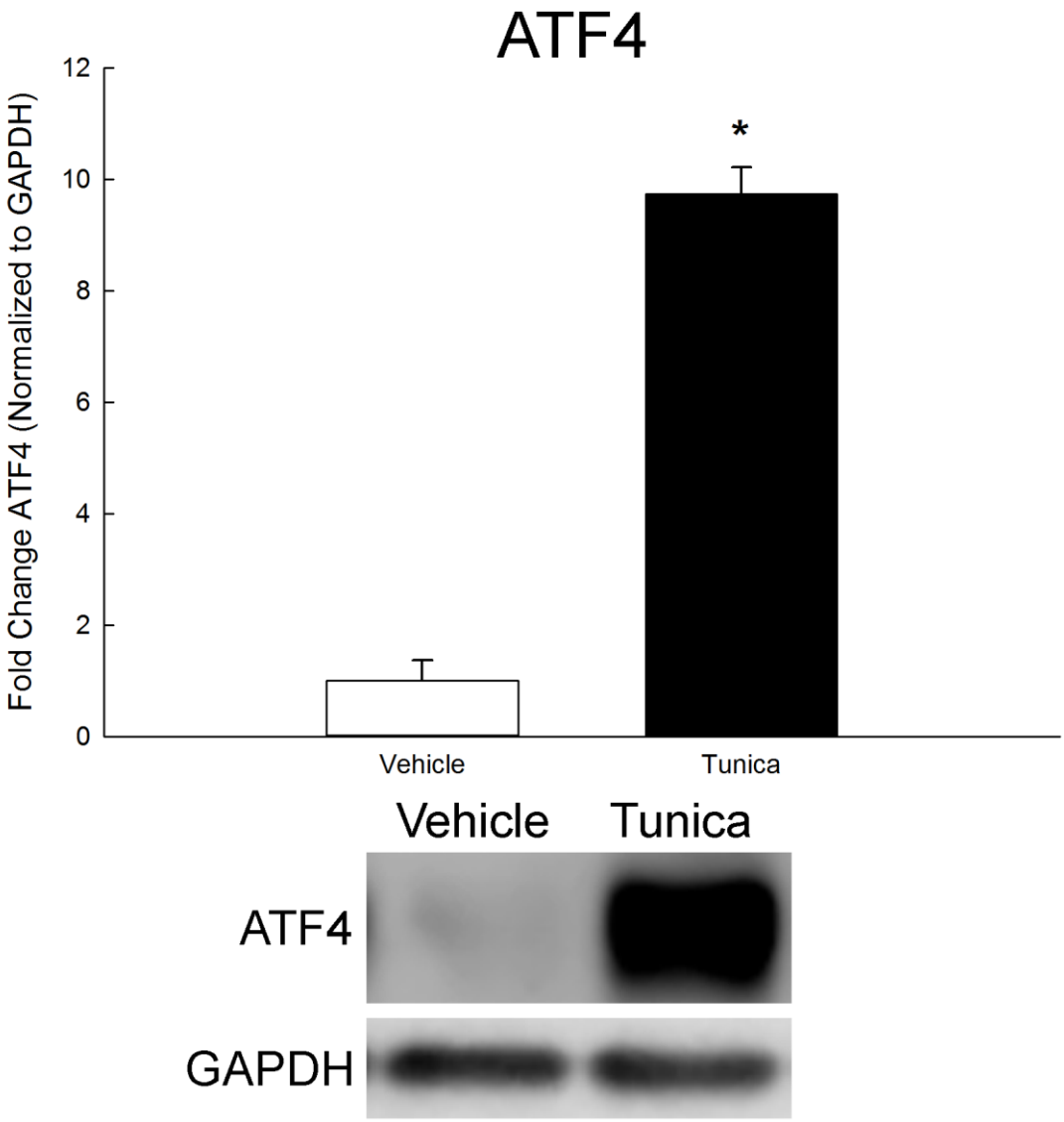

Figure 4.7 Comparison of the effects of tunicamycin on ATF4 in MN9D dopaminergic neuronal cell culture. tunicamycin was added to DMEM media to a concentration of 2 µg/ml, cells were collected 12 hours later and processed for Western blots (n=3, with 3 technical repliates). Western blots were used to quantify ATF4 normalized to GAPDH. Columns indicate the group means, error bars represent +1 standard error of the mean ,and significance ($p \leq 0.05$; t-test) is indicated with an asterisk.

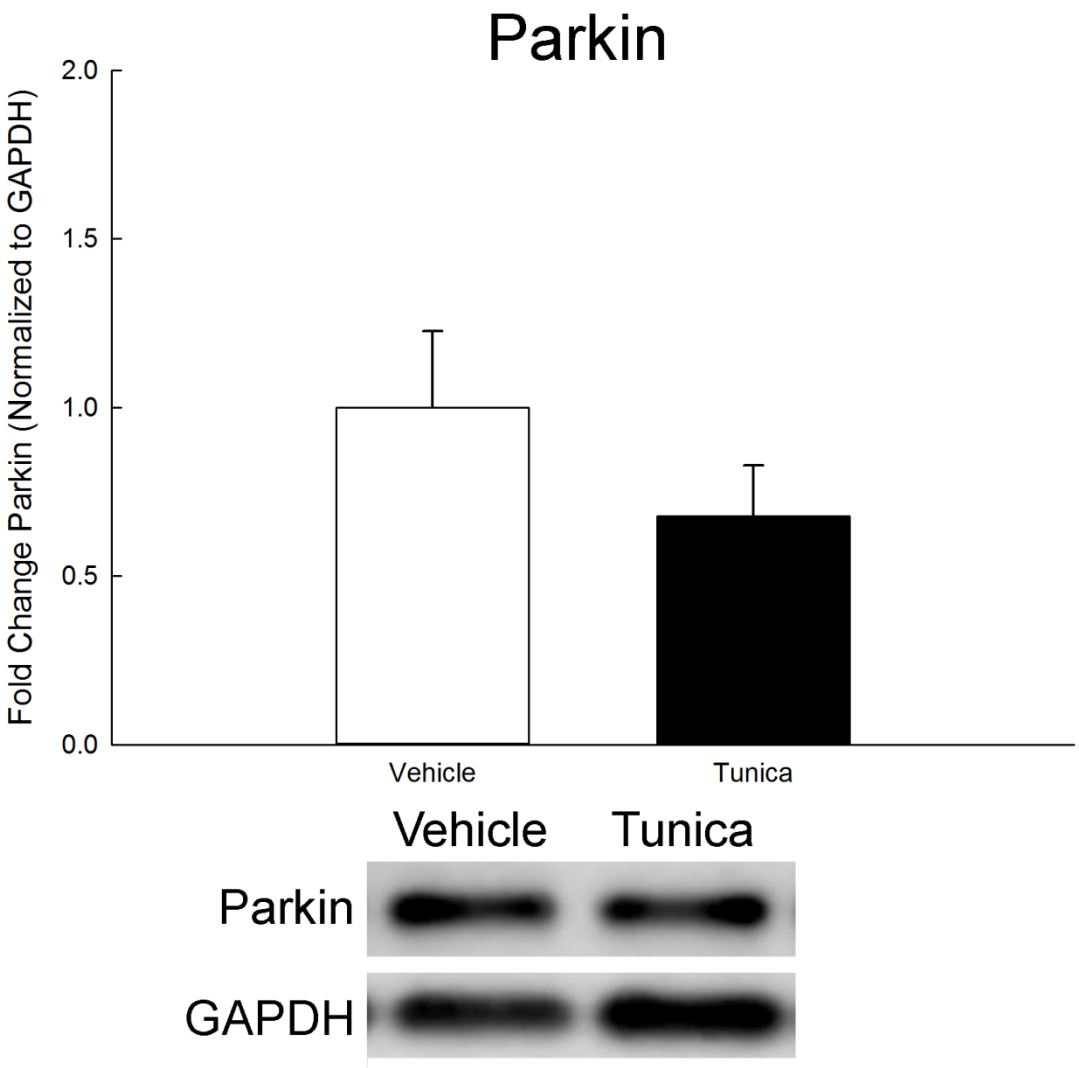

Figure 4.8 Comparison of the effects of tunicamycin on parkin in MN9D dopaminergic neuronal cell culture. tunicamycin was added to DMEM media to a concentration of 2 µg/ml, cells were collected 12 hours later and processed for Western blots (n=3, with 3 technical repliates). Western blots were used to quantify parkin normalized to GAPDH. Columns indicate the group means, error bars represent +1 standard error of the mean.

Discussion

It was expected that if ATF4 acts as a transcriptional activator of parkin following acute neurotoxicant exposure, then it would increase in the ARC and not the SN in response to MPTP administration. The lack of expression change of ATF4 is unexpected and contradictory to what was previously reported in the literature. There was also no change in a key regulator of ATF4, phosphorylated eIF2α. ATF4 was shown in SHSY-5Y and PC12 neuronal cell lines to act as transcriptional activators of parkin (Sun et al., 2013; Bouman et al., 2012). In addition, MPP^+ was shown in PC12 cells to increase ATF4 expression, as well as induce ER stress (Sun et al., 2013). The lack of ATF4 expression could be explained by differences in the model used in these studies. PC12 cells are derived from a pheochromocytoma from a rat adrenal medulla and used in a pure neuronal culture, whereas the brain regions examined in the present study are a mixed population of cells that contain DA neurons, more complex than the cell culture model.

Another caveat is the amount of neurotoxicant exposure. In the ME and ST, MPP^+ at its highest reported levels (4 h post-MPTP) are around 400 pg/μg of protein and 80 pg/μg respectively (Benskey et al., 2012). In comparison, Sun et al. used 1 mM of MPP^+. The formula weight of MPP^+ is 170.23 g/mol, which equates to cellular exposure of 170.23 ng MPP^+ per ml of solution. In comparison, the MN9D dopaminergic neuronal cell line shows significant loss of DA stores with 100 μM (Choi et al., 1999). There is also no

circulation in the cell culture model, where over time MPP^+ would be flushed from the tissue *in vivo*.

To further explore the use of a cell culture model, the MN9D cell line was used. MN9D cells when differentiated synthesize, release and reuptake DA (Balasooriya and Wimalasena, 2007; Choi et al., 1992). Unlike the ARC and the SN, ATF4 expression in MN9D cells did change in response to MPP^+, an approximately 3 fold increase, however there was no change in parkin. To focus directly on ER stress and ATF4, tunicamycin was used to cause an UPR. Tunicamycin caused an almost 9 fold increase in ATF4, a more drastic response than MPP^+ caused. Even with high levels of ATF4, parkin expression remains unchanged. Taken together this suggests that MPTP is not causing sufficient ER stress in the brain regions of interest, and that at least in MN9D cells, ER stress and ATF4 are not driving parkin expression.

Nrf1 and Nrf2

Results

Expression of Nrf1 protein was unchanged after MPTP in both the ARC and SN. In the ARC, fold change of the ER bound 120 kDa Nrf1 protein in the saline control mice was 1.00 ± 0.09, at 6 h post-MPTP it was 0.77 ± 0.12 and 0.85 ± 0.13 in 24 h post-MPTP (**Figure 4.9**). Fold change in the SN of the active 95 kDa Nrf1 protein in the saline control mice was 1.00 ± 0.13, at 6 h post-MPTP it was 0.87 ± 0.12 and 0.77 ± 0.14 in 24 h post-MPTP

(**Figure 4.10**) In the SN, fold change of the ER bound 120 kDa Nrf1 protein in the saline control mice was 1.00 ± 0.19, at 6 h post-MPTP it was 0.82 ± 0.23 and 0.68 ± 0.26 in 24 h post-MPTP (**Figure 4.9**). Fold change in the SN of the active 95 kDa Nrf1 protein in the saline control mice was 1.00 ± 0.17, at 6 h post-MPTP it was 1.08 ± 0.13 and 0.70 ± 0.22 in 24 h post-MPTP (**Figure 4.10**).

Expression of Nrf2 protein was unchanged at 6 h post-MPTP in both the ARC and SN. In the ARC, fold change Nrf2 protein in the saline control mice was 1.00 ± 0.06, and 1.16 ± 0.13 in 6 h post-MPTP treated mice (**Figure 4.11**). In the SN, fold change Nrf2 protein in the saline control mice was 1.00 ± 0.22, and 1.35 ± 0.24 in 6 h post-MPTP treated mice (**Figure 4.12**). Due to questions regarding the reliability of the Nrf2 antibody, Nrf2 knock-out (KO) mice were explored as a control and parkin protein was measured in the ARC and SN. Fold difference for parkin protein in the ARC of wild-type (WT) mice was 1.00 ± 0.45, and parkin in the Nrf2 KO mice was 8.98 ± 0.08 (**Figure 4.13**). Fold difference parkin protein in the SN of wild-type (WT) mice was 1.00 ± 0.16, and parkin in the Nrf2 KO mice was 3.13 ± 0.02 (**Figure 4.14**).

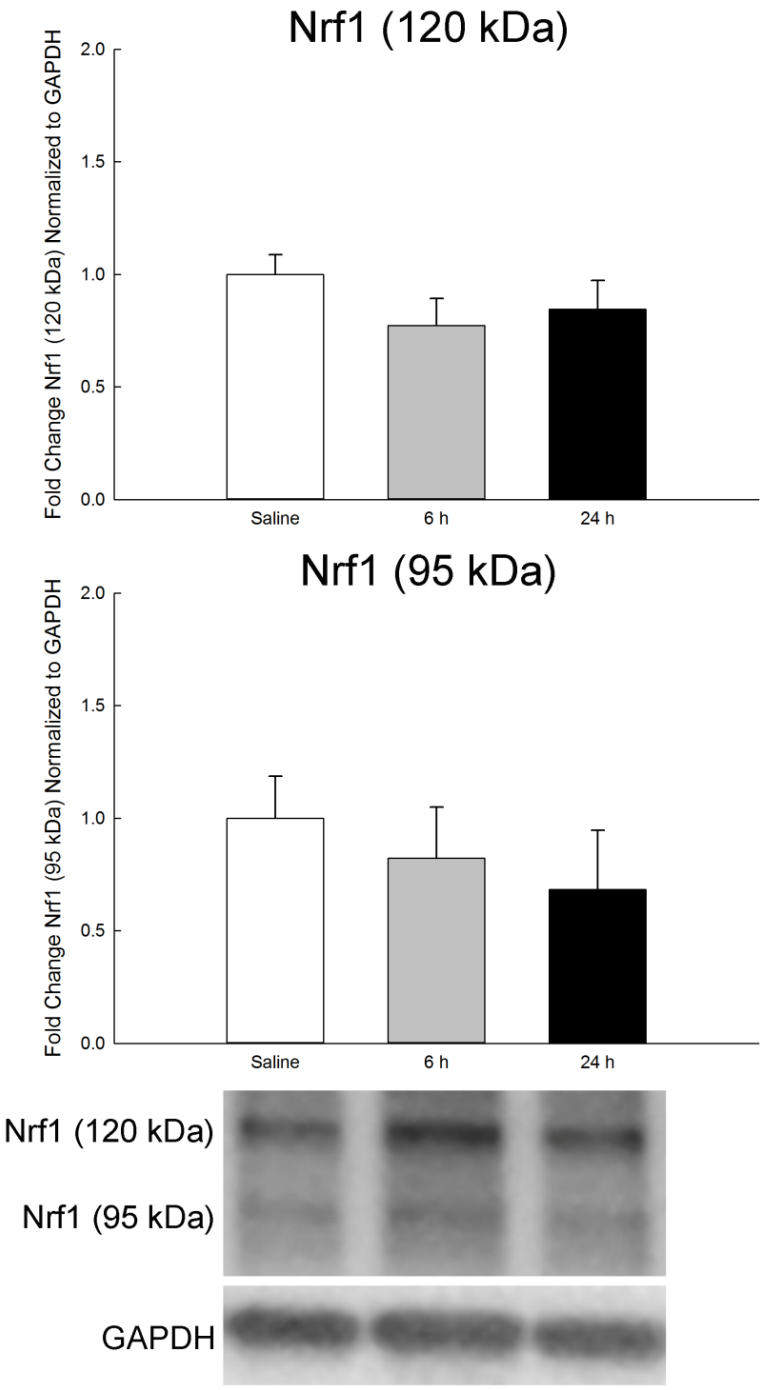

Figure 4.9 Comparison of the effects of MPTP on Nrf1 (120 and 95 kDa) in the ARC of mice. Male C57Bl/6J mice were treated with either saline (10 ml/kg; s.c.) or MPTP (20 mg/kg; s.c.) and killed by decapitation 6 h after injection (n=8/group). Brains were sectioned, ARC were microdissected, protein isolated and Western blots used to quantify Nrf1 normalized to GAPDH. Columns indicate the group means, error bars represent +1 standard error of the mean.

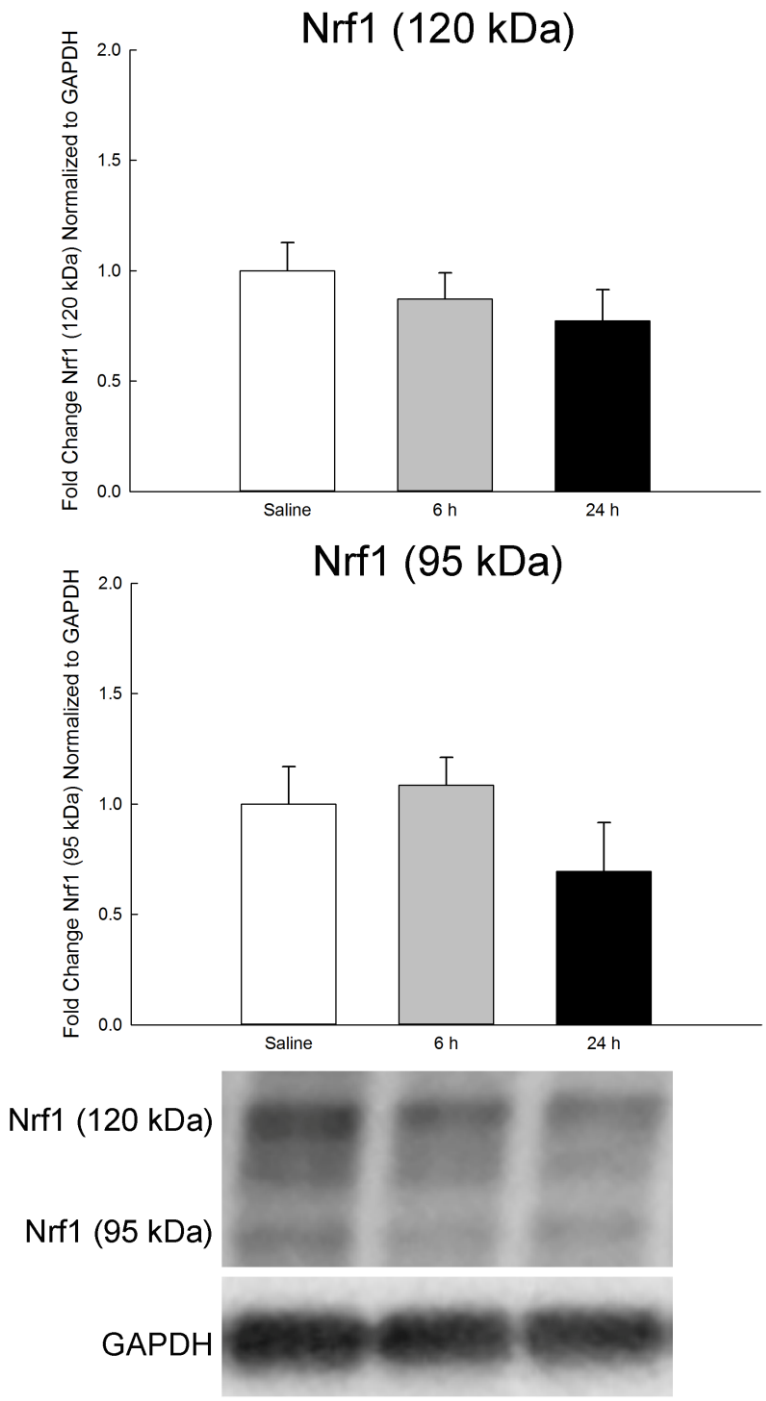

Figure 4.10 Comparison of the effects of MPTP on Nrf1 (120 and 95 kDa) in the SN of mice. Male C57Bl/6J mice were treated with either saline (10 ml/kg; s.c.) or MPTP (20 mg/kg; s.c.) and killed by decapitation 6 h after injection (n=8/group). Brains were sectioned, SN were microdissected, protein isolated and Western blots used to quantify Nrf1 normalized to GAPDH. Columns indicate the group means, error bars represent +1 standard error of the mean.

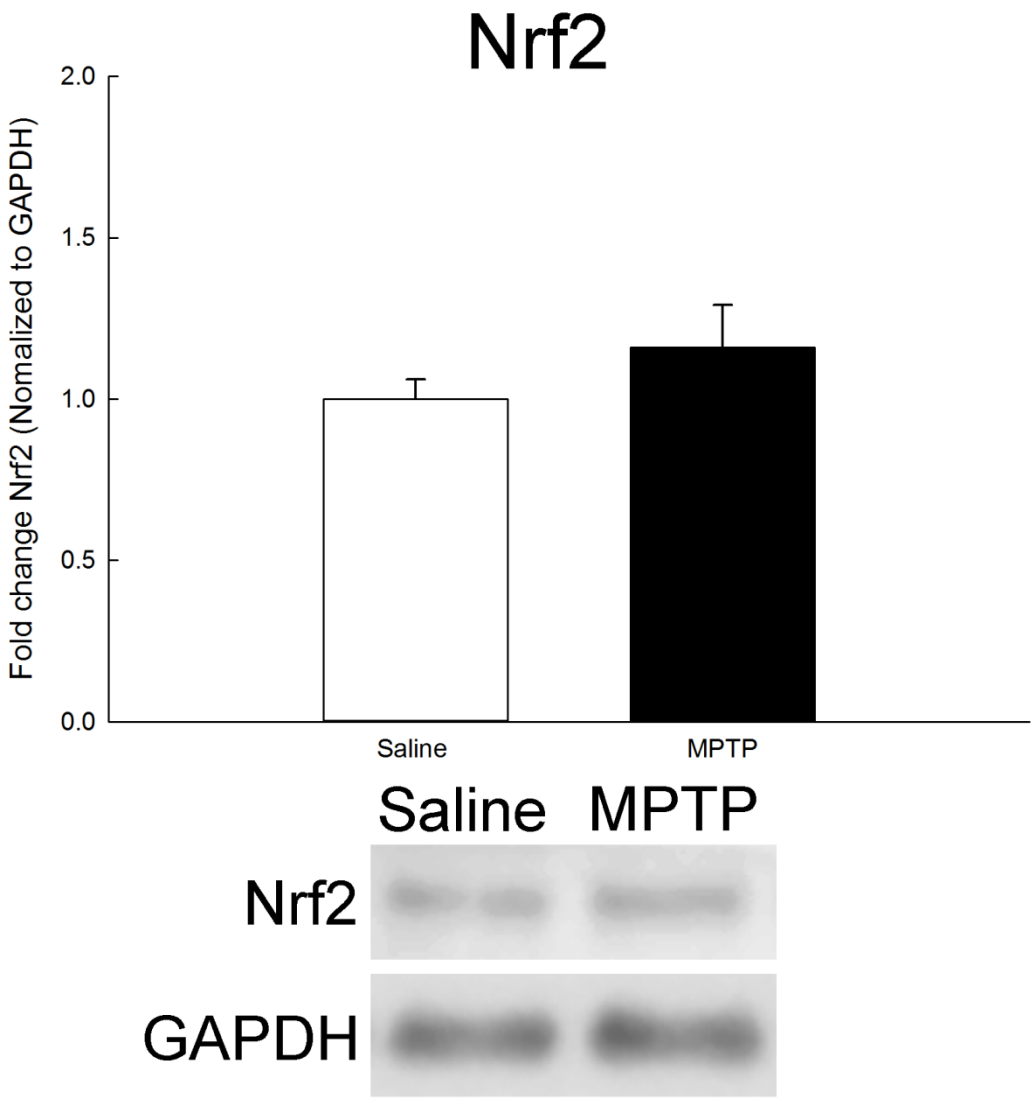

Figure 4.11 Comparison of the effects of MPTP on Nrf2 in the ARC of mice. Male C57Bl/6J mice were treated with either saline (10 ml/kg; s.c.) or MPTP (20 mg/kg; s.c.) and killed by decapitation 6 h after injection (n=8/group). Brains were sectioned, ARC were microdissected, protein isolated and Western blots used to quantify Nrf2 normalized to GAPDH. Columns indicate the group means, error bars represent +1 standard error of the mean.

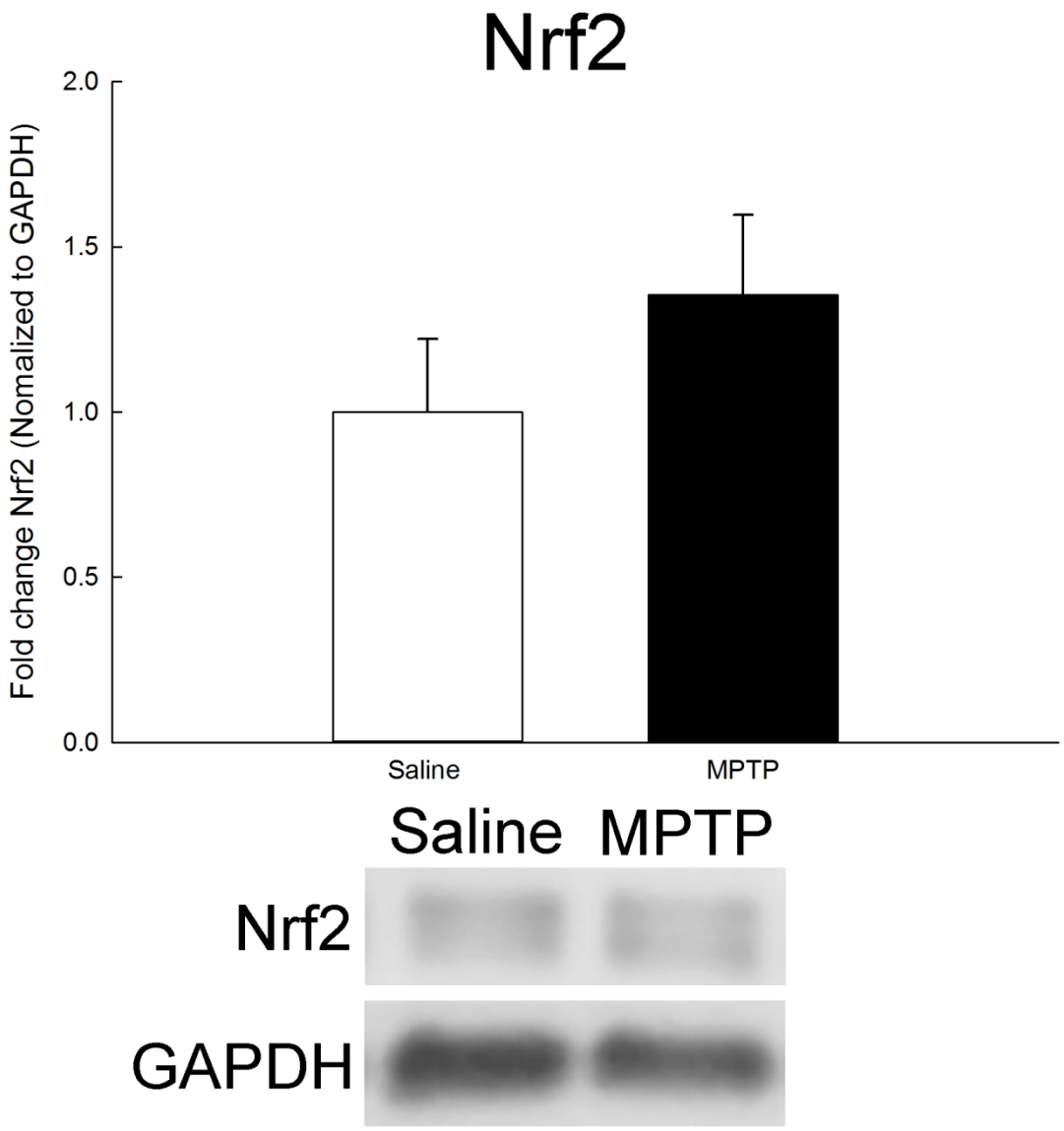

Figure 4.12 Comparison of the effects of MPTP on Nrf2 in the SN of mice. Male C57Bl/6J mice were treated with either saline (10 ml/kg; s.c.) or MPTP (20 mg/kg; s.c.) and killed by decapitation 6 h after injection (n=8/group). Brains were sectioned, SN were microdissected, protein isolated and Western blots used to quantify Nrf2 normalized to GAPDH. Columns indicate the group means, error bars represent +1 standard error of the mean.

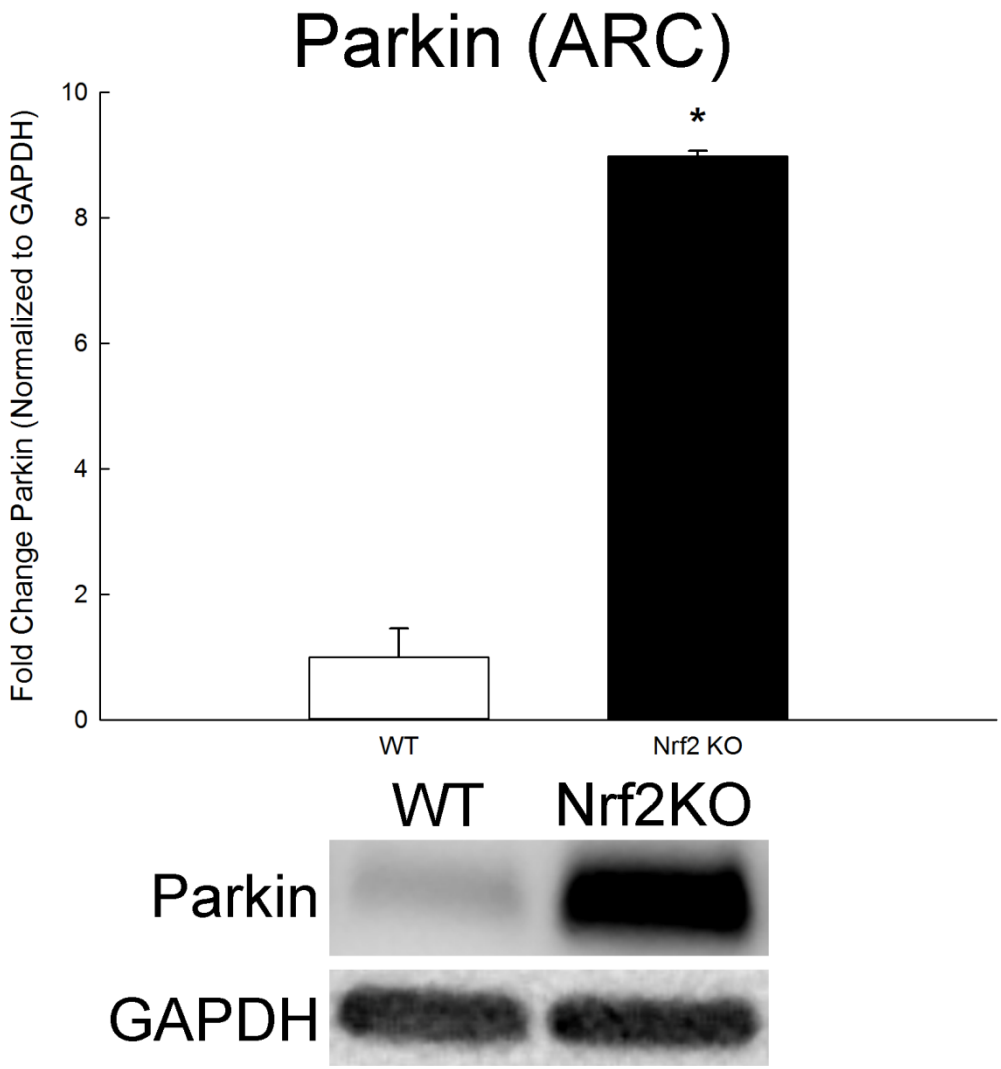

Figure 4.13 Parkin expression in the ARC of WT and Nrf2KO mice. Male C57Bl/6J and Nrf2KO mice were injected with saline (10 ml/kg; s.c.) and killed by decapitation 24 h after injection (n=8/group). Brains were sectioned, ARC were microdissected, protein isolated and Western blots used to quantify parkin normalized to GAPDH. Columns indicate the group means, error bars represent +1 standard error of the mean. An asterisk indicates values that are significantly different ($p < 0.05$; t-test) from vehicle-treated controls.

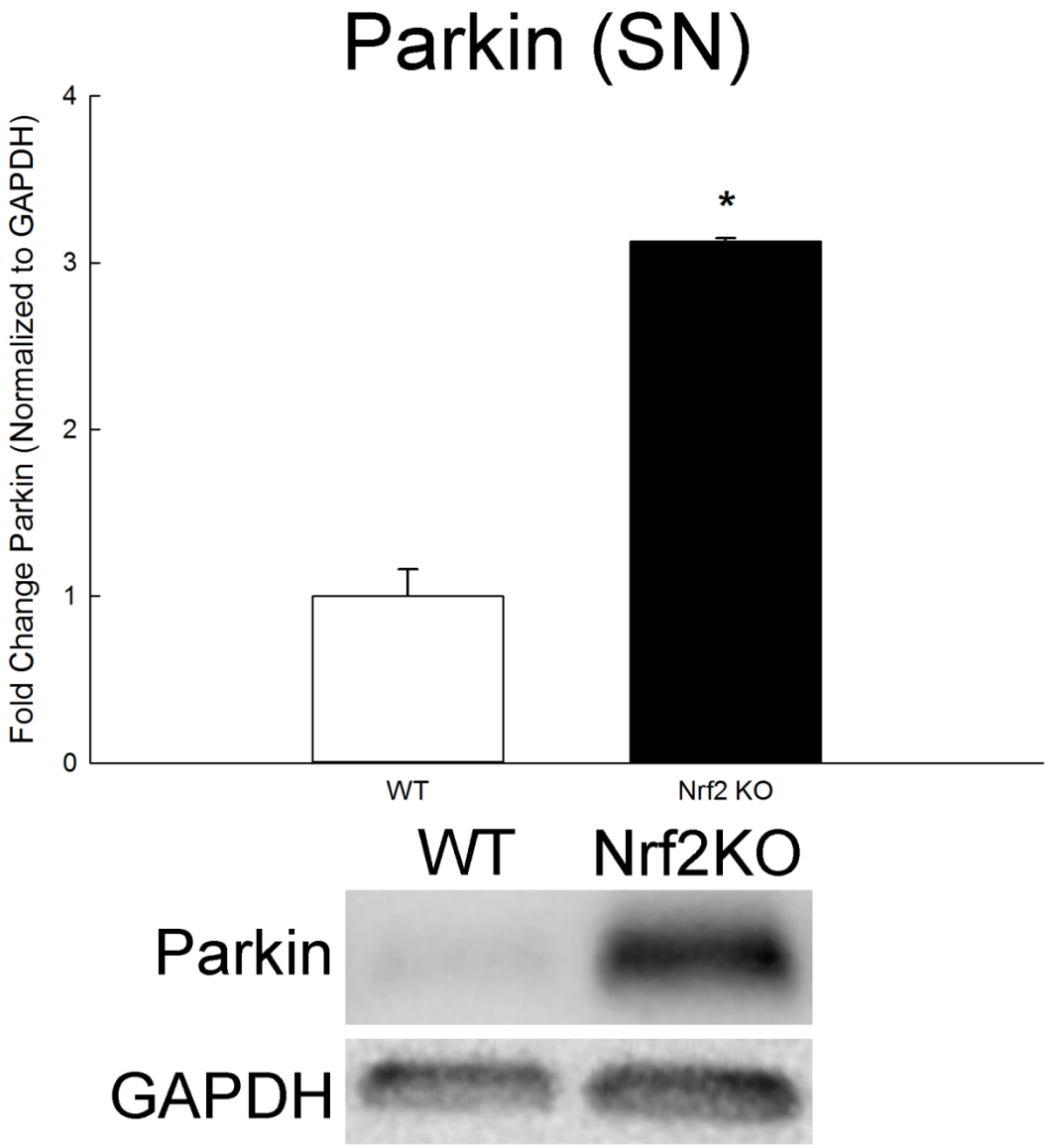

Figure 4.14 Parkin expression in the SN of WT and Nrf2KO mice. Male C57Bl/6J and Nrf2KO mice were injected with saline (10 ml/kg; s.c.) and killed by decapitation 24 h after injection (n=8/group). Brains were sectioned, SN were microdissected, protein isolated and Western blots used to quantify parkin normalized to GAPDH. Columns indicate the group means, error bars represent +1 standard error of the mean.

Discussion

Expression of Nrf1 was measured at 6 h and 24 h post-MPTP with no observable change in the ARC or SN. These results suggest that Nrf1 is not a transcription factor mediating neurotoxicant-induced activation of parkin promoter activity in the ARC. The role of Nrf1 in response to ER stress and proteasome dysfunction, and the lack of change in Nrf1 at either time-point suggest the extent of these stressors is not sufficient to increase Nrf1 or cause a shift to the 95 kDa active form (Digaleh et al., 2013; Steffin et al., 2010; Radhakrishnan et al., 2014). Based on the lack of change in ATF4, phosphorylated eIF2α, or Nrf1 acute MPTP does not appear to cause significant ER stress. MPTP does cause differential effects on proteasome activity, with decreased activity in the ST and not in the ME (Lansdell, et al., in preparation). Similarly, this loss of proteasome function in the ST following acute neurotoxicant exposure is most likely not severe enough to elicit a Nrf1 response, nor does it alter ST parkin expression (Benskey et al., 2013).

The focus of Nrf2 as a transcription factor driving neurotoxicant-induced parkin expression is based on the assumption of increased oxidative stress caused by MPTP. At 6 h post-MPTP the only region where ROS accumulates is the ME, though there is no change in Nrf2 in the ARC. Since Nrf2 reacts to oxidative stress, the lack of change in Nrf2 is unexpected. Similarly there was no change in the SN, but this is congruent with a lack of change in ROS

in the ST and SN 6 h post-MPTP. The interpretation of these results comes with a few caveats. Changes in Nrf2 expression could be short-lived, as Nrf2 normally has a half-life of less than 20 min (Itoh et al., 2004). In order to measure an accumulation of Nrf2 a proteasome inhibitor would be needed, however this causes its own problems, as a proteasome inhibitor would alter other transcription factors, such as Nrf1. There is also the issue that available Nrf2 antibodies are non-specific, with additional bands present on Western blots. In the case of the antibody used in the present studies, there was one clear band present that was slightly smaller than the 75 kDa weight ladder marker. The predicted size of Nrf2 being 68 kDa, this appeared to be the correct band.

Additional follow-up experiments using available Nrf2KO mice compared to WT C57Blj6 mice was performed to further examine if there is a link between Nrf2 and parkin. In these animals parkin expression was determined to be significantly higher in the Nrf2KO mice in both the ARC and SN. This contradicts earlier predictions that Nrf2 is a transcriptional activator of parkin, but would support the role of Nrf2 as a transcriptional repressor. This is not unprecedented since Nrf2 has been observed to act as a transcriptional repressor of the RON tyrosine kinase receptor in MDA MB 231 cells, derived from mammary tissue (Thangasamy et al., 2011). Though this could be the case, alternatively higher parkin expression in Nrf2KO mice

could be a compensatory mechanism in animals with a life-long deficit of functional Nrf2.

NRF1

Results

Expression of NRF1 protein was unchanged at 6 h post-MPTP in both the ARC and SN. In the ARC, fold change for NRF1 protein in the saline control mice was 1.00 ± 0.24, and 0.84 ± 0.22 for 6 h post-MPTP treated mice (**Figure 4.15**). In the SN, fold change for NRF1 protein in the saline control mice was 1.00 ± 0.19, and 1.06 ± 0.17 for 6 h post-MPTP treated mice (**Figure 4.16**).

Since NRF1 is related to mitochondrial biogenesis and MPP^+ inhibits mitochondrial Complex I activity and produces oxidative stress, ROS was measured as an index of oxidative stress after neurotoxicant exposure using a 2', 7'-dichlorofluorescin diacetate (DCF-DA) assay. In measuring the production of ROS, the only change at 6 h post-MPTP occurred in the ME. At basal levels, the ME had 3458.81 ± 399.02 arbitrary units (au)/μg protein. At 6 h post-MPTP, the ME had 6700.40 ± 1249.46 au/μg protein (**Figure 4.17**). In the ARC, basal levels were 838.60 ± 109.88 au/μg protein, and 1114.14 ± 127.69 at 6 h post-MPTP (**Figure 4.18**). In the ST, basal levels were 459.25 ± 48.50 au/μg protein, and 580.04 ± 68.65 at 6 h post-MPTP

(**Figure 4.19**). In the SN, basal levels were 459.43 ± 43.04 au/µg protein, and 572.65 ± 33.84 at 6 h post-MPTP (**Figure 4.20**).

In addition to comparisons made between vehicle and MPTP treated mice, comparisons were also made between brain regions at basal levels in control mice. Comparing the axon terminal region (ME) to the cell body region (ARC) of the TIDA neurons, the ARC have lower levels of ROS (**Figure 4.21**). Comparing the axon terminal region (ST) to the cell body region (SN) of the NSDA neurons, there was no difference in ROS levels (**Figure 4.22**). In comparing the two sets of axon terminal regions, the ME had higher levels of ROS than the ST (**Figure 4.23**). Comparing the two sets of cell body regions, the ARC had higher levels of ROS than the SN (**Figure 4.24**).

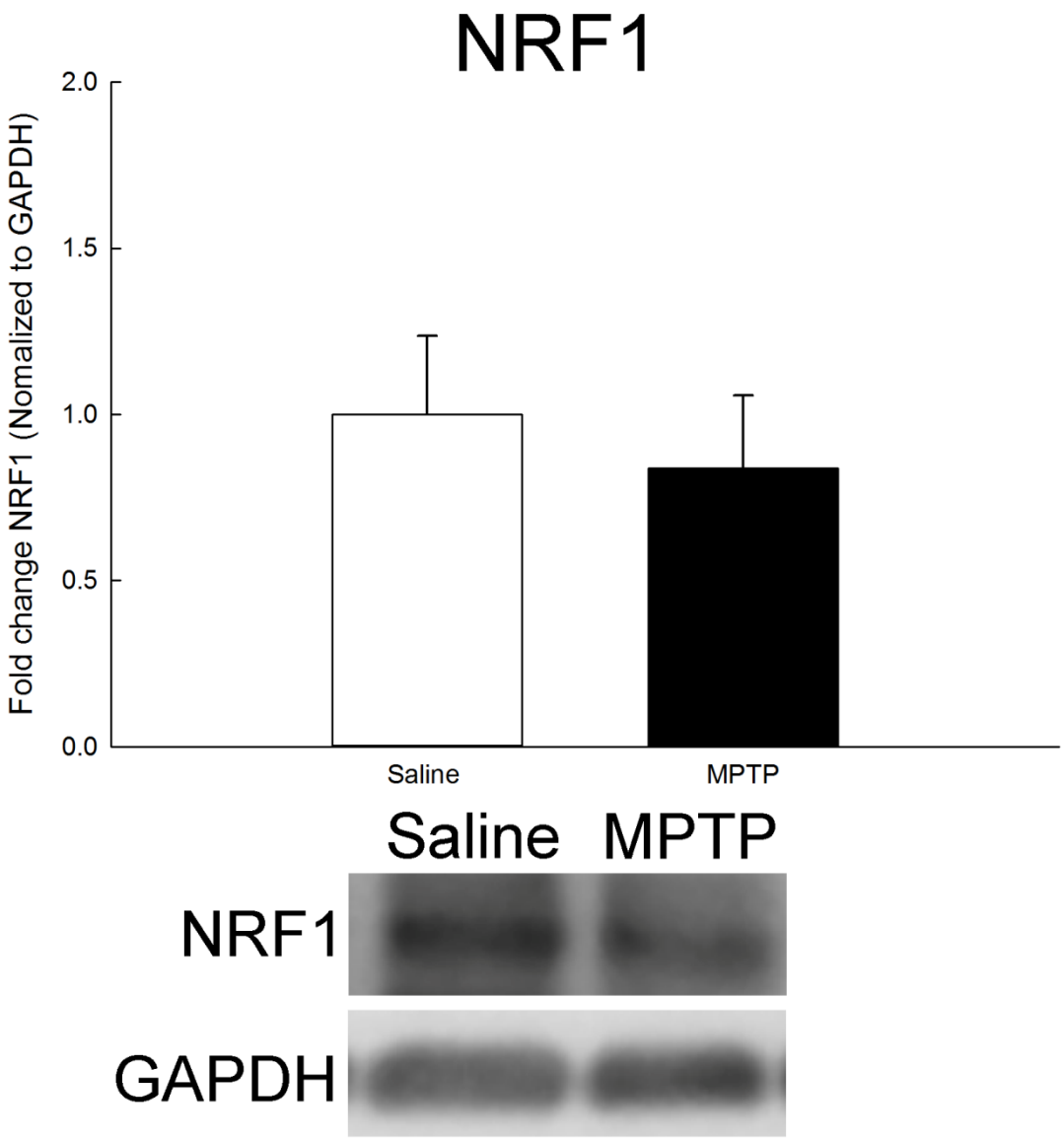

Figure 4.15 Comparison of the effects of MPTP on NRF1 in the ARC of mice. Male C57Bl/6J mice were treated with either saline (10 ml/kg; s.c.) or MPTP (20 mg/kg; s.c.) and killed by decapitation 6 h after injection (n=8/group). Brains were sectioned, ARC were microdissected, protein isolated and Western blots used to quantify NRF1 normalized to GAPDH. Columns indicate the group means, error bars represent +1 standard error of the mean.

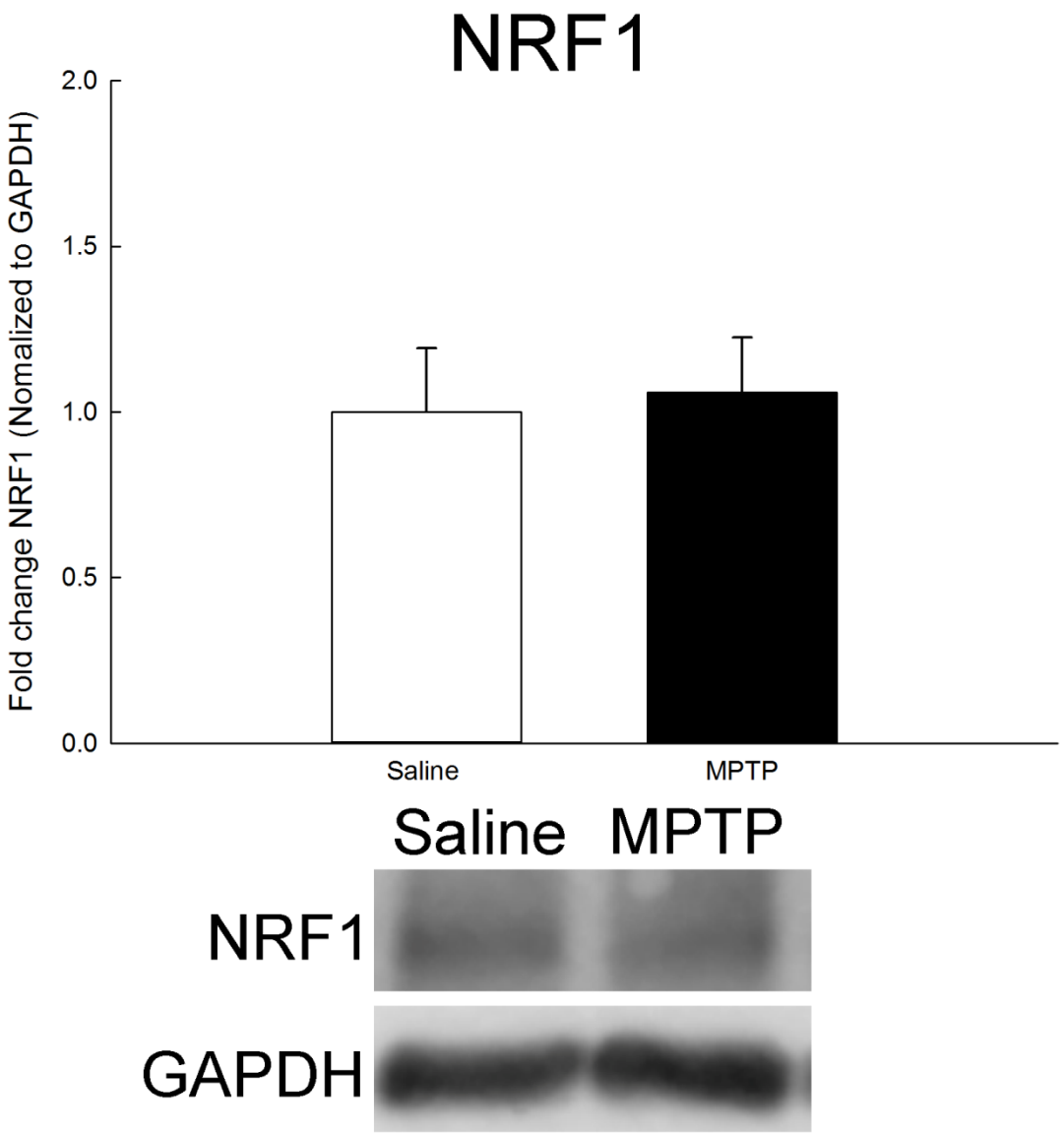

Figure 4.16 Comparison of the effects of MPTP on NRF1 in the SN of mice. Male C57Bl/6J mice were treated with either saline (10 ml/kg; s.c.) or MPTP (20 mg/kg; s.c.) and killed by decapitation 6 h after injection (n=8/group). Brains were sectioned, SN were microdissected, protein isolated and Western blots used to quantify NRF1 normalized to GAPDH. Columns indicate the group means, error bars represent +1 standard error of the mean.

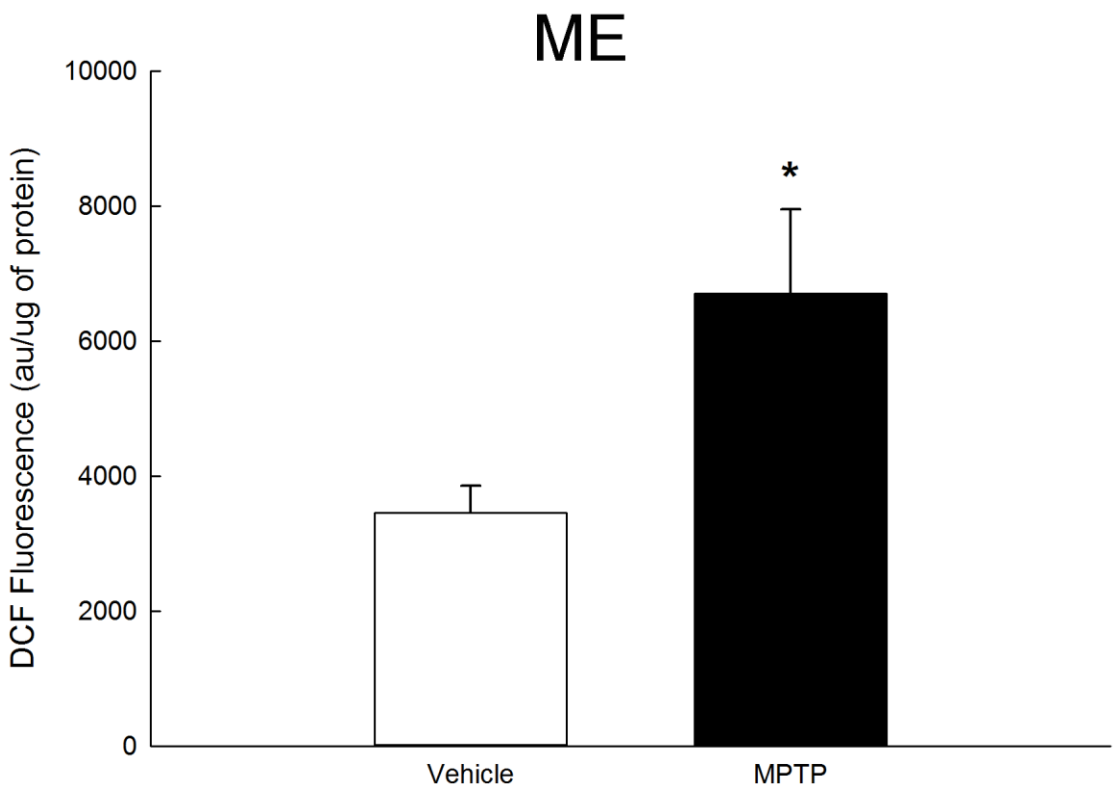

Figure 4.17 Comparison of the effects of MPTP on ROS formation and accumulation in the ME of mice. Male C57Bl/6J mice were treated with either saline (10 ml/kg; s.c.) or MPTP (20 mg/kg; s.c.) and killed by decapitation 6 h after injection (n=8/group). ME were microdissected, protein isolated and a DCF-DA assay was used to quantify fluorescence generated by ROS. Fluorescence was measured in arbitrary units and normalized to protein. Columns indicate the group means, error bars represent +1 standard error of the mean, and significance ($p \leq 0.05$; t-test) is indicated with an asterisk.

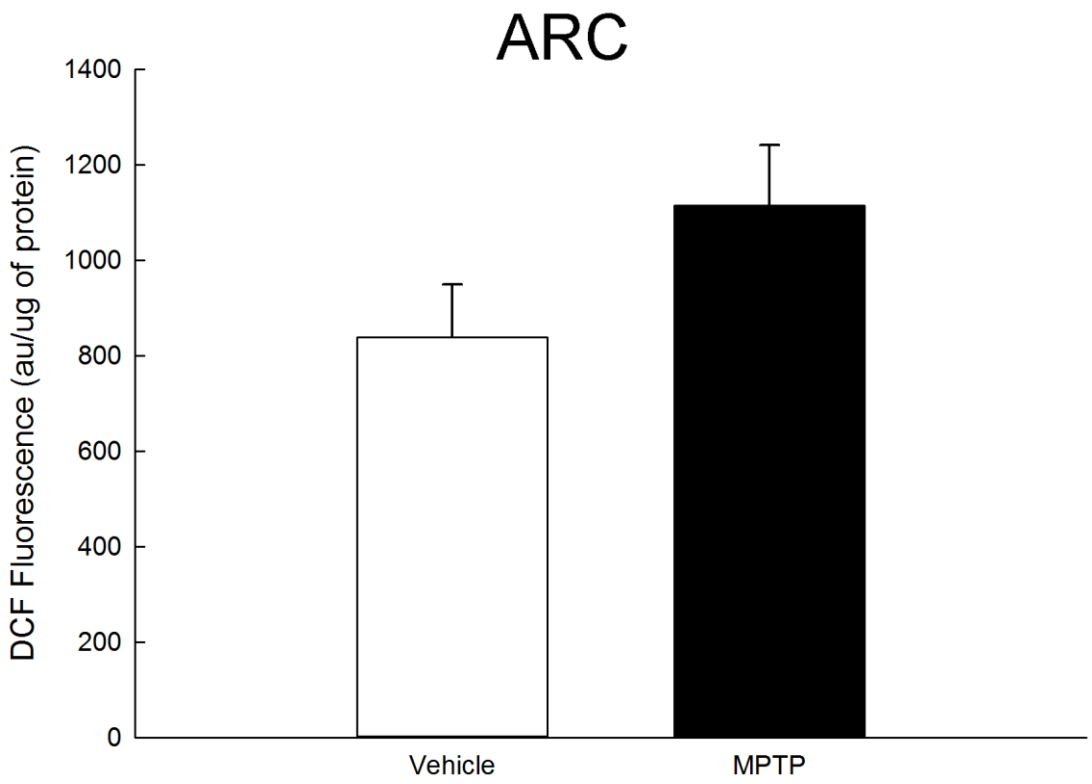

Figure 4.18 Comparison of the effects of MPTP on ROS formation and accumulation in the ARC of mice. Male C57Bl/6J mice were treated with either saline (10 ml/kg; s.c.) or MPTP (20 mg/kg; s.c.) and killed by decapitation 6 h after injection (n=8/group). ARC were microdissected, protein isolated and a DCF-DA assay was used to quantify fluorescence generated by ROS. Fluorescence was measured in arbitrary units and normalized to protein. Columns indicate the group means, error bars represent +1 standard error of the mean.

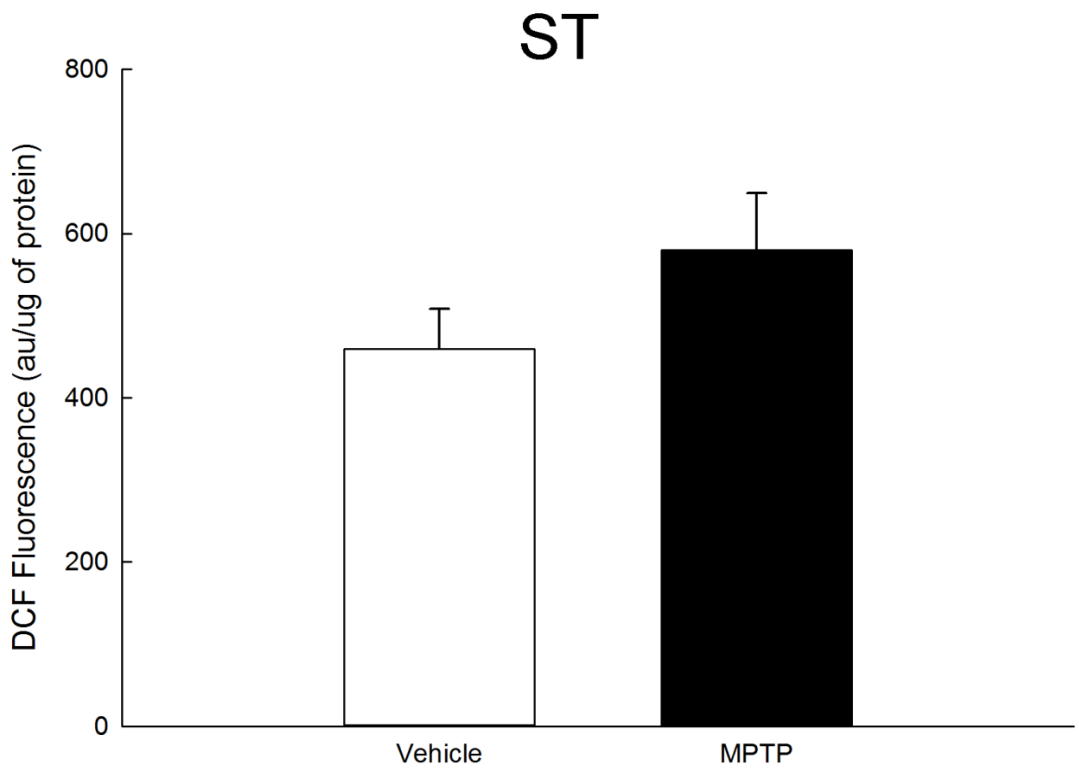

Figure 4.19 Comparison of the effects of MPTP on ROS formation and accumulation in the ST of mice. Male C57Bl/6J mice were treated with either saline (10 ml/kg; s.c.) or MPTP (20 mg/kg; s.c.) and killed by decapitation 6 h after injection (n=8/group). ST were microdissected, protein isolated and a DCF-DA assay was used to quantify fluorescence generated by ROS. Fluorescence was measured in arbitrary units and normalized to protein. Columns indicate the group means, error bars represent +1 standard error of the mean.

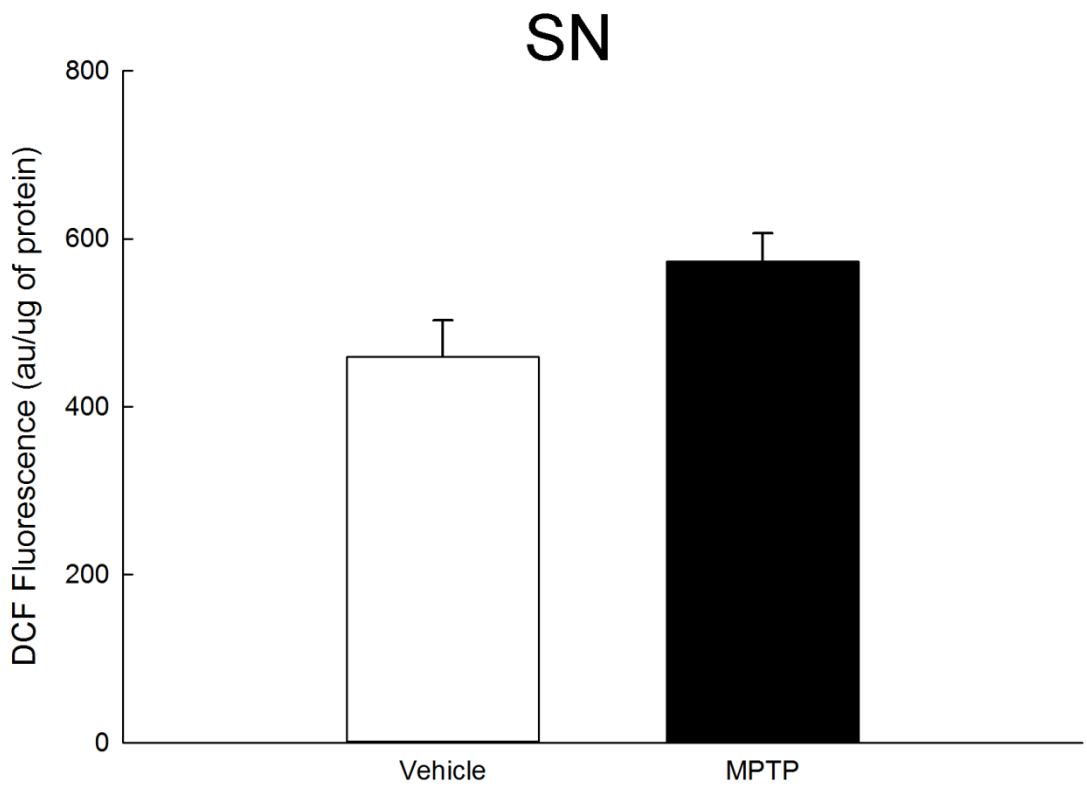

Figure 4.20 Comparison of the effects of MPTP on ROS formation and accumulation in the SN of mice. Male C57Bl/6J mice were treated with either saline (10 ml/kg; s.c.) or MPTP (20 mg/kg; s.c.) and killed by decapitation 6 h after injection (n=8/group). SN were microdissected, protein isolated and a DCF-DA assay was used to quantify fluorescence generated by ROS. Fluorescence was measured in arbitrary units and normalized to protein. Columns indicate the group means, error bars represent +1 standard error of the mean.

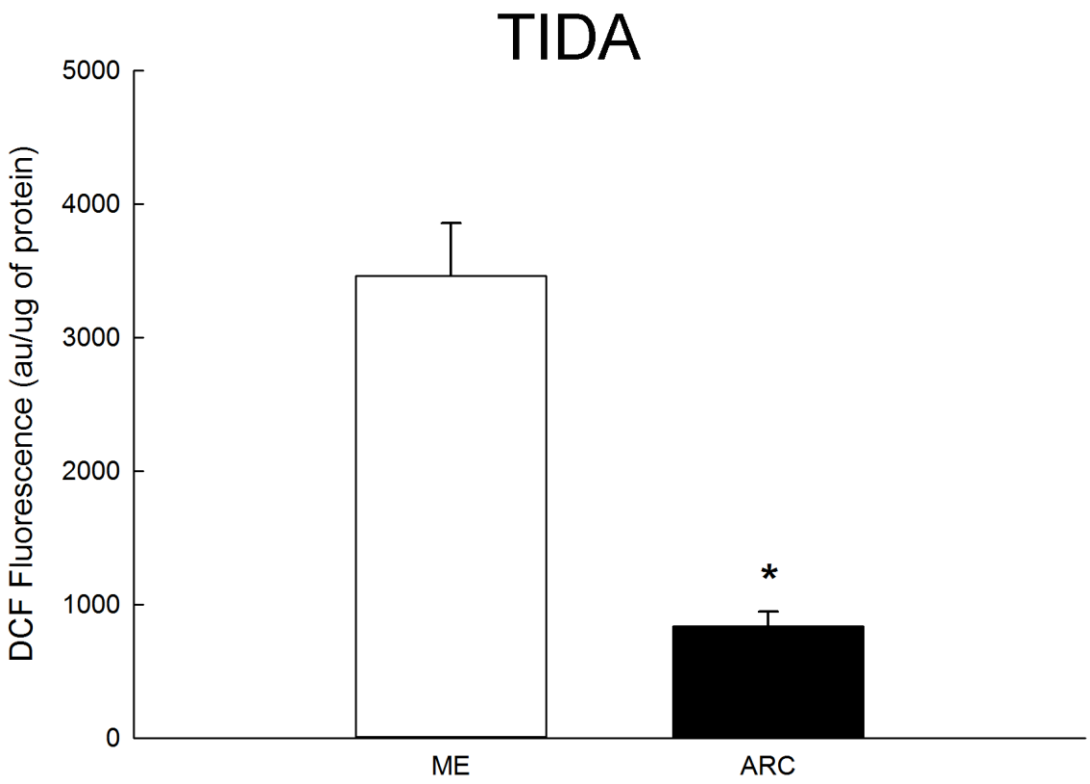

Figure 4.21 Comparison of ROS presence in brain regions containing TIDA neurons. Male C57Bl/6J mice were treated with either saline (10 ml/kg; s.c.) or MPTP (20 mg/kg; s.c.) and killed by decapitation 6 h after injection (n=8/group). ME and ARC were microdissected, protein isolated and a DCF-DA assay was used to quantify fluorescence generated by ROS. Fluorescence was measured in arbitrary units and normalized to protein. Columns indicate the group means, error bars represent +1 standard error of the mean, and significance ($p \leq 0.05$; paired t-test) is indicated with an asterisk.

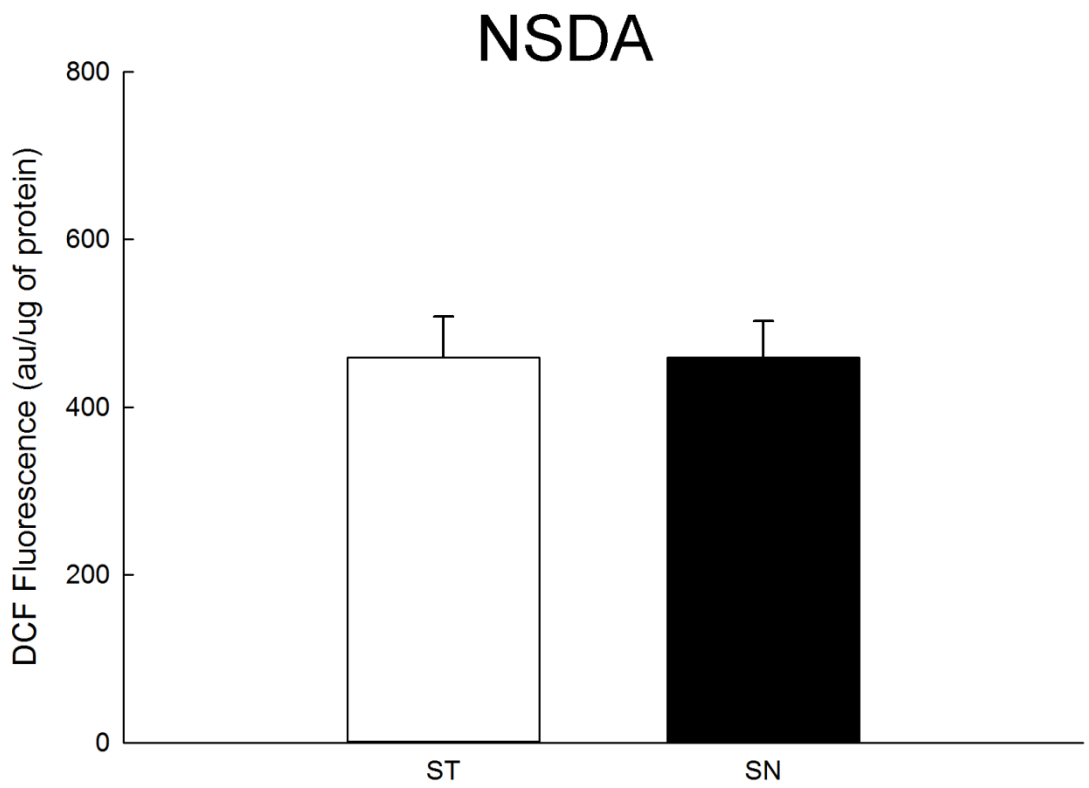

Figure 4.22 Comparison of ROS presence in brain regions containing NSDA neurons. Male C57Bl/6J mice were treated with either saline (10 ml/kg; s.c.) or MPTP (20 mg/kg; s.c.) and killed by decapitation 6 h after injection (n=8/group). ST and SN were microdissected, protein isolated and a DCF-DA assay was used to quantify fluorescence generated by ROS. Fluorescence was measured in arbitrary units and normalized to protein. Columns indicate the group means, error bars represent +1 standard error of the mean.

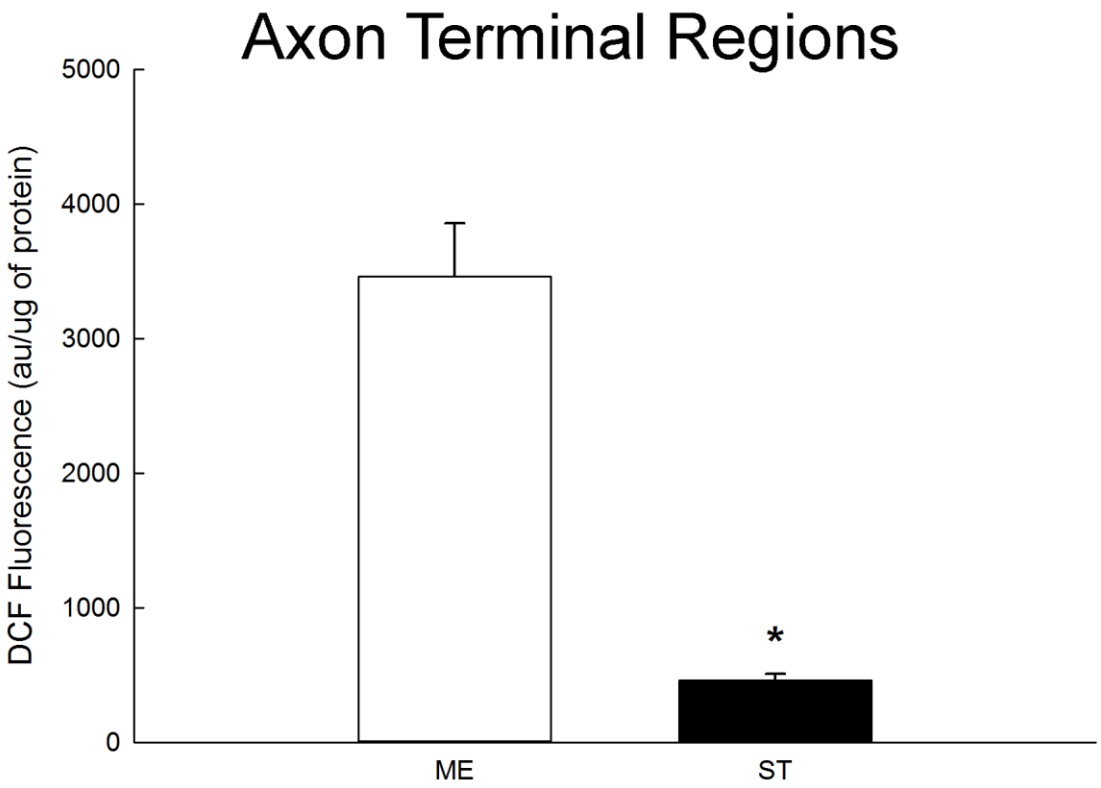

Figure 4.23 Comparison of ROS presence in brain regions containing axon terminals of the TIDA or NSDA neurons. Male C57Bl/6J mice were treated with either saline (10 ml/kg; s.c.) or MPTP (20 mg/kg; s.c.) and killed by decapitation 6 h after injection (n=8/group). ME and ST were microdissected, protein isolated and a DCF-DA assay was used to quantify fluorescence generated by ROS. Fluorescence was measured in arbitrary units and normalized to protein. Columns indicate the group means, error bars represent +1 standard error of the mean, and significance ($p \leq 0.05$; paired t-test) is indicated with an asterisk.

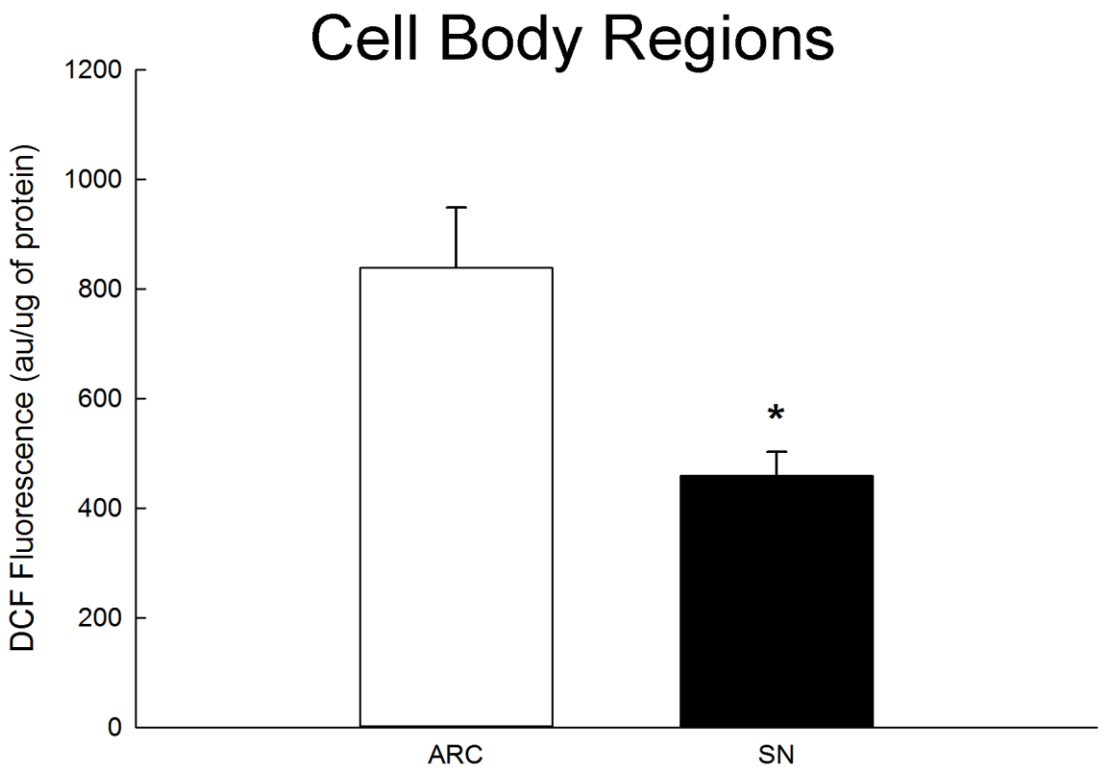

Figure 4.24 Comparison of ROS presence in brain regions containing cell bodies of the TIDA or NSDA neurons. Male C57Bl/6J mice were treated with either saline (10 ml/kg; s.c.) or MPTP (20 mg/kg; s.c.) and killed by decapitation 6 h after injection (n=8/group). ARC and SN were microdissected, protein isolated and a DCF-DA assay was used to quantify fluorescence generated by ROS. Fluorescence was measured in arbitrary units and normalized to protein. Columns indicate the group means, error bars represent +1 standard error of the mean, and significance ($p \leq 0.05$; paired t-test) is indicated with an asterisk.

Discussion

The lack of any observed change of NRF1 in either the ARC or SN does not rule out the possibility of NRF1 being a transcription factor of parkin. Rather, it suggests that NRF1 is probably not involved in initiating the increased expression of parkin in the ARC in response to acute neurotoxicant exposure. NRF1 was measured at 6 h post-MPTP, though this is enough time for MPP^+ to accumulate in the axon terminals and for DA stores to be depleted (Behrouz et al., 2007; Benskey et al., 2012), it may not be enough time for mitochondrial damage and induction of mitochondrial biogenesis to occur. Since mitochondria damaged by MPP^+ should lead to increased ROS accumulation and oxidative stress, ROS levels were examined in the present study. The only region where ROS levels increase at 6 h post-MPTP is the ME. This is possibly because the axon terminals of the TIDA neurons are located outside the blood-brain barrier and as such were exposed to higher levels of MPP^+ than the NSDA neurons (Benskey et al., 2012). Interestingly, levels of ROS are higher in both the cell body and axon terminal regions of the TIDA neurons as compared to the NSDA neurons. This suggest that the TIDA neurons are normally predisposed to compensate for higher levels of oxidative stress and expression of parkin may play a role in this process.

It is possible that NRF1 expression changes at later time-points after MPTP, possibly due to mitochondrial biogenesis or as a downstream effect of parkin. Rather than NRF1 initiating parkin expression, it is possible that the

changes in parkin expression could alter NRF1 via PARIS-PGC-1α (Shin et al., 2011). In the ARC increased parkin could lead to decreased PARIS, increased PGC-1α, and as an effect, increased NRF1. The opposite would be expected to occur in the SN, where decreased parkin could lead to increased PARIS, which would negatively regulate PGC-1α and either decrease or maintain NRF1 expression. If this is the case, it is possible that parkin and NRF1 are acting in a feed-forward loop, where parkin is initiating NRF1 expression, and NRF1 acts to increase parkin, until either parkin or NRF1 expression returns to basal levels.

SRY

Results

Expression of SRY protein was unchanged at 6 h post-MPTP in both the ARC and SN. In the ARC, fold change for SRY protein in the saline control mice was 1.00 ± 0.21, and 3.18 ± 0.30 for 6 h post-MPTP treated mice (**Figure 4.25**). In the SN, fold change for SRY protein in the saline control mice was 1.00 ± 0.07, and 0.72 ± 0.21 for 6 h post-MPTP treated mice (**Figure 4.26**).

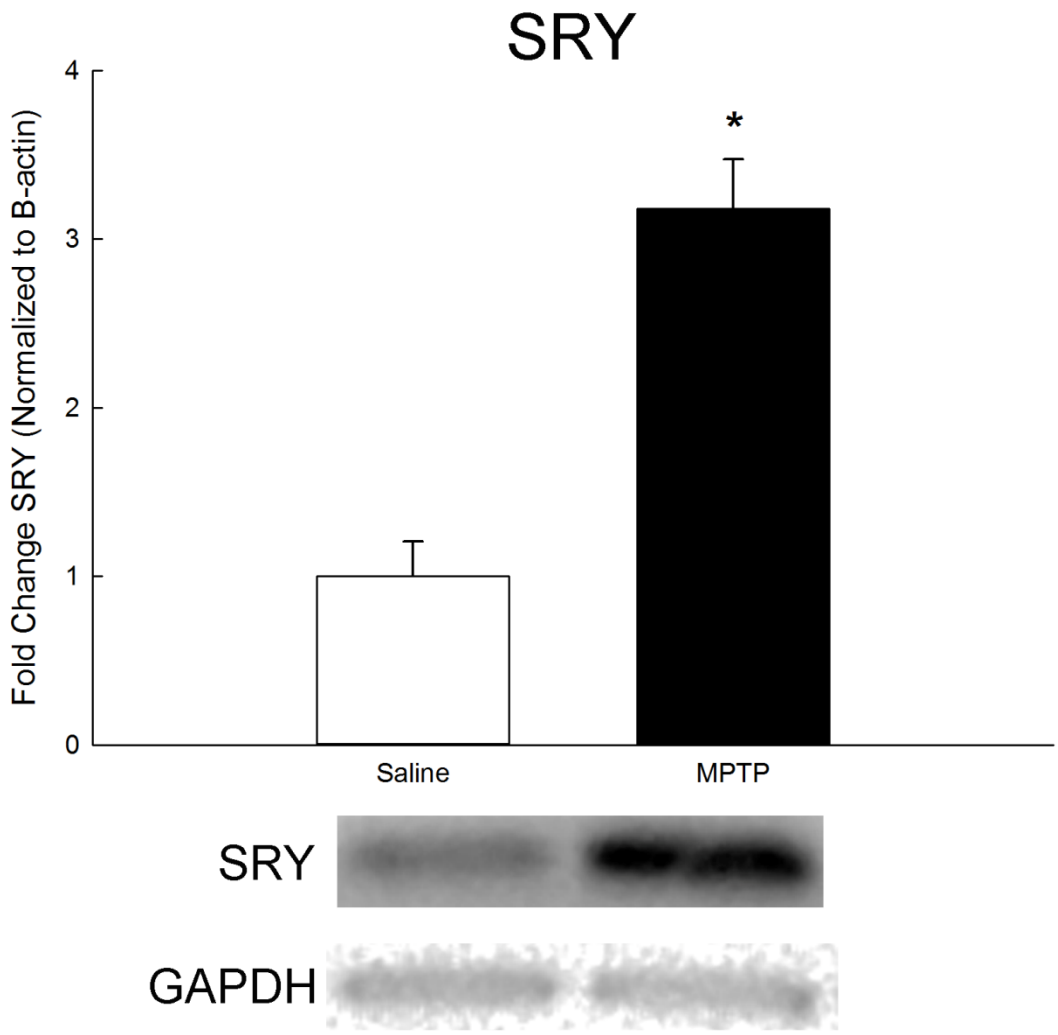

Figure 4.25 Comparison of the effects of MPTP on SRY in the ARC of mice. Male C57Bl/6J mice were treated with either saline (10 ml/kg; s.c.) or MPTP (20 mg/kg; s.c.) and killed by decapitation 6 h after injection (n=8/group). Brains were sectioned, ARC were microdissected, protein isolated and Western blots used to quantify SRY normalized to β-actin. Columns indicate the group means, error bars represent +1 standard error of the mean. An asterisk indicates values that are significantly different ($p < 0.05$; t-test) from vehicle-treated controls.

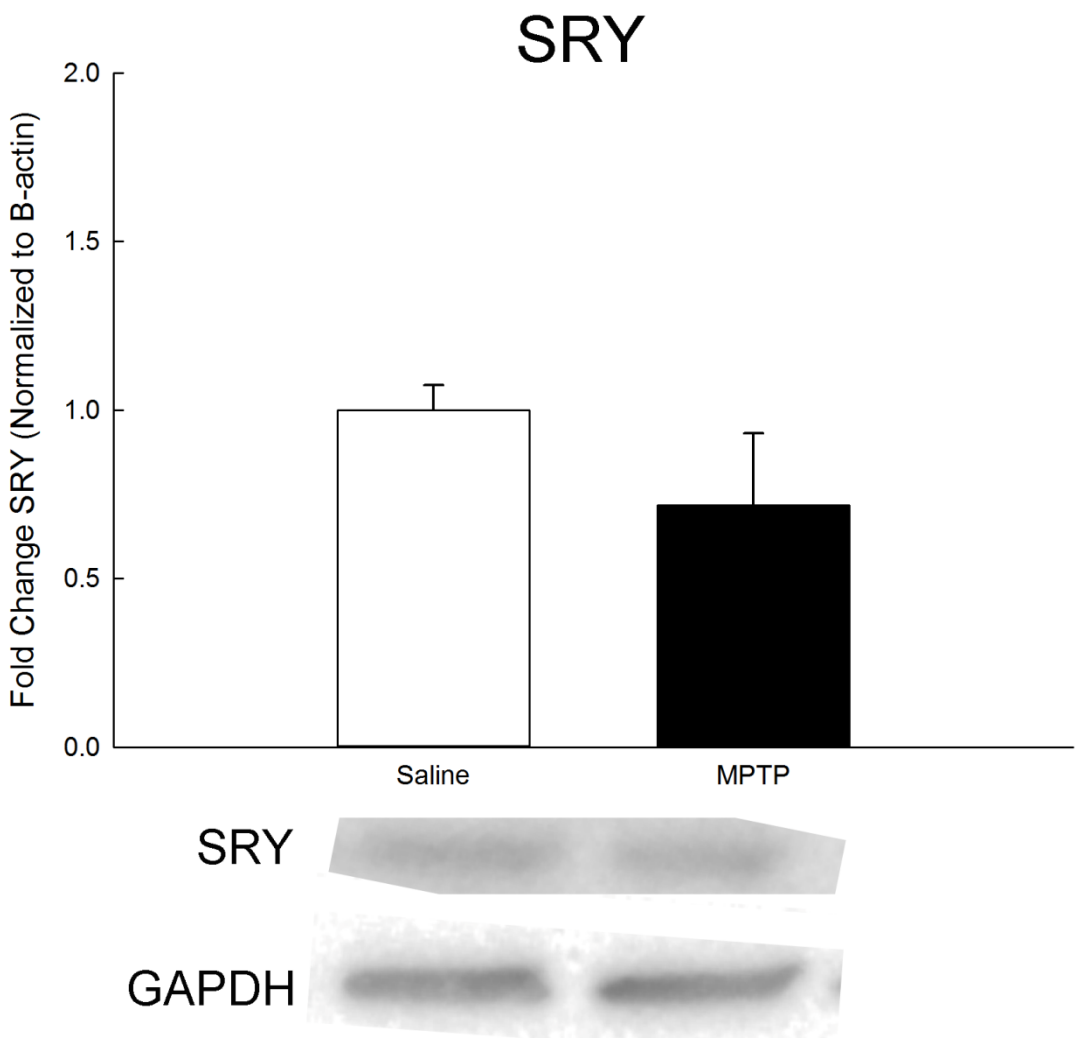

Figure 4.26 Comparison of the effects of MPTP on SRY in the SN of mice. Male C57Bl/6J mice were treated with either saline (10 ml/kg; s.c.) or MPTP (20 mg/kg; s.c.) and killed by decapitation 6 h after injection (n=8/group). Brains were sectioned, SN were microdissected, protein isolated and Western blots used to quantify SRY normalized to β-actin. Columns indicate the group means, error bars represent +1 standard error of the mean.

Discussion

SRY had potential to be a transcriptional regulator of parkin, as it has been shown to be in DA neurons and interact with the same DNA sites as AP-1 transcription factors (Dewing et al., 2006; Milsted et al., 2004). Expression of SRY appears to mirror parkin expression, i.e., SRY increases in the ARC and not the SN 6 h post-MPTP exposure. The specificity of the antibody however does pose an issue. Initial trials of the antibody for Western blots used tissue from both male and female specific mouse tissue (testis, ovaries and brains from each examined), with a faint band at the predicted size of 24 kDa only present in the tissue from male mice. The issue is the antibodies commercially available were raised in mice and the secondary antibody recognizes mouse antibodies. The band at 24 kDa assumed to initially be SRY also was present in controls where the primary antibodies were not added to the blots. This also is the approximate weight of light chain IgG in mice, which is most likely what was measured in these experiments, instead of SRY.

Although this suggests that SRY appears to be absent or not at a measureable level in the brain regions examined, it does suggest that there is an immune response that occurs in the ARC at 6 h post-MPTP that does not occur in the SN. If the band in light chain IgG, the increase in the ARC may be due to its position outside of the blood-brain barrier, where the TIDA axon terminals are exposed to circulating blood in the hypophyseal portal

system. Regardless, SRY does not appear to be a strongly expressed protein and there are better candidates available, additionally significantly more optimization of SRY would be required for further studies involving this protein.

AP-1

Results

The AP-1 transcription factors examined were c-Fos, c-Jun, FosB, ΔFosB, JunD, and ΔJunD. In the ARC, fold change for c-Fos protein in the saline control mice was 1.00 ± 0.06, and 1.14 ± 0.12 for 6 h post-MPTP treated mice (**Figure 4.27**). In the SN, fold change for c-Fos protein in the saline control mice was 1.00 ± 0.05, and 0.95 ± 0.18 for 6 h post-MPTP treated mice (**Figure 4.28**). Fold change for c-Jun protein in the the ARC of saline control mice was 1.00 ± 0.16, and 0.96 ± 0.20 for 6 h post-MPTP treated mice (**Figure 4.29**). In the SN, fold change c-Jun protein in the saline control mice was 1.00 ± 0.18, and 1.07 ± 0.22 in 6 h post-MPTP treated mice (**Figure 4.30**).

Expression of FosB and ΔFosB increased after MPTP, but only in the ARC. Fold change for FosB protein in the saline control mice was 1.00 ± 0.11, and 4.67 ± 0.14 for 6 h post-MPTP treated mice (**Figure 4.31**). In the SN, fold change for FosB protein in the saline control mice was 1.00 ± 0.06, and 1.13 ± 0.07 for 6 h post-MPTP treated mice (**Figure 4.32**). Fold change for ΔFosB

protein in the ARC of saline control mice was 1.00 ± 0.07, and 2.60 ± 0.12 for 6 h post-MPTP treated mice (Figure 4.33). In the SN, fold change for ΔFosB protein in the saline control mice was 1.00 ± 0.05, and 1.07 ± 0.08 for 6 h post-MPTP treated mice (Figure 4.34).

JunD and ΔJunD are the predominant binding partners of FosB and ΔFosB. In the ARC, fold change for JunD protein in the saline control mice was 1.00 ± 0.15, and 0.88 ± 0.12 for 6 h post-MPTP treated mice (Figure 4.35). In the SN, fold change for JunD protein in the saline control mice was 1.00 ± 0.22, and 0.86 ± 0.21 for 6 h post-MPTP treated mice (Figure 4.36). Fold change for ΔJunD protein in the ARC of saline control mice was 1.00 ± 0.17, and 0.63 ± 0.11 for 6 h post-MPTP treated mice (Figure 4.37). In the SN, fold change for ΔJunD protein in the saline control mice was 1.00 ± 0.22, and 0.77 ± 0.20 for 6 h post-MPTP treated mice (Figure 4.38).

Another potential factor is the ratio of ΔJunD to JunD, since ΔJunD is a dominant negative protein and will inhibit the function of any basic leucine zipper transcription factor that dimerizes with it (ref). The ΔJunD/JunD ratio in the ARC was 0.23 ± 0.04 in the saline control mice and 0.19 ± 0.02 at 6 h post-MPTP. In the SN, the ΔJunD/JunD was 0.47 ± 0.04 in the saline control mice and 0.42 ± 0.02 at 6 h post-MPTP (Figure 4.39 and 4.40). Though there was no change in the ratio after MPTP administration within each region, the ΔJunD/JunD ratio in the SN was about twice as high than in the ARC (Figure 4.39).

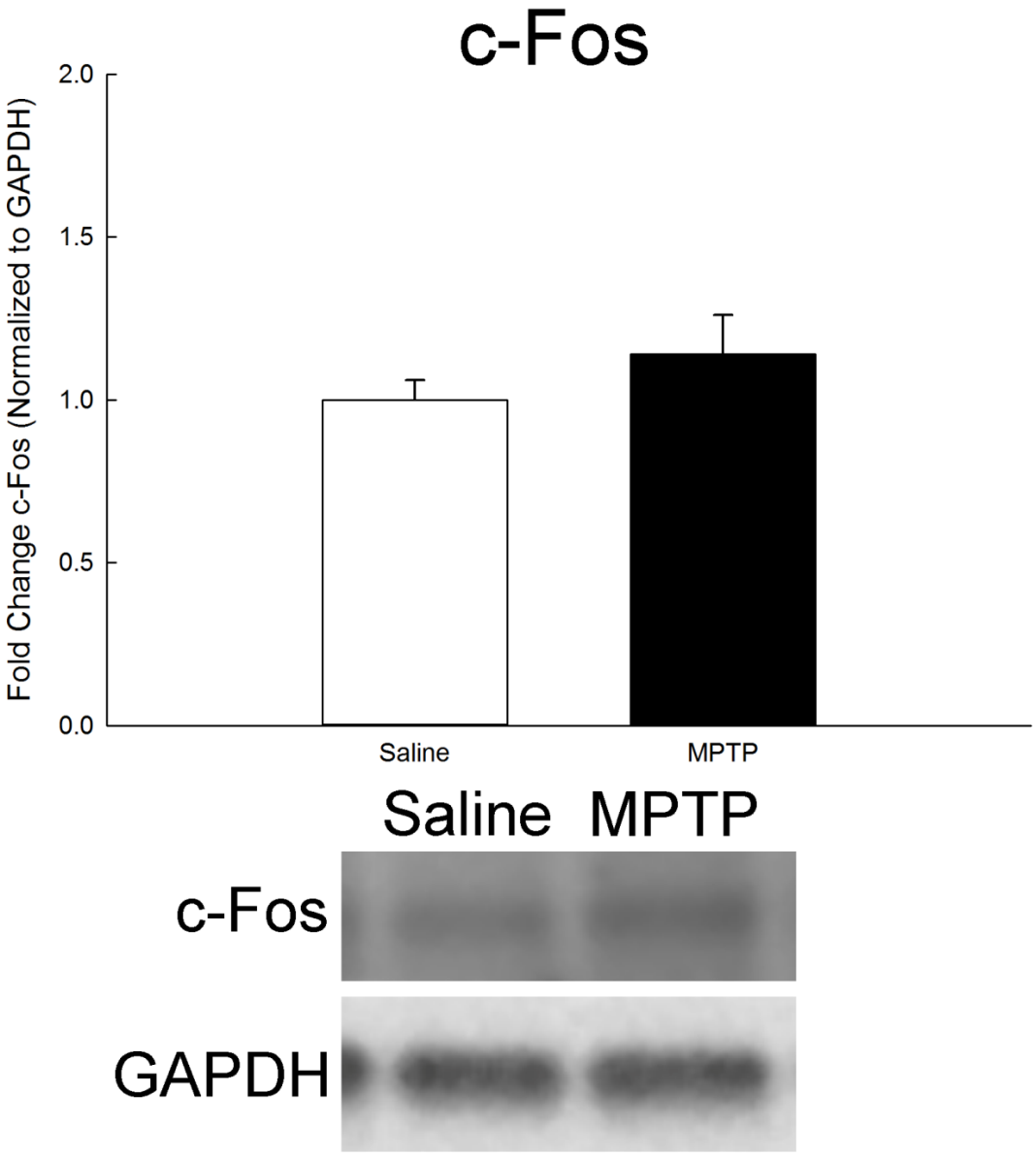

Figure 4.27 Comparison of the effects of MPTP on c-Fos in the ARC of mice. Male C57Bl/6J mice were treated with either saline (10 ml/kg; s.c.) or MPTP (20 mg/kg; s.c.) and killed by decapitation 6 h after injection (n=8/group). Brains were sectioned, ARC were microdissected, protein isolated and Western blots used to quantify c-Fos normalized to GAPDH. Columns indicate the group means, error bars represent +1 standard error of the mean.

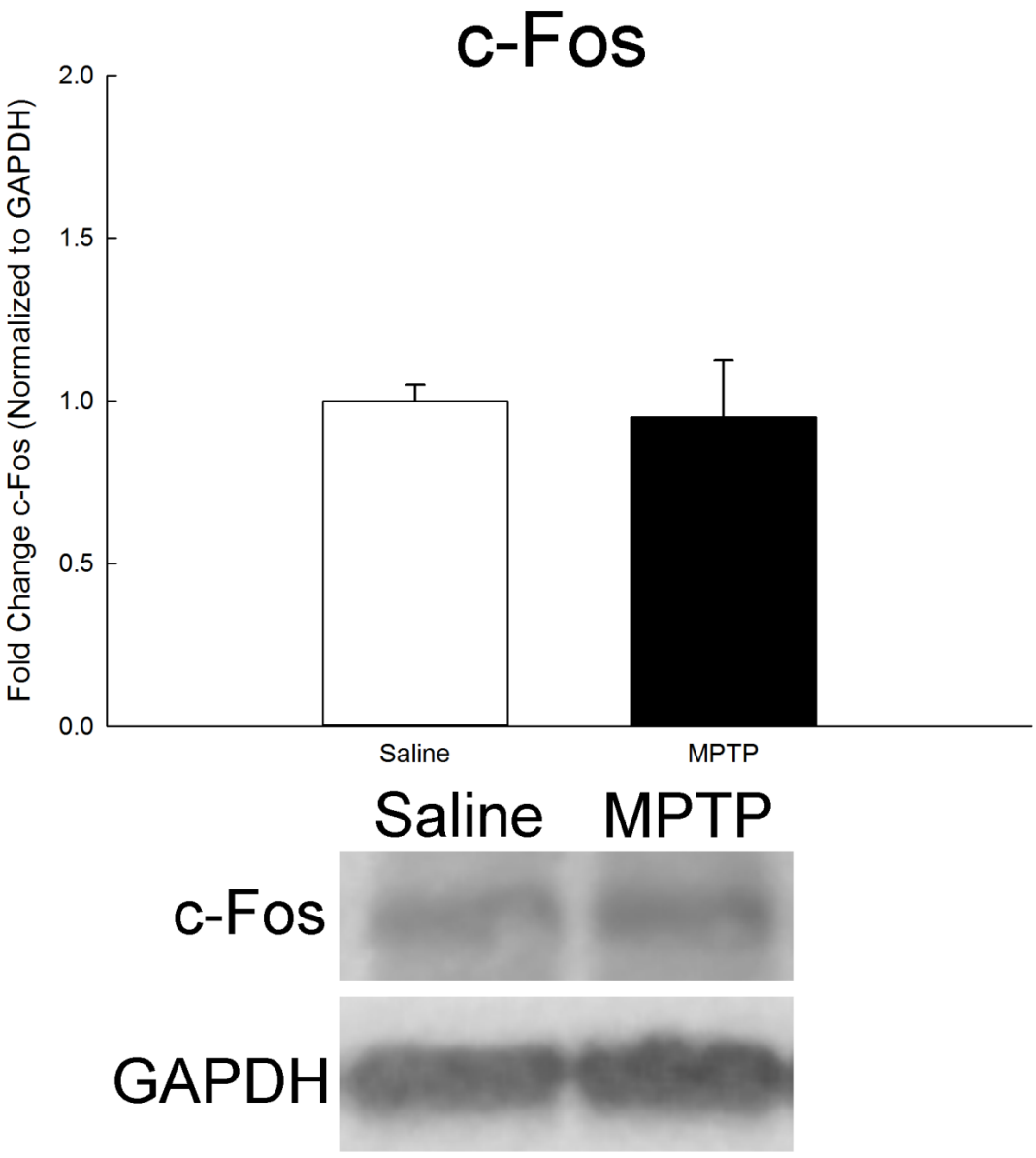

Figure 4.28 Comparison of the effects of MPTP on c-Fos in the SN of mice. Male C57Bl/6J mice were treated with either saline (10 ml/kg; s.c.) or MPTP (20 mg/kg; s.c.) and killed by decapitation 6 h after injection (n=8/group). Brains were sectioned, SN were microdissected, protein isolated and Western blots used to quantify c-Fos normalized to GAPDH. Columns indicate the group means, error bars represent +1 standard error of the mean.

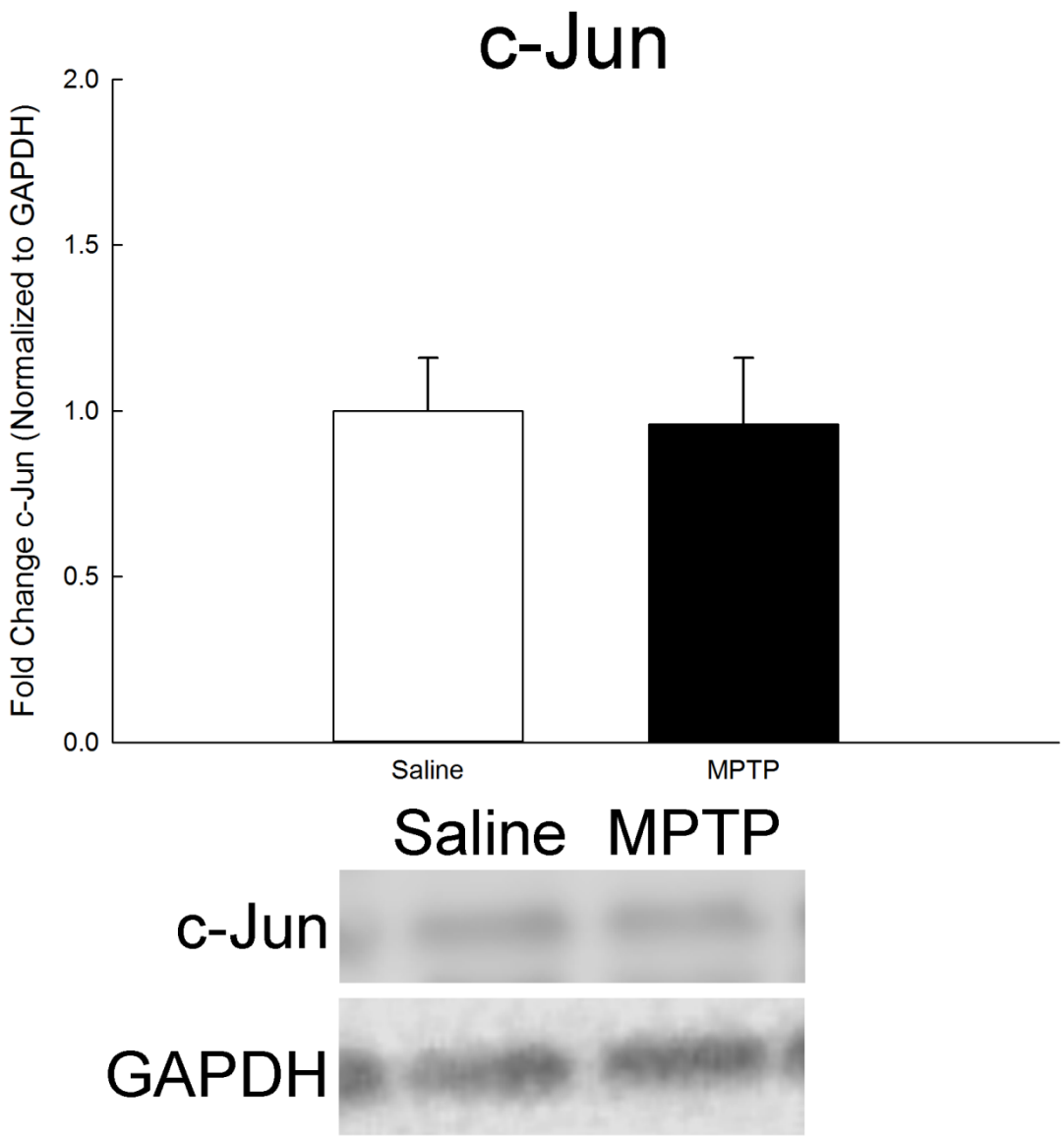

Figure 4.29 Comparison of the effects of MPTP on c-Jun in the ARC of mice. Male C57Bl/6J mice were treated with either saline (10 ml/kg; s.c.) or MPTP (20 mg/kg; s.c.) and killed by decapitation 6 h after injection (n=8/group). Brains were sectioned, ARC were microdissected, protein isolated and Western blots used to quantify c-Jun normalized to GAPDH. Columns indicate the group means, error bars represent +1 standard error of the mean.

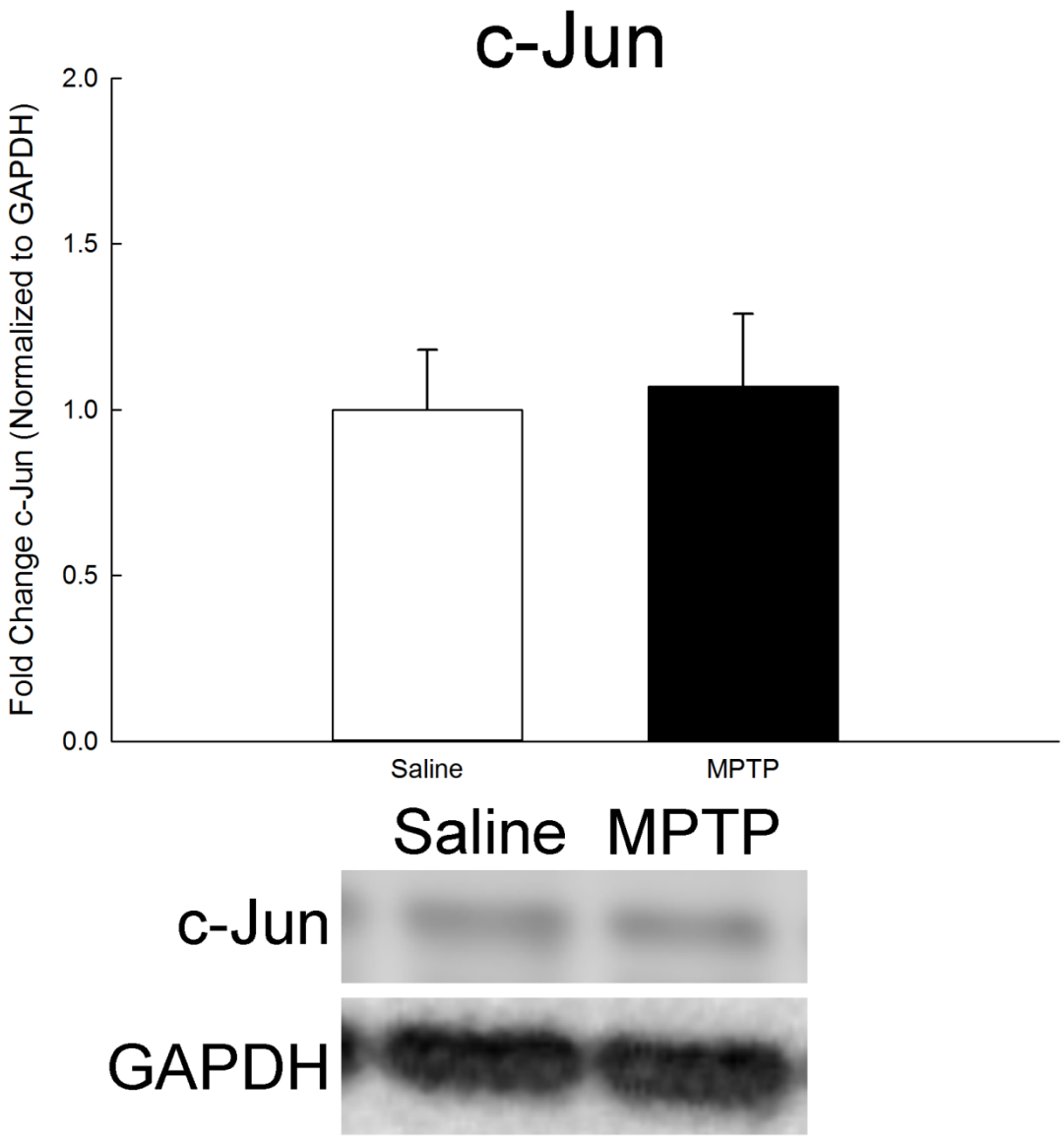

Figure 4.30 Comparison of the effects of MPTP on c-Jun in the SN of mice. Male C57Bl/6J mice were treated with either saline (10 ml/kg; s.c.) or MPTP (20 mg/kg; s.c.) and killed by decapitation 6 h after injection (n=8/group). Brains were sectioned, SN were microdissected, protein isolated and Western blots used to quantify c-Jun normalized to GAPDH. Columns indicate the group means, error bars represent +1 standard error of the mean.

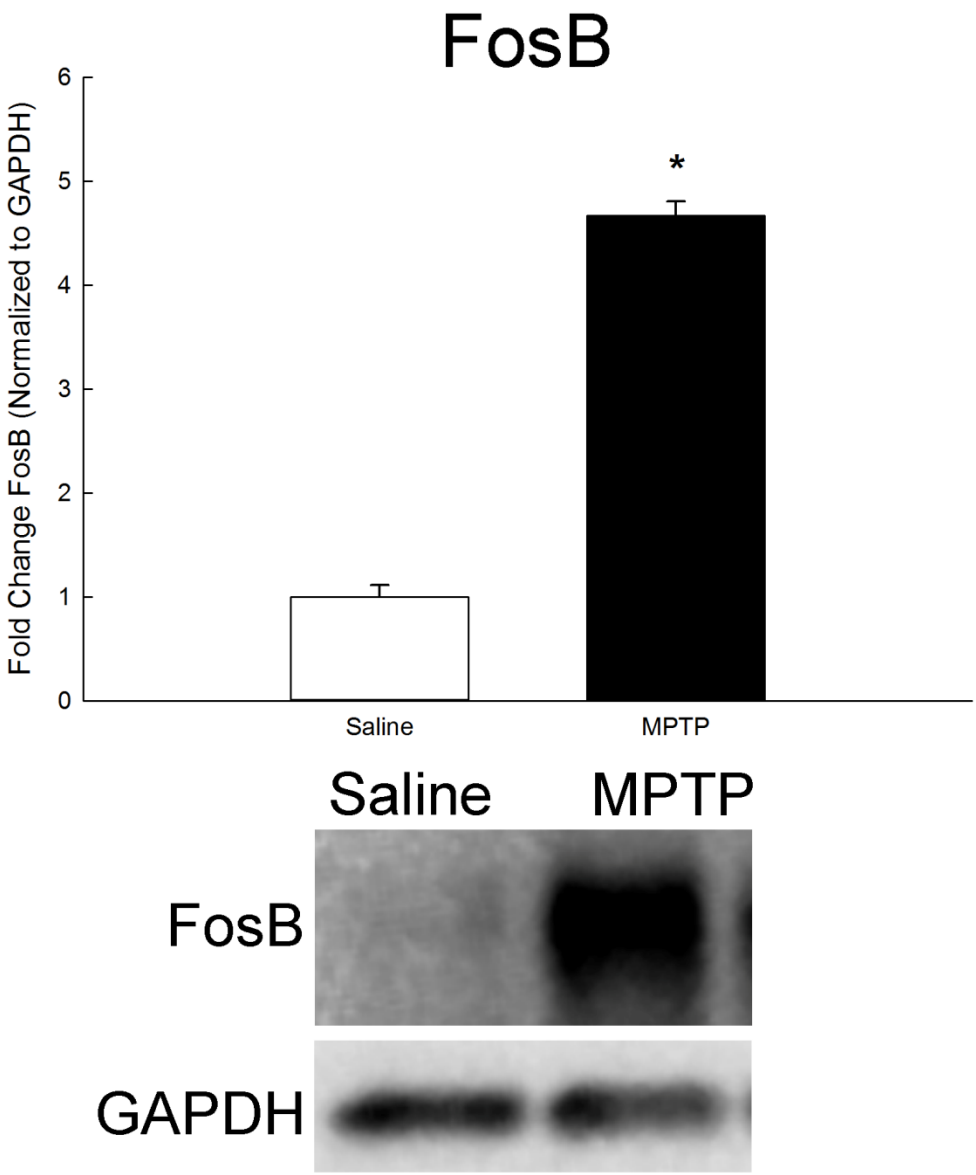

Figure 4.31 Comparison of the effects of MPTP on FosB in the ARC of mice. Male C57Bl/6J mice were treated with either saline (10 ml/kg; s.c.) or MPTP (20 mg/kg; s.c.) and killed by decapitation 6 h after injection (n=8/group). Brains were sectioned, ARC were microdissected, protein isolated and Western blots used to quantify FosB normalized to GAPDH. Columns indicate the group means, error bars represent +1 standard error of the mean. An asterisk indicates values that are significantly different ($p < 0.05$; t-test) from vehicle-treated controls.

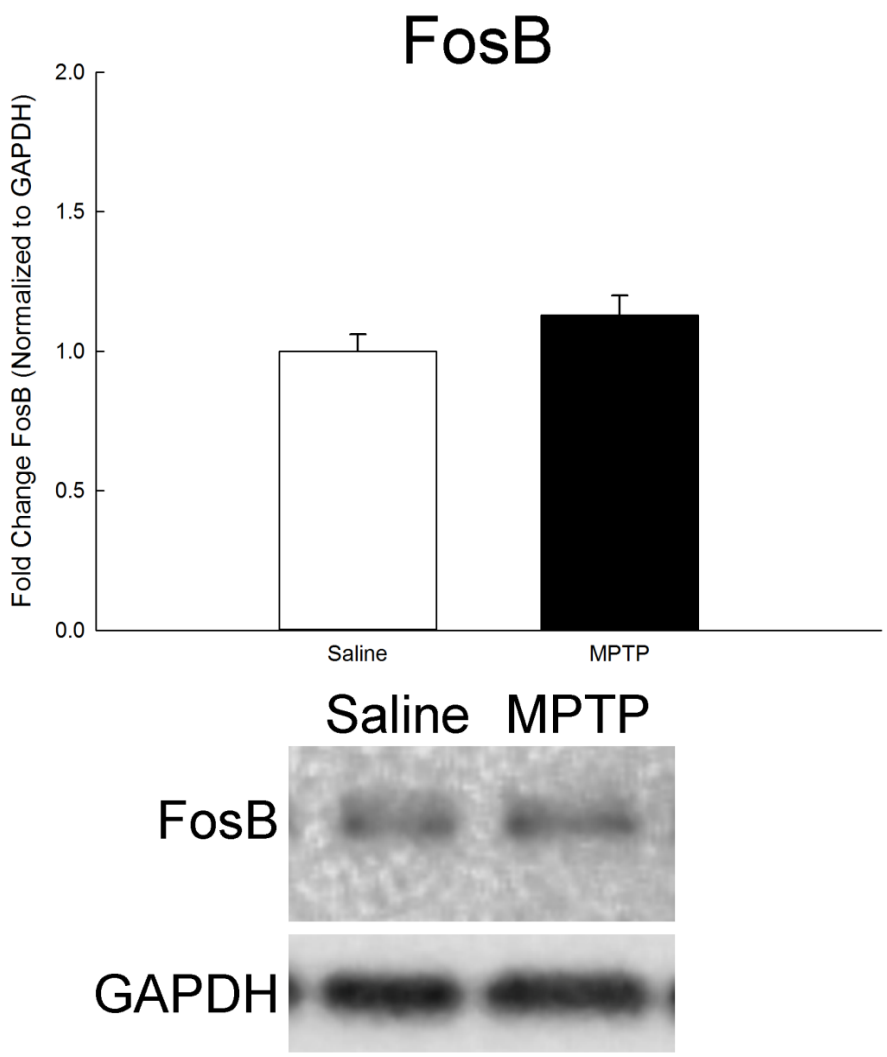

Figure 4.32 Comparison of the effects of MPTP on FosB in the SN of mice. Male C57Bl/6J mice were treated with either saline (10 ml/kg; s.c.) or MPTP (20 mg/kg; s.c.) and killed by decapitation 6 h after injection (n=8/group). Brains were sectioned, SN were microdissected, protein isolated and Western blots used to quantify FosB normalized to GAPDH. Columns indicate the group means, error bars represent +1 standard error of the mean.

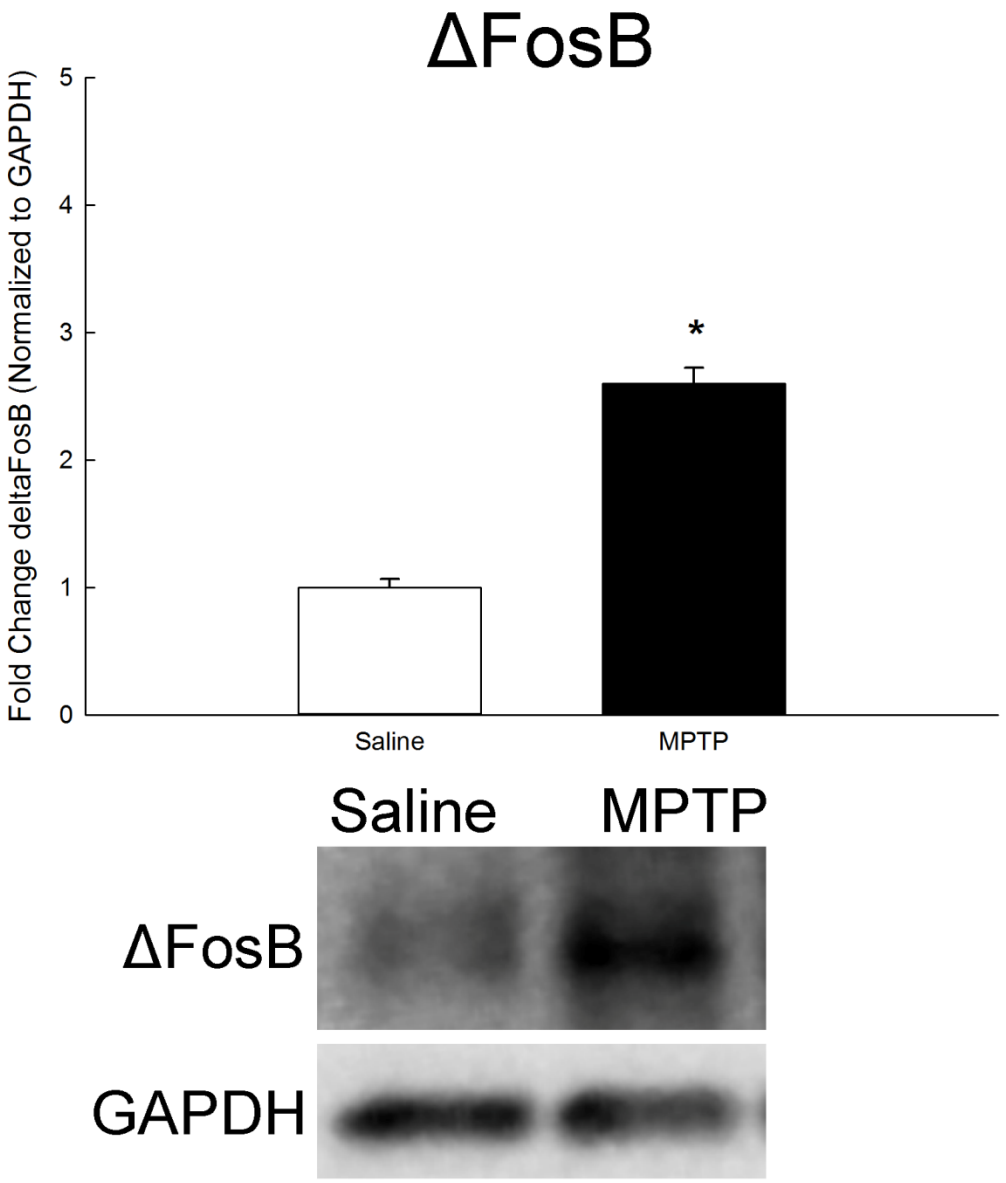

Figure 4.33 Comparison of the effects of MPTP on ΔFosB in the ARC of mice. Male C57Bl/6J mice were treated with either saline (10 ml/kg; s.c.) or MPTP (20 mg/kg; s.c.) and killed by decapitation 6 h after injection (n=8/group). Brains were sectioned, ARC were microdissected, protein isolated and Western blots used to quantify ΔFosB normalized to GAPDH. Columns indicate the group means, error bars represent +1 standard error of the mean. An asterisk indicates values that are significantly different ($p < 0.05$; t-test) from vehicle-treated controls.

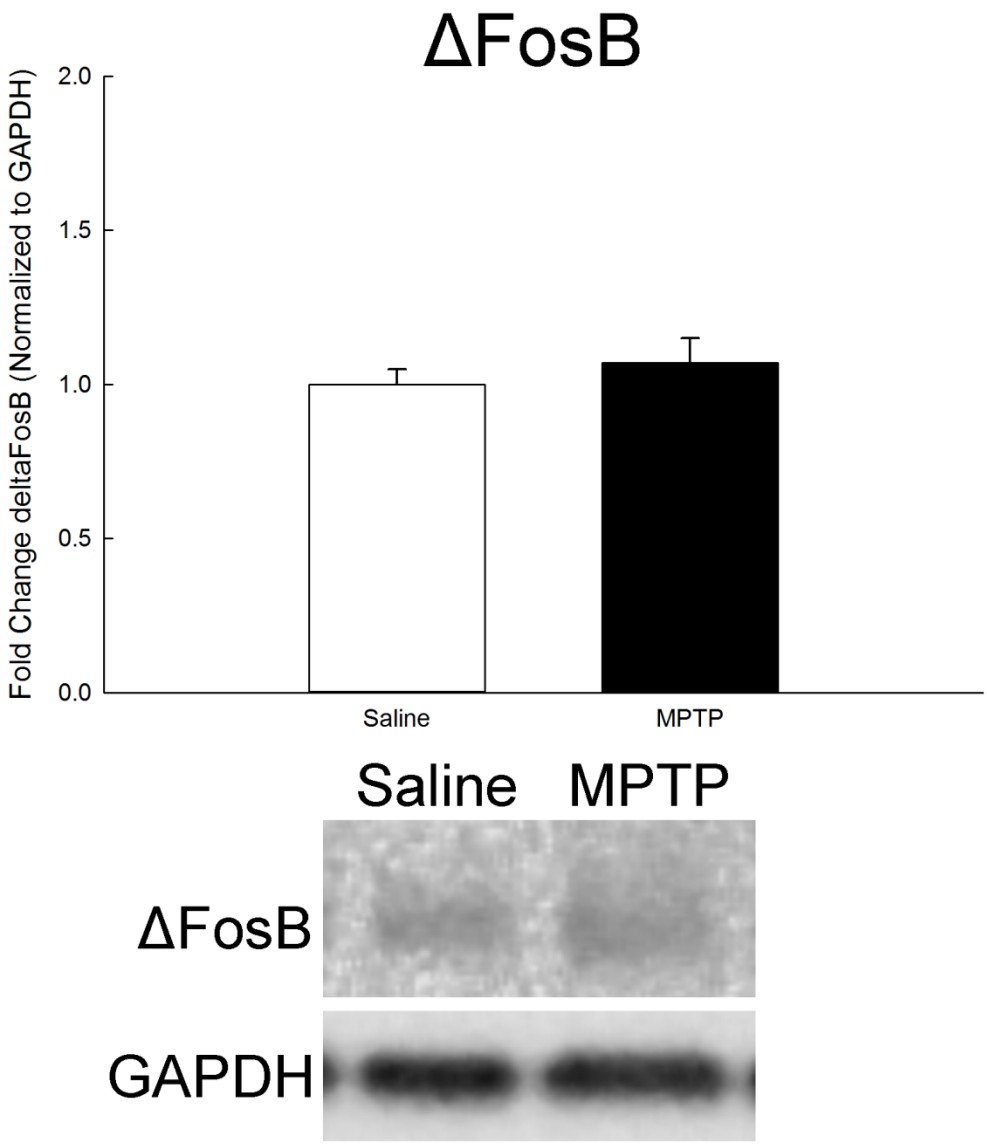

Figure 4.34 Comparison of the effects of MPTP on ΔFosB in the SN of mice. Male C57Bl/6J mice were treated with either saline (10 ml/kg; s.c.) or MPTP (20 mg/kg; s.c.) and killed by decapitation 6 h after injection (n=8/group). Brains were sectioned, SN were microdissected, protein isolated and Western blots used to quantify ΔFosB normalized to GAPDH. Columns indicate the group means, error bars represent +1 standard error of the mean.

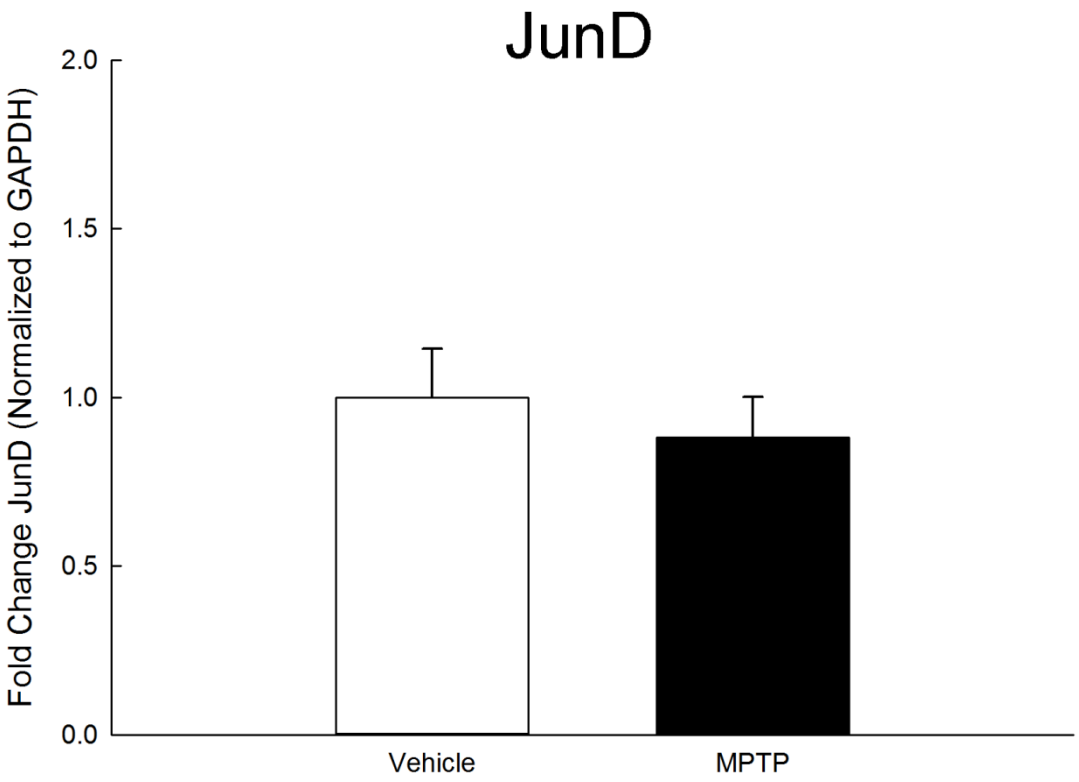

Figure 4.35 Comparison of the effects of MPTP on JunD in the ARC of mice. Male C57Bl/6J mice were treated with either saline (10 ml/kg; s.c.) or MPTP (20 mg/kg; s.c.) and killed by decapitation 6 h after injection (n=8/group). Brains were sectioned, ARC were microdissected, protein isolated and Western blots used to quantify JunD normalized to GAPDH. Columns indicate the group means, error bars represent +1 standard error of the mean.

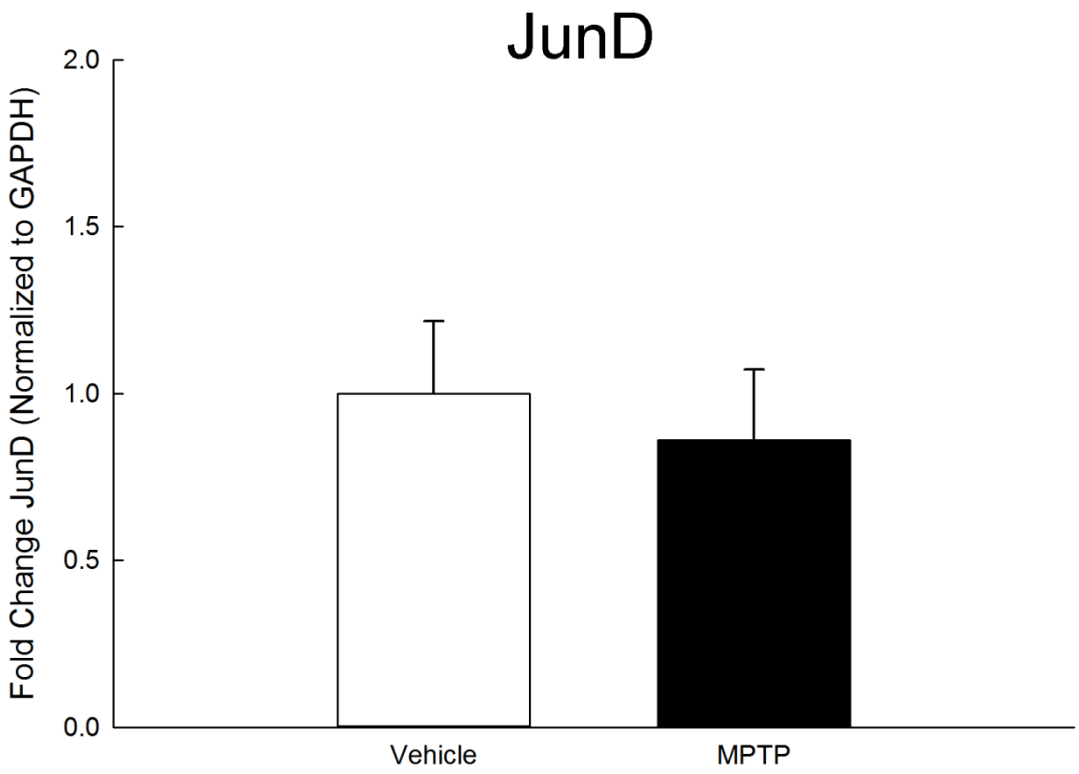

Figure 4.36 Comparison of the effects of MPTP on JunD in the SN of mice. Male C57Bl/6J mice were treated with either saline (10 ml/kg; s.c.) or MPTP (20 mg/kg; s.c.) and killed by decapitation 6 h after injection (n=8/group). Brains were sectioned, SN were microdissected, protein isolated and Western blots used to quantify JunD normalized to GAPDH. Columns indicate the group means, error bars represent +1 standard error of the mean.

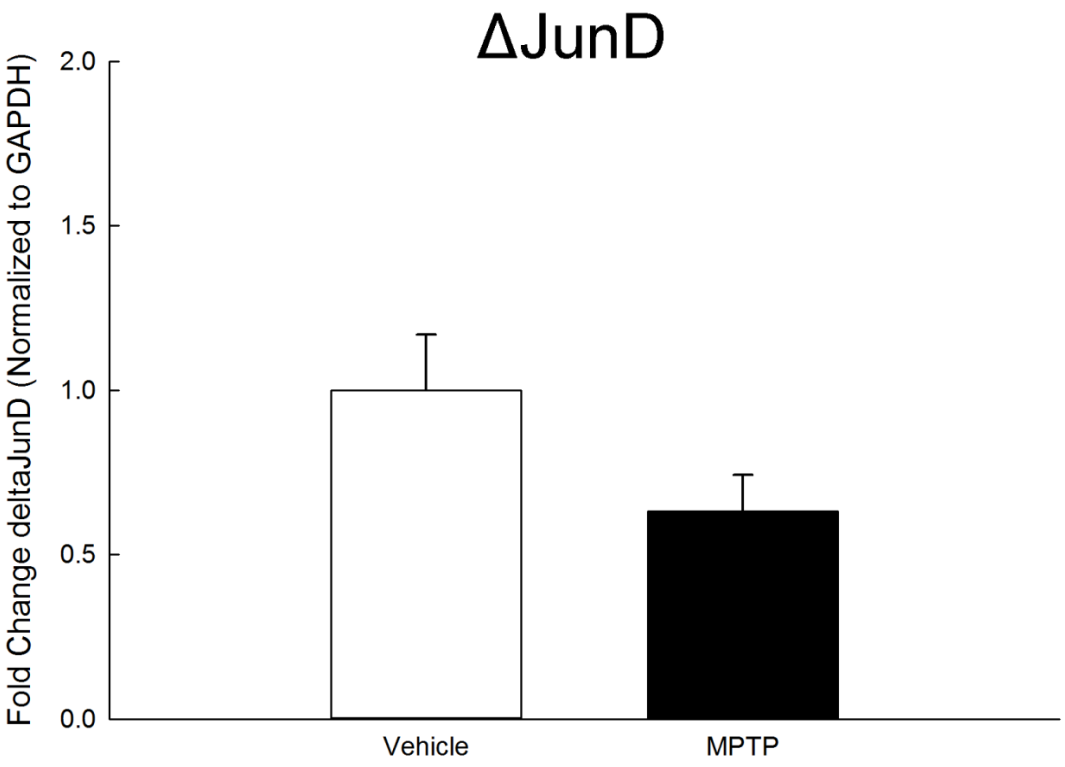

Figure 4.37 Comparison of the effects of MPTP on ΔJunD in the ARC of mice. Male C57Bl/6J mice were treated with either saline (10 ml/kg; s.c.) or MPTP (20 mg/kg; s.c.) and killed by decapitation 6 h after injection (n=8/group). Brains were sectioned, ARC were microdissected, protein isolated and Western blots used to quantify ΔJunD normalized to GAPDH. Columns indicate the group means, error bars represent +1 standard error of the mean.

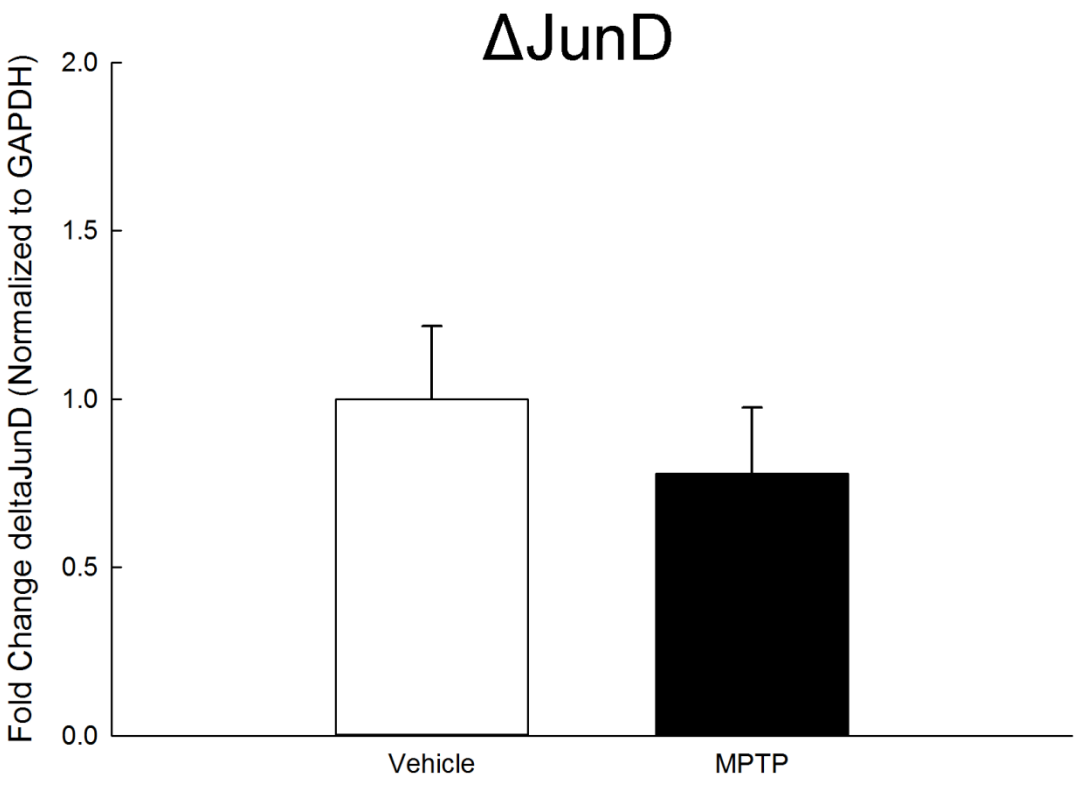

Figure 4.38 Comparison of the effects of MPTP on ΔJunD in the SN of mice. Male C57Bl/6J mice were treated with either saline (10 ml/kg; s.c.) or MPTP (20 mg/kg; s.c.) and killed by decapitation 6 h after injection (n=8/group). Brains were sectioned, SN were microdissected, protein isolated and Western blots used to quantify ΔJunD normalized to GAPDH. Columns indicate the group means, error bars represent +1 standard error of the mean.

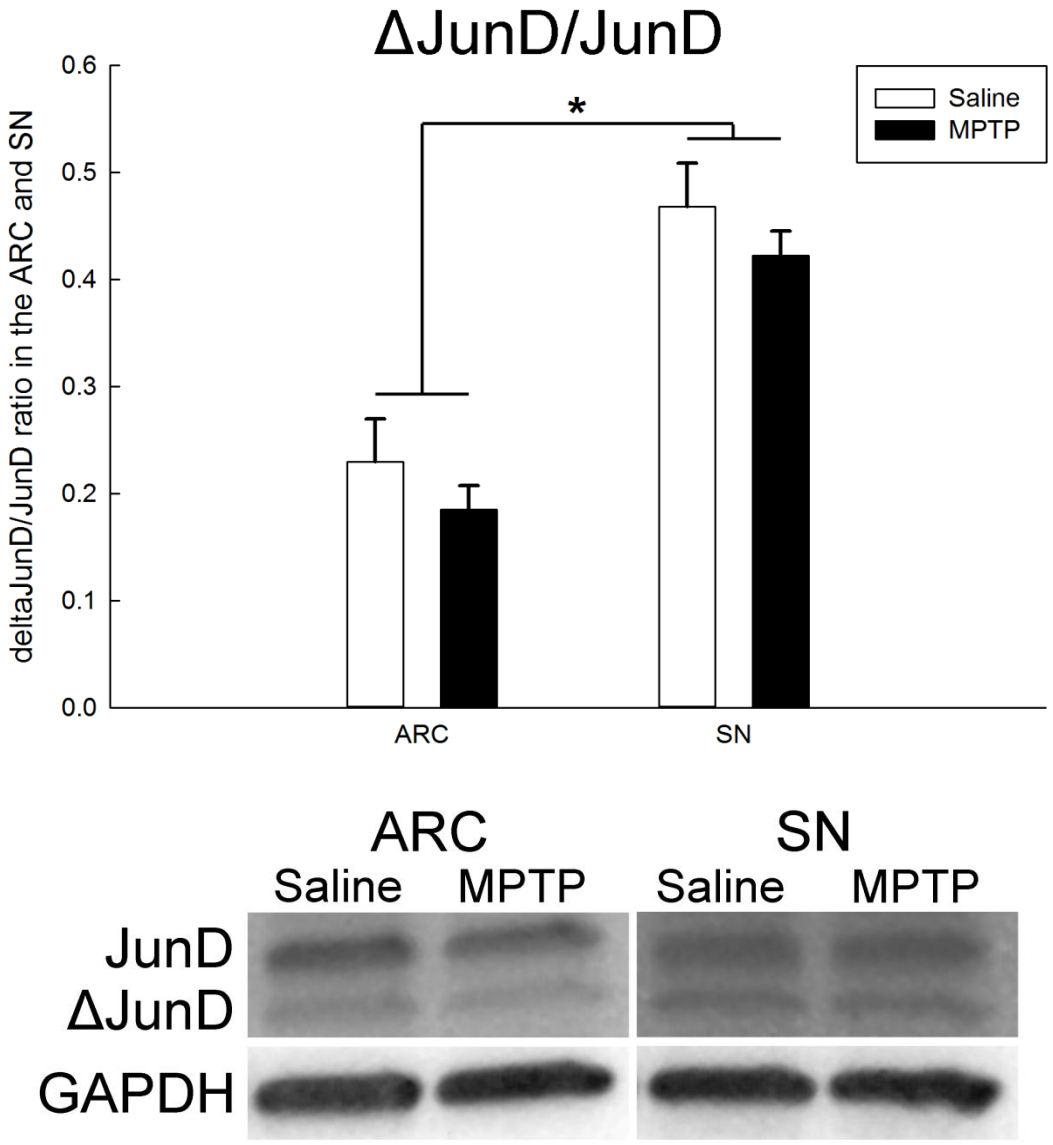

Figure 4.39 Comparison of the effects of MPTP on the ratio of ΔJunD/JunD in the ARC and SN of mice. Male C57Bl/6J mice were treated with either saline (10 ml/kg; s.c.) or MPTP (20 mg/kg; s.c.) and sacrificed 6 h after injection (n=8/group). Brains were sectioned, ARC and SN were microdissected, protein isolated and Western blots used to quantify JunD and ΔJunD. Columns indicate the group means, error bars represent +1 standard error of the mean. An asterisk indicates values that are significantly different ($p < 0.05$; t-test) from vehicle-treated controls.

Discussion

Within the group of AP-1 proteins examined in the present study, only FosB and ΔFosB are responsive to MPTP, and only in the ARC. The MPTP-induced increase in FosB and ΔFosB expression in the ARC corresponds with activation of parkin expression and sparing of TIDA neurons located in this brain region (Behrouz et al, 2007; Benskey et al., 2012; 2013; 2015). Additionally, neither FosB or ΔFosB expression were altered in the SN following MPTP, which corresponds with a lack of effect of this neurotoxicant on parkin expression and the higher susceptibility of NSDA neurons located in this region to degeneration following neurotoxicant exposure and degeneration in PD (Behrouz et al, 2007; Matzuk et al., 1985; Heikkila et al., 1984; Benskey et al., 2012, 2013, 2015)

Previous studies reported that FosB/ΔFosB protein and mRNA expression are increased in the ST following MPTP exposure (Perez-Otano et al., 1998). MPTP exposure paradigms used in these studies required more aggressive toxicant exposure (e.g., multiple repeated doses of MPTP) to observe any changes in striatal ΔFosB expression (Perez-Otano et al., 1998; Potashkin et al., 2007). Most likely the changes in FosB occur in medium spiny neurons of the striatum, perhaps in response to axonopathy of NSDA neurons and loss of DA receptor-mediated regulation of these neurons (Gerfen et al., 2011; Albin et al., 1989).

The expression of c-Fos and c-Jun were previously reported to increase the SN following multiple or high doses of MPTP (Duchemin et al., 1992; Nishi, 1997; Chen et al., 2001). These high dose MPTP paradigms are more severe than the acute single injection paradigm used in these experiments, which could explain why no increases in c-Fos or c-Jun were observed in the SN. In contrast to FosB and ΔFosB, the expression of c-Fos or c-Jun does not change in the ARC at any of the times examined in response to MPTP. It is possible however that expression of these immediate early transcription factors increases prior to the 6 h time-point. Additionally, phosphorylation of c-Fos, c-Jun, or both may occur to modulate activity independent of steady state levels of these transcription factors to promote parkin transcription.

Though JunD and ΔJunD expression do not change at 6 h post-MPTP in the ARC or the SN, they are still relevant proteins that are potential transcription factors of parkin. JunD dimerizes with FosB or ΔFosB to produce a functional transcription factor. Lack of change in JunD suggests that it is present at sufficient levels to dimerize with FosB. ΔJunD also can bind to the FosBs, however this blocks the ability of the dimer to function as a transcription factor (Berton et al., 2009; Struhl, 1988). Because of this the ratio of ΔJunD to JunD in the ARC and SN are interesting. In the SN the ΔJunD/JunD ratio is twice as high as the ARC. This holds true for in vehicle and MPTP (6h post-injection) samples. These results suggest that the higher

ratio of ΔJunD/JunD in the SN could block or attenuate any effect that the FosBs have in cells in the SN.

Overall Conclusions

From the eleven transcription factors examined at 6 h-post MPTP, FosB and ΔFosB are the best transcription factor candidates to mediate acute neurotoxicant-induced parkin expression. Both FosB and ΔFosB are differentially expressed between the ARC and SN, mirroring parkin expression (only increasing in the ARC and not the SN). Expression of both increase prior to parkin, as would be expected of a transcription factor that is initiating the differential expression of parkin. ΔFosB expression also has the potential to last as long as parkin expression. The half-life of ΔFosB *in vitro* is greater than eight days and MPTP-induced ΔFosB in the ST is elevated for at least seven days (Chen et al., 1997; Perez-Otano et al., 1998). The long-term expression of ΔFosB, as well as its nature to accumulate could potentially explain long-term parkin expression in the ARC after chronic MPTP exposure (Nestler, 2001; Kelz et al., 1999; Benskey et al., 2013). To further examine the potential of FosB and ΔFosB as transcriptional activators of parkin, further analysis of their temporal expression patterns and cellular localization is required.

Chapter 5: Examination of FosB/ΔFosB Expression and Localization in the ARC and SN

Introduction

In the analyses of putative parkin promoter transcription factors 6 h post-MPTP, only the expression of FosB and ΔFosB is confirmed to be correlated with parkin expression, i.e., increasing in the ARC but not in the SN. FosB and ΔFosB have previously been shown to increase in the ST after multiple doses of MPTP, but not in the SN (Pérez-Otaño et al., 1998; Potashkin et al., 2007). The caveat to this is that these changes are most likely not occurring in the DA neurons, since the cell bodies of these neurons are located in the SN. More likely the changes occur in the post-synaptic medium spiny neurons in response to the disruptive effects of MPTP on the axon terminals of the NSDA neurons in the ST.

FosB and ΔFosB are both encoded in the *FosB* gene. While a full-length transcript produces FosB, ΔFosB is a truncated protein produced through alternative splicing lacking 101 amino acids on the C-terminal end (Nakabeppu and Nathans, 1991). ΔFosB lacks two degron domains, which results in increased stability and accumulation following multiple stimuli (Nakabeppu and Nathans, 1991). ΔFosB stability and transcriptional activity can also be increased through phosphorylation by casein kinase 2 (Ulery et al., 2006; Ulery and Nestler, 2007). The stability and known target genes of

ΔFosB are also known to have a role in drug addiction and desensitization (Nestler, 2008).

Having already examined the expression of FosB, ΔFosB and other AP-1 transcription factors at 6 h post MPTP, a more complete temporal profile of these transcription factors is required. Additionally, as potential transcription factors of parkin, an increase in the nuclei of TIDA neurons in the ARC is predicted, as a transcription factor must be present in the nucleus to interact with DNA.

Temporal Expression of AP-1 Transcription Factors

Results

As with the 6 h post-MPTP results, FosB and ΔFosB proteins are differentially expressed between brain regions. In the ARC, FosB expression increased approximately 3-fold by 4 h post-MPTP and declined to two-fold by 12 and 24 h post-MPTP (**Figures 5.1 and 5.3**). ΔFosB expression also increased by approximately 3-fold by 4 h post-MPTP and this increase was maintained up to 24 h post-MPTP (**Figures 5.2 and 5.3**). Although both FosB and ΔFosB are present in the SN of control mice, there was no change in expression of either protein at any time following MPTP treatment (**Figures 5.1, 5.2 and 5.4**).

As for the other potential components of the AP-1 transcription factors that were not observed to change at 6 h post-MPTP, there was also no

change at any of the times examined. There was no change in c-Fos measured in the ARC or in the SN at 4, 6, 8, 12, or 24 h post-MPTP (**Figures 5.5-5.7**). There was no change in c-Jun measured in the ARC or in the SN at 4, 6, 8, 12, or 24 h post-MPTP (**Figures 5.8-5.10**). JunD and ΔJunD, the AP-1 transcription factors that predominantly dimerize with FosB and ΔFosB, also displayed no change in protein at any of the times measured (**Figures 5.11-5.14**). MPTP did not change the ratio of ΔJunD/JunD in either the ARC or SN, though as with the previous results at 6 h post-MPTP, the ΔJunD/JunD was higher in the SN (**Figure 5.15**). These results demonstrate that FosB and ΔFosB are the only AP-1 transcription factors that show differential response to neurotoxicant exposure between brain regions.

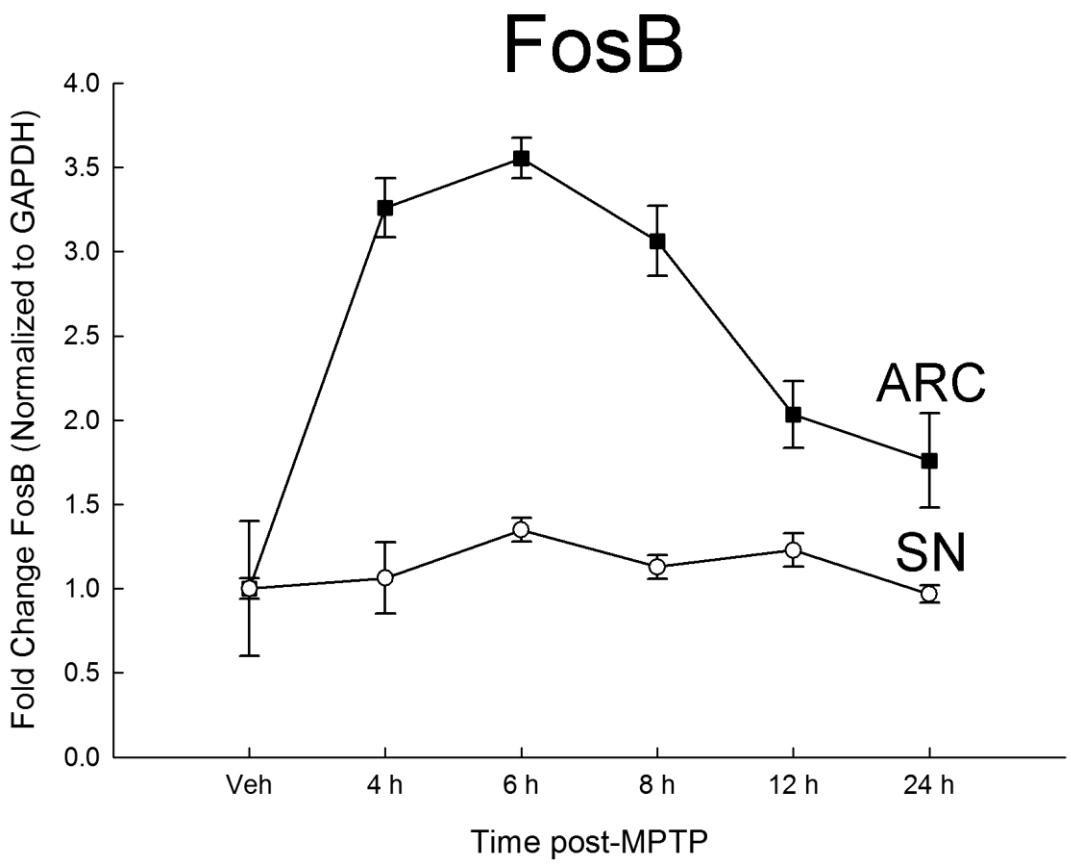

Figure 5.1 Time course effects of MPTP on FosB expression in the ARC and SN. Male C57Bl/6J mice were treated with either saline (10 ml/kg; s.c.) or MPTP (20 mg/kg; s.c.) and killed by decapitation 4, 6, 8, 12, or 24 h post-injection (n=8/group). Brains were sectioned, ARC and SN were microdissected, protein isolated and Western blots used to quantify FosB normalized to GAPDH. Mean fold change are represented by shapes with ± 1 standard error of the mean. Values significantly different ($p<0.05$; one-way ANOVA) from the vehicle controls are denoted with filled shapes.

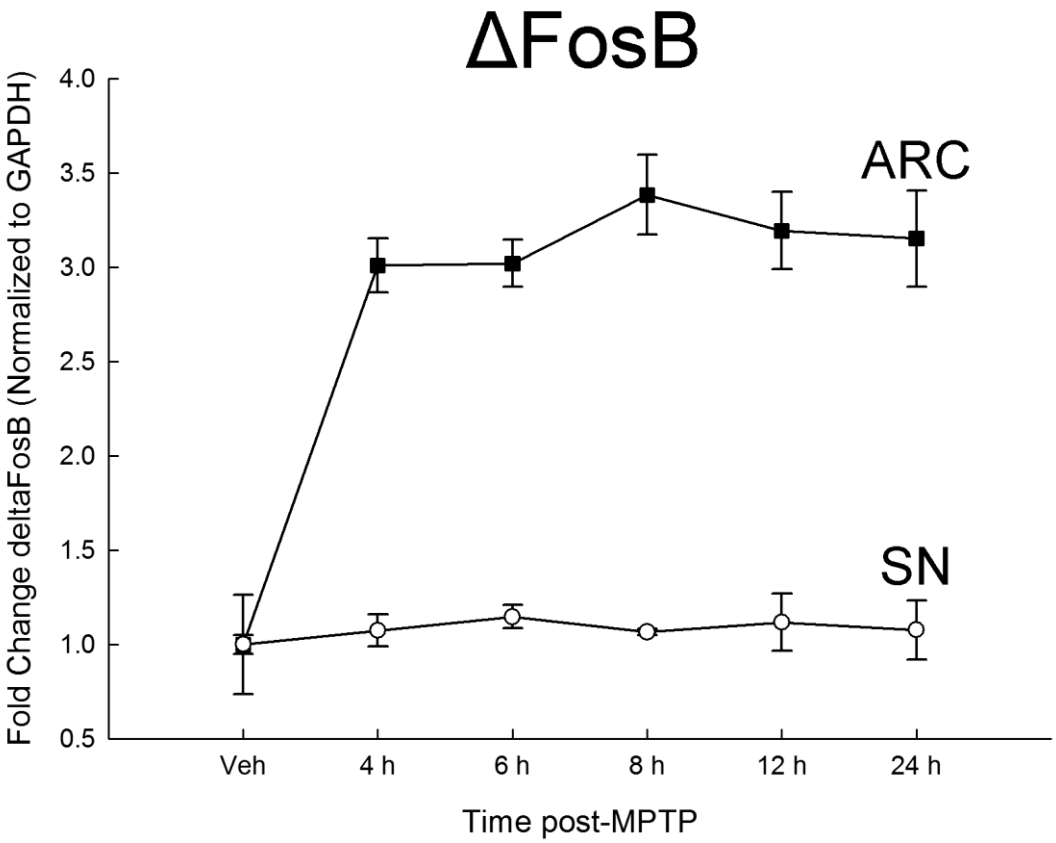

Figure 5.2 Time course effects of MPTP on ΔFosB expression in the ARC and SN. Male C57Bl/6J mice were treated with either saline (10 ml/kg; s.c.) or MPTP (20 mg/kg; s.c.) and killed by decapitation 4, 6, 8, 12, or 24 h post-injection (n=8/group). Brains were sectioned, ARC and SN were microdissected, protein isolated and Western blots used to quantify ΔFosB normalized to GAPDH. Mean fold change are represented by shapes with ± 1 standard error of the mean. Values significantly different ($p<0.05$; one-way ANOVA) from the vehicle controls are denoted with filled shapes.

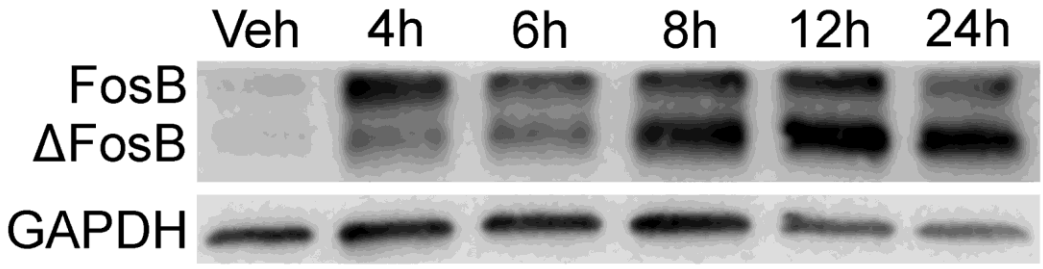

Figure 5.3 Representative Western blots for FosB and ΔFosB in the ARC at 4, 6, 8, 12, or 24 h post-MPTP. FosB and ΔFosB were normalized to GAPDH.

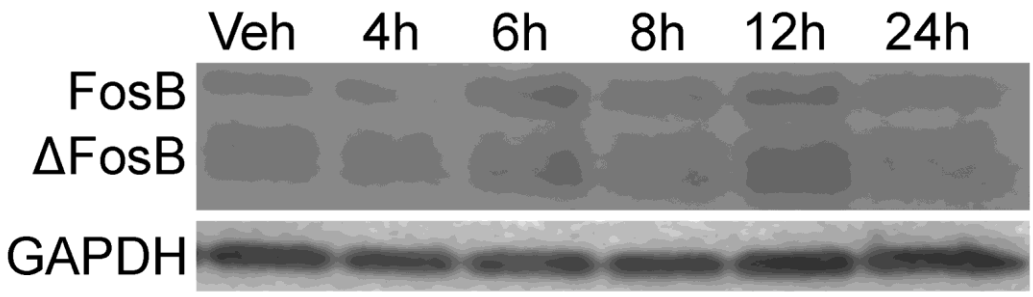

Figure 5.4 Representative Western blots for FosB and ΔFosB in the SN at 4, 6, 8, 12, or 24 h post-MPTP. FosB and ΔFosB were normalized to GAPDH.

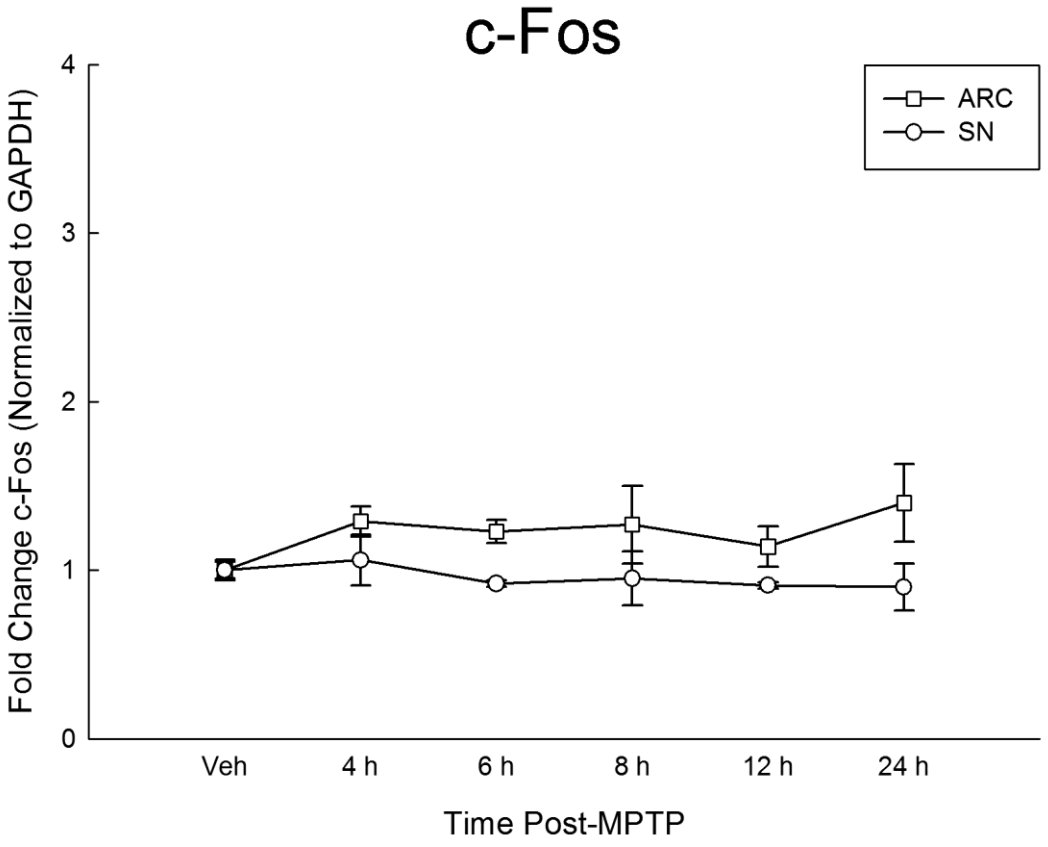

Figure 5.5 Time course effects of MPTP on c-Fos expression in the ARC and SN. Male C57Bl/6J mice were treated with either saline (10 ml/kg; s.c.) or MPTP (20 mg/kg; s.c.) and killed by decapitation 4, 6, 8, 12, or 24 h post-injection (n=8/group). Brains were sectioned, ARC and SN were microdissected, protein isolated and Western blots used to quantify c-Fos normalized to GAPDH. Mean fold change are represented by shapes with ± 1 standard error of the mean. Values significantly different ($p<0.05$; one-way ANOVA) from the vehicle controls are denoted with filled shapes.

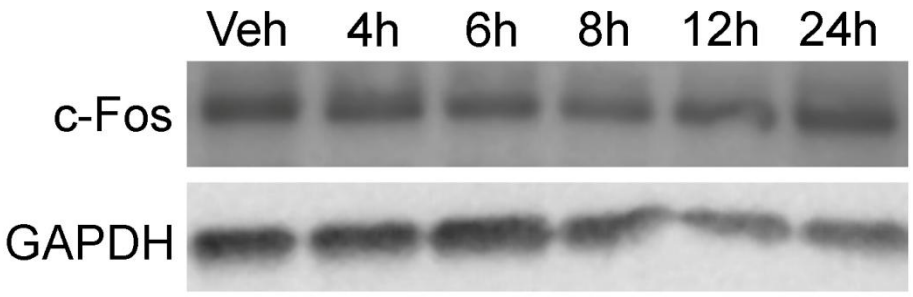

Figure 5.6 Representative Western blots for c-Fos in the ARC at 4, 6, 8, 12, or 24 h post-MPTP. c-Fos was normalized to GAPDH.

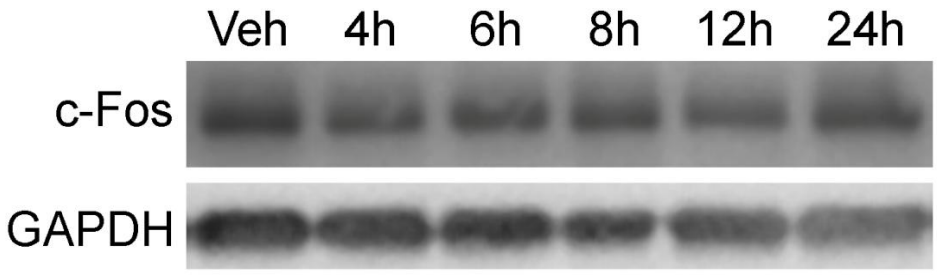

Figure 5.7 Representative Western blots for c-Fos in the SN at 4, 6, 8, 12, or 24 h post-MPTP. c-Fos was normalized to GAPDH.

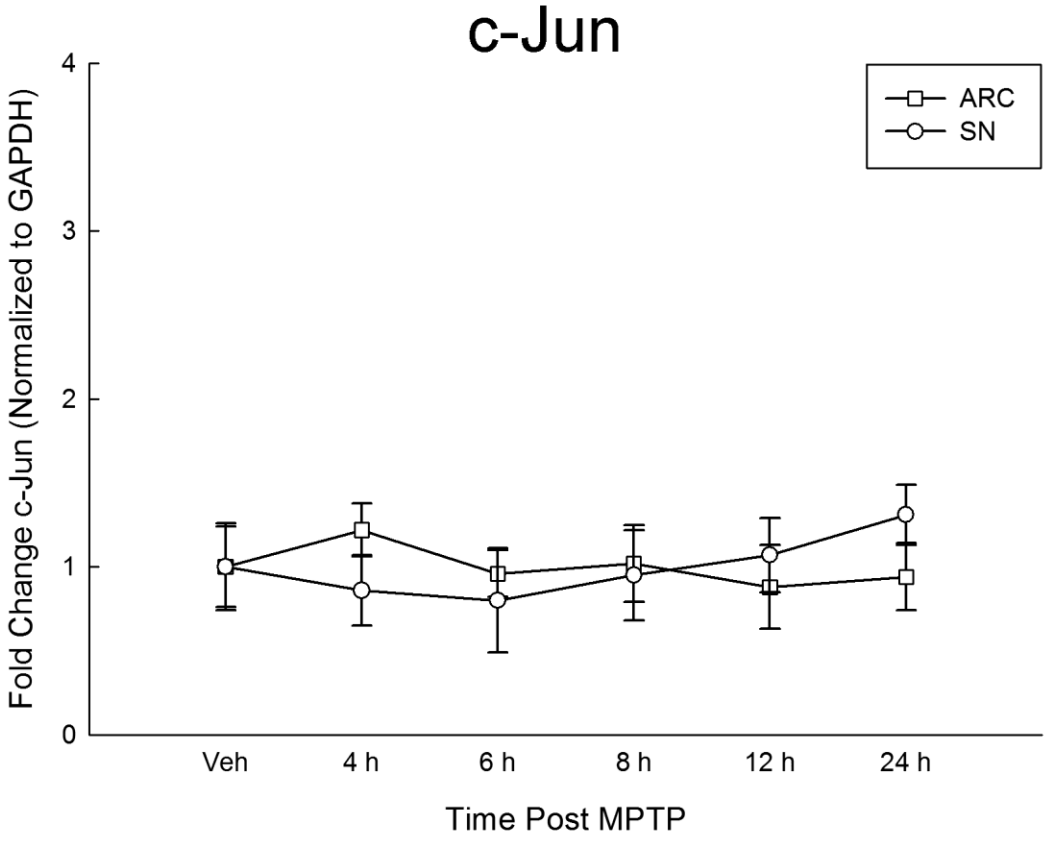

Figure 5.8 Time course effects of MPTP on c-Jun expression in the ARC and SN. Male C57Bl/6J mice were treated with either saline (10 ml/kg; s.c.) or MPTP (20 mg/kg; s.c.) and killed by decapitation 4, 6, 8, 12, or 24 h post-injection (n=8/group). Brains were sectioned, ARC and SN were microdissected, protein isolated and Western blots used to quantify c-Jun normalized to GAPDH. Mean fold change are represented by shapes with ± 1 standard error of the mean. Values significantly different ($p<0.05$; one-way ANOVA) from the vehicle controls are denoted with filled shapes.

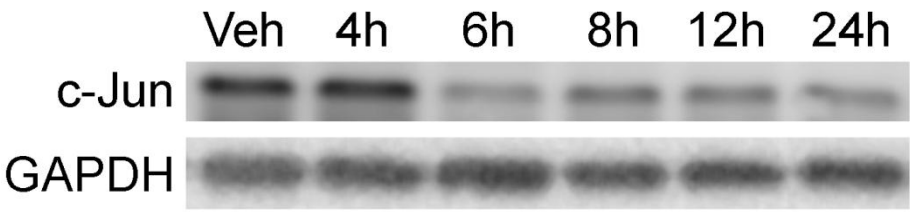

Figure 5.9 Representative Western blots for c-Jun in the ARC at 4, 6, 8, 12, or 24 h post-MPTP. c-Jun was normalized to GAPDH.

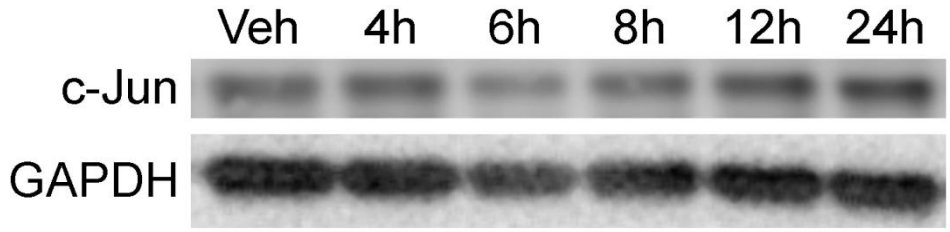

Figure 5.10 Representative Western blots for c-Jun in the SN at 4, 6, 8, 12, or 24 h post-MPTP. c-Jun was normalized to GAPDH.

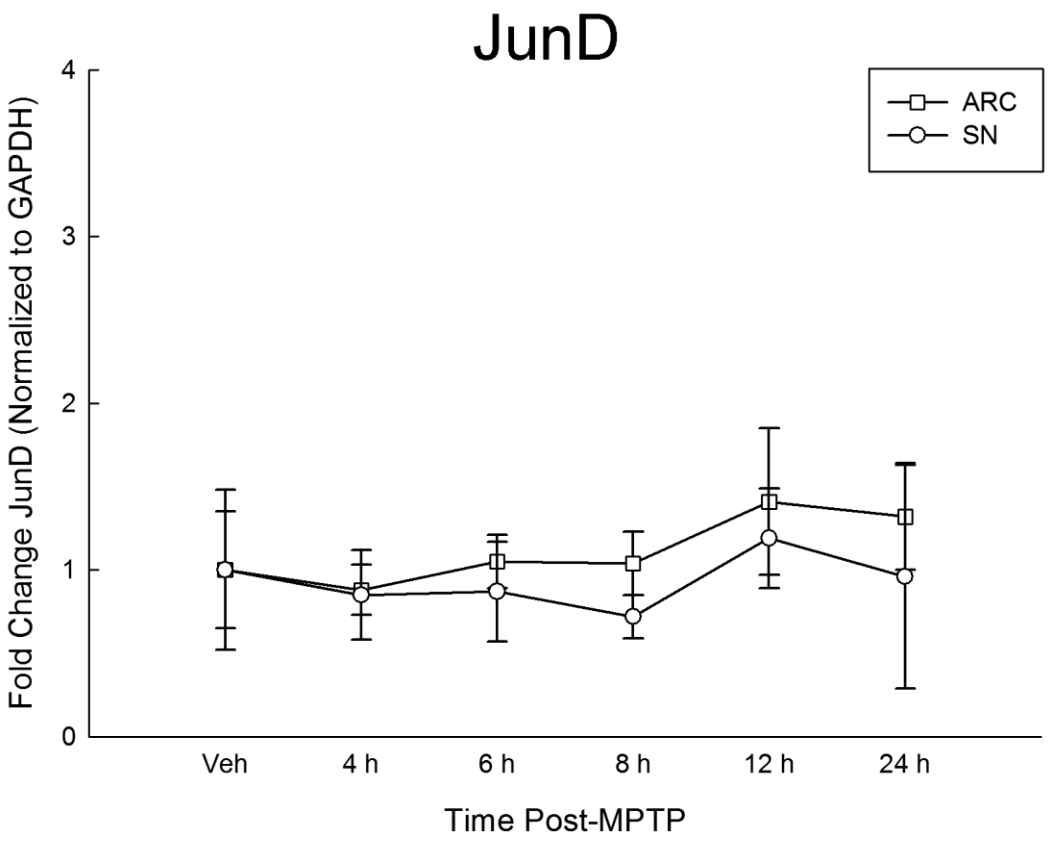

Figure 5.11 Time course effects of MPTP on JunD expression in the ARC and SN. Male C57Bl/6J mice were treated with either saline (10 ml/kg; s.c.) or MPTP (20 mg/kg; s.c.) and killed by decapitation 4, 6, 8, 12, or 24 h post-injection (n=8/group). Brains were sectioned, ARC and SN were microdissected, protein isolated and Western blots used to quantify JunD normalized to GAPDH. Mean fold change are represented by shapes with ± 1 standard error of the mean. Values significantly different ($p<0.05$; one-way ANOVA) from the vehicle controls are denoted with filled shapes.

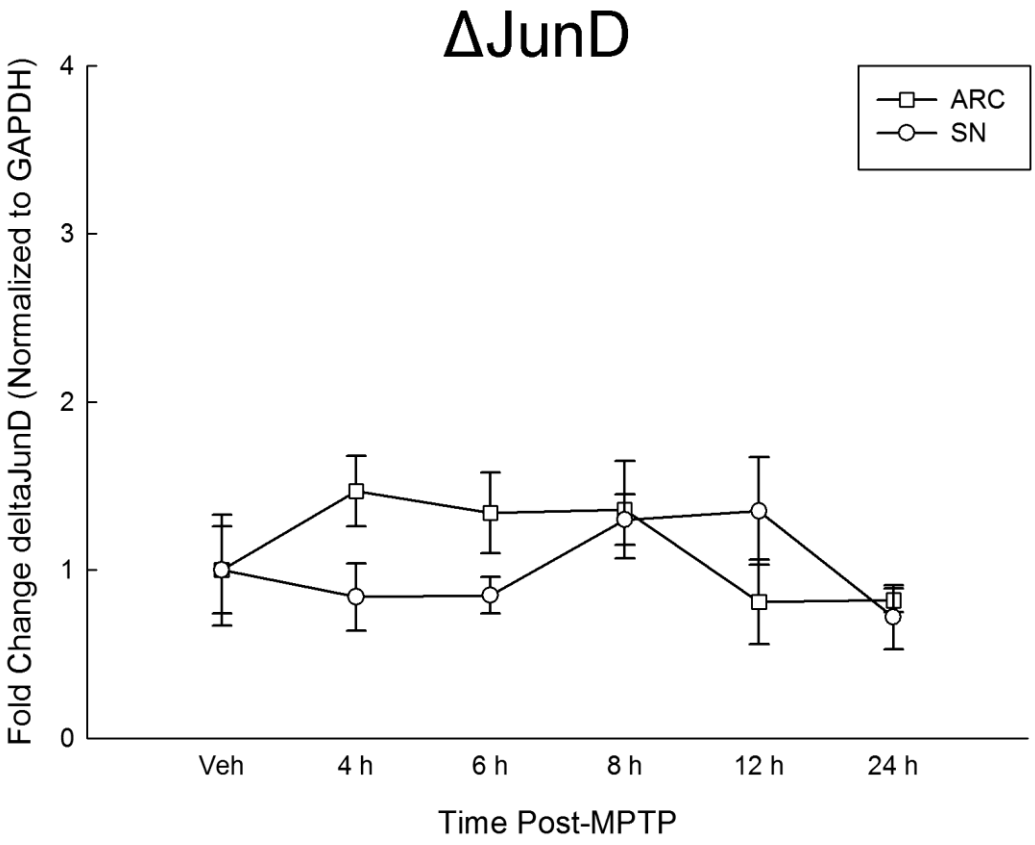

Figure 5.12 Time course effects of MPTP on ΔJunD expression in the ARC and SN. Male C57Bl/6J mice were treated with either saline (10 ml/kg; s.c.) or MPTP (20 mg/kg; s.c.) and killed by decapitation 4, 6, 8, 12, or 24 h post-injection (n=8/group). Brains were sectioned, ARC and SN were microdissected, protein isolated and Western blots used to quantify ΔJunD normalized to GAPDH. Mean fold change are represented by shapes with ± 1 standard error of the mean. Values significantly different ($p<0.05$; one-way ANOVA) from the vehicle controls are denoted with filled shapes.

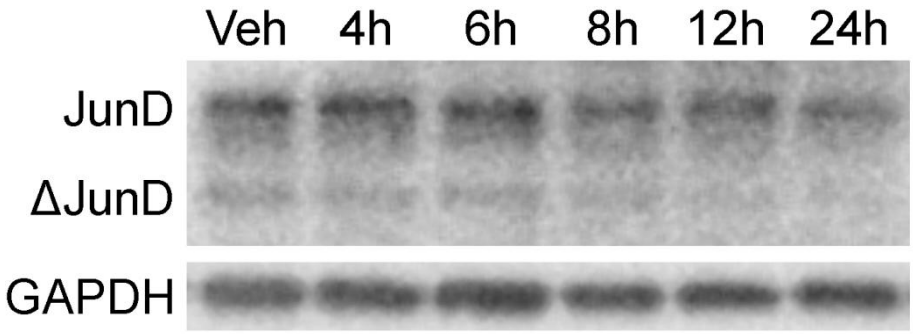

Figure 5.13 Representative Western blots for JunD and ΔJunD in the ARC at 4, 6, 8, 12, or 24 h post-MPTP. JunD and ΔJunD were normalized to GAPDH.

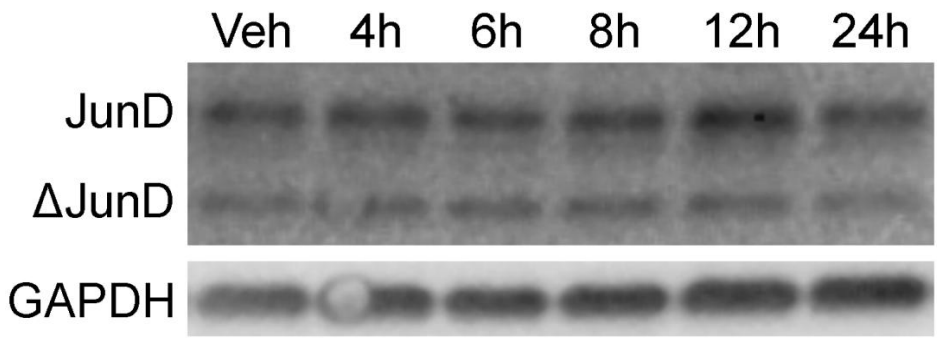

Figure 5.14 Representative Western blots for JunD and ΔJunD in the SN at 4, 6, 8, 12, or 24 h post-MPTP. JunD and ΔJunD were normalized to GAPDH.

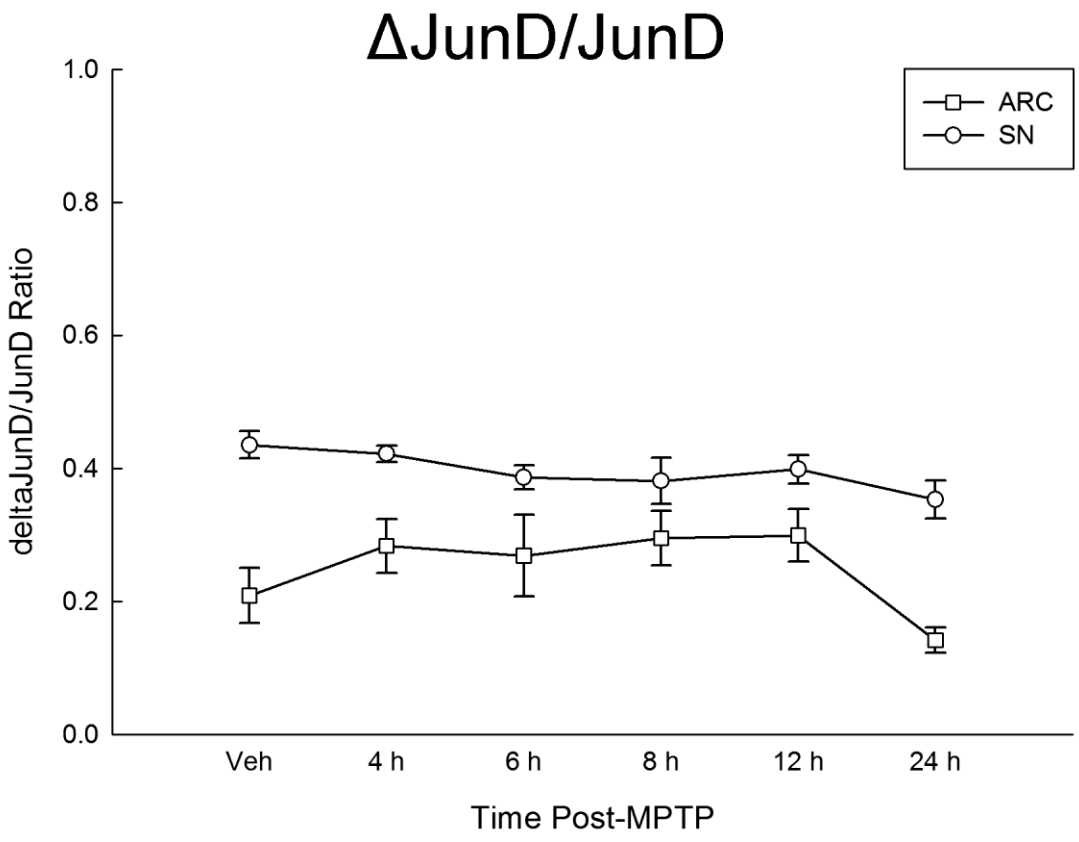

Figure 5.15 Time course effects of MPTP on ΔJunD/JunD ratio expression in the ARC and SN. Male C57Bl/6J mice were treated with either saline (10 ml/kg; s.c.) or MPTP (20 mg/kg; s.c.) and killed by decapitation 4, 6, 8, 12, or 24 h post-injection (n=8/group). Brains were sectioned, ARC and SN were microdissected, protein isolated and Western blots used to quantify ΔJunD and JunD. Mean ratio of ΔJunD/JunD are represented by shapes with ± 1 standard error of the mean.

Time-courses shown in Figures 5.1 and 5.2 reveal that FosB and ΔFosB expression both peak as early as 4 h post-MPTP. An early time-course experiment was performed to determine how rapidly FosB and ΔFosB expression increase after MPTP administration. In the ARC, FosB expression increased approximately 3-fold by 1 h post-MPTP and this increase was maintained at 2 and 4 h post MPTP (**Figures 5.16 and 5.18**). An increase in ΔFosB expression was delayed until 2 h post-MPTP, where expression levels were approximately 2-fold and 4-fold higher than control at 2 and 4 h post-MPTP treatment (**Figures 5.17 and 5.18**). In the SN, there was no change in expression of either FosB or ΔFosB at 1, 2 or 4 h after MPTP (**Figures 5.16, 5.17 and 5.19**).

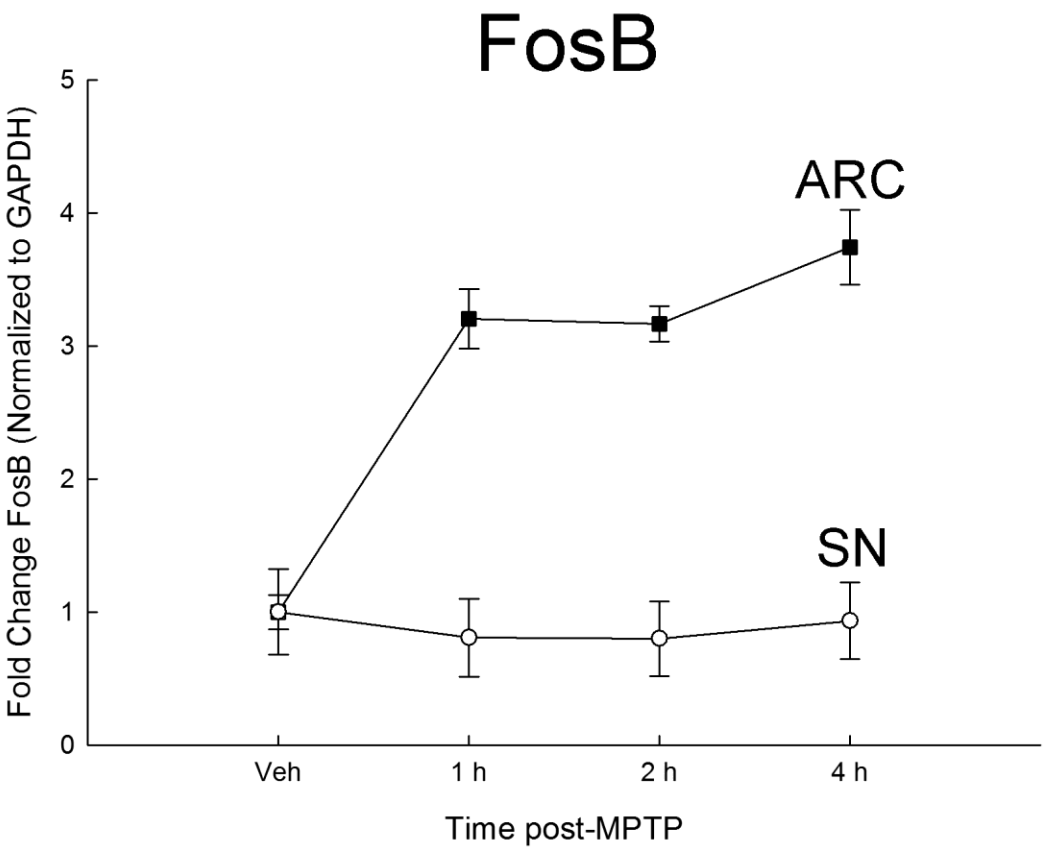

Figure 5.16 Early time course effects of MPTP on FosB expression in the ARC and SN. Male C57Bl/6J mice were treated with either saline (10 ml/kg; s.c.) or MPTP (20 mg/kg; s.c.) and killed by decapitation 1, 2, or 4 h post-injection (n=8/group). Brains were sectioned, ARC and SN were microdissected, protein isolated and Western blots used to quantify FosB normalized to GAPDH. Mean fold change are represented by shapes with ± 1 standard error of the mean. Values significantly different ($p<0.05$; one-way ANOVA) from the vehicle controls are denoted with filled shapes.

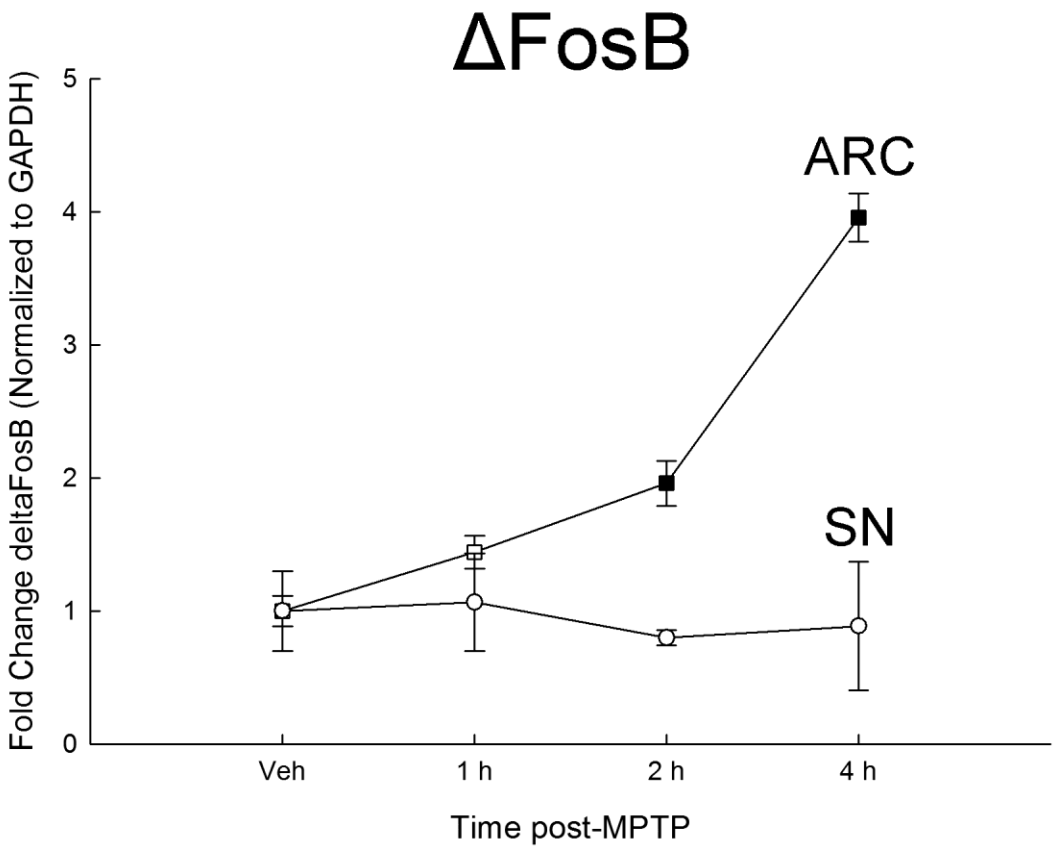

Figure 5.17 Early time course effects of MPTP on ΔFosB expression in the ARC and SN. Male C57Bl/6J mice were treated with either saline (10 ml/kg; s.c.) or MPTP (20 mg/kg; s.c.) and killed by decapitation 1, 2, or 4 h post-injection (n=8/group). Brains were sectioned, ARC and SN were microdissected, protein isolated and Western blots used to quantify ΔFosB normalized to GAPDH. Mean fold change are represented by shapes with ± 1 standard error of the mean. Values significantly different ($p<0.05$; one-way ANOVA) from the vehicle controls are denoted with filled shapes.

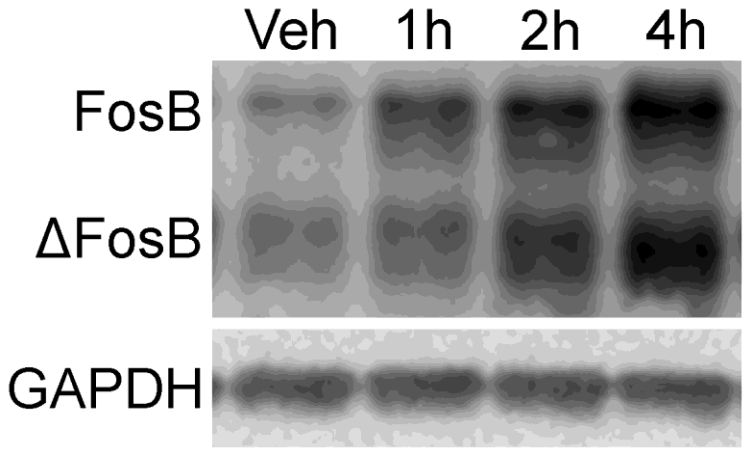

Figure 5.18 Representative Western blots for FosB and ΔFosB in the ARC at 1, 2, or 4 h post-MPTP. FosB and ΔFosB were normalized to GAPDH.

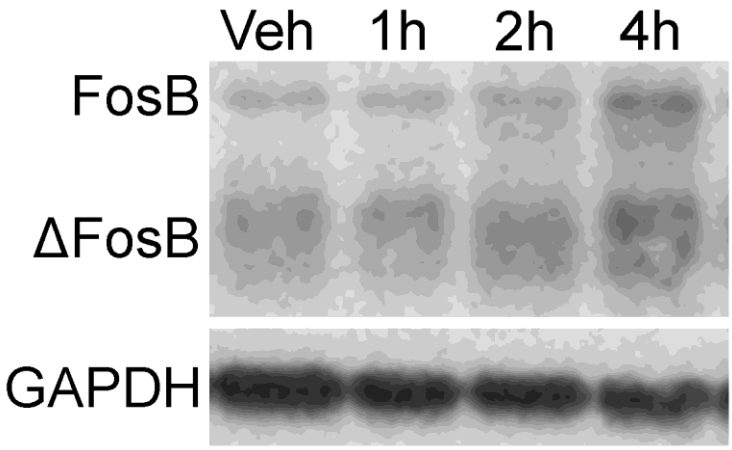

Figure 5.19 Representative Western blots for FosB and ΔFosB in the SN at 1, 2, or 4 h post-MPTP. FosB and ΔFosB were normalized to GAPDH.

Discussion

Similar to parkin and consistent with the 6 h post-MPTP results, FosB and ΔFosB only increase in the ARC, and not the SN. A single injection of MPTP induces FosB expression as early as 1 h post-MPTP and ΔFosB as early as 2 h post-MPTP. Increased expression of both FosB and ΔFosB in the ARC precedes increases in parkin mRNA at 8 h and protein at 12 h post-MPTP (Benskey et al., 2012). Activation of differential expression of FosB and ΔFosB between brain regions is consistent with the expectations of transcription factors mediating neurotoxicant-induced differential parkin expression.

Unlike FosB and ΔFosB, expression of the other AP-1 proteins does not change at 4, 6, 8, 12, or 24 h post-MPTP. This does not rule out the possibility that expression changes occur earlier than 4 h, or onset and return to basal levels was too rapid and occurred between time-points measured. As activity of the proteins can be altered independent of expression via post-translational modifications, such as phosphorylation, it is possible that phosphorylated c-Fos or c-Jun, could be possible transcription factors of parkin. Though not initially measured, this offers a future direction to explore in addition to FosB and ΔFosB.

Though they are the preferred proteins FosB and ΔFosB dimerize with, JunD and ΔJunD expression remains unchanged after MPTP. Increased expression of ΔJunD would contradict the proposed function of the FosBs as

transcriptional activators of parkin. However, an increase in JunD would be expected to be beneficial to increases in FosB and ΔFosB proteins. Within the cells, expression of JunD may be sufficient to pair with the FosBs. Comparably, in Sprague-Dawley rats there has been shown to be moderate expression of JunD at basal levels in the ARC and even lower levels in the SN (Herdegen et al., 1995). Alternatively, ΔFosB expression could be at high enough levels for ΔFosB homodimers to form and ΔFosB act independent of JunD (Jorissen et al., 2007). Regardless, the expression patterns of FosB and ΔFosB fit the predicted qualifications of a transcriptional activator, which warrants further examination of the *FosB* gene.

Sub-Cellular Localization of FosB and ΔFosB

Results

Transcription factors need to localize to the nucleus in order to interact with DNA, therefore FosB and ΔFosB levels in cytoplasmic and nuclear fractions were examined in the ARC and SN. In the ARC, both FosB and ΔFosB increased in the cytoplasmic fraction approximately 3- fold 6 h at 6 h post-MPTP (**Figures 5.20 and 5.22**). Expression of FosB in the nuclear fraction did not change after MPTP, however, ΔFosB increased approximately 3-fold in the nuclear fraction 6 h following treatment (**Figures 5.21 and 5.22**). FosB and ΔFosB in the cytoplasmic or nuclear fractions of the SN following MPTP did not change (**Figures 5.23-5.25**).

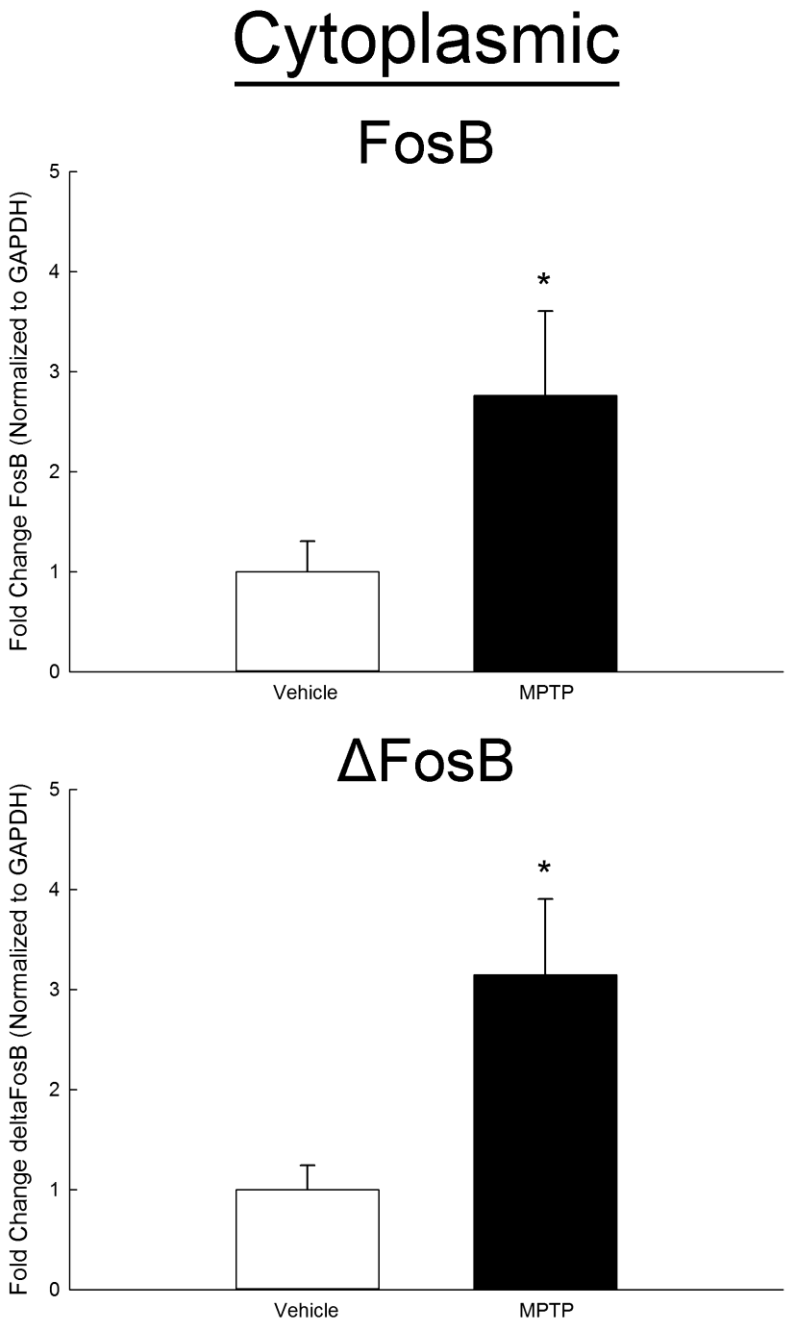

Figure 5.20 Effects of MPTP on FosB and ΔFosB in cytoplasmic fractions derived from the ARC. Male C57Bl/6J mice were treated with either saline (10 ml/kg; s.c.) or MPTP (20 mg/kg; s.c.) and killed by decapitation 6 h post-injection (n=8/group). The ARC was microdissected from fresh/unfrozen tissue, cytoplasmic and nuclear fractions separated, and Western blots used to quantify FosB and ΔFosB normalized to GAPDH. Columns indicate the group means, error bars represent +1 standard error of the mean. An asterisk indicates values that are significantly different ($p < 0.05$; t-test) from vehicle-treated controls.

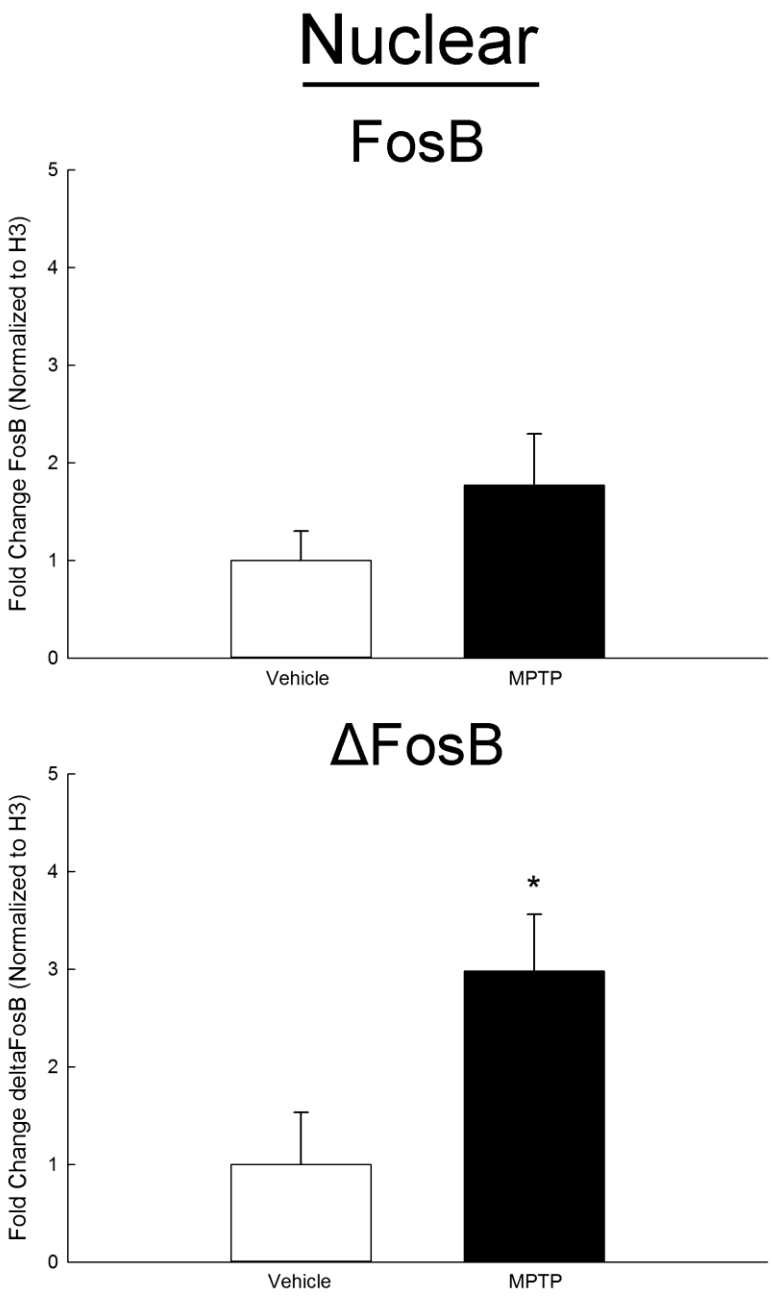

Figure 5.21 Effects of MPTP on FosB and ΔFosB in nuclear fractions derived from the ARC. Male C57Bl/6J mice were treated with either saline (10 ml/kg; s.c.) or MPTP (20 mg/kg; s.c.) and killed by decapitation 6 h post-injection (n=8/group). The ARC was microdissected from fresh/unfrozen tissue, cytoplasmic and nuclear fractions separated, and Western blots used to quantify FosB and ΔFosB normalized to histone protein H3. Columns indicate the group means, error bars represent +1 standard error of the mean. An asterisk indicates values that are significantly different ($p < 0.05$; t-test) from vehicle-treated controls.

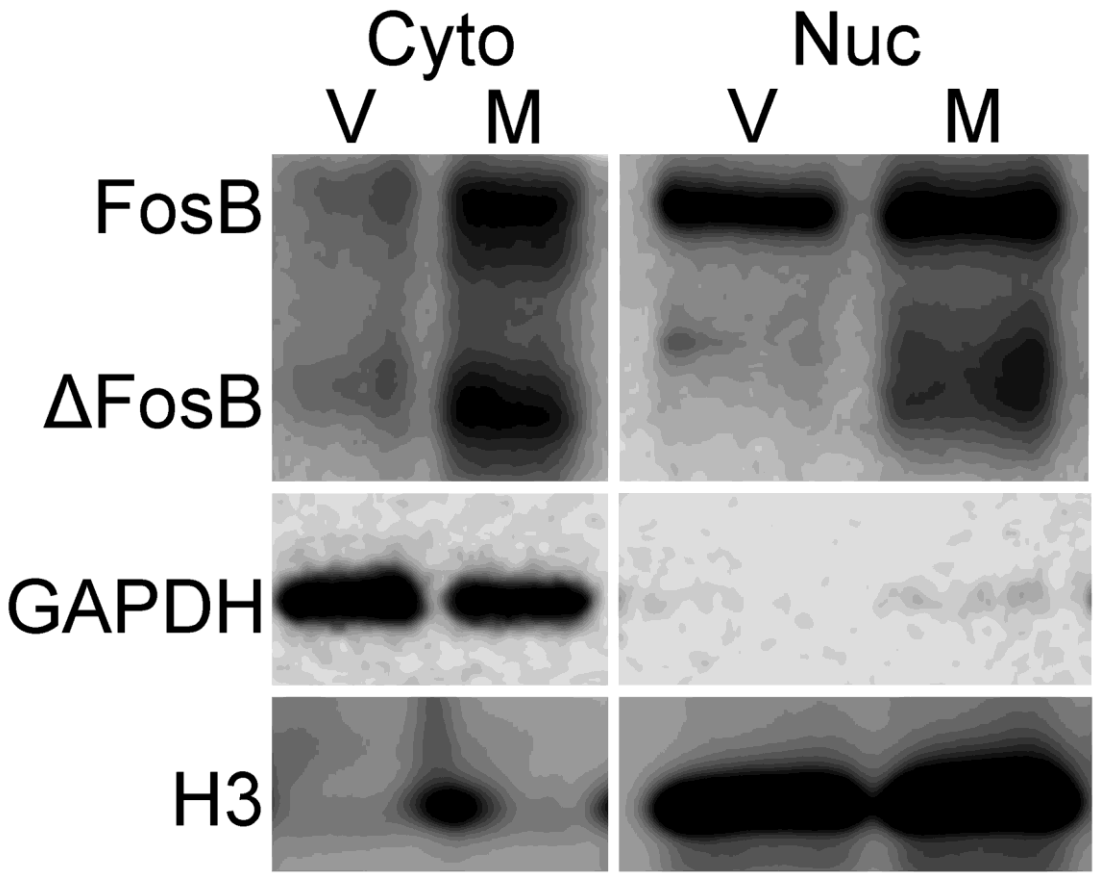

Figure 5.22 Representative Western blots for FosB and ΔFosB in cytoplasmic and nuclear fractions derived from the ARC at 6 h post-MPTP. FosB and ΔFosB were normalized to GAPDH in the cytoplasmic fraction and histone protein H3 in the nuclear fraction.

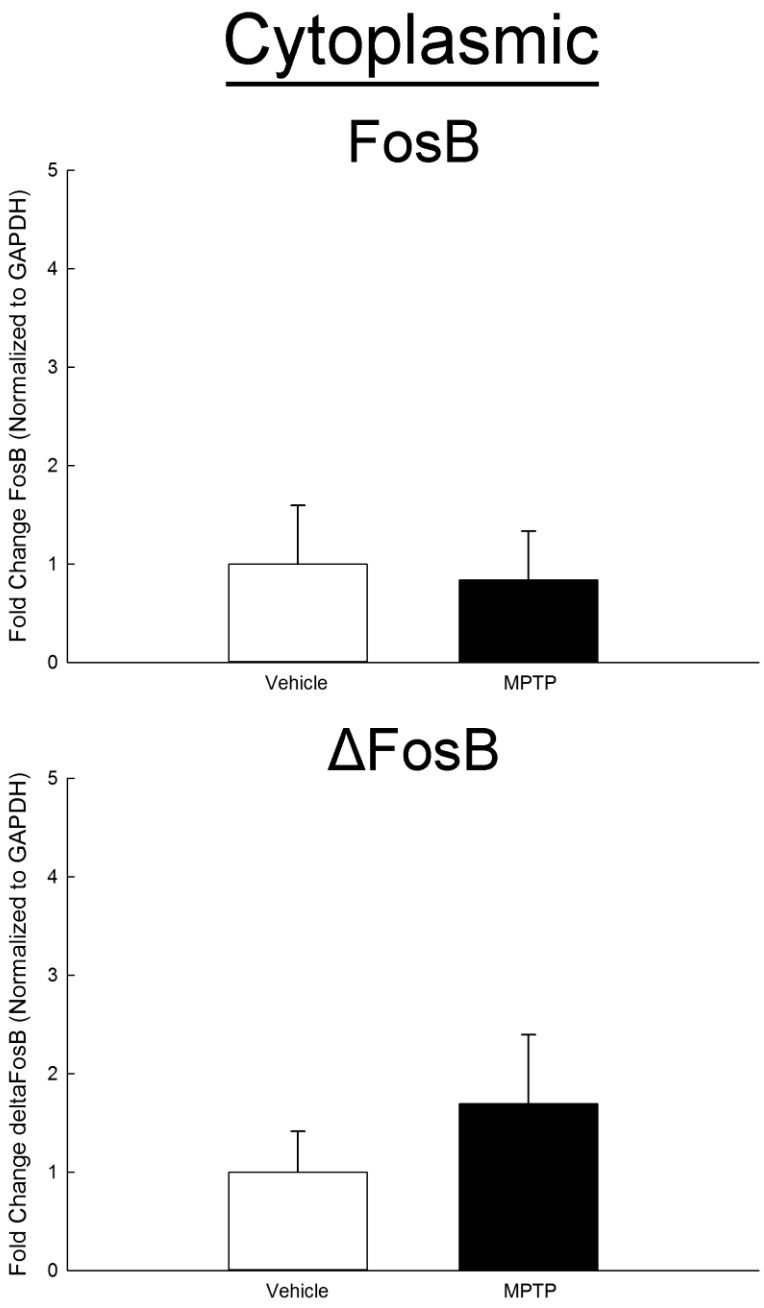

Figure 5.23 Effects of MPTP on FosB and ΔFosB in cytoplasmic fractions derived from the SN. Male C57Bl/6J mice were treated with either saline (10 ml/kg; s.c.) or MPTP (20 mg/kg; s.c.) and killed by decapitation 6 h post-injection (n=8/group). The SN was microdissected from fresh/unfrozen tissue, cytoplasmic and nuclear fractions separated, and Western blots used to quantify FosB and ΔFosB normalized to GAPDH. Columns indicate the group means, error bars represent +1 standard error of the mean. An asterisk indicates values that are significantly different ($p < 0.05$; t-test) from vehicle-treated controls.

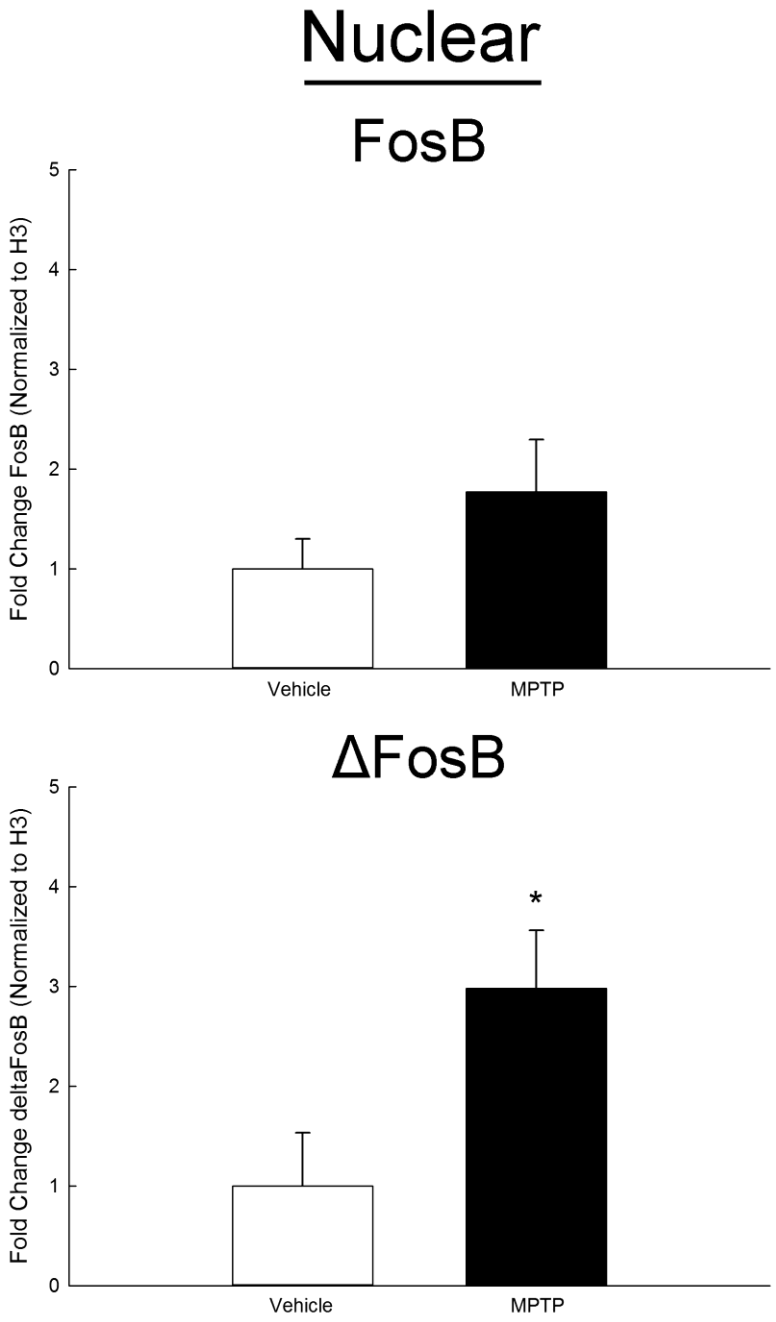

Figure 5.24 Effects of MPTP on FosB and ΔFosB in nuclear fractions derived from the SN. Male C57Bl/6J mice were treated with either saline (10 ml/kg; s.c.) or MPTP (20 mg/kg; s.c.) and killed by decapitation 6 h post-injection (n=8/group). The SN was microdissected from fresh/unfrozen tissue, cytoplasmic and nuclear fractions separated, and Western blots used to quantify FosB and ΔFosB normalized to histone protein H3. Columns indicate the group means, error bars represent +1 standard error of the mean. An asterisk indicates values that are significantly different ($p < 0.05$; t-test) from vehicle-treated controls.

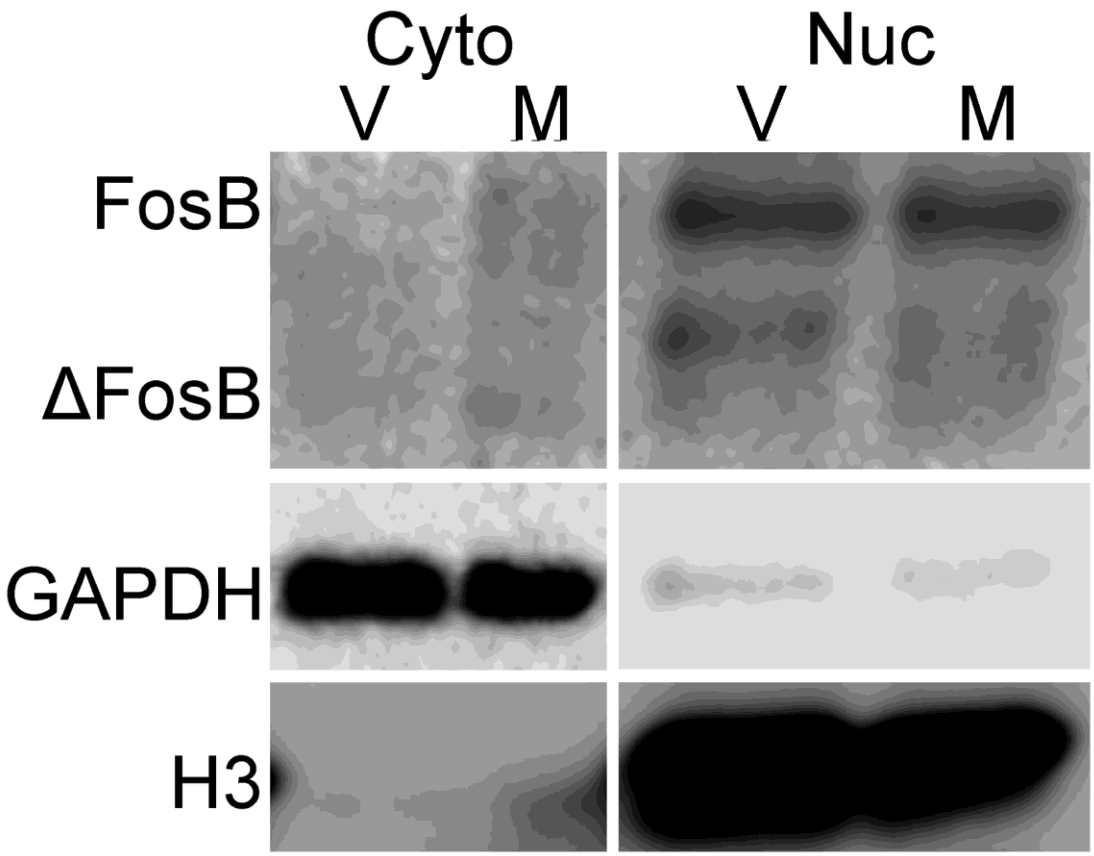

Figure 5.25 Representative Western blots for FosB and ΔFosB in cytoplasmic and nuclear fractions derived from the SN at 6 h post-MPTP. FosB and ΔFosB were normalized to GAPDH in the cytoplasmic fraction and histone protein H3 in the nuclear fraction.

Discussion

In order for FosB and ΔFosB to act as transcription factors in response to neurotoxicant exposure they must localize to the nucleus. Based on Western blots using cytoplasmic and nuclear fractions, FosB and ΔFosB were found to be present in both the cytoplasm and nuclei in the ARC and SN. As observed in previous experiments (Chapters 4 and 5), FosB and ΔFosB expression only changes in the ARC, with no change observed quantitative change in the amount of these transcription factors in whole SN tissue. There was also no change in localization in the SN, i.e., no increases or decreases in either cytoplasmic or nuclear fractions. In the ARC however, ΔFosB increases in both the cytoplasm and nuclei, with FosB only increasing in the cytoplasm by 6 h post-MPTP. These results are consistent with the hypothesis that ΔFosB may act as a transcription factor of parkin mediating neurotoxicant-induced activation of the parkin promoter. Elevated levels in cytoplasmic FosB (in the absence of nuclear localization) suggests that this transcription factor does not regulate parkin expression for prolonged periods (i.e. 6 h) after neurotoxicant exposure. It is likely that FosB is an early initiator of the parkin promoter, with the truncated ΔFosB form supplanting FosB as a prolonged regulator of the parkin promoter. This hypothesis is consistent with the known function of the FosB family of transcription factors in addiction (Nestler 2008).

Increased nuclear localization of ΔFosB could be due to phosphorylation at serine 27 by casein kinase 2. Phosphorylayion of ΔFosB increases the stability and transcriptional activity of ΔFosB, but not FosB (Ulery and Nestler et al., 2007). When casein kinase 2 is inhibited, translocation of ΔFosB into the nucleus decreases (Ulery and Nestler et al., 2007). By extension, this suggests that ΔFosB phosphorylation causes translocation into the nucleus and could explain why ΔFosB, and not FosB increases in the nuclear fraction at 6 h. Additionally, high concentrations of dimers containing ΔFosB residing in the nuclei may prevent additional translocation of FosB into the nucleus.

Localization of Total FosB in DA Neurons, Total Neurons, and Glial Cells

Results

Relative levels of FosB and ΔFosB were measured in regions containing cell bodies of TIDA or NSDA neurons, but to determine if FosB and ΔFosB are located in nuclei of TIDA and NSDA neurons immunofluorescent staining was required. The antibody used for FosB and ΔFosB in this analysis recognizes both FosB and ΔFosB isoforms. This was paired with an antibody against TH, the rate limiting enzyme in DA synthesis and a marker for DA neurons in the ARC and SN. Sections through the ARC and SN of vehicle and 6 h post-MPTP mice were stained and imaged (**Figure 5.26**). Total numbers of TH-immunoreactive neurons with and without FosB in the nuclei were counted.

The percentage of TH-immunoreactive neurons with FosB stained nuclei were calculated for each brain region of individual mice and averaged across treatment groups. In the ARC of vehicle-treated mice approximately 90% of TH neurons had total FosBs localized to nuclei and this did not change 6 h post-MPTP treatment (Table 5.1). In the SN of vehicle-treated mice approximately 90% of TH neurons had total FosBs localized to the nuclei and this did not change at 6 h post-MPTP (Table 5.1).

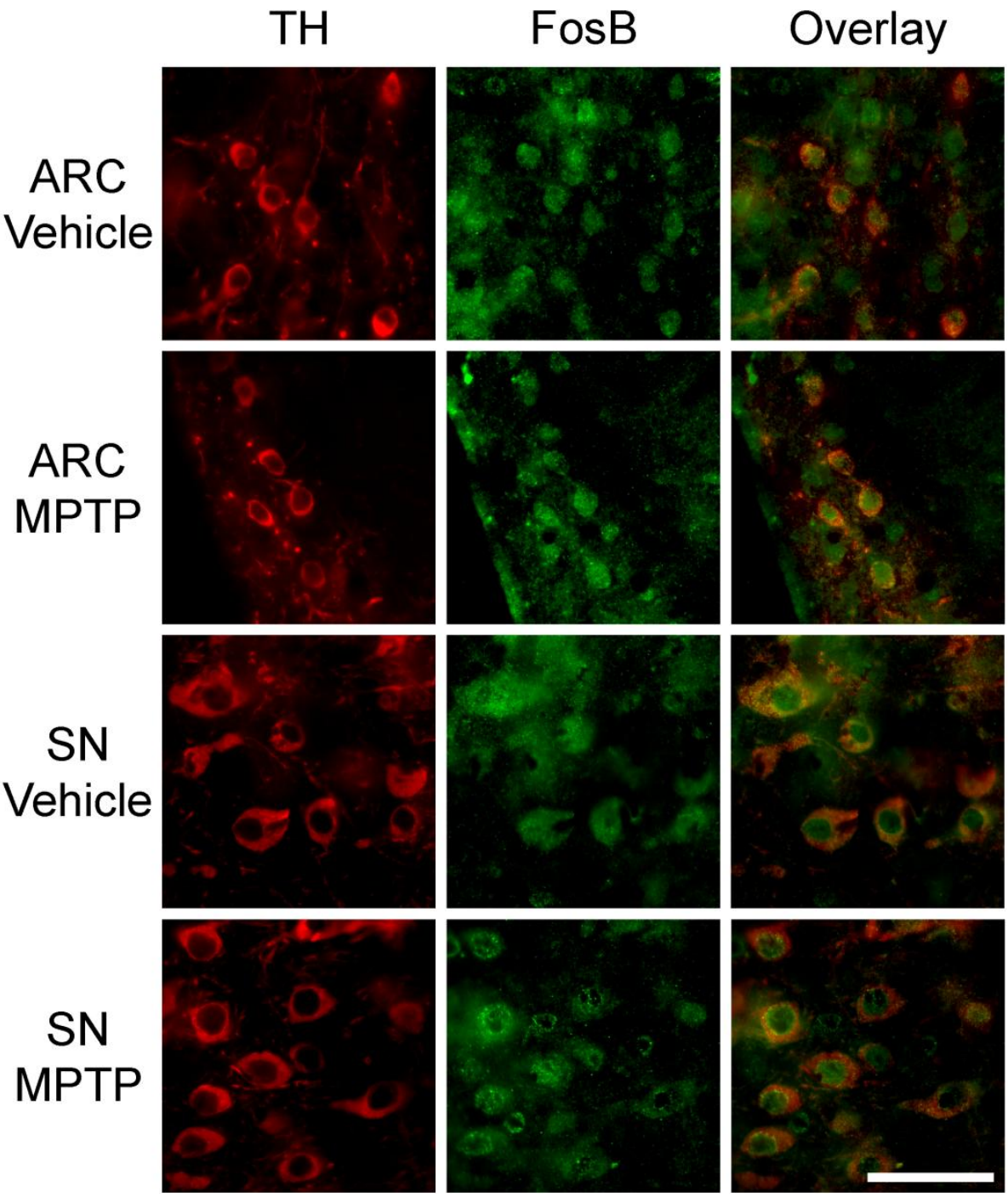

Figure 5.26 Total FosB (FosB and ΔFosB) localization in nuclei of TH-immunoreactive neurons in the ARC and SN. Male C57Bl/6J mice were treated with either saline (10 ml/kg; s.c.) or MPTP (20 mg/kg; s.c.) and perfused 6 h later (n=5/group). Sections 20 μm thick were cut and immunofluoresence used to co-localize total FosB in TH positive neurons. Sections 100 μm apart were imaged and TH-immunoreactive cells with and without total FosB in the nuclei were quantified. Scale bar is 50 μm.

Changes in FosB and ΔFosB expression from tissue samples could potentially be occurring in non-DA neurons. To examine this possibility, an antibody against NeuN was used. NeuN is a neuronal splicing factor and a phenotype independent neuronal marker. A majority (>95%) of all ARC and SN neurons in vehicle and 6 h post-MPTP mice exhibited nuclear staining for FosB, with no change after MPTP (**Figure 5.27 and Table 5.1**).

Another possibility was that FosB and ΔFosB were occurring in non-neuronal cells, such as glial cells. The glial marker, GFAP (glial fibrillary acidic protein), was used with the antibody for the FosBs to stain sections from the ARC and SN of vehicle and 6 h post-MPTP treated mice. Only a small percentage (~10%) of cells stained with GFAP co-localized with total FosB (~10%) in the ARC and SN of both vehicle and MPTP treated animals (**Figure 5.28 and Table 5.1**).

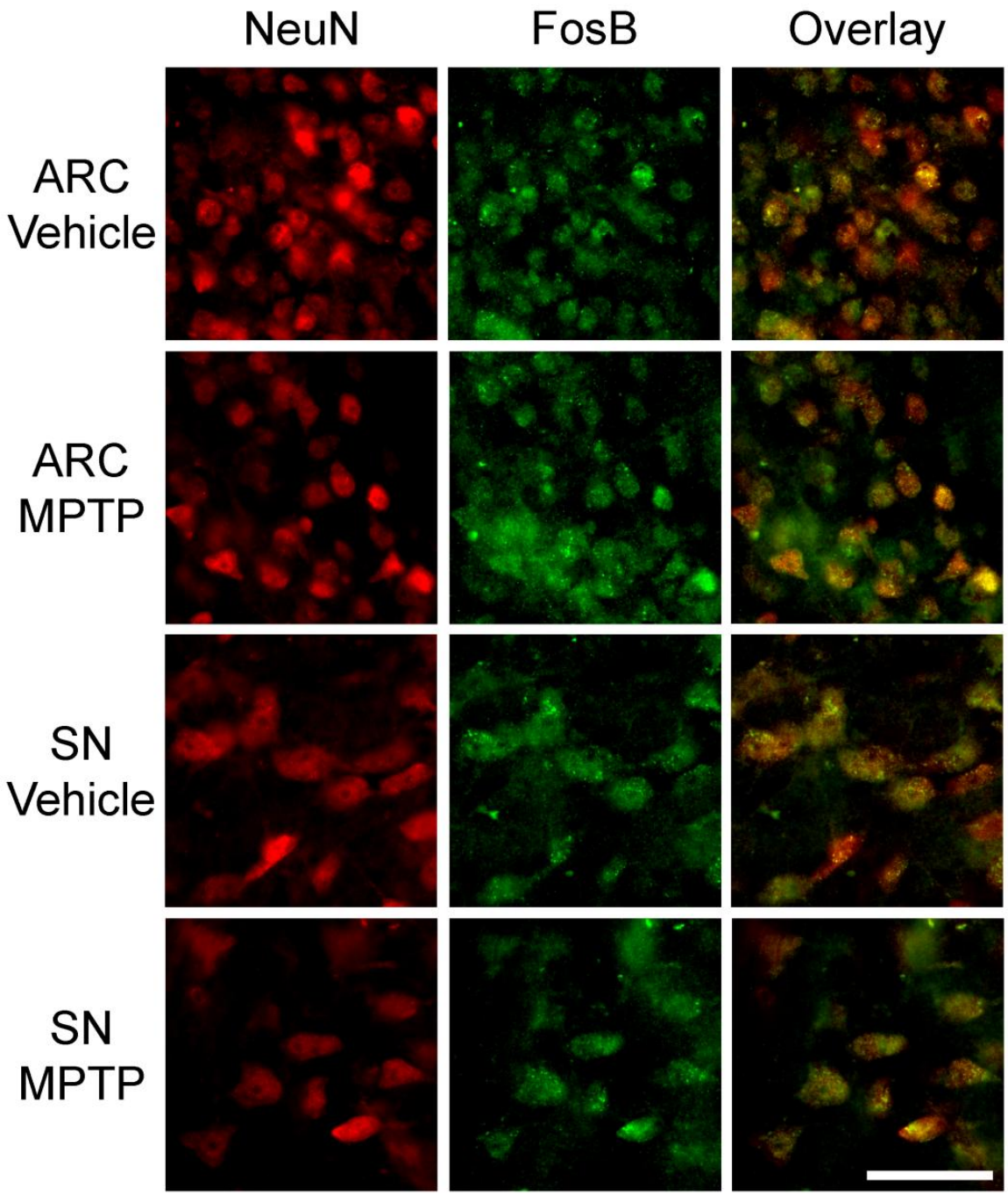

Figure 5.27 Total FosB (FosB and ΔFosB) localization in the nuclei of all neurons in the ARC and SN. Male C57Bl/6J mice were treated with either saline (10 ml/kg; s.c.) or MPTP (20 mg/kg; s.c.) and perfused 6 h later (n=5/group). Sections 20 μm thick were cut and immunofluoresence used to co-localize total FosB in NeuN positive neurons. Sections 100 μm apart were imaged and NeuN-immunoreactive cells with and without total FosB in the nuclei were quantified. Scale bar is 50 μm.

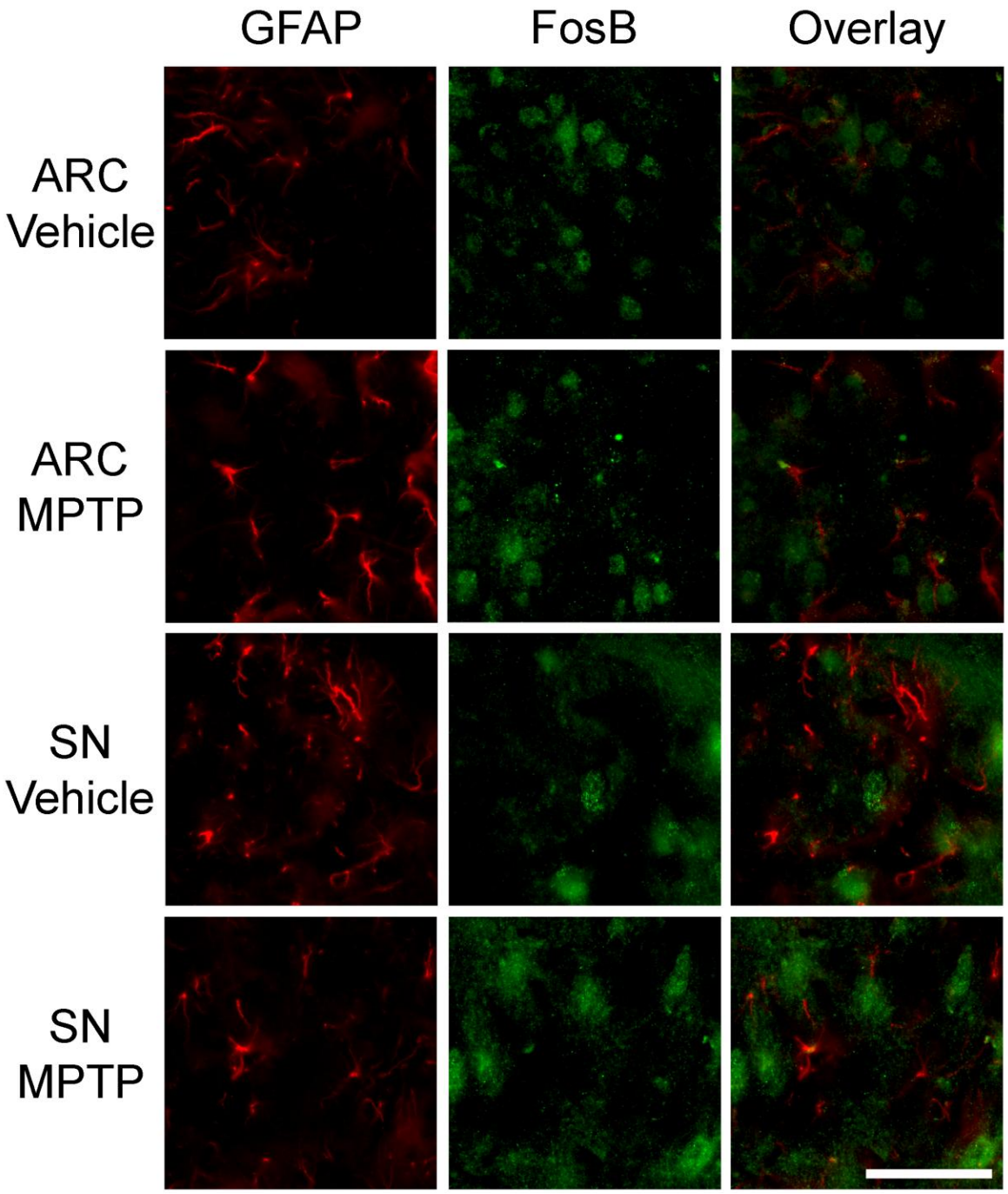

Figure 5.28 Total FosB (FosB and ΔFosB) localization in glial cells in the ARC and SN. Male C57Bl/6J mice were treated with either saline (10 ml/kg; s.c.) or MPTP (20 mg/kg; s.c.) and perfused 6 h later (n=5/group). Sections 20 µm thick were cut and immunofluoresence used to co-localize total FosB in GFAP positive cells. Sections 100 µm apart were imaged and GFAP-immunoreactive cells with and without total FosB in the nuclei were quantified. Scale bar is 50 µm.

Table 5.1 Mean percentage of TH-immunoreactive neurons, total neurons, and glial cells containing total FosB.

Cells	Treatment	ARC	SN
DA Neurons	Vehicle	90.6% ± 0.4%	92.5% ± 0.4%
	MPTP	88.8% ± 1.3%	90.5% ± 0.8%
Total Neurons	Vehicle	98.7% ± 0.9%	97.7% ± 0.9%
	MPTP	98.5% ± 0.6%	97.9% ± 0.6%
Glial Cells	Vehicle	8.0% ± 2.7%	11.7% ± 4.6%
	MPTP	7.6% ± 1.4%	11.1% ± 3.4%

Discussion

FosB and ΔFosB measurements in cytoplasmic and nuclear fractions in isolated brain regions only partially addresses what is happening in DA neurons. To further resolve whether these changes occur in DA neurons dual immunofluorescent staining was used to locate total FosB in TH immunoreactive neurons at 6 h post-MPTP. An overwhelming majority (i.e. 90%) of TH immunoreactive neurons contained FosB in there nuclei. There was no change in the percentage of TH neurons with total FosB in their nuclei after MPTP in either NSDA neurons in the SN or TIDA neurons in the ARC. The lack of increase in the numbers of DA neurons with total FosB in the nuclei in the ARC suggests that the observed increase in FosB and ΔFosB protein occurs within individual TIDA neurons, rather than a recruitment in the numbers of TIDA neurons expressing FosB/ΔFosB.

Alternatively, the number of non-TH neurons or glia expressing total FosB could be increasing. Both NeuN and GFAP staining for total neurons and glia show no change in the number of cells expressing total FosB 6 h post-MPTP. In the ARC and SN, almost all of the neurons observed express FosB to some degree. Though other neurons express total FosB in the ARC, the increase in FosB and ΔFosB is most likely occurring in DA neurons due to the selectivity of MPP^+ for the DA transporter (Bezard et al., 1998; Javitch et al., 1985). As with neurons, both astrocytes and microglia have been shown to have the potential to express FosB and ΔFosB (Nomaru et al., 2014).

However, in the ARC and SN, there is a low percentage of glia co-localizing with FosB. Considering the low number of total FosB expressing glia, the increase in FosB and ΔFosB observed in the Western blots are not likely due to changes in glial cells.

Long-Term Effects of MPTP on FosB and ΔFosB Expression

Results

As the ΔFosB protein has long half-life and is constant with the expectations of a transcription factor of parkin, and extended time-course was performed. Effects of MPTP on DA vesicular stores, DA synthesis, release, and re-uptake pathway, body weight, FosB and ΔFosB, and parkin at 1, 3, and 7 d post-MPTP were determined. DA concentrations (an index of vesicular neurotransmitter storage) in the ST were decreased to about 25% of same day vehicle controls at 1, 3, and 7 d after a single injection of MPTP (**Figure 5.29**). Comparably, DA concentrations in the ME after MPTP were not significantly different from the respective same day vehicle controls, showing full recovery of neurotransmitter stores in the ME (**Figure 5.30**). In addition to the depleting effect of MPTP on DA ,TH in the ST was decreased to approximately 50% of controls at 1, 3, and 7 d post-MPTP with no recovery (**Figures 5.31 and 5.32**). Concentrations of the DA uptake transporter DAT in the ST was decreased 50% of the control (or lower) at 1, 3, and 7 d post-MPTP (**Figures 5.33 and 5.35**). In contrast, levels of the DA vesicular

transporter VMAT2 in the ST did not change at 1, 3, and 7 d post-MPTP (Figures 5.34 and 5.35).

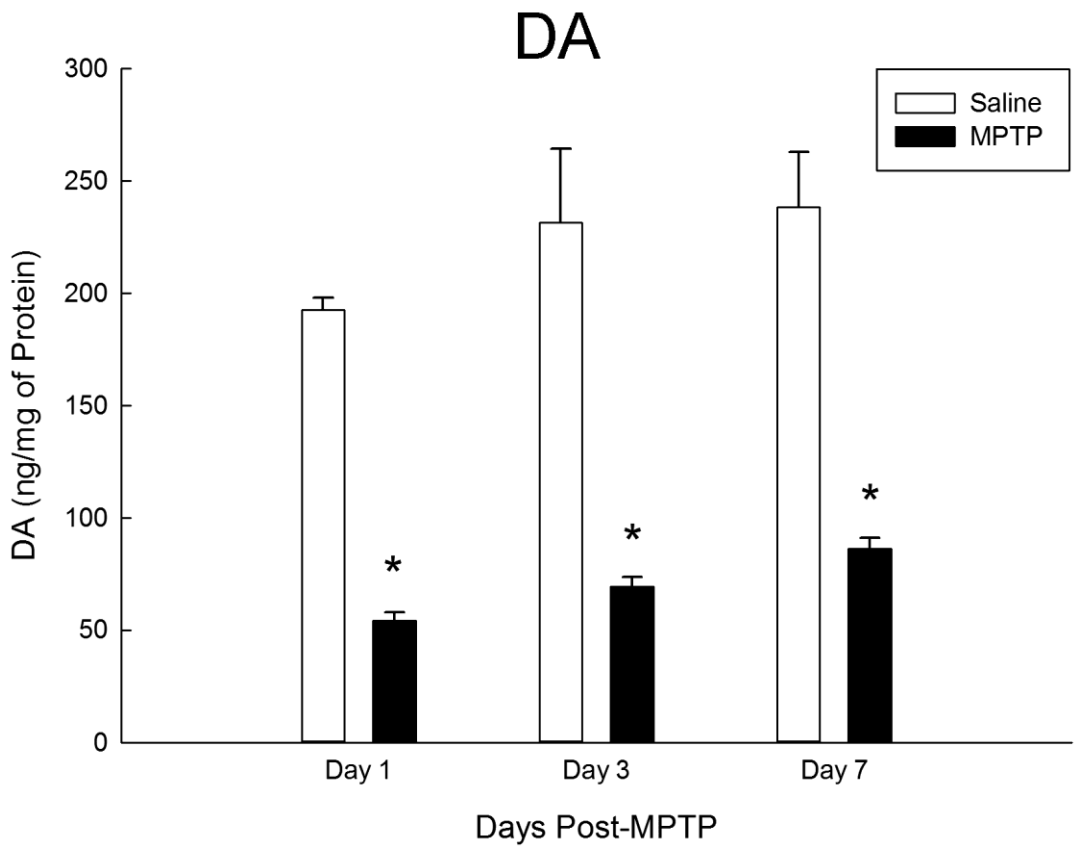

Figure 5.29 Extended time course effects of MPTP on DA concentration in the ST. Male C57Bl/6J mice were treated with either saline (10 ml/kg; s.c.) or MPTP (20 mg/kg; s.c.) and killed by decapitation 1, 3, or 7 d post-injection (n=8/group). Brains were sectioned, ST was microdissected, and samples were prepared for neurochemistry. Columns indicate the group means, error bars represent +1 standard error of the mean. An asterisk indicates values that are significantly different ($p < 0.05$; t-test) from the same day vehicle-treated controls.

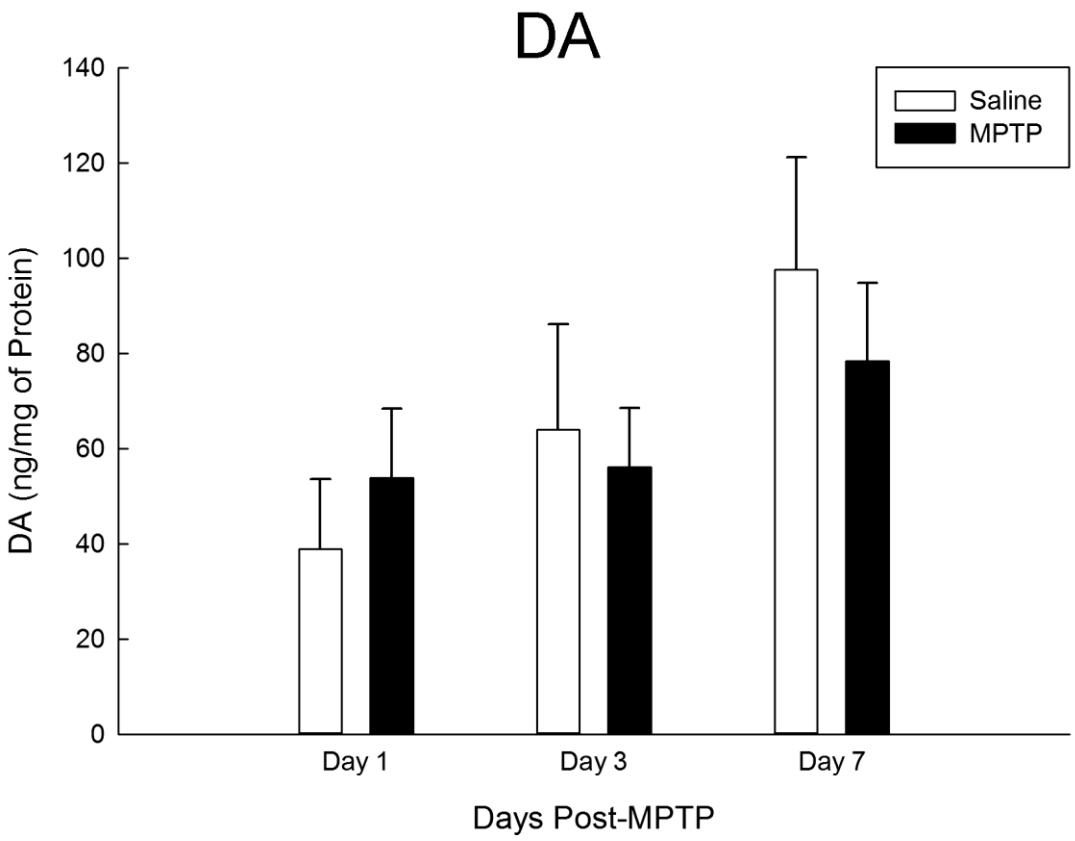

Figure 5.30 Extended time course effects of MPTP on DA concentration in the ME. Male C57Bl/6J mice were treated with either saline (10 ml/kg; s.c.) or MPTP (20 mg/kg; s.c.) and killed by decapitation 1, 3, or 7 d post-injection (n=8/group). Brains were sectioned, ME was microdissected, and samples were prepared for neurochemistry. Columns indicate the group means, error bars represent +1 standard error of the mean. An asterisk indicates values that are significantly different ($p < 0.05$; t-test) from the same day vehicle-treated controls.

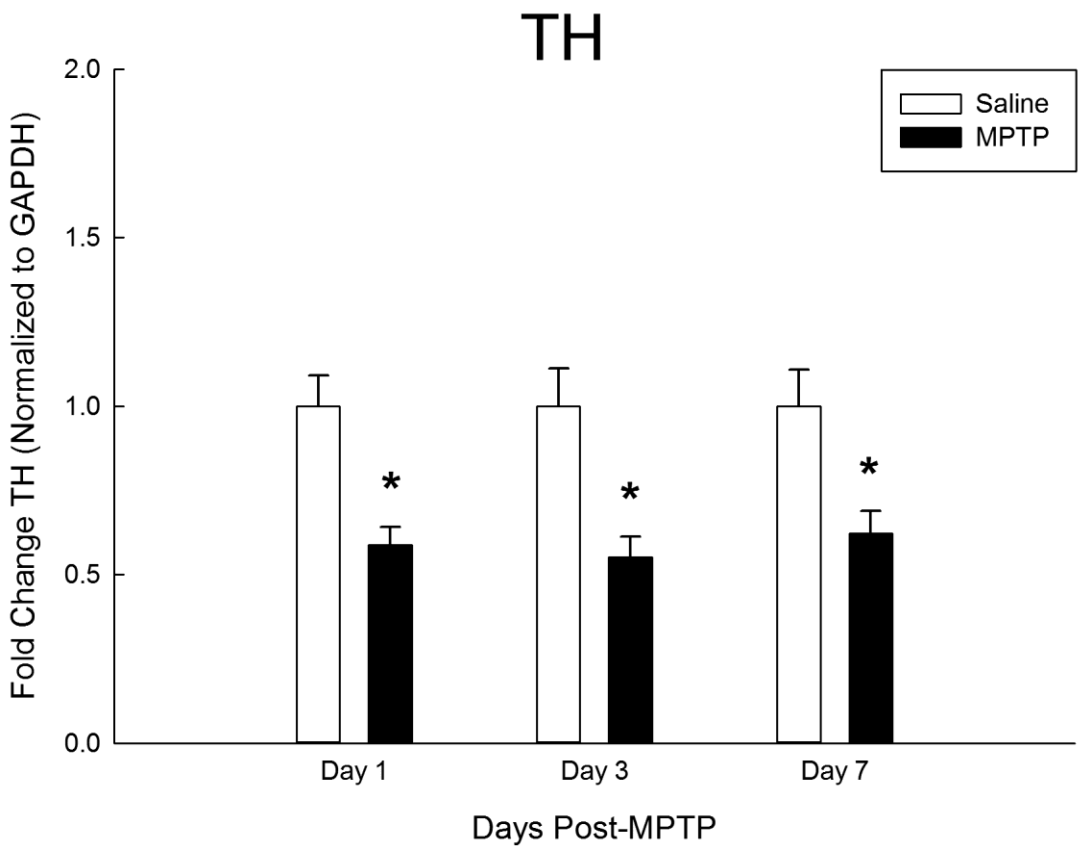

Figure 5.31 Extended time course effects of MPTP on TH expression in the ST. Male C57Bl/6J mice were treated with either saline (10 ml/kg; s.c.) or MPTP (20 mg/kg; s.c.) and killed by decapitation 1, 3, or 7 d post-injection (n=8/group). Brains were sectioned, ST was microdissected, protein isolated, and Western blots used to quantify TH normalized to GAPDH. Columns indicate the group means, error bars represent +1 standard error of the mean. An asterisk indicates values that are significantly different ($p < 0.05$; t-test) from the same day vehicle-treated controls.

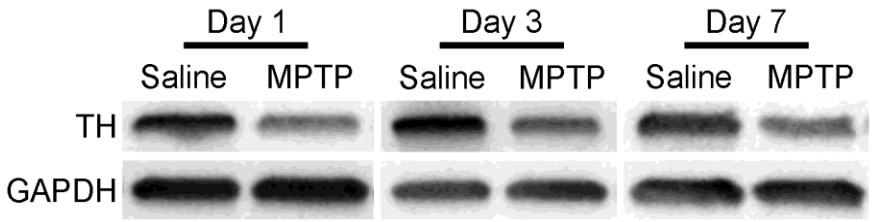

Figure 5.32 Representative Western blots for TH in the ST at 1, 3, or 7 d post-MPTP. TH was normalized to GAPDH.

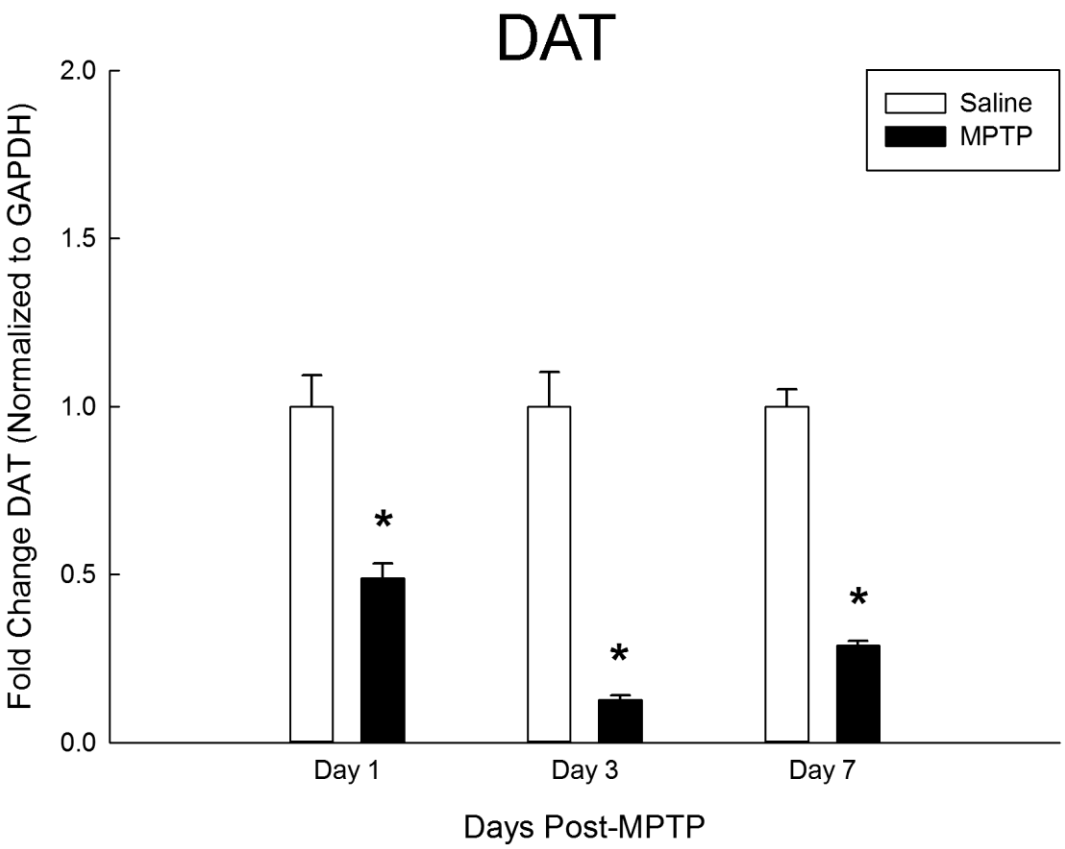

Figure 5.33 Extended time course effects of MPTP on DAT expression in the ST. Male C57Bl/6J mice were treated with either saline (10 ml/kg; s.c.) or MPTP (20 mg/kg; s.c.) and killed by decapitation 1, 3, or 7 d post-injection (n=8/group). Brains were sectioned, ST was microdissected, protein isolated, and Western blots used to quantify DAT normalized to GAPDH. Columns indicate the group means, error bars represent +1 standard error of the mean. An asterisk indicates values that are significantly different ($p < 0.05$; t-test) from the same day vehicle-treated controls.

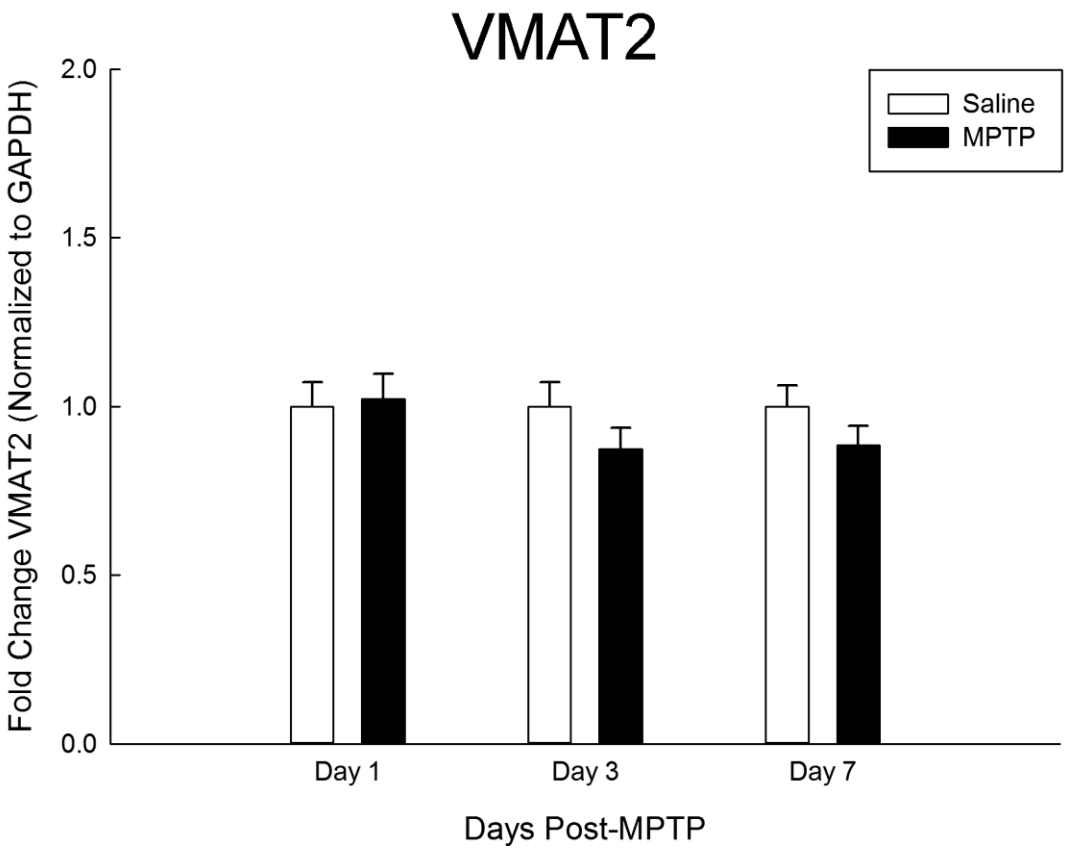

Figure 5.34 Extended time course effects of MPTP on VMAT expression in the ST. Male C57Bl/6J mice were treated with either saline (10 ml/kg; s.c.) or MPTP (20 mg/kg; s.c.) and killed by decapitation 1, 3, or 7 d post-injection (n=8/group). Brains were sectioned, ST was microdissected, protein isolated, and Western blots used to quantify VMAT normalized to GAPDH. Columns indicate the group means, error bars represent +1 standard error of the mean. An asterisk indicates values that are significantly different ($p < 0.05$; t-test) from the same day vehicle-treated controls.

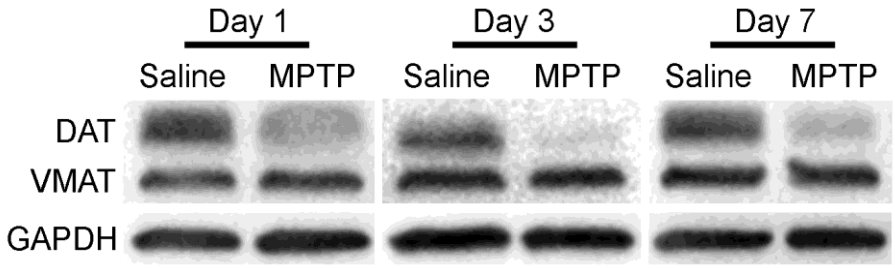

Figure 5.35 Representative Western blots for DAT and VMAT in the ST at 1, 3, or 7 d post-MPTP. DAT and VMAT were normalized to GAPDH.

In addition to the DA pathway, there were also changes in body weight. Animals were weighed just prior to neurotoxicant administration and then just prior to sacrifice either 1, 3 or 3 days later. MPTP treated animals at 1 and 3 d post-MPTP lost weight compared to same day vehicle controls. By 7 d post-MPTP, MPTP and vehicle animals had gained weight, with no difference in weight gain between groups (**Figure 5.36**).

Consistent with Figure 5.1, FosB at 1 d post-MPTP was approximately 2-fold higher in the ARC than in same day vehicle mice (**Figure 5.37 and 5.39**). FosB levels at 3 and 7 d post-MPTP were not different than same day vehicle controls (**Figure 5.37 and 5.39**). ΔFosB expression was approximately 3-fold higher in the ARC than the same day vehicle control at 1 d post-MPTP, but drops to about 1.5 fold higher than same day vehicle control at 7 d post-MPTP (**Figure 5.38 and 5.39**). Parkin, a potential downstream target of the FosBs, was found to be approximately 1.5 fold higher in the ARC than same day vehicle controls at 1, 3, and 7 d post-MPTP (**Figure 5.40 and 5.41**). In the SN there was no significant change in parkin protein at 1, 3, or 7 d post-MPTP (**Figure 5.42 and 5.43**).

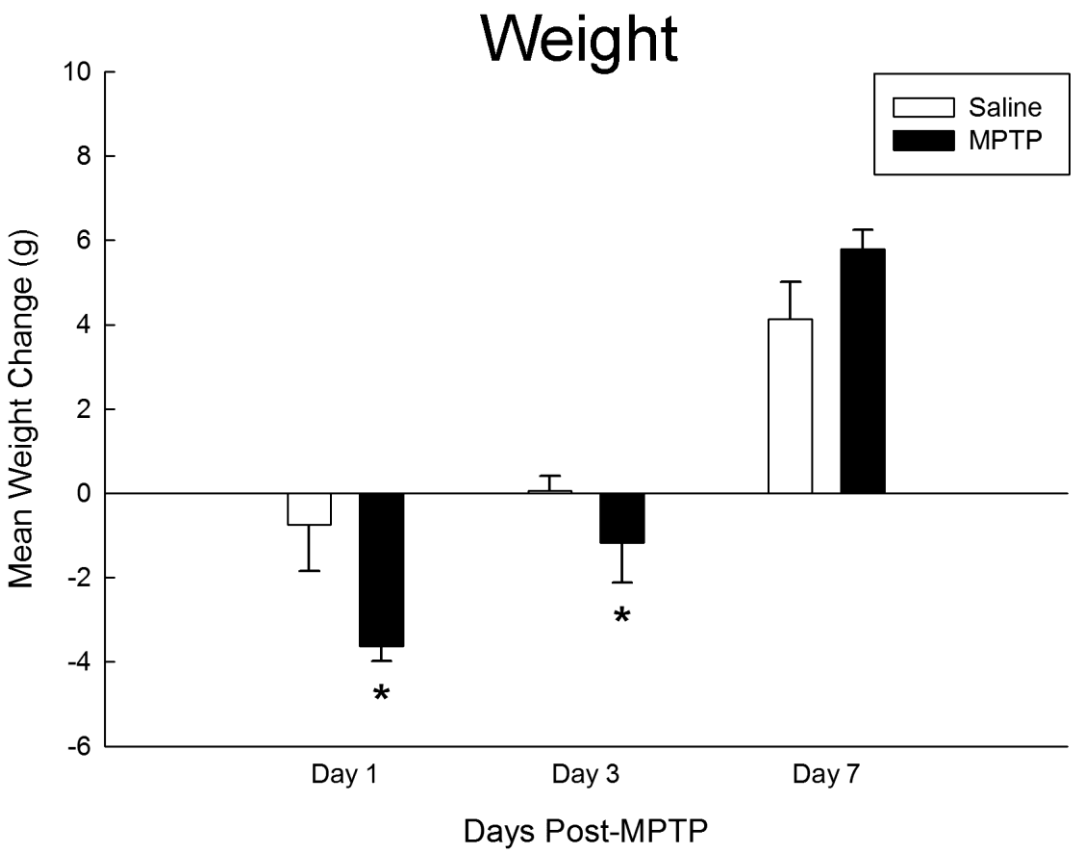

Figure 5.36 Extended time course effects of MPTP on weight change. Male C57Bl/6J mice were weighed prior to being treated with either saline (10 ml/kg; s.c.) or MPTP (20 mg/kg; s.c.) and reweighed prior to being killed by decapitation 1, 3, or 7 d post-injection (n=8/group). Change from the starting weight was calculated for each animal. Columns indicate the group means, error bars represent +1 standard error of the mean. An asterisk indicates values that are significantly different ($p < 0.05$; t-test) from the same day vehicle-treated controls.

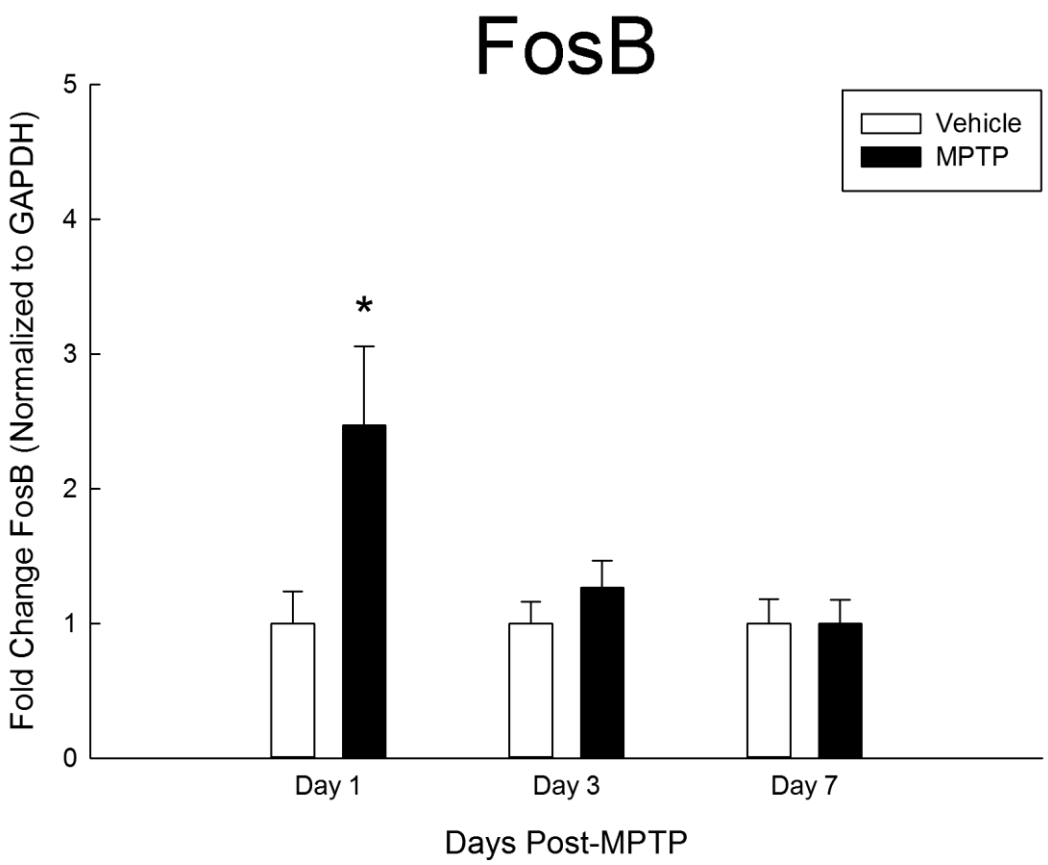

Figure 5.37 Extended time course effects of MPTP on FosB expression in the ARC. Male C57Bl/6J mice were treated with either saline (10 ml/kg; s.c.) or MPTP (20 mg/kg; s.c.) and killed by decapitation 1, 3, or 7 d post-injection (n=8/group). Brains were sectioned, ARC was microdissected, protein isolated, and Western blots used to quantify FosB normalized to GAPDH. Columns indicate the group means, error bars represent +1 standard error of the mean. An asterisk indicates values that are significantly different ($p < 0.05$; t-test) from the same day vehicle-treated controls.

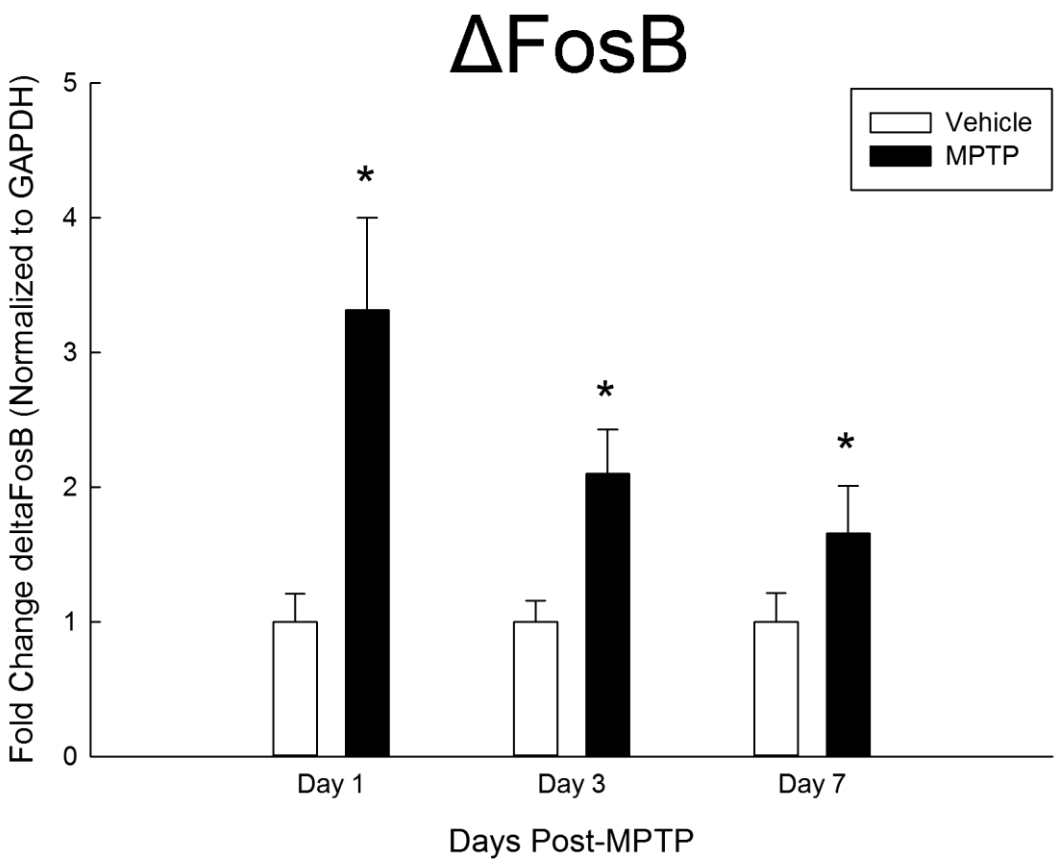

Figure 5.38 Extended time course effects of MPTP on ΔFosB expression in the ARC. Male C57Bl/6J mice were treated with either saline (10 ml/kg; s.c.) or MPTP (20 mg/kg; s.c.) and killed by decapitation 1, 3, or 7 d post-injection (n=8/group). Brains were sectioned, ARC was microdissected, protein isolated, and Western blots used to quantify ΔFosB normalized to GAPDH. Columns indicate the group means, error bars represent +1 standard error of the mean. An asterisk indicates values that are significantly different ($p < 0.05$; t-test) from the same day vehicle-treated controls.

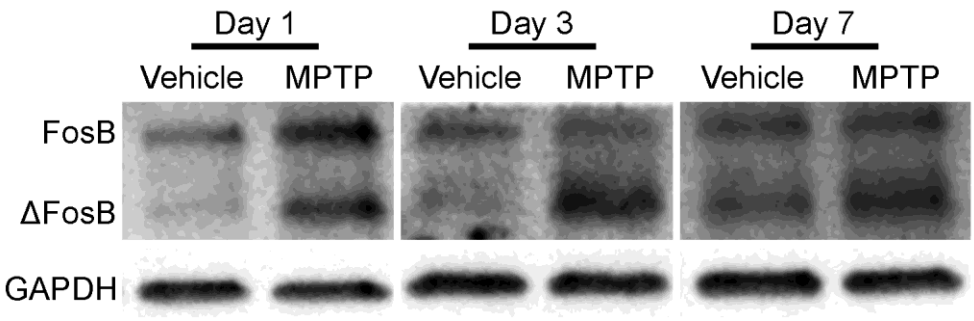

Figure 5.39 Representative Western blots for FosB and ΔFosB in the ARC at 1, 3, or 7 d post-MPTP. FosB and ΔFosB were normalized to GAPDH.

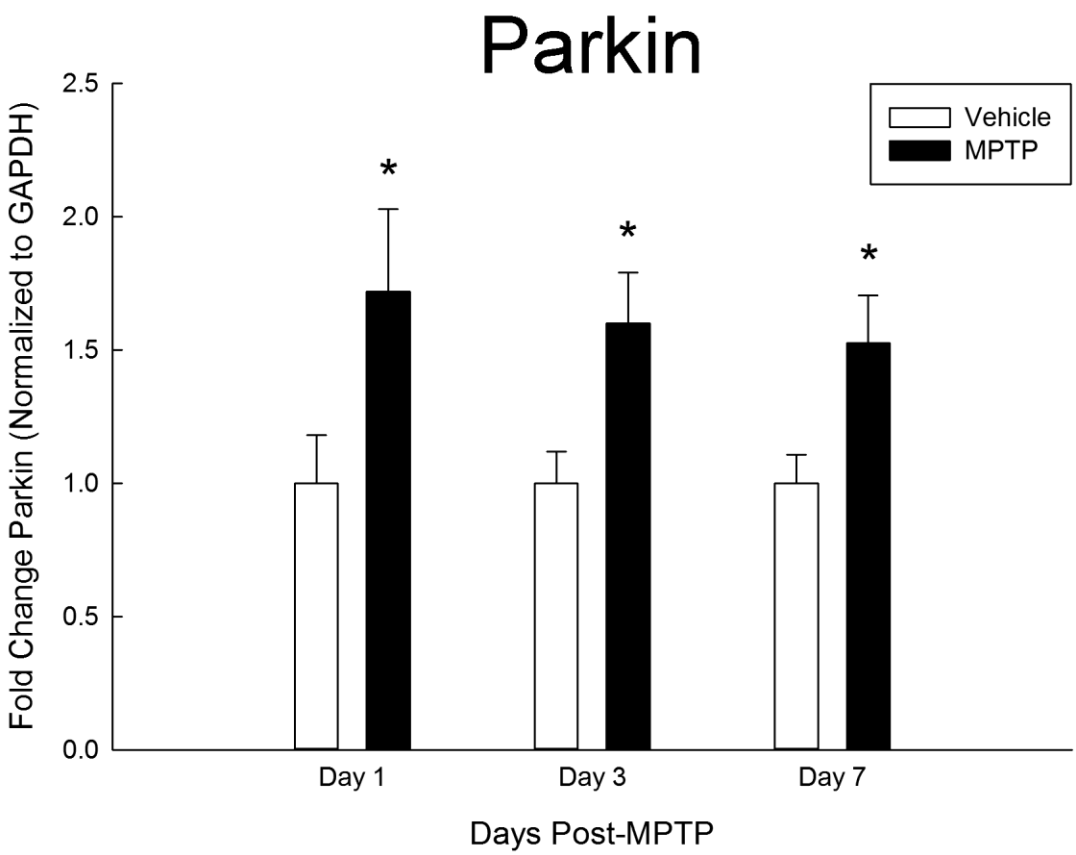

Figure 5.40 Extended time course effects of MPTP on parkin expression in the ARC. Male C57Bl/6J mice were treated with either saline (10 ml/kg; s.c.) or MPTP (20 mg/kg; s.c.) and killed by decapitation 1, 3, or 7 d post-injection (n=8/group). Brains were sectioned, ARC was microdissected, protein isolated, and Western blots used to quantify parkin normalized to GAPDH. Columns indicate the group means, error bars represent +1 standard error of the mean. An asterisk indicates values that are significantly different ($p < 0.05$; t-test) from the same day vehicle-treated controls.

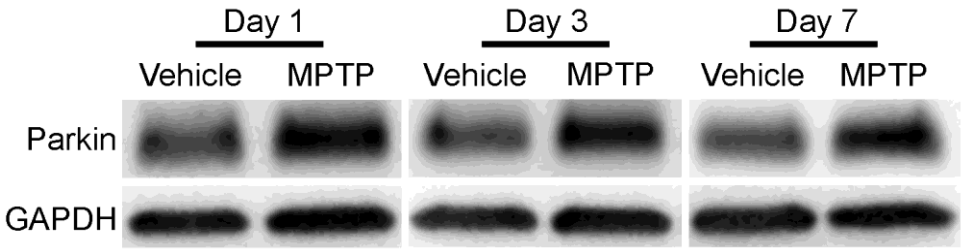

Figure 5.41 Representative Western blots for parkin in the ARC at 1, 3, or 7 d post-MPTP. Parkin was normalized to GAPDH.

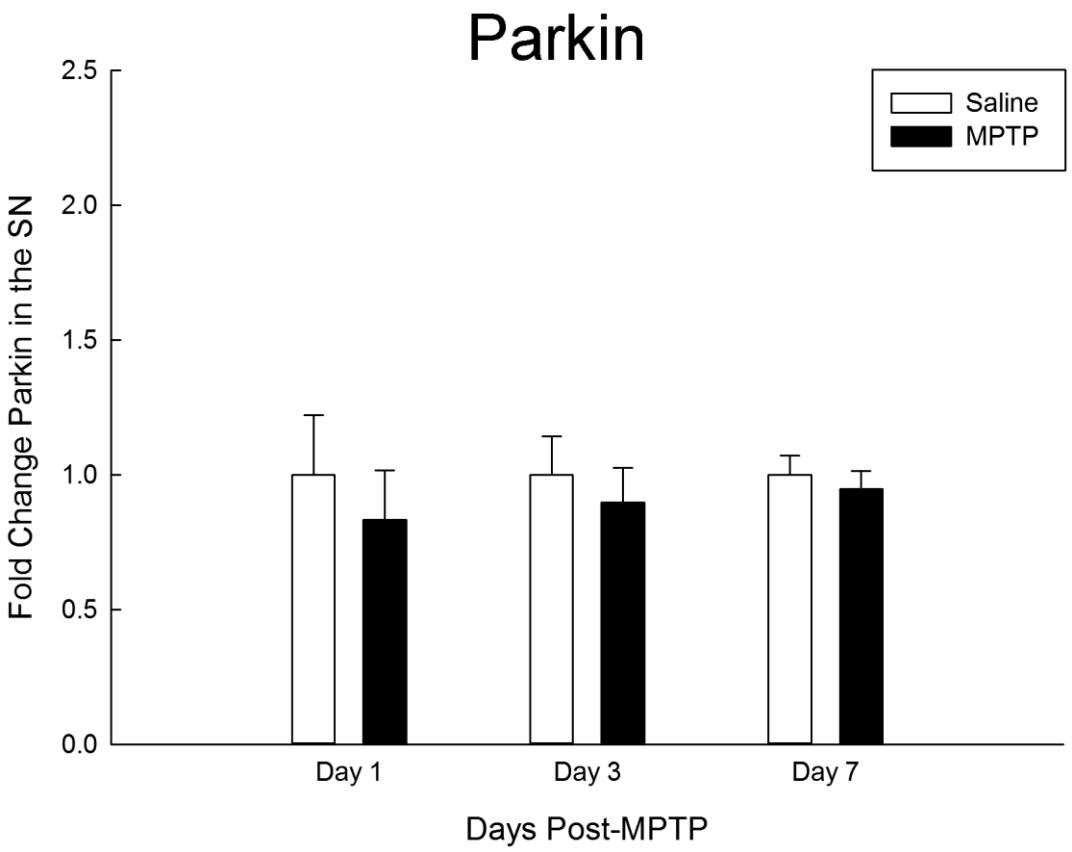

Figure 5.42 Extended time course effects of MPTP on parkin expression in the SN. Male C57Bl/6J mice were treated with either saline (10 ml/kg; s.c.) or MPTP (20 mg/kg; s.c.) and killed by decapitation 1, 3, or 7 d post-injection (n=8/group). Brains were sectioned, SN was microdissected, protein isolated, and Western blots used to quantify parkin normalized to GAPDH. Columns indicate the group means, error bars represent +1 standard error of the mean. An asterisk indicates values that are significantly different ($p < 0.05$; t-test) from the same day vehicle-treated controls.

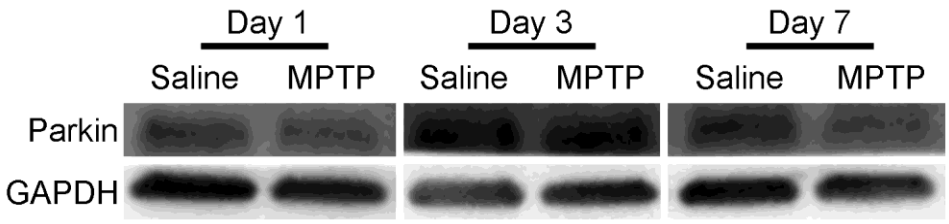

Figure 5.43 Representative Western blots for parkin in the SN at 1, 3, or 7 d post-MPTP. Parkin was normalized to GAPDH.

Correlation tests were performed comparing neurotoxicant-induced changes in FosB and ΔFosB with parkin. Pearson correlation coefficients calculated for FosB and parkin were 0.463 for the vehicle control, 0.517 at 1 d post-MPTP, -0.912 at 3 d post-MPTP, and 0.396 at 7 d post-MPTP (**Table 5.2**). Spearman correlation coefficients calculated for FosB and parkin were 0.381 for the vehicle control, 0.786 at 1 d post-MPTP, -0.874 at 3 d post-MPTP, and 0.667 at 7 d post-MPTP (**Table 5.2**). Pearson correlation coefficients calculated for ΔFosB and parkin were -0.349 for the vehicle control, 0.885 at 1 d post-MPTP, 0.899 at 3 d post-MPTP, and 0.894 at 7 d post-MPTP (**Table 5.2**). Spearman correlation coefficients calculated for ΔFosB and parkin were -0.0476 for the vehicle control, 0.929 at 1 d post-MPTP, 0.922 at 3 d post-MPTP, and 0.738 at 7 d post-MPTP (**Table 5.2**). In addition to Pearson and Spearman correlation coefficients, linear regressions were plotted for FosB and ΔFosB at 1, 3, and 7 days post-MPTP (**Figures 5.44 and 5.45**). The r^2 values for FosB and parkin were 0.214 for the vehicle control, 0.267 at 1 d post-MPTP, 0.832 at 3 d post-MPTP, and 0.157 at 7 d post-MPTP. The r^2 values for ΔFosB and parkin were 0.121 for the vehicle control, 0.782 at 1 d post-MPTP, 0.807 at 3 d post-MPTP, and 0.799 at 7 d post-MPTP.

Table 5.2 Pearson and Spearman correlation statistics in the comparison of FosB and ΔFosB to parkin.

Treatment	Protein Compared	Pearson Coefficient	Pearson P-value	Spearman Coefficient	Spearman P-value
Vehicle	FosB	0.463	0.248	0.381	0.321
	deltaFosB	-0.349	0.397	-0.0476	0.885
1 day post-MPTP	FosB	0.517	0.19	0.786	0.015
	deltaFosB	0.885	0.0035	0.929	0.001
3 days post-MPTP	FosB	-0.912	0.0016	-0.874	0.001
	deltaFosB	0.899	0.0024	0.922	0.001
7 days post-MPTP	FosB	0.396	0.332	0.667	0.059
	deltaFosB	0.894	0.0028	0.738	0.029

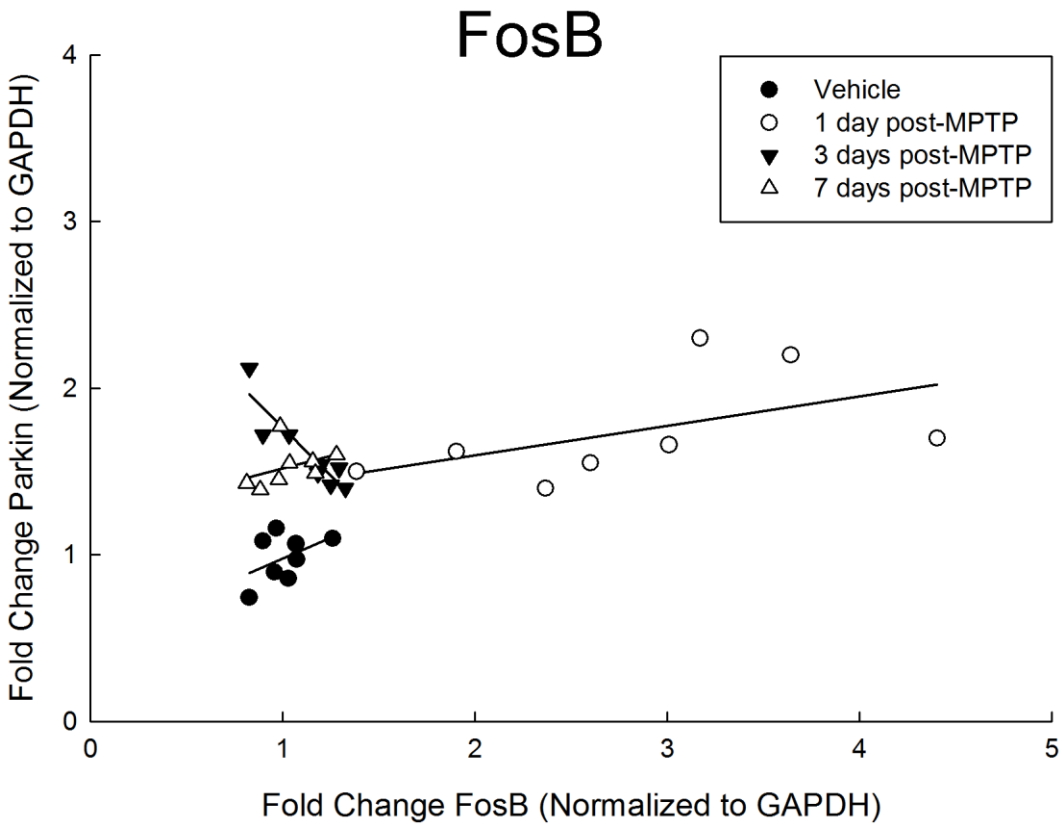

Figure 5.44 Linear regressions plotted for FosB as compared to parkin at 1, 3, and 7 days post-MPTP. FosB and parkin were normalized to GAPDH, fold change calculated based on same day vehicle control. Vehicle control shown was from 1 day post-injection, which does not statistically differ from 3 or 7 day controls.

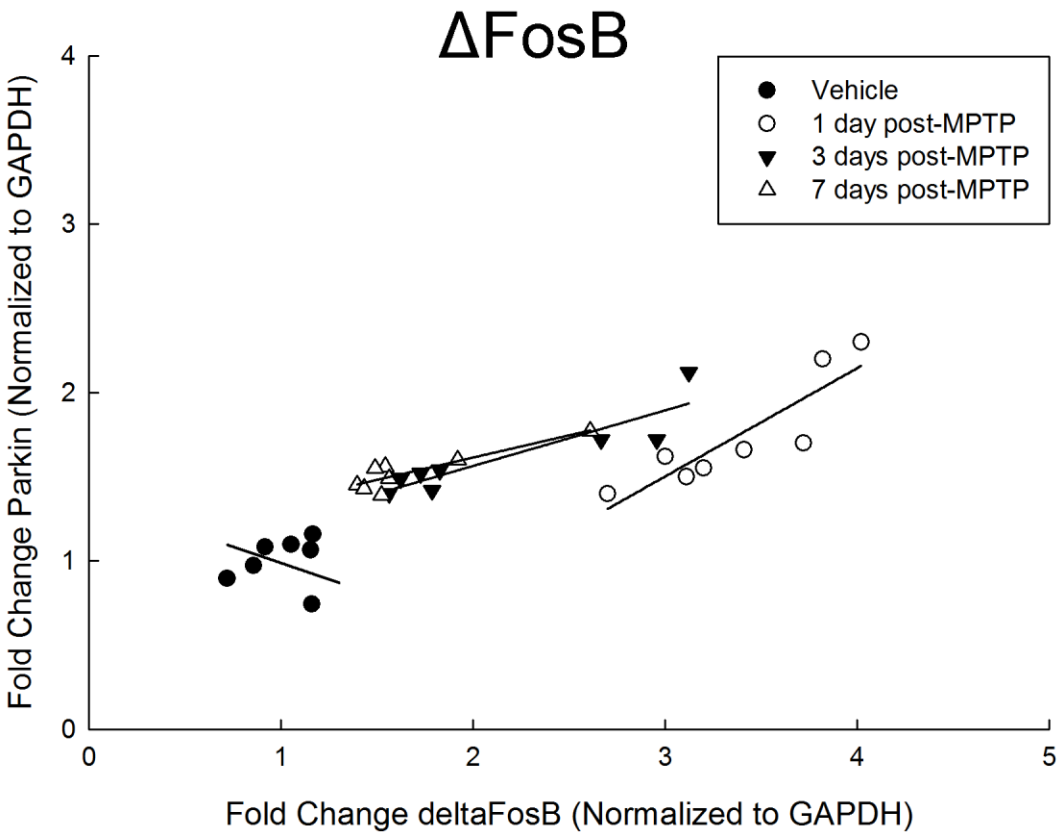

Figure 5.45 Linear regressions plotted for ΔFosB as compared to parkin at 1, 3, and 7 days post-MPTP. ΔFosB and parkin were normalized to GAPDH, fold change calculated based on same day vehicle control. Vehicle control shown was from 1 day post-injection, which does not statistically differ from 3 or 7 day controls.

Discussion

Acute MPTP has long-lasting effects in brain regions containing the NSDA and TIDA neurons. Similar to the differential recovery in the ST and ME at 1 d post-MPTP, there was no recovery in the ST of stored DA and complete recovery in the ME. These effects on DA stores in the ST are long lasting, with no sign of recovery up to 7 d post-MPTP. In addition to DA stores affected in the ST, deficiencies in proteins involved in DA synthesis and re-uptake persist. Both TH and DAT in the ST decrease with no signs of recovery up to 7 d post-MPTP. The losses observed in both of these proteins that are normally located in axon terminals suggest that MPTP administration may have resulted in axonopathy. A caveat to this is the steady-state expression of VMAT2 protein. As VMAT2 is found on synaptic vesicle membranes, no change in this protein suggests that the number of synaptic vesicles in the terminals does not change. Therefore either an axonopathy occurs and VMAT2 is up-regulated to compensate for axon loss in unlesioned neurons, or axonopathy does not occur and MPTP-induced decreases in TH and DAT are due to long-term down-regulation.

Decreases in DAT have been shown to precede cell death and loss of axon terminals of the NSDA neurons in response to MPTP (Muroyama et al., 2011; Kurosaki et al., 2003). Long-term decreases in DAT and TH support the hypothesis that axonopathy to some degree occurs after acute MPTP exposure. VMAT2 levels have been shown to correspond to neuron survival

in response to MPTP, where higher levels of VMAT2 results in resilience to neurotoxicant exposure (Lohr et al., 2016). Taken together, the results suggest axonopathy occurs and VMAT2 is a compensator mechanism that aids the remaining neurons in survival. To further examine axonopathy, a silver stain could be used to show axon density, or an additional axon marker could be used, such as synaptobrevin, synapsin, or synaptosomal associated protein of 25 kDa (SNAP25).

The finding that increased parkin in the ARC is maintained up to 7 d post-MPTP lends support to the hypothesis that FosB and ΔFosB act as transcription factors of parkin. The normal half-life of parkin is about 8 h, so transcription factors of parkin would need to be constantly present over all 7 d after MPTP (Hyun et al., 2002). ΔFosB levels in the ARC are elevated up to 7 d post-MPTP, consistent with the highly stable nature of ΔFosB and expectations of a transcription factor of parkin (Nestler, 2001). These findings also may explain the observation that parkin protein is elevated following chronic MPTP treatment. In one chronic MPTP experiment mice treated every 3.5 d for 35 d were allowed to recover 21 d, and even after the recovery period, parkin remained elevated in the ARC (Benskey et al., 2013). Accumulation of stable ΔFosB seems a reasonable explanation for why parkin expression is maintained over 21 d. Within individual mice there is a strong correlation between FosB and parkin expression only at 1 d post-MPTP, consistent with a role for early regulation of the parkin promoter by

the FosB family member. On the other hand, the long term regulator ΔFosB is highly correlated with elevated parkin protein at 1, 3, and 7 d post-MPTP. These results further strengthen the support for FosB and ΔFosB as transcriptional activators of parkin in the ARC, with ΔFosB contributing to the long-term expression of parkin.

Overall Conclusions

Consistent with the results presented in the previous chapter for 6 h post-MPTP exposure, data presented in this chapter reveal that the temporal expression of FosB and ΔFosB are differentially expressed the ARC and SN. In the ARC, expression of both FosBs increases by 2 h post-MPTP (well before parkin) and elevated levels of ΔFosB are maintained for at least 7 d post-MPTP, similar to the long-term parkin expression caused by MPTP. Taken together, the presence of total FosB in DA neurons, increase of ΔFosB in nuclei in the ARC after MPTP, the temporal expression of FosB and ΔFosB, and a correlation between ΔFosB and parkin expression are all consistent with the expectations of FosB and ΔFosB as transcriptional activators of parkin.

Chapter 6: Effects of Experimental Manipulation of ΔFosB on Parkin Expression in Cell Culture and in the ARC and SN

Introduction

The data presented in the previous chapter is consistent with the hypothesis that FosB and ΔFosB are transcription factors mediating the stimulatory effects of MPTP on parkin expression. Between both proteins, ΔFosB is the better candidate. ΔFosB is not only located in TIDA neurons in the ARC, but also levels of ΔFosB increase in the nuclear fraction of ARC extracts after MPTP. Long-term expression of ΔFosB correlates with expression of parkin and could account for long-term elevated parkin levels in the ARC in both acute and chronic models of MPTP (Benskey et al., 2013). MPTP has many potential deleterious effects in central DA neurons including generation of ROS and ER stress, but it is not known what causes the differential expression of the FosBs that results in the corresponding regional differences in the pattern of parkin expression after acute neurotoxicant exposure.

The *FosB* gene is regulated by both cAMP response element-binding protein (CREB) and serum response factor (SRF) (Morgan and Curran, 1995; Vialou et al., 2012). Multiple stimuli, such as growth factors, serum, neurotransmitters, and calcium, can lead to phosphorylation and therefore increased activity of CREB and SRF. CREB can be phosphorylated by protein

kinase A (PKA), calmodulin-dependent protein kinase II (CaMKII), calmodulin-dependent protein kinase IV (CaMKIV), protein kinase B, and p90 ribosomal S6 kinase (Sun et al., 1994; Delghandi et al., 2005; Du et al., 1998; Bohm et al., 1995). SRF can be phosphorylated by Casein kinase 2, calmodulin-dependent protein kinase IV (CaMKII), protein kinase A, and mitogen-activated protein kinase-activated protein kinase 2 (Chang et al., 2013; Miranti et al., 1995; Heidenreich et al., 1999; Blaker et al., 2009). Common pathways between phosphorylation of CREB and SRF are PKA and the CaMKs. PKA is activated by cAMP, which can accumulate due to adenylate cyclase and the G-protein coupled receptors. The CaMKs are regulated by the presence of Ca^{2+}. Changes in Ca^{2+} are common in neurons, as an influx of Ca^{2+} is required in neurons for neurotransmitter release into the synapse. In addition, ER stress and mitochondrial dysfunction can both cause Ca^{2+} accumulation in cells and subsequent CaMK activation (Deniaud et al., 2008; Arnould et al., 2002). In total, many of the stresses that MPTP is known to cause are potential induces of CREB and/or SRF phosphorylation. Through studying the pathways that may be involved in the differential induction of transcription of the *FosB* gene in different brain regions, further upstream information on parkin regulation may be revealed. In addition to possible mechanisms that may induce expression of the FosBs and parkin in response to neurotoxicant induced stress, expression of the FosBs can be

manipulated to determine if changes in FosB or ΔFosB effect parkin expression.

Expression of the FosBs can be induced through known means, such as PMA (phorbol 12-myristate 13-acetate, also called 12-O-tertradecanoylphorbol-12-acetate or TPA). PMA exposure of cells in culture induces expression of AP-1 proteins, including FosB (Limb et al., 2009; Gavala et al., 2010; Frigo et al., 2004; Yoza et al., 1992). FosB or ΔFosB protein can also be expressed *in vivo* via the use of adeno-associated viruses (AAV), recapitulating the downstream effects underlying addiction, hippocampal-dependent learning and memory, and levadopa induced dyskinesia (Hedges et al., 2009; Cao et al., 2010; Zhang et al., 2014; Eagle et al., 2015).

ΔJunD is a dominant negative protein that blocks the actions of FosB and ΔFosB (Been et al., 2013; Berton et al., 2009). ΔJunD is a truncated form of JunD that lacks 48 amino acids on the N-terminal end (Yazgan and Pfarr, 2002; Struhl, 1988). As the N-terminal end contains the DNA binding domain, but not the basic leucine zipper domain, dimers containing ΔJunD can form, but these are not functional as transcription factors. The experiments described in this chapter utilize PMA *in vitro*, and AAV-induced overexpression of ΔFosB and ΔJunD *in vivo* methods to determine if there is a causal link between FosBs and parkin expression under basal conditions and following neurotoxicant exposure.

Transcriptional Activators of the FosB Gene

Results

CREB and SRF, known transcriptional activators of *FosB* were measured at 1, 2 and 4 h after MPTP as a strategy to identify mechanisms underlying the MPTP-induced increase in FosB and ΔFosB in the ARC. Phosphorylated CREB (Ser133), increased over 2-fold by 1 h post-MPTP in the ARC and remained elevated at 4 h post-MPTP (**Figures 6.1 and 6.5**). In the SN, phosphorylated CREB decreased by 1 and 2 h post-MPTP, and returned to basal levels by 4 h post-MPTP (**Figures 6.1 and 6.5**). The expression of total CREB protein in the ARC or SN did not change at 1, 2, or 4 h post MPTP (**Figures 6.2 and 6.6**). Phosphorylated SRF (Ser103) increased to approximately 2-fold at 1 and 2 h post-MPTP in the ARC and returned to basal levels by 4 h post-MPTP (**Figures 6.3 and 6.5**). Phosphorylated SRF did not change in the SN at any of the time points examined (**Figures 6.3 and 6.5**), There was no change in total SRF in the ARC or SN (**Figures 6.4 and 6.6**).

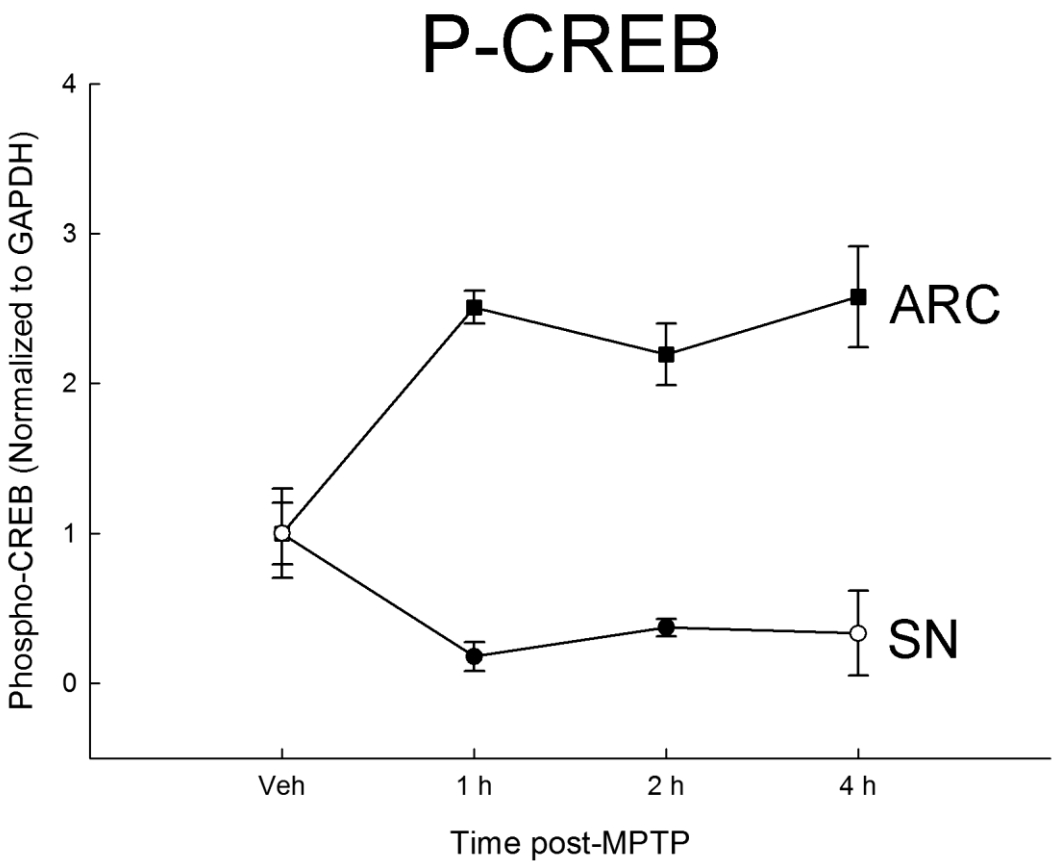

Figure 6.1 Early time course effects of MPTP on phosphorylated CREB (Ser133) in the ARC and SN. Male C57Bl/6J mice were treated with either saline (10 ml/kg; s.c.) or MPTP (20 mg/kg; s.c.) and killed by decapitation 1, 2, or 4 h post-injection (n=8/group). Brains were sectioned, ARC and SN were microdissected, protein isolated and Western blots used to quantify phosphorylated CREB normalized to GAPDH. Mean fold change are represented by shapes with ± 1 standard error of the mean. Values significantly different ($p<0.05$; one-way ANOVA) from the vehicle controls are denoted with filled shapes.

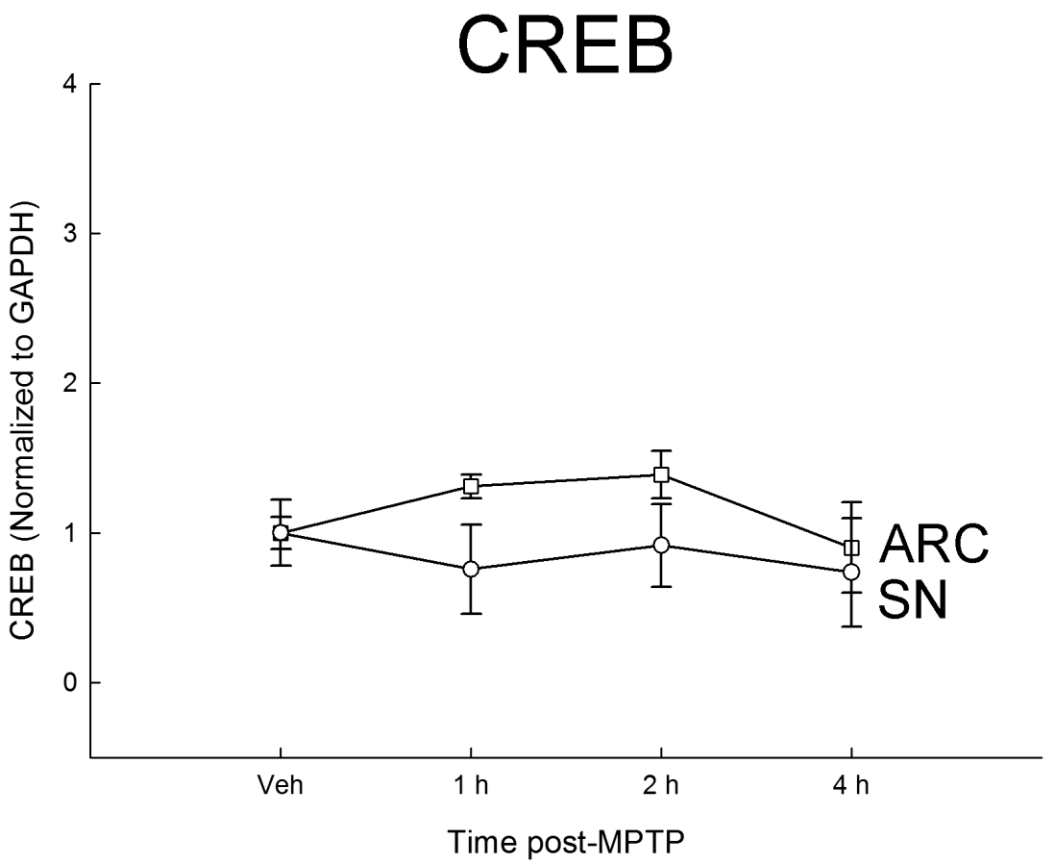

Figure 6.2 Early time course effects of MPTP on total CREB in the ARC and SN. Male C57Bl/6J mice were treated with either saline (10 ml/kg; s.c.) or MPTP (20 mg/kg; s.c.) and killed by decapitation 1, 2, or 4 h post-injection (n=8/group). Brains were sectioned, ARC and SN were microdissected, protein isolated and Western blots used to quantify CREB normalized to GAPDH. Mean fold change are represented by shapes with ± 1 standard error of the mean.

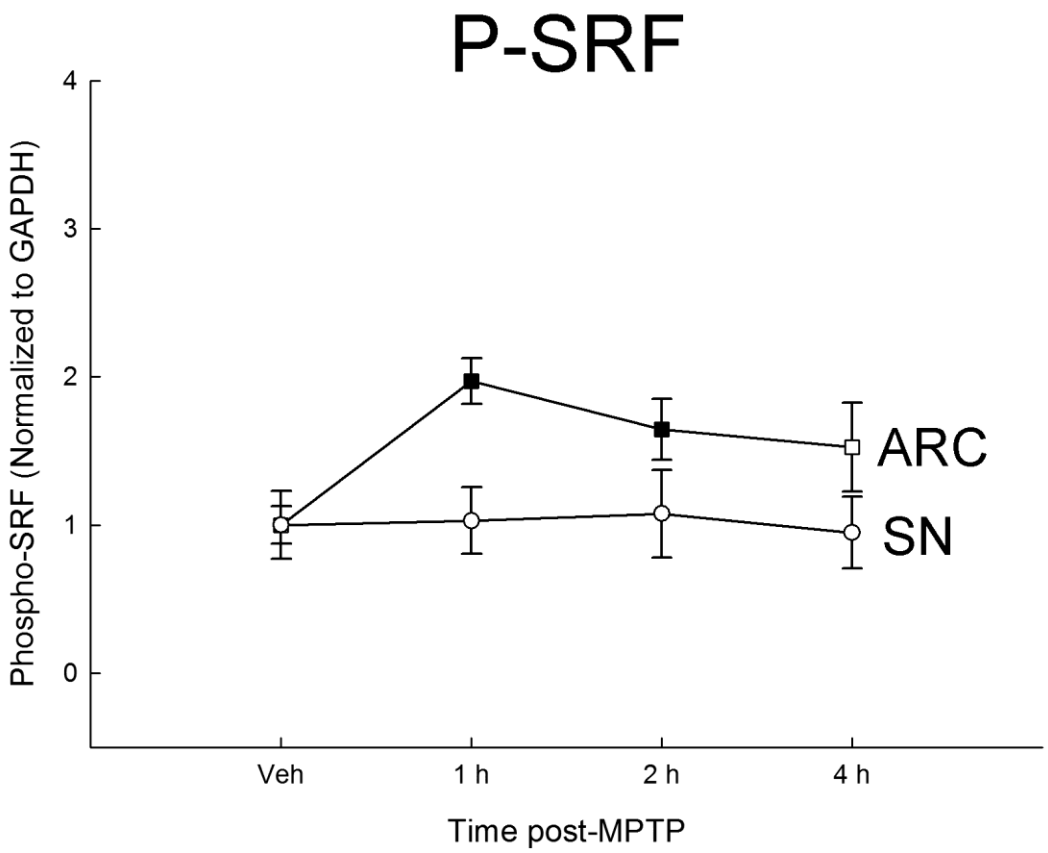

Figure 6.3 Early time course effects of MPTP on phosphorylated SRF (Ser103) in the ARC and SN. Male C57Bl/6J mice were treated with either saline (10 ml/kg; s.c.) or MPTP (20 mg/kg; s.c.) and killed by decapitation 1, 2, or 4 h post-injection (n=8/group). Brains were sectioned, ARC and SN were microdissected, protein isolated and Western blots used to quantify phosphorylated SRF normalized to GAPDH. Mean fold change are represented by shapes with ± 1 standard error of the mean. Values significantly different ($p<0.05$; one-way ANOVA) from the vehicle controls are denoted with filled shapes.

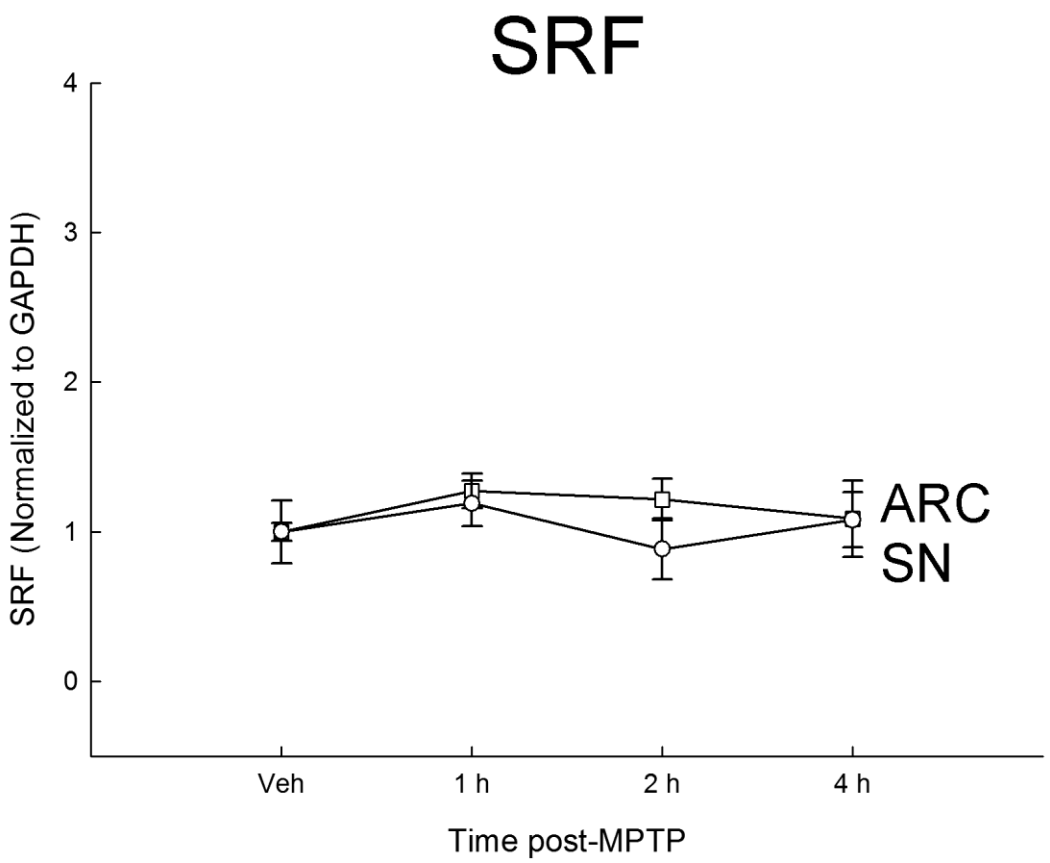

Figure 6.4 Early time course effects of MPTP on total SRF in the ARC and SN. Male C57Bl/6J mice were treated with either saline (10 ml/kg; s.c.) or MPTP (20 mg/kg; s.c.) and killed by decapitation 1, 2, or 4 h post-injection (n=8/group). Brains were sectioned, ARC and SN were microdissected, protein isolated and Western blots used to quantify SRF normalized to GAPDH. Mean fold change are represented by shapes with ± 1 standard error of the mean.

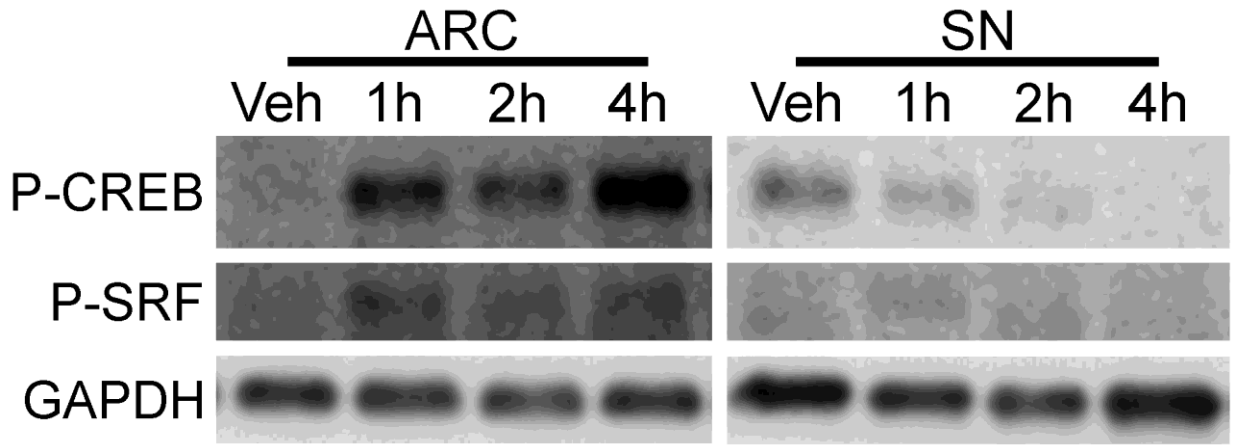

Figure 6.5 Representative Western blots for phosphorylated CREB (Ser133) and phosphorylated SRF (Ser103) in the ARC and SN at 1, 2, or 4 h post-MPTP. Phosphorylated CREB and SRF were normalized to GAPDH.

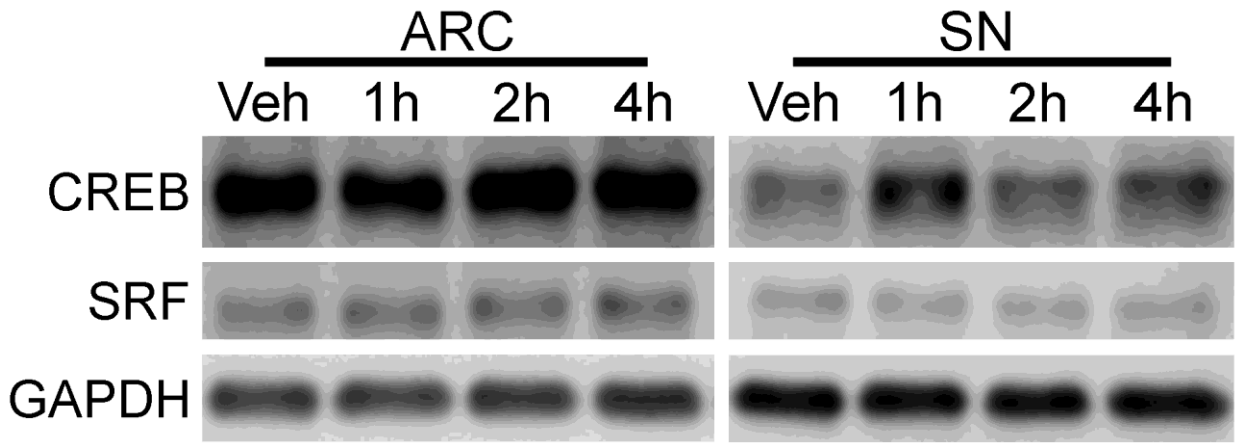

Figure 6.6 Representative Western blots for total CREB and SRF in the ARC and SN at 1, 2, or 4 h post-MPTP. CREB and SRF were normalized to GAPDH.

Discussion

In order to elucidate a potential mechanism for differential expression of parkin following acute MPTP exposure known transcriptional activators of the *FosB* gene, SRF and CREB, were examined (Vialou et al., 2012). Both CREB and SRF have been shown to have a potential role in the response to oxidative stress in neurons (Lee et al., 2009; Rieker et al., 2012). Phosphorylated SRF and CREB both increase early (by 1 h) after MPTP in the ARC but not the SN. Total SRF and CREB expression is not effected by MPTP, suggesting that increased kinase activity, rather than transcription leads to the increases the phosphorylated forms.

In relation to FosB and ΔFosB expression, both phosphorylated SRF and CREB expression are consistent with these transcription factors acting on the *FosB* gene. Though FosB is already elevated by 1 h post-MPTP, ΔFosB levels are not elevated until 2 h and do not peak until 4 h post-MPTP. Since ΔFosB is still in the process of increasing, this suggests that transcription factors are acting at the *FosB* promoter during this timeframe. At both 1 and 2 h post-MPTP phosphorylated SRF levels are elevated and at 1, 2 and 4 h post-MPTP phosphorylated CREB is elevated. Though none of the time points measured show the increase in phosphorylated SRF or CREB preceding FosB expression, the differential expression between the ARC and SN and the temporal expression of phosphorylated SRF and CREB are consistent with their known roles as transcriptional activators of FosB.

In addition to interactions with the *FosB* gene, phosphorylation of SRF and CREB are potentially activators of other genes that could aid in the recovery of the TIDA neurons. The loss of SRF for example, has been shown to increase the sensitivity of NSDA neurons to MPTP (Rieker er al., 2012). This suggests that the increase of phosphorylated SRF could be beneficial to the TIDA neurons, possibly through activation of FosB/ΔFosB expression.

FosB and ΔFosB in the MN9D Dopaminergic Cell Line

Results

To better study FosB and ΔFosB in a pure neuronal population, the neuroblastoma-derived MN9D cell line was used. As with NSDA neurons in the brain in response to MPTP administration *in vivo*, addition of its active metabolite MPP^+ *in vitro* results in decreased stored DA in MN9D cells (**Figure 6.7**). MPP^+ however did not decrease MN9D cell viability at least out to 24 h post-MPP^+ (**Figure 6.8**). As anticipated, MPP^+ did not cause a change in FosB or ΔFosB expression in MN9D cells at 6 or 12 h post-MPP^+ (**Figure 6.9-6.11**). Parkin expression in MN9D cells at 6 and 12 h post-MPP^+ also did not change (**Figure 6.12 and 6.13**).

PMA was used to induce expression of AP-1 transcription factors FosB and ΔFosB in MN9D cells. Both FosB and ΔFosB were increased in the MN9D cells at 6 and 12 h post-PMA. FosB had a fold change of 2.61 ± 0.29 at 6 h and 2.48 ± 0.05 at 12 h post-PMA (**Figure 5.14 and 5.16**). ΔFosB had a fold

change of 3.68 ± 0.16 at 6 h and 3.11 ± 0.32 at 12 h post-PMA (**Figure 5.15 and 5.16**). Although FosB and ΔFosB expression is activated by PMA, there was no change in parkin expression (**Figure 5.17 and 5.18**).

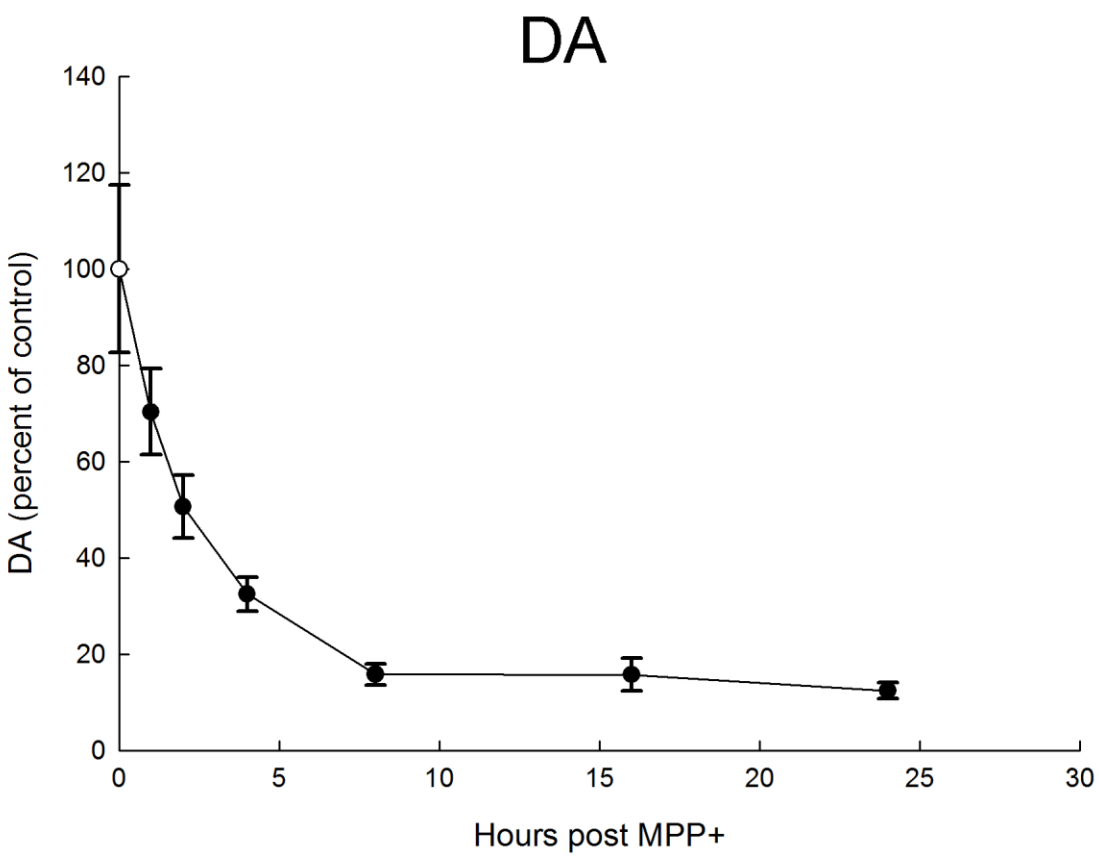

Figure 6.7 Effects of MPP^+ on stored DA in MN9D cells. MN9D cells were treated with 200 μM MPP^+ in DMEM media. Cells were collected at 0.5, 1, 2, 4, 8, 16, and 24 h post-MPP^+ and prepared for neurochemical analysis. Time-points are plotted as percent of control and are represented by circles with ± 1 standard error of the mean. Values significantly different ($p<0.05$; one-way ANOVA) from the vehicle controls are denoted with filled circles.

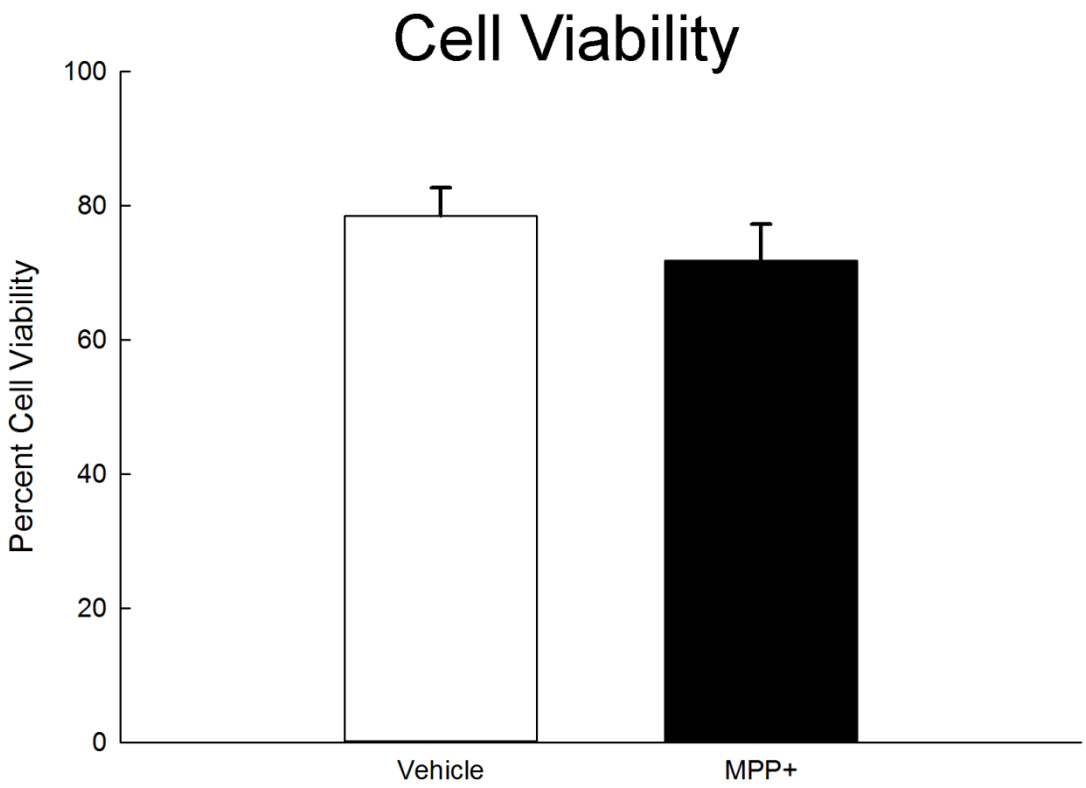

Figure 6.8 Cell viability of MN9D cells at 24 h post MPP^+. MN9D cells were treated with 200 μM MPP^+ in DMEM media. Cells were collected at 24 h post-MPP^+ and a trypan blue assay used to assess cell viability. Mean percent of viable cells are plotted as columns with error bars representing + 1 standard error of the mean.

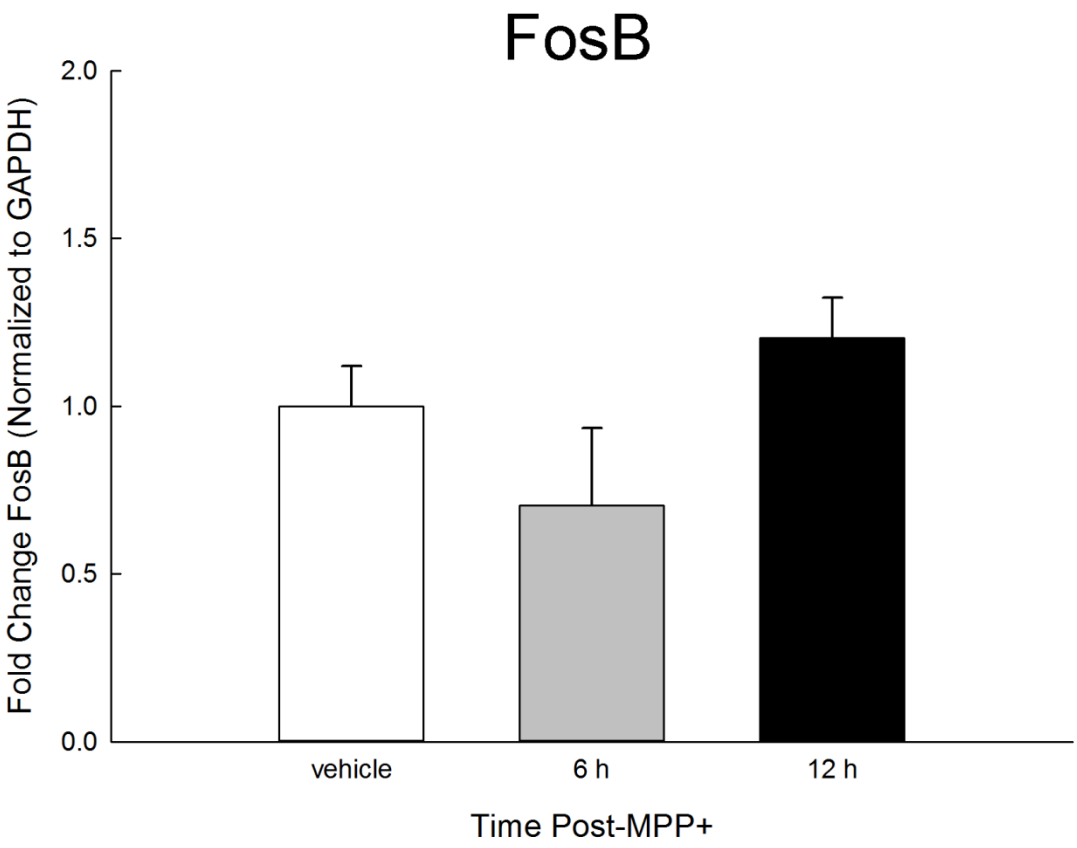

Figure 6.9 FosB expression in MN9D cells at 6 and 12 h post MPP$^+$. MN9D cells were treated with 200 µM MPP$^+$ in DMEM media. Cells were collected at 6 and 12 h post-MPP$^+$, protein isolated, and Western blots used to quantify FosB normalized to GAPDH. Mean fold change from vehicle control is represented by columns with error bars representing + 1 standard error of the mean.

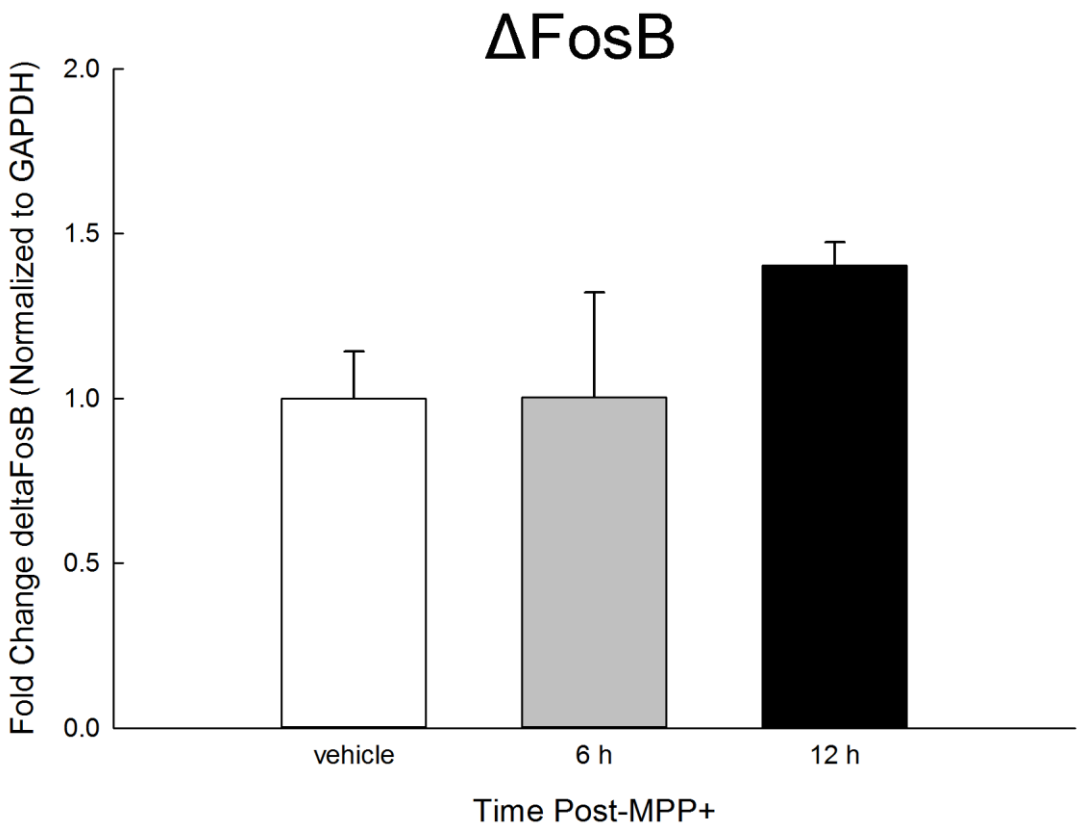

Figure 6.10 ΔFosB expression in MN9D cells at 6 and 12 h post MPP^+. MN9D cells were treated with 200 μM MPP^+ in DMEM media. Cells were collected at 6 and 12 h post-MPP^+, protein isolated, and Western blots used to quantify ΔFosB normalized to GAPDH. Mean fold change from vehicle control is represented by columns with error bars representing + 1 standard error of the mean.

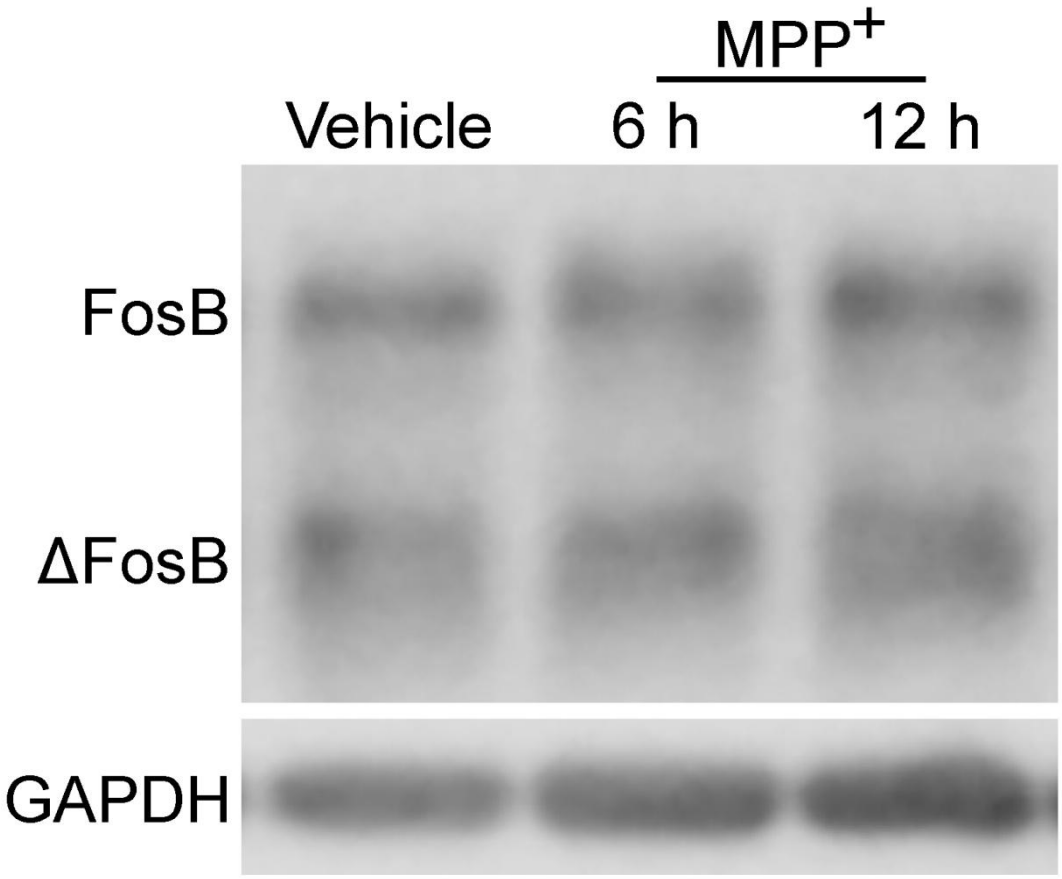

Figure 6.11 Representative Western blot for FosB and ΔFosB in MN9D cells at 6 and 12 h post-MPP$^+$. FosB and ΔFosB were normalized to GAPDH.

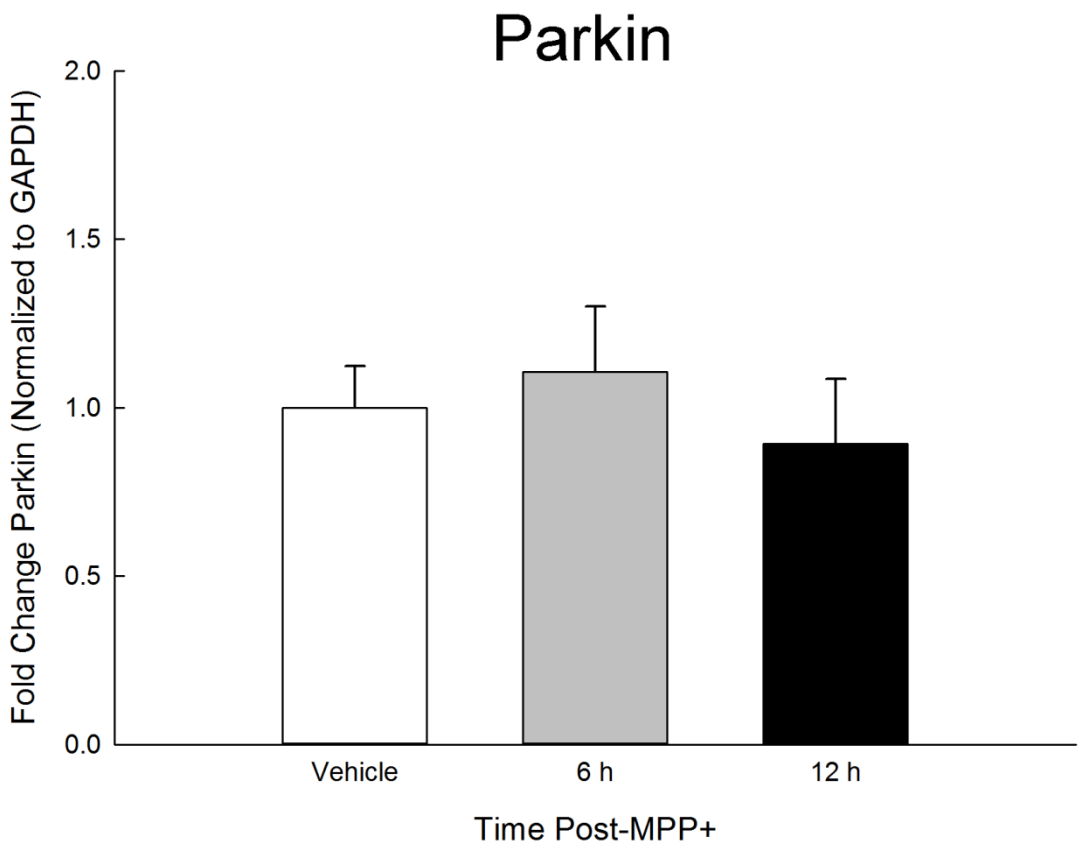

Figure 6.12 Parkin expression in MN9D cells at 6 and 12 h post MPP^+. MN9D cells were treated with 200 μM MPP^+ in DMEM media. Cells were collected at 6 and 12 h post-MPP^+, protein isolated, and Western blots used to quantify parkin normalized to GAPDH. Mean fold change from vehicle control is represented by columns with error bars representing + 1 standard error of the mean.

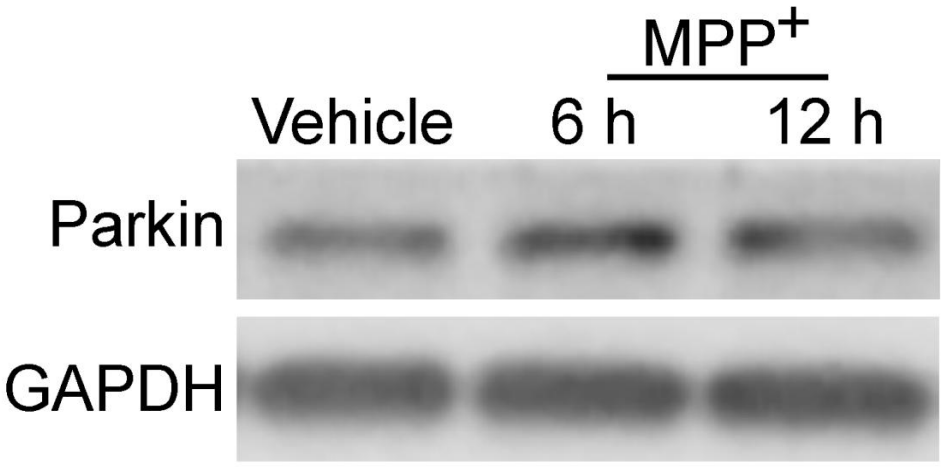

Figure 6.13 Representative Western blot for parkin in MN9D cells at 6 and 12 h post-MPP$^+$. Parkin was normalized to GAPDH.

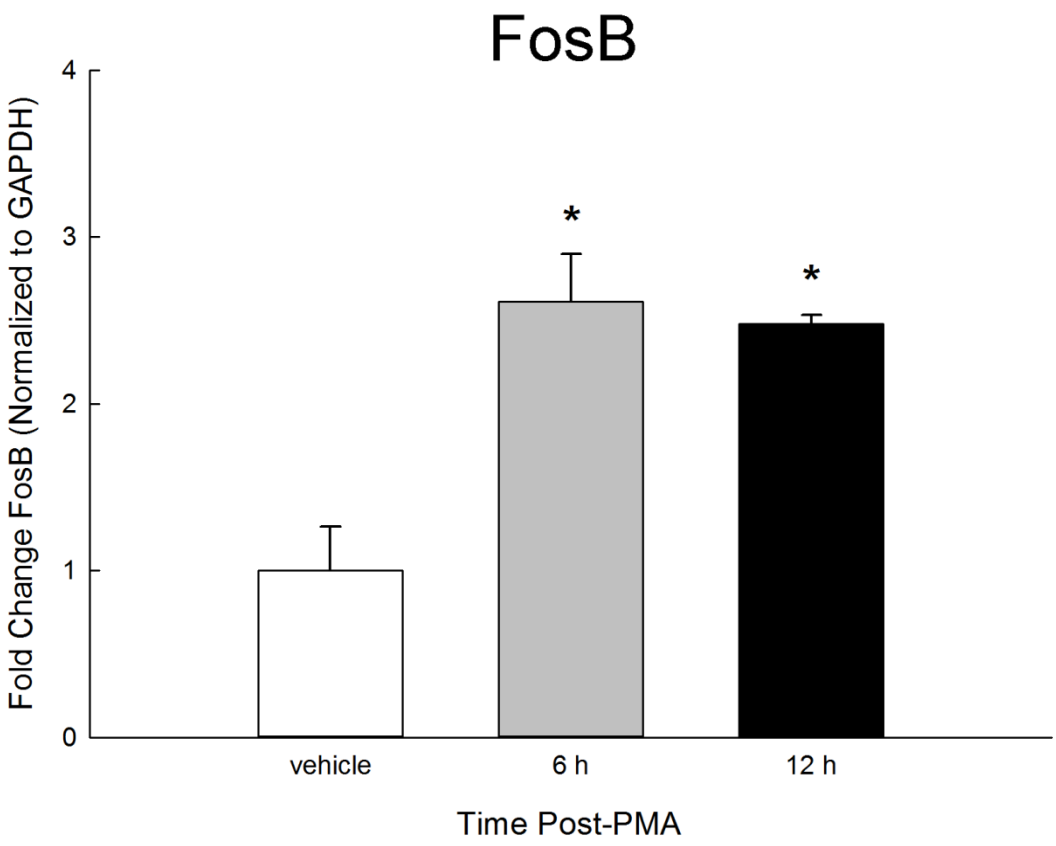

Figure 6.14 FosB expression in MN9D cells at 6 and 12 h post PMA. MN9D cells were treated with 50 μM PMA in DMEM media. Cells were collected at 6 and 12 h post-PMA, protein isolated, and Western blots used to quantify FosB normalized to GAPDH. Mean fold change from vehicle control is represented by columns with error bars representing + 1 standard error of the mean. Values significantly different ($p<0.05$; one-way ANOVA) from the vehicle controls are denoted with asterisks.

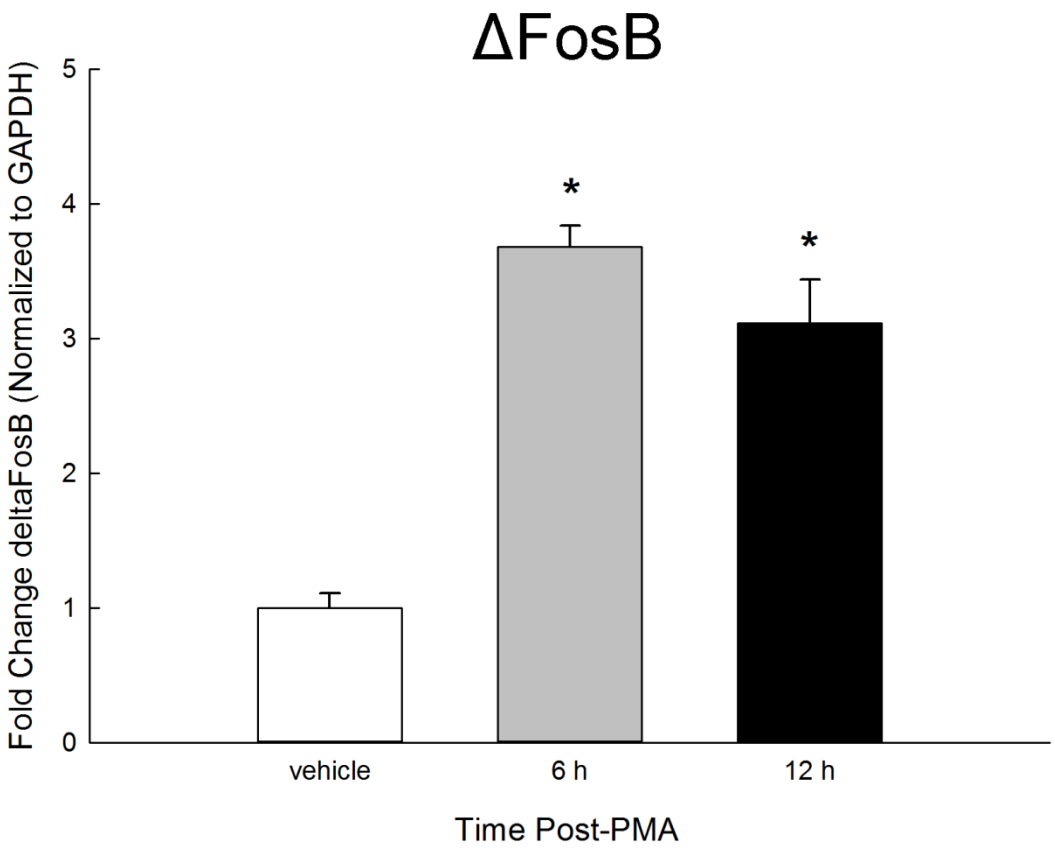

Figure 6.15 ΔFosB expression in MN9D cells at 6 and 12 h post PMA. MN9D cells were treated with 50 μM PMA in DMEM media. Cells were collected at 6 and 12 h post-PMA, protein isolated, and Western blots used to quantify ΔFosB normalized to GAPDH. Mean fold change from vehicle control is represented by columns with error bars representing + 1 standard error of the mean. Values significantly different ($p<0.05$; one-way ANOVA) from the vehicle controls are denoted with asterisks.

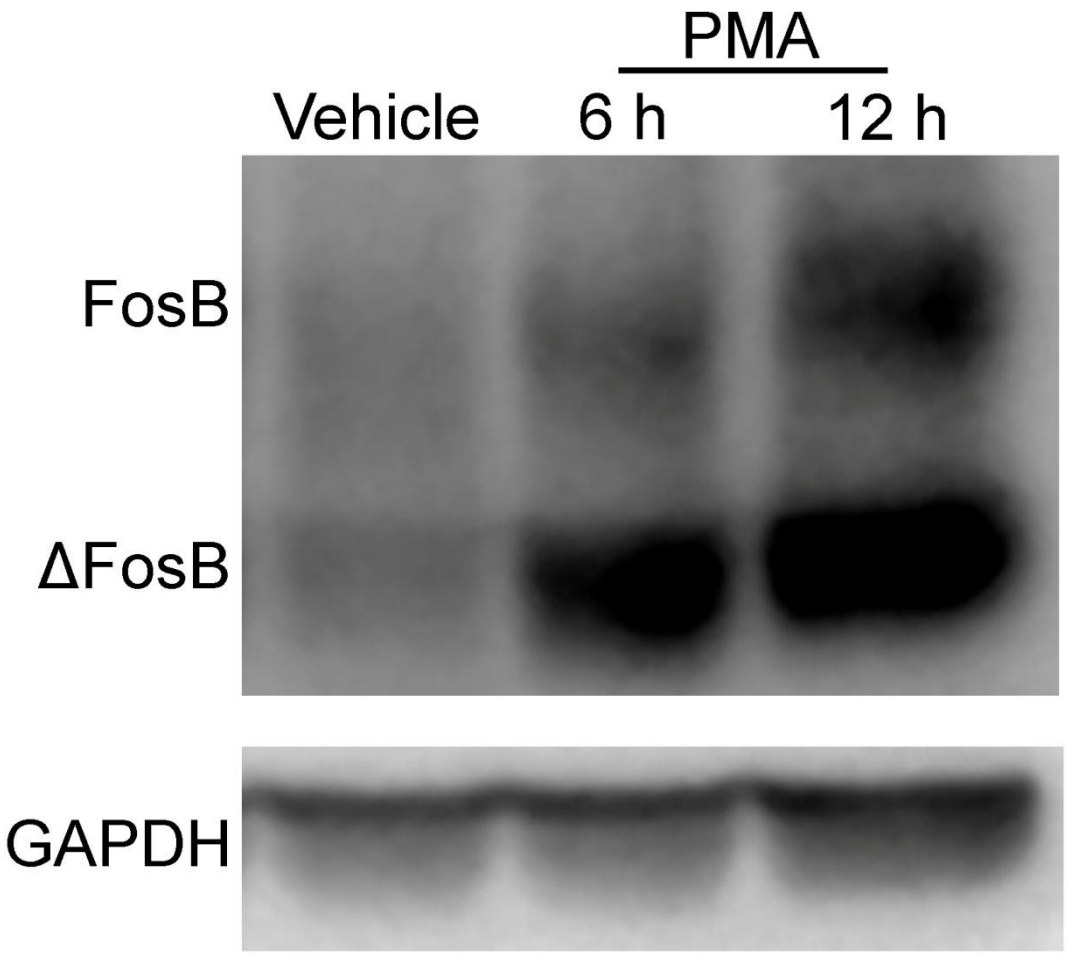

Figure 6.16 Representative Western blot for FosB and ΔFosB in MN9D cells at 6 and 12 h post-PMA. FosB and ΔFosB were normalized to GAPDH.

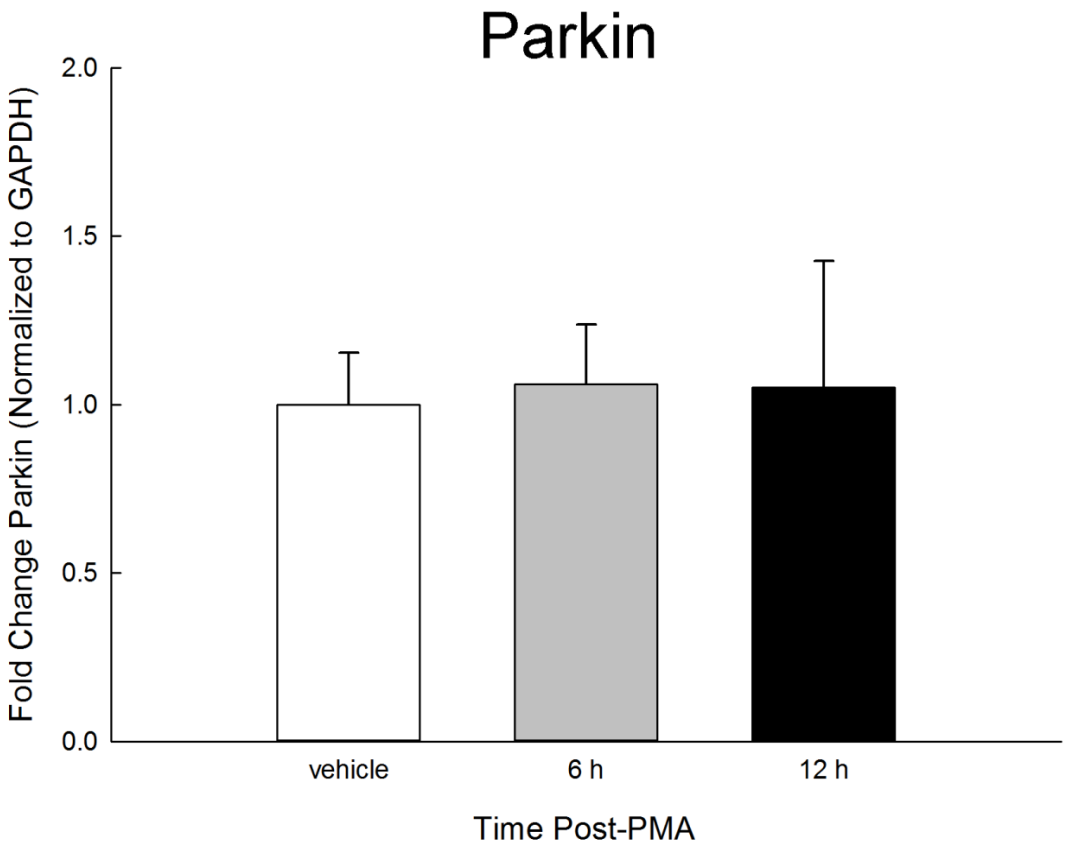

Figure 6.17 Parkin expression in MN9D cells at 6 and 12 h post PMA. MN9D cells were treated with 50 μM PMA in DMEM media. Cells were collected at 6 and 12 h post-PMA, protein isolated, and Western blots used to quantify parkin normalized to GAPDH. Mean fold change from vehicle control is represented by columns with error bars representing + 1 standard error of the mean.

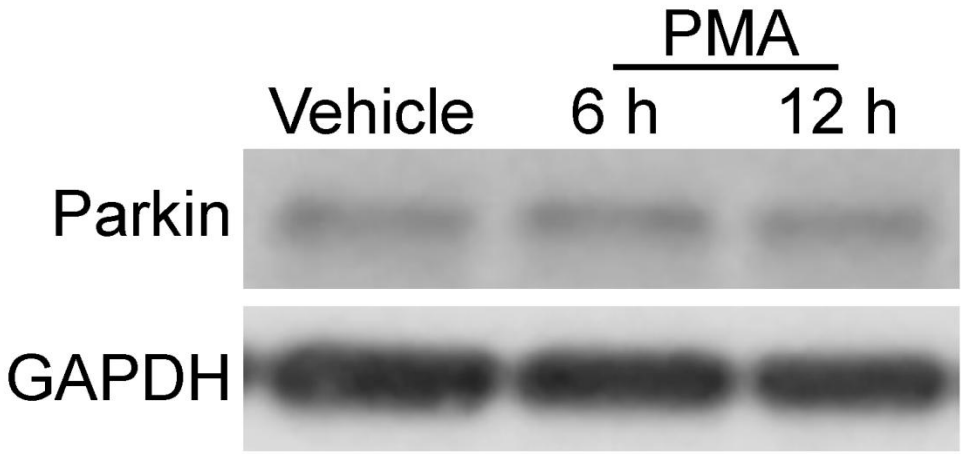

Figure 6.18 Representative Western blot for parkin in MN9D cells at 6 and 12 h post-PMA. Parkin was normalized to GAPDH.

Discussion

Results from the *in vitro* experiments reveal that MN9D cells closely resemble what has been previously found for NSDA neurons in the SN. Indeed, MPP^+ (the active metabolite of MPTP) leads to a rapid, time-dependent decrease in cellular stored DA that does not recover by 24 h after treatment. With no change observed in cell viability, this loss in DA is not the result of cell loss. It is also important to note that there is no increase in ROS in MN9D cells at the concentration of MPP^+ used (Choi et al., 1999). The absence of any change in FosB or ΔFosB also mirrors the lack of change in these transcription factors in the SN. Moreover, then was no there was no change in parkin in these cells. This is slightly different than the SN, where parkin in the SN decreases by 24 h after MPTP (Benskey et al., 2012). Comparing the MN9D cells to the ARC, the two are completely different in regards to DA stores, and expression of FosBs and parkin. MN9D cells do not recover DA stores by 24 h after neurotoxicant exposure nor do these cells have increased expression of FosBs or parkin as is seen in the ARC (Benskey et al., 2012). Accordingly, MN9D cells responses are more like those of NSDA neurons than the TIDA neurons, as such, MN9D cells are not a good model to study transcription factor mediated parkin expression following neurotoxicant exposure.

PMA is a phorbol ester commonly used *in vitro* to stimulate expression of AP-1 transcription factors including FosBs (Lee et al., 1997). To determine if

induction of AP-1 transcription factor expression is linked to activation of parkin expression MN9D cells were treated with PMA. With PMA, FosB and ΔFosB expression increases, however there is no increase in parkin, suggesting that FosB and ΔFosB may not be direct transcription factors of parkin in this neuroblastoma cell line. There are a few caveats to this interpretation.

While PMA was used to induce AP-1 transcription factors in these experiments, this induction is not specific to just FosB or ΔFosB. PMA leads to global up-regulation of AP-1 transcription factors, and in other neuronal cell lines such as SHSY-5Y cells, is used to terminally differentiate cells (Balasooriya and Wimalasena, 2007). MN9D cells are a fusion of mouse embryonic ventral mesencephalic neurons with neuroblastoma cells (Choi et al., 1992). As such the MN9D cells are an immortalized cell line that are continually dividing. MN9D cells will continue to divide until terminally differentiated, at which time the cells express DAT, become able to uptake DA, and take on the appearance of a typical neuron (cell body with projections) (Balasooriya and Wimalasena, 2007; Choi et al., 1992).

Differentiation of MN9D cells can be achieved through exposure to sodium butyrate over a period of days. Sodium butyrate is a histone deacetylase inhibitor, and should cause increased expression of genes not usually expressed as highly. The differentiation processes itself has the potential to alter both parkin and AP-1 expression. In some cell lines sodium butyrate

increases the activation of AP-1 transcription factors, while in other cells lines it decreases activity (Alva-Murillo et al., 2015; Andoh et al., 1999; He et al., 2016). If AP-1 misregulation caused by sodium butyrate in the differentiation process increases parkin, then parkin expression could be high enough that a ceiling effect is reached. As parkin is both an E3 ligase and a substrate of itself, parkin levels should only be able to increase to a certain extent before expression plateaus (Zhang et al., 2000; Imai et al., 2001). Overall, the MN9D cells do not appear to be the best model in which to study the relationship between parkin, the FosBs, and differential susceptibility of neurons.

AAV-ΔFosB Expression in the ARC and SN

Results

To directly determine the effects of increases in ΔFosB expression on parkin protein in the ARC an SN, an AAV-ΔFosB vector was stereotaxically bilaterally injected into the ARC or unilaterally injected in the SN. In the ARC of mice receiving AAV-ΔFosB, parkin was 1.71 ± 0.17 fold higher than the AAV-GFP control at 1.00 ± 0.12 (**Figures 6.19 and 6.20**). In the ipsilateral SN that received AAV-ΔFosB, parkin levels were 1.92 ± 0.36 fold higher than the AAV-GFP control contralateral SN at 1.00 ± 0.08 (**Figures 6.21 and 6.22**).

Unilateral injection of the AAV-ΔFosB vector in the SN did not cause neurochemical changes in NSDA neurons terminating in the ST. DA in the ST

was 271.19 ± 15.95 ng/mg of protein in the AAV-GFP control side and 245.56 ± 22.36 ng/mg of protein in the AAV-ΔFosB side (**Figure 6.23**). DOPAC in the ST was 24.85 ± 1.29 ng/mg of protein in the AAV-GFP control side and 23.52 ± 1.69 ng/mg of protein in the AAV-ΔFosB side (**Figure 6.24**). DOPAC/DA ratio in the ST was 0.089 ± 0.0035 in the AAV-GFP control side and 0.091 ± 0.0036 ng/mg in the AAV-ΔFosB side (**Figure 6.25**). On contrast, bilateral injection into the ARC altered DA stores axon terminals of TIDA neurons in the ME. DA in the ME was 56.08 ± 8.60 ng/mg of protein in the AAV-GFP control mice and 188.02 ± 21.73 ng/mg of protein in mice that received AAV-ΔFosB in the ARC (**Figure 6.26**).

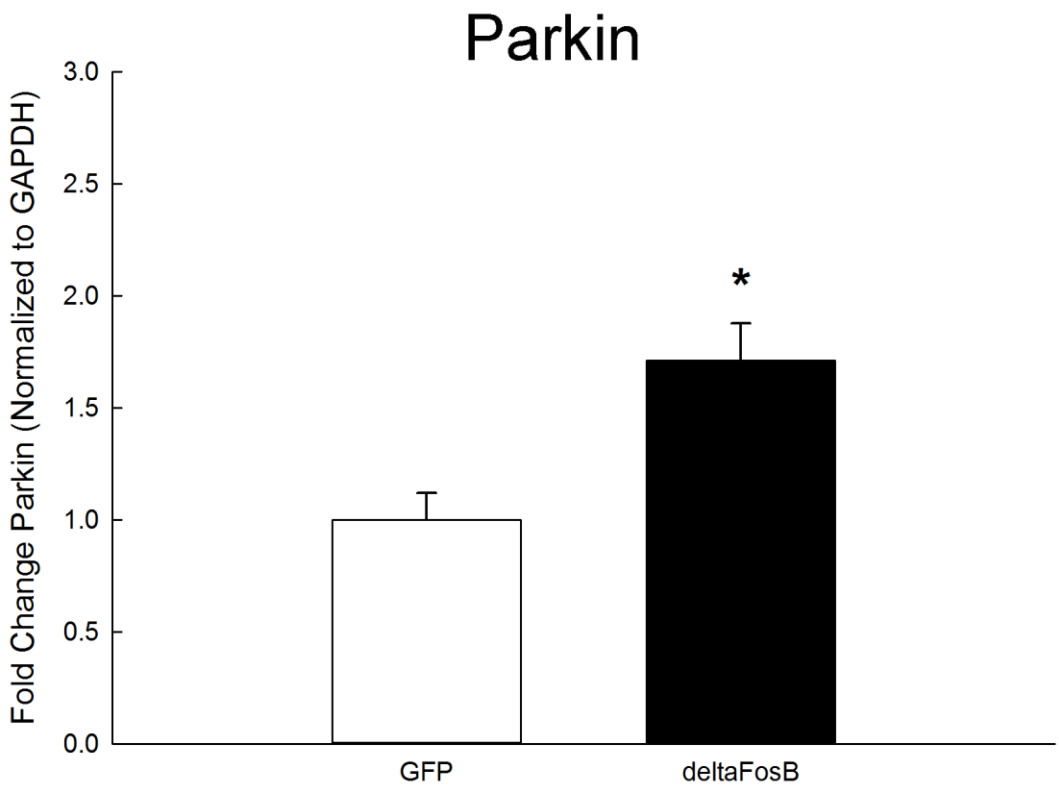

Figure 6.19 Parkin in the ARC after AAV-ΔFosB- mediated overexpression. An AAV-ΔFosB vector or AAV-GFP control vector was stereotaxically injected into the ARC of male C57Bl/6J mice. Injections were bilateral, with mice receiving either AAV-GFP or AAV-ΔFosB. Mice were allowed to recover for four weeks and killed by decapitation (n=8/group). Brains were sectioned, ARC was microdissected, protein isolated and Western blots used to quantify parkin normalized to GAPDH. Mean fold change from vehicle control is represented by columns with error bars representing + 1 standard error of the mean. Values significantly different ($p<0.05$; t-test) from the vehicle controls are denoted with asterisks.

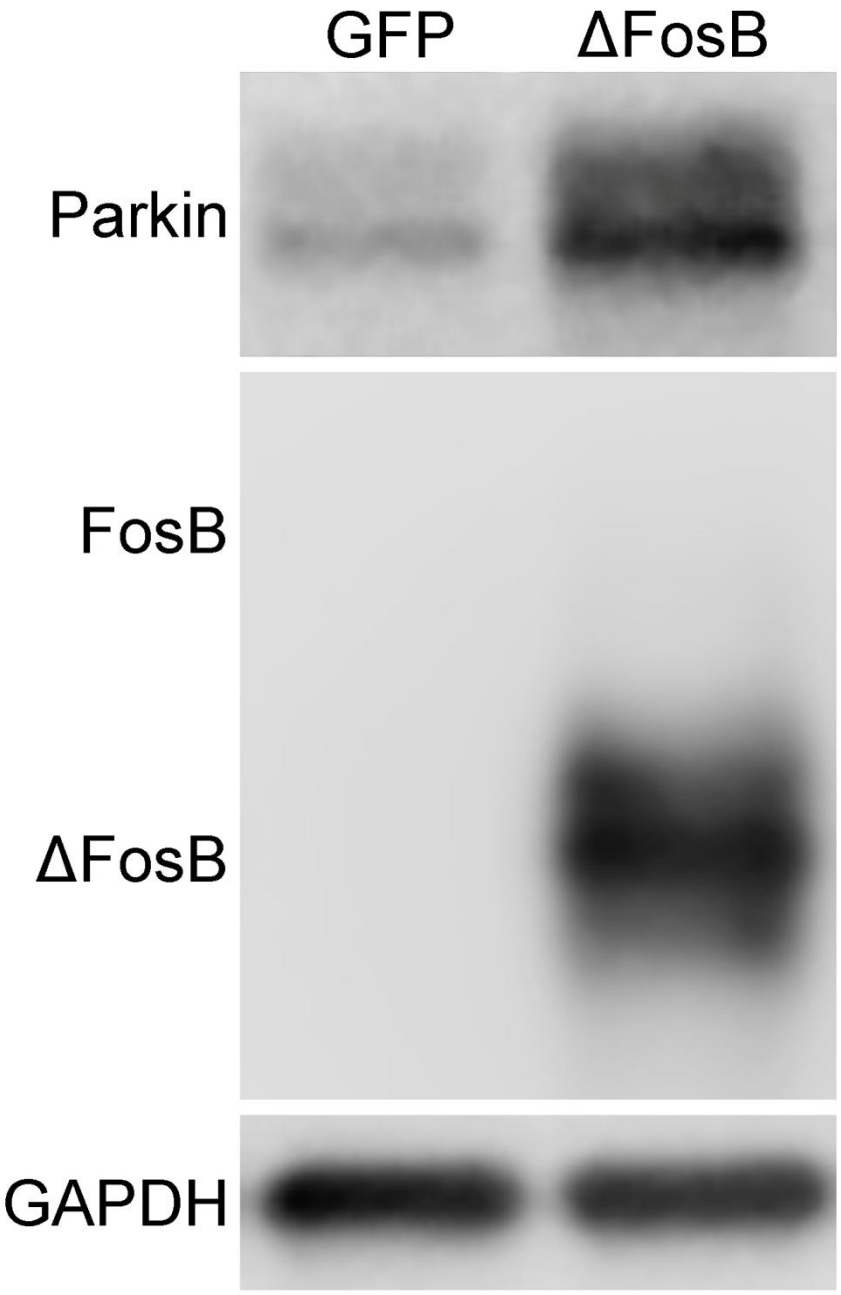

Figure 6.20 Representative Western blots for parkin, FosB and ΔFosB in the ARC of mice injected with either AAV-GFP or AAV-ΔFosB. Parkin, FosB, and ΔFosB were normalized to GAPDH.

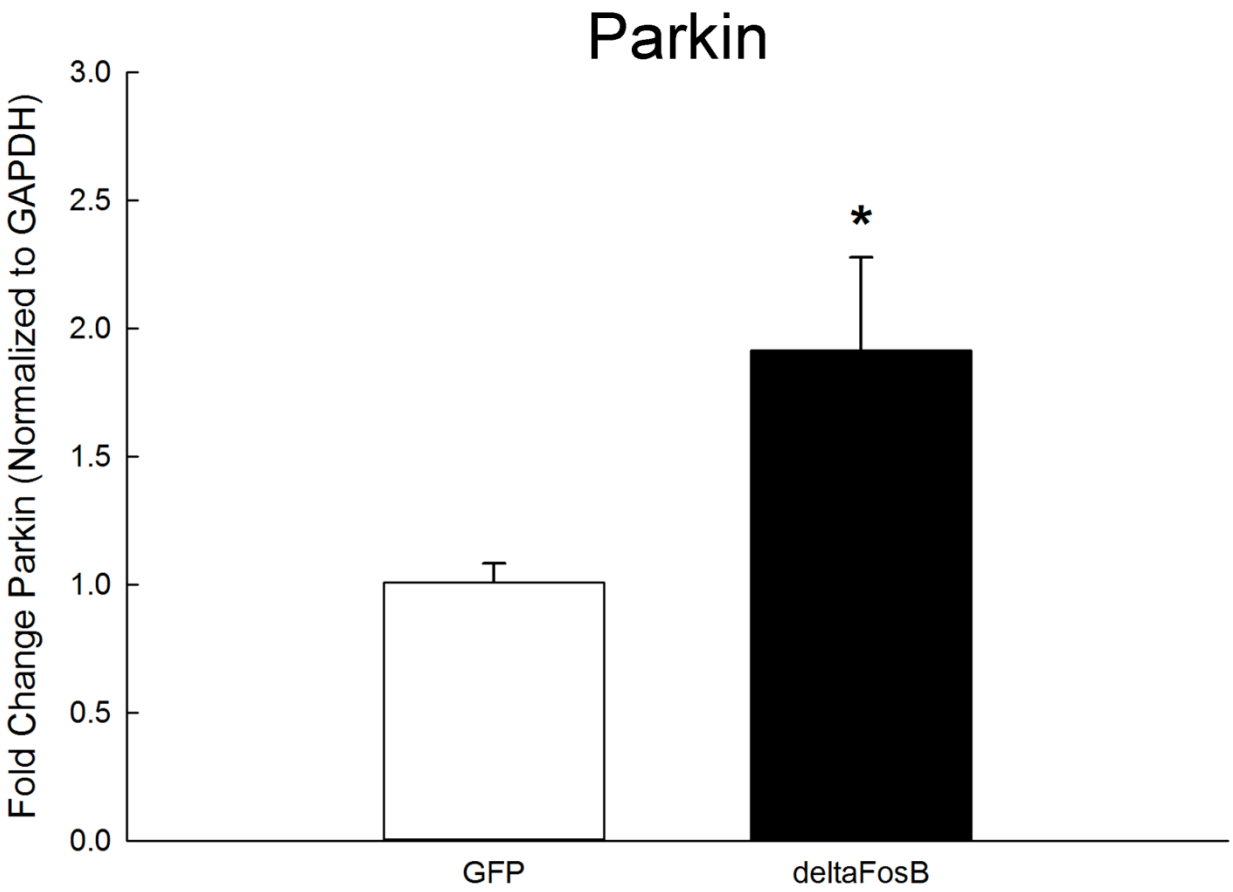

Figure 6.21 Parkin in the SN after AAV-ΔFosB-mediated overexpression. An AAV-ΔFosB vector or AAV-GFP control vector was stereotaxically injected into the SN of male C57Bl/6J mice. Injections were unilateral, with one hemisphere receiving AAV-GFP and the other AAV-ΔFosB. Mice were allowed to recover for four weeks and killed by decapitation (n=8/group). Brains were sectioned, SN was microdissected, protein isolated and Western blots used to quantify parkin normalized to GAPDH. Mean fold change from vehicle control is represented by columns with error bars representing + 1 standard error of the mean. Values significantly different ($p<0.05$; paired t-test) from the vehicle controls are denoted with asterisks.

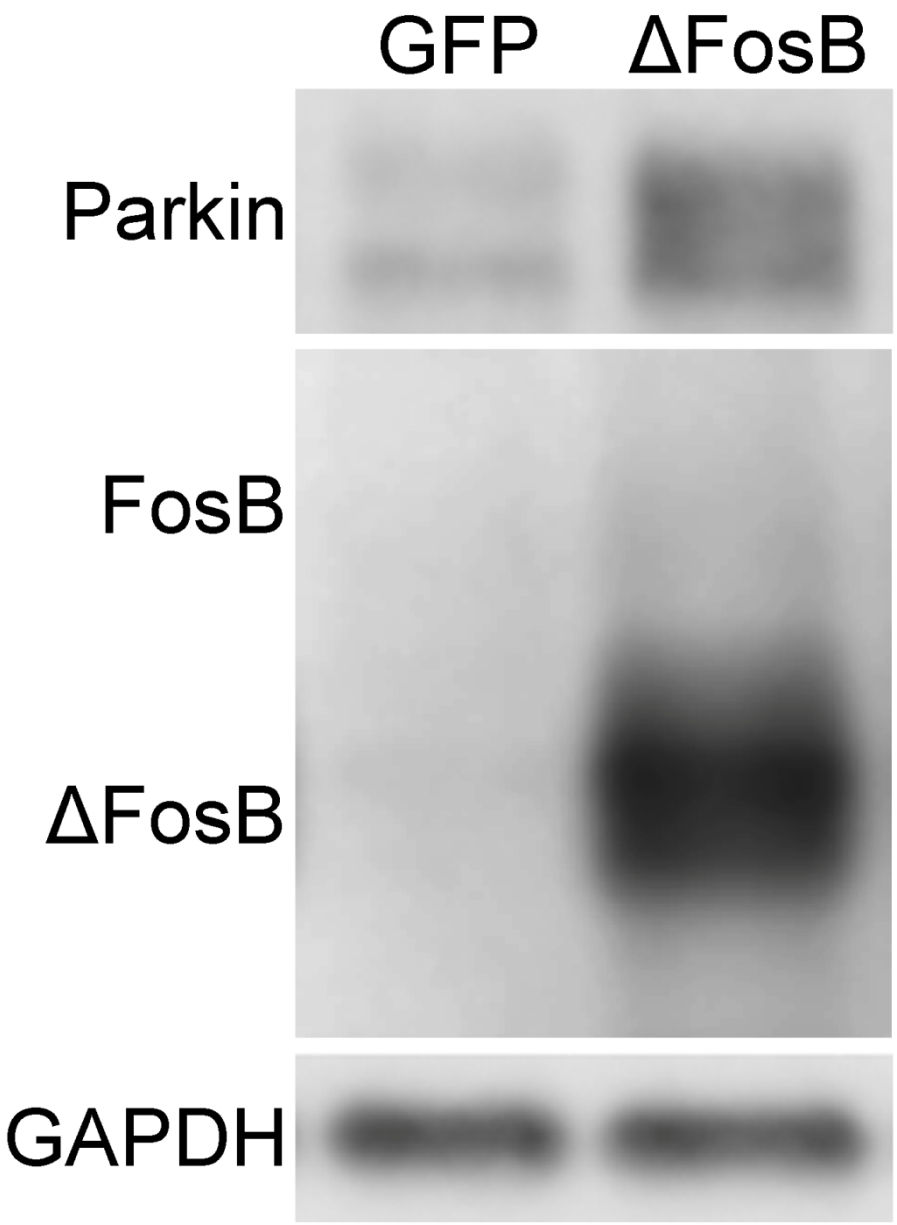

Figure 6.22 Representative Western blots for parkin, FosB and ΔFosB in the SN of mice injected with either AAV-GFP or AAV-ΔFosB. Parkin, FosB, and ΔFosB were normalized to GAPDH.

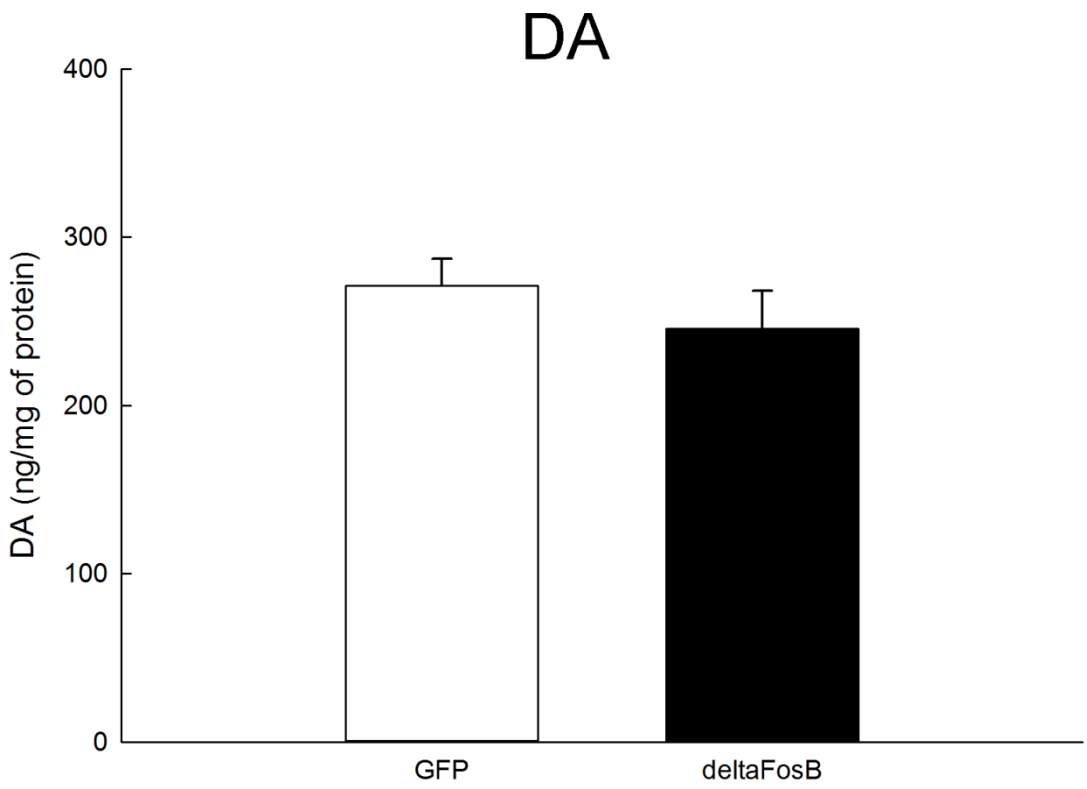

Figure 6.23 DA concentration in the ST after AAV-ΔFosB. An AAV-ΔFosB vector or AAV-GFP control vector was stereotaxically injected into the SN of male C57Bl/6J mice. Injections were unilateral, with one hemisphere receiving AAV-GFP and the other AAV-ΔFosB. Mice were allowed to recover for four weeks and killed by decapitation (n=8/group). Brains were sectioned, ST was microdissected and processed for neurochemical analysis. Mean fold change from vehicle control is represented by columns with error bars representing + 1 standard error of the mean. Values significantly different ($p<0.05$; paired t-test) from the vehicle controls are denoted with asterisks.

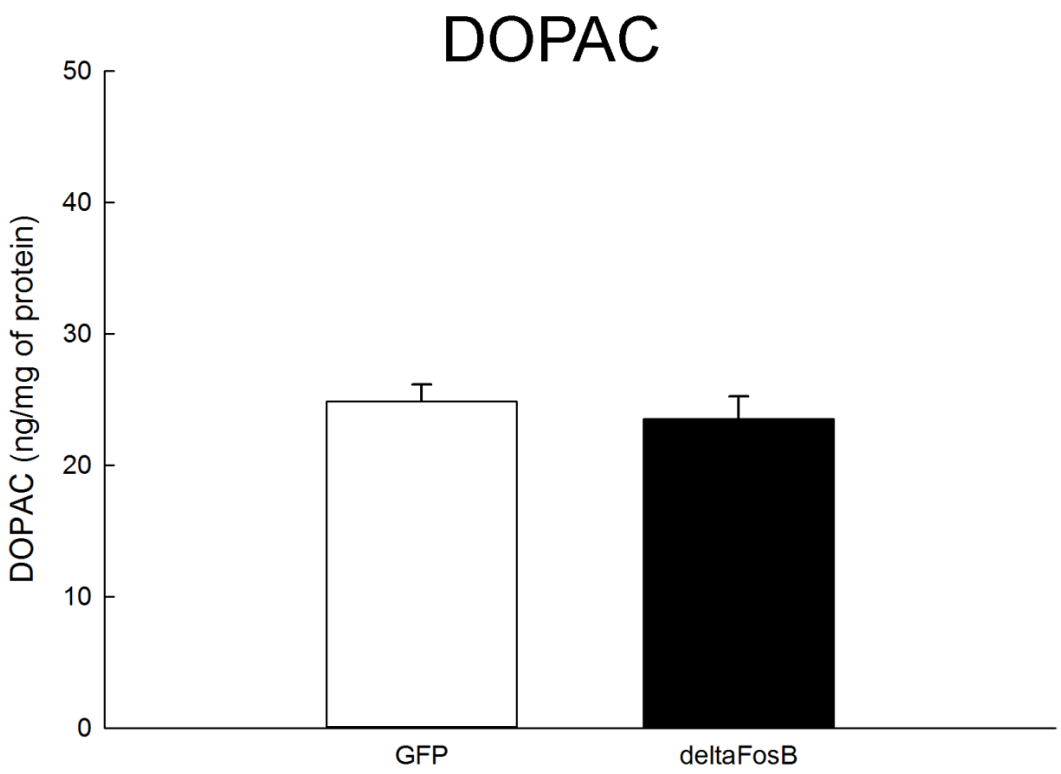

Figure 6.24 DOPAC concentration in the ST after AAV-ΔFosB. An AAV-ΔFosB vector or AAV-GFP control vector was stereotaxically injected into the SN of male C57Bl/6J mice. Injections were unilateral, with one hemisphere receiving AAV-GFP and the other AAV-ΔFosB. Mice were allowed to recover for four weeks and killed by decapitation (n=8/group). Brains were sectioned, ST was microdissected and processed for neurochemical analysis. Mean fold change from vehicle control is represented by columns with error bars representing + 1 standard error of the mean.

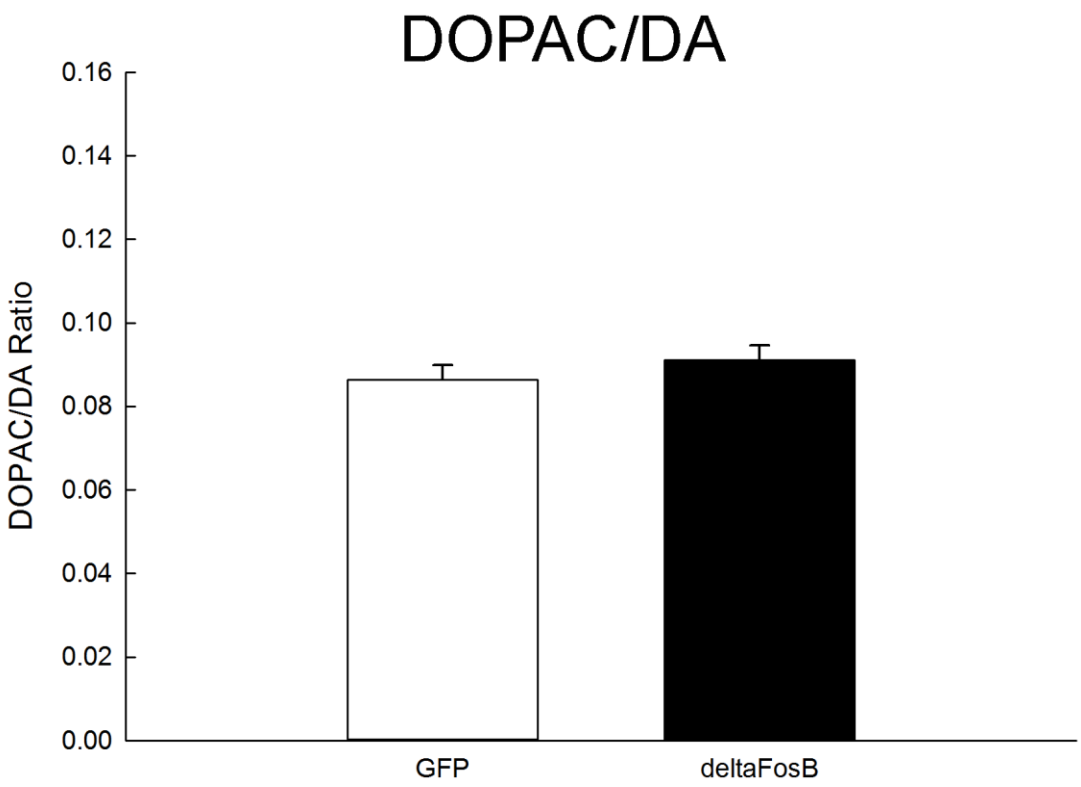

Figure 6.25 DOPAC/DA ratio in the ST after AAV-ΔFosB. An AAV-ΔFosB vector or AAV-GFP control vector was stereotaxically injected into the SN of male C57Bl/6J mice. Injections were unilateral, with one hemisphere receiving AAV-GFP and the other AAV-ΔFosB. Mice were allowed to recover for four weeks and killed by decapitation (n=8/group). Brains were sectioned, ST was microdissected and processed for neurochemical analysis. Mean fold change from vehicle control is represented by columns with error bars representing + 1 standard error of the mean.

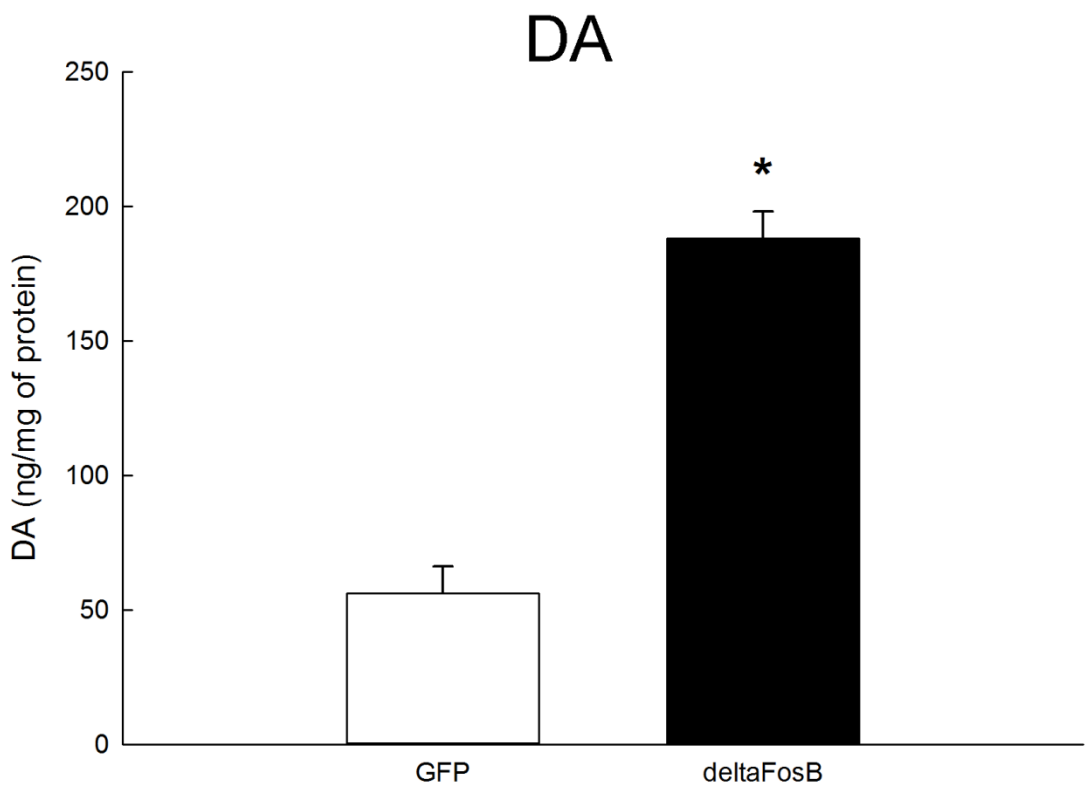

Figure 6.26 DA concentrations in the ME after AAV-ΔFosB. An AAV-ΔFosB vector or AAV-GFP control vector was stereotaxically injected into the ARC of male C57Bl/6J mice. Injections were made bilaterally with mice receiving either AAV-GFP or AAV-ΔFosB. Mice were allowed to recover for four weeks and killed by decapitation (n=8/group). ME were microdissected and processed for neurochemical analysis. Mean fold change from vehicle control is represented by columns with error bars representing + 1 standard error of the mean. Values significantly different ($p<0.05$; paired t-test) from the vehicle controls are denoted with asterisks.

Discussion

The neurochemical analysis after AAV-ΔFosB injection in the ARC and SN provides another difference between neurons. In the ST, AAV-ΔFosB injection in the SN does not alter DA stores, nor does it effect DA metabolism, as shown by the lack of change in the DOPAC/DA ratio. In the ME, AAV-ΔFosB injection in the ARC leads to an increase in DA stores in TIDA axon terminals, possibly through increased DA synthesis. TH is the rate-limiting enzyme in DA synthesis in TIDA neurons (Lookingland and Moore, 2005). FosB as well as other AP-1 transcription factors are known to bind to TPA-response elements within the TH promoter and regulate the expression of TH (Gizang-Ginsberg and Ziff, 1994; Yukimasa et al., 1999;). The way AP-1 transcription factors effect TH expression varies in different tissues, for example in PC12 cells, AP-1 represses TH expression, where in F9, NIH3T3 cells and a rodent model it can increase TH expression (Ghee et al., 1998; Gizang-Ginsberg and Ziff, 1994; Chae et al., 1996). Though ΔFosB is not directly studied, it essentially acts the same as FosB, with the same binding partners. It is reasonable to assume that the increase in DA in the ME is due to ΔFosB acting on the TH promoter, though future studies should be performed to examine TH expression and activity in these neurons.

As for the lack of increase in DA or DA metabolism in the ST, this may be explained by tissue specific differences (Ghee et al., 1998). The NSDA neurons have D2 presynaptic autoreceptors located on their axon terminals

in the ST that can directly regulate and inhibit TH and DA synthesis. If over-expression of ΔFosB does increase DA synthesis and release, the D2 autoreceptors may repress DA synthesis back to basal levels. Reports of D2 autoreceptor regulation of the TIDA neurons varies (Timmerman et al., 1995; Berry and Gudelsky, 1991). The lack of D2 autoreceptor inhibition of DA synthesis in axon terminals of TIDA neurons in the ME could explain how DA stores could increase in the ME.

Viral mediated overexpression of ΔFosB increases parkin in both the ARC and SN. The AAV-ΔFosB used in the experiment is serotype 2, known to effect neurons, and has been shown to not infect glial cells (Zachariou et al., 2006). This suggests that changes caused by AAV-ΔFosB in the ARC and SN occur in neurons in these regions, of which TIDA and NSDA neurons comprise a large portion. The increase in parkin in both regions is consistent with the hypothesis that ΔFosB is a transcription factor of parkin, and that increased expression of this transcription factor is sufficient to increase parkin expression in these neurons. To further elucidate the role ΔFosB plays in regulating parkin in response to neurotoxicant exposure, ΔJunD was employed to block the action of FosB and ΔFosB.

AAV-ΔJunD Expression in the ARC in the Presence of MPTP

Results

An AAV-ΔJunD vector was stereotaxically injected bilaterally in the ARC as a method to block parkin expression in the ARC and DA recovery in the ME after acute MPTP exposure. In the ARC of mice that received AAV-GFP and saline, mean fold change FosB was 1.00 ± 0.17, in mice that received AAV-GFP and MPTP, mean fold change FosB was 3.75 ± 0.19, in mice that received AAV-ΔJunD and saline, mean fold change FosB was 1.10 ± 0.16, and in mice that received AAV-ΔJunD and MPTP, mean fold change FosB was 2.46 ± 0.80 (**Figures 6.27 and 6.29**). As for ΔFosB in the ARC, mice that received AAV-GFP and saline, mean fold change ΔFosB was 1.00 ± 0.18, in mice that received AAV-GFP and MPTP, mean fold change ΔFosB was 6.81 ± 0.10, in mice that received AAV-ΔJunD and saline, mean fold change ΔFosB was 0.99 ± 0.28, and in mice that received AAV-ΔJunD and MPTP, mean fold change ΔFosB was 6.49 ± 0.08 (**Figures 6.28 and 6.29**).

Parkin in the ARC increased with MPTP in AAV-GFP control mice, but did not change in the mice that received AAV-ΔJunD with or without MPTP present. In the ARC, mice that received AAV-GFP and saline, mean fold change parkin was 1.00 ± 0.08, in mice that received AAV-GFP and MPTP, mean fold change parkin was 2.21 ± 0.11, in mice that received AAV-ΔJunD and saline, mean fold change parkin was 1.10 ± 0.07, and in mice that

received AAV-ΔJunD and MPTP, mean fold change parkin was 1.43 ± 0.14 (Figures 6.30 and 6.31).

Injection of the AAV-ΔJunD vector in the ARC did not change stored DA in axon terminals of TIDA neurons in the ME. DA in the ME was 56.08 ± 8.60 ng/mg of protein in the AAV-GFP control mice that received saline, and 42.19 ± 4.60 ng/mg of protein those that received MPTP. In mice that AAV-ΔJunD that received saline 47.99 ± 11.29 ng/mg of protein and 32.98 ± 7.41 ng/mg of protein those that received MPTP (Figure 6.32).

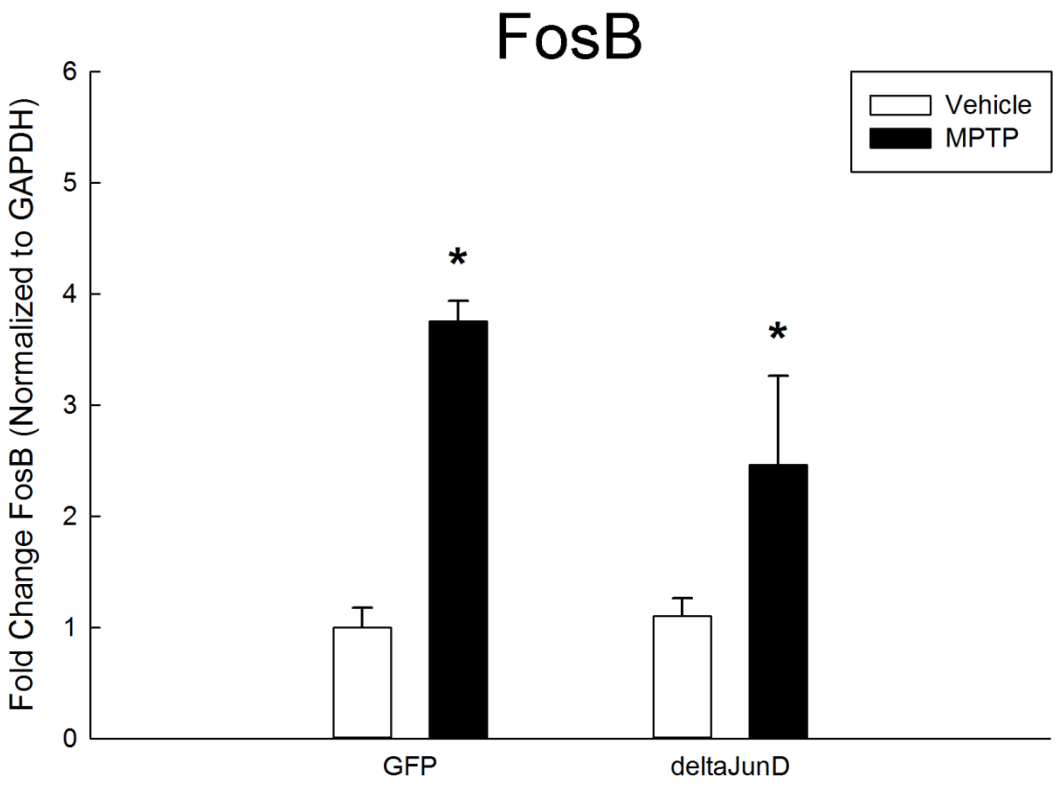

Figure 6.27 FosB in the ARC after AAV-ΔJunD expression and 24 h post-MPTP. An AAV-ΔJunD vector or AAV-GFP control vector was stereotaxically injected into the ARC of male C57Bl/6J mice. Injections were bilateral, with mice receiving either AAV-GFP or AAV-ΔFosB. Mice were allowed to recover for four weeks and killed by decapitation (n=8/group). Brains were sectioned, ARC was microdissected, protein isolated and Western blots used to quantify FosB normalized to GAPDH. Mean fold change from AAV-GFP vehicle control is represented by columns with error bars representing + 1 standard error of the mean. Values significantly different ($p<0.05$; two-way ANOVA) from the vehicle controls are denoted with asterisks.

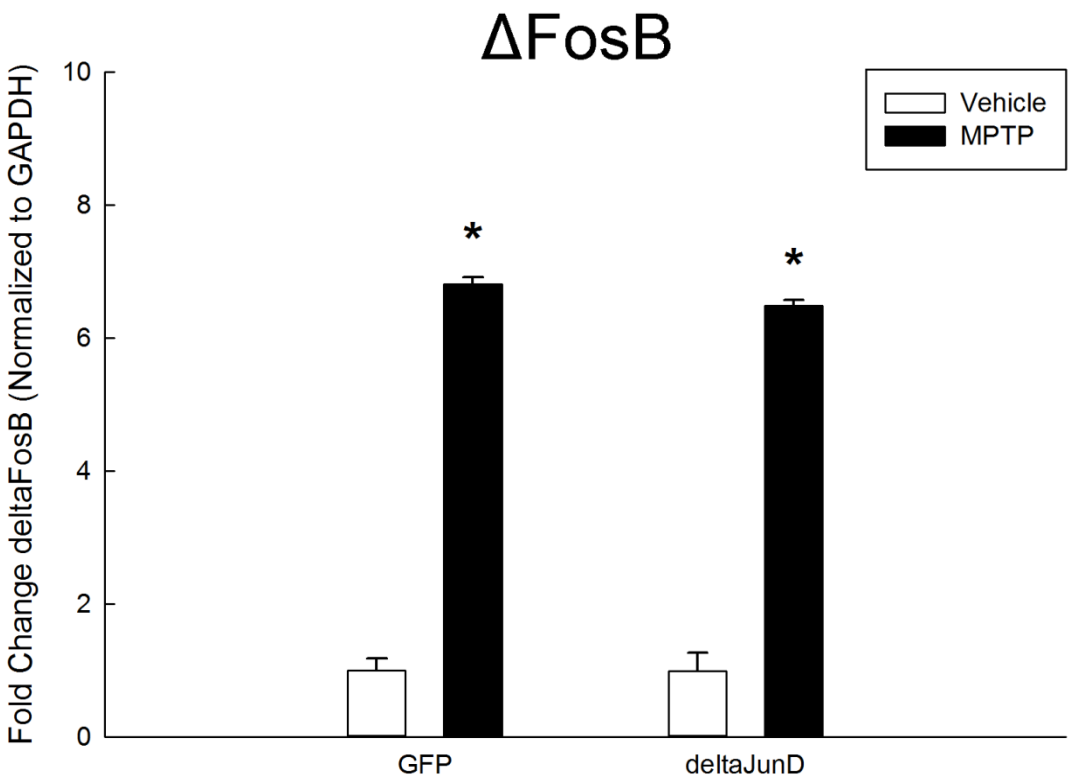

Figure 6.28 ΔFosB in the ARC after AAV-ΔJunD expression and 24 h post-MPTP. An AAV-ΔJunD vector or AAV-GFP control vector was stereotaxically injected into the ARC of male C57Bl/6J mice. Injections were bilateral, with mice receiving either AAV-GFP or AAV-ΔFosB. Mice were allowed to recover for four weeks and killed by decapitation (n=8/group). Brains were sectioned, ARC was microdissected, protein isolated and Western blots used to quantify ΔFosB normalized to GAPDH. Mean fold change from AAV-GFP vehicle control is represented by columns with error bars representing + 1 standard error of the mean. Values significantly different ($p<0.05$; two-way ANOVA) from the vehicle controls are denoted with asterisks.

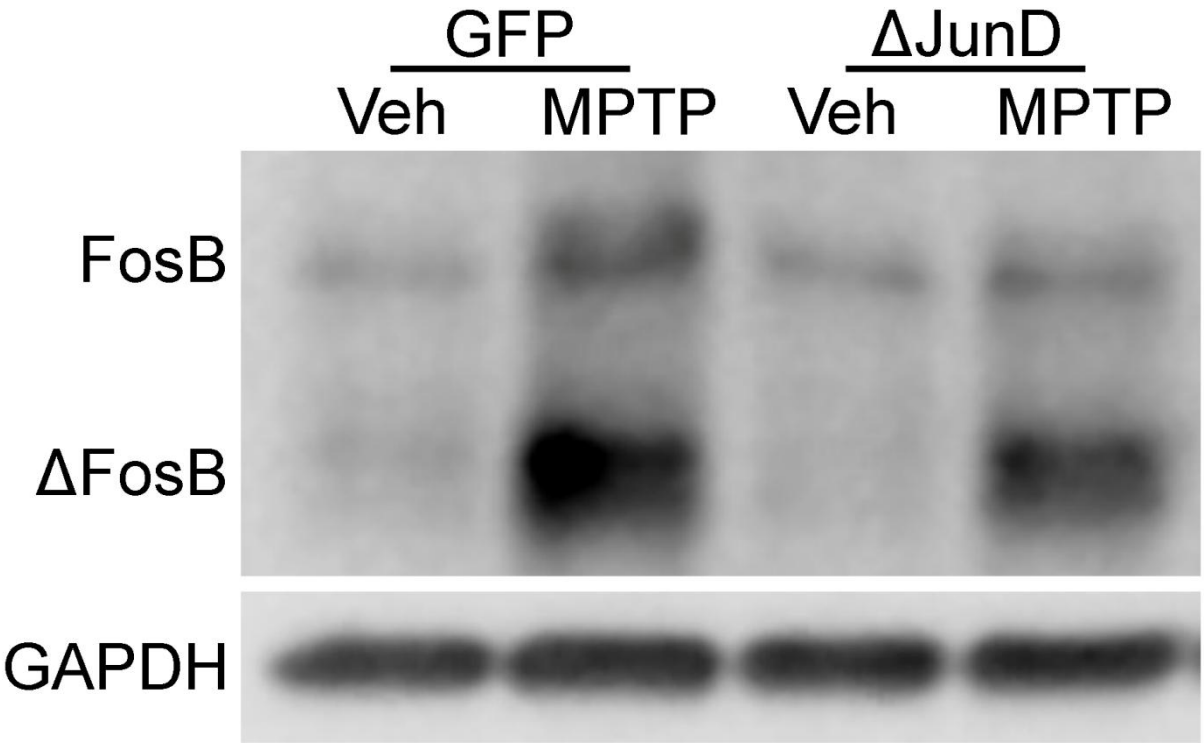

Figure 6.29 Representative Western blots for FosB and ΔFosB in the ARC of mice injected with either AAV-GFP or AAV-ΔFosB and MPTP. FosB, and ΔFosB were normalized to GAPDH.

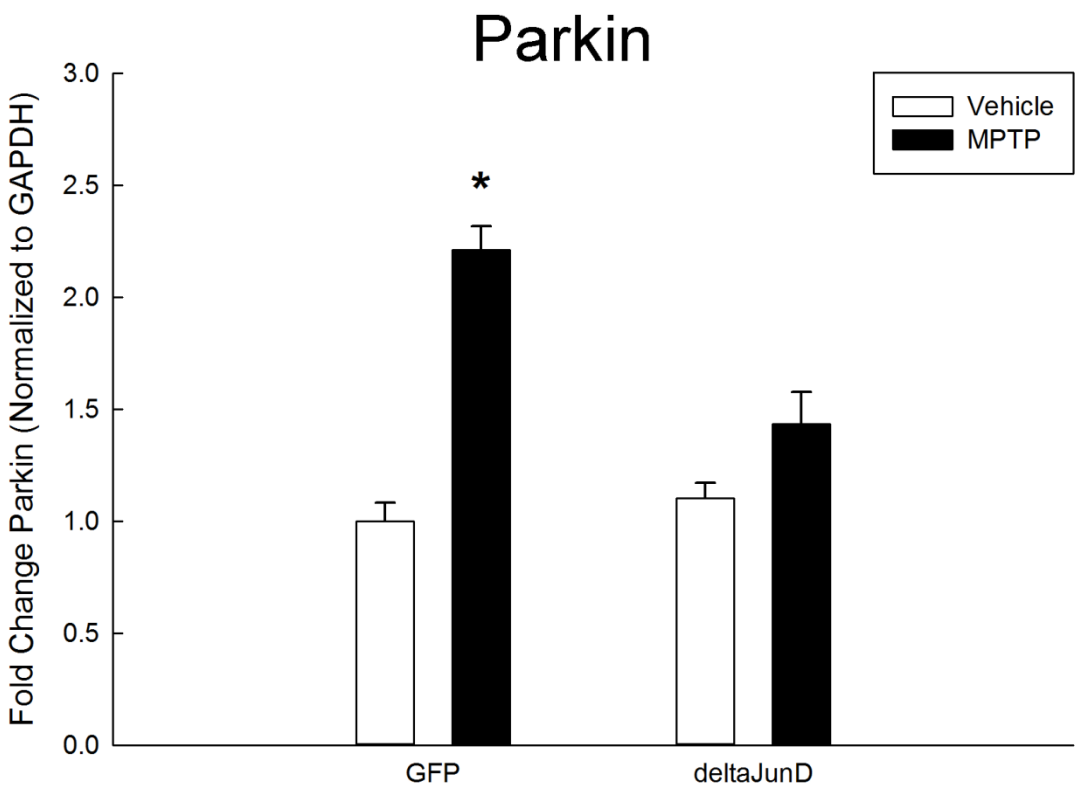

Figure 6.30 Parkin in the ARC after AAV-ΔJunD expression and 24 h post-MPTP. An AAV-ΔJunD vector or AAV-GFP control vector was stereotaxically injected into the ARC of male C57Bl/6J mice. Injections were bilateral, with mice receiving either AAV-GFP or AAV-ΔFosB. Mice were allowed to recover for four weeks and killed by decapitation (n=8/group). Brains were sectioned, ARC was microdissected, protein isolated and Western blots used to quantify parkin normalized to GAPDH. Mean fold change from AAV-GFP vehicle control is represented by columns with error bars representing + 1 standard error of the mean. Values significantly different ($p<0.05$; two-way ANOVA) from the vehicle controls are denoted with asterisks.

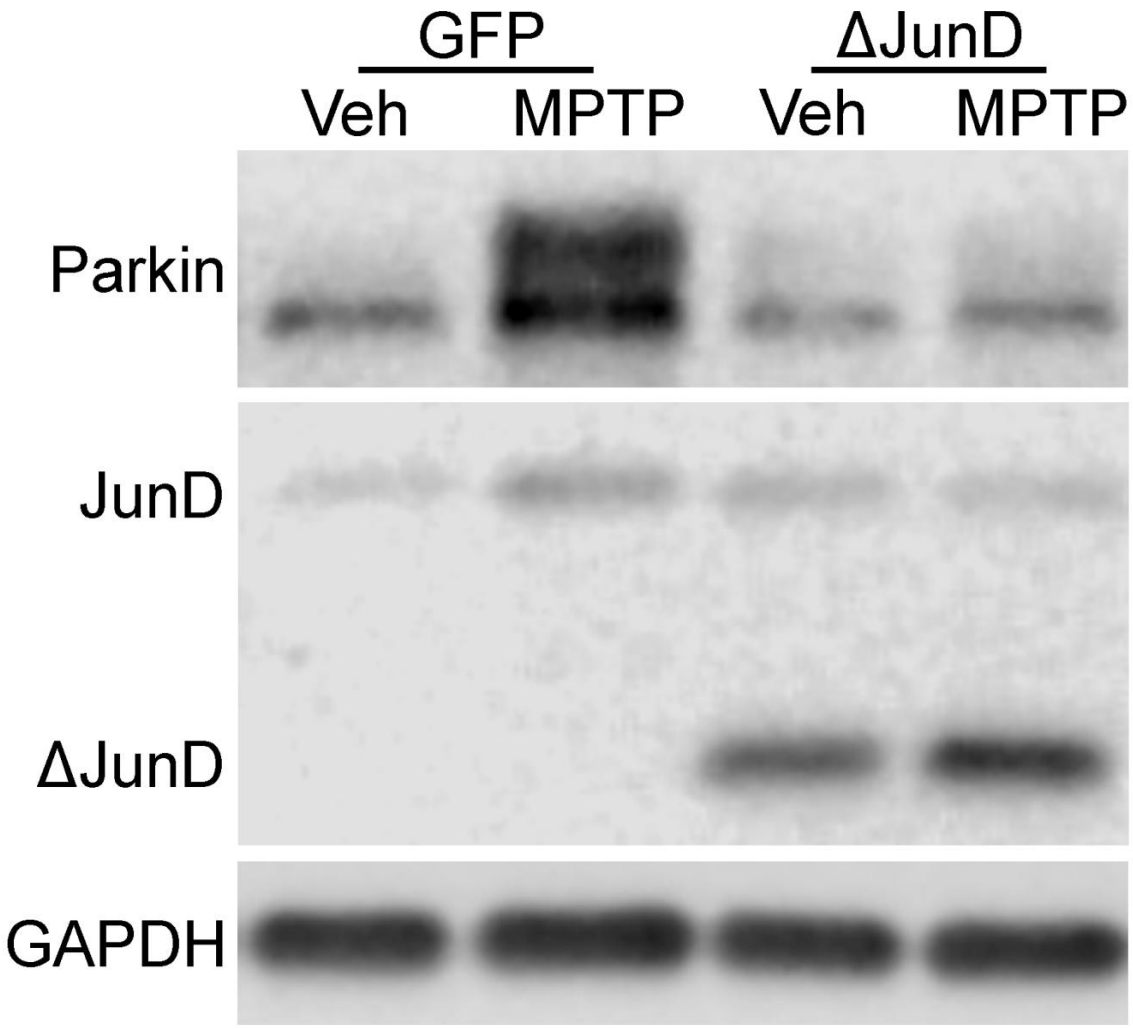

Figure 6.31 Representative Western blots for parkin, JunD and ΔJunD in the ARC of mice injected with either AAV-GFP or AAV-ΔFosB and MPTP. Parkin, JunD, and ΔJunD were normalized to GAPDH.

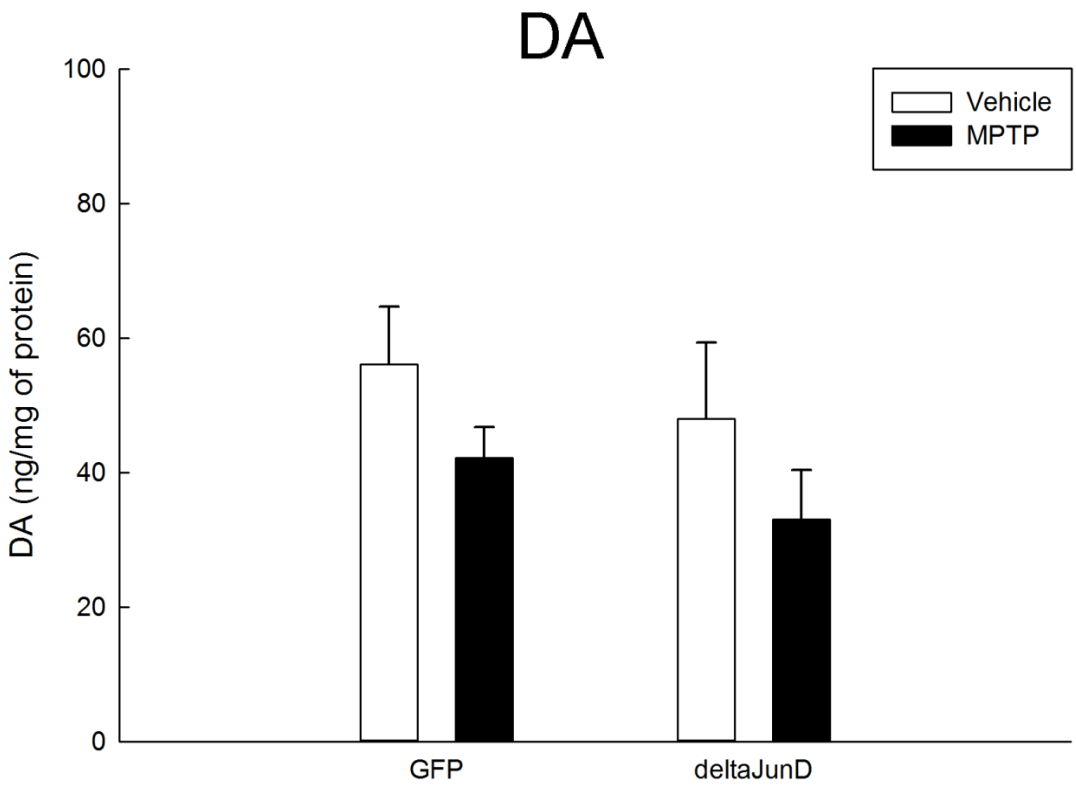

Figure 6.32 DA concentrations in the ME after AAV-ΔJunD and 24 h post-MPTP. An AAV-ΔJunD vector or AAV-GFP control vector was stereotaxically injected into the ARC of male C57Bl/6J mice. Injections were bilateral, with mice receiving either AAV-GFP or AAV-ΔJunD. Mice were allowed to recover for four weeks and killed by decapitation (n=8/group; two-way ANOVA). ME were microdissected and processed for neurochemical analysis. Mean fold change from vehicle control is represented by columns with error bars representing + 1 standard error of the mean.

Discussion

Overexpression of ΔJunD in the ARC does not affect DA in the ME. DA levels in the ME of mice that were injected with AAV-GFP or AAV-ΔJunD are not different from each other. DA was not different in the ME 24 h after MPTP consistent with previous published reports from our laboratory (Behrouz, et al., 2007; Benskey, et al., 2012), even in the presence of overexpressed ΔJunD. This indicates that the FosB-induced increase in parkin is not required for DA recovery in the ME after MPTP. The caveat to these results is that the data appears to be trending towards there not being a recovery of DA in MPTP-treated mice that received AAV-ΔJunD in the ARC. This trend and the effect of ΔJunD on parkin expression would be consistent with the requirement of parkin for recovery of the TIDA neurons (Benskey et al., 2015).

Overexpression of ΔJunD in the ARC blocks the effects of FosB and ΔFosB on parkin expression. Indeed, overexpression of ΔJunD attenuates the expression of parkin, however it does not effect MPTP-induced FosB or ΔFosB expression. The ability of ΔJunD to block the up-regulation of parkin following acute neurotoxicant exposure, and the preferential dimerization of ΔJunD with the FosBs supports the hypothesis that the FosBs are in a pathway that directly regulates parkin.

Overall Conclusions

Phosphorylation of CREB and SRF upstream transcriptional activators of *FosB* is consistent with the regional differences in expression patterns of FosB and ΔFosB following acute neurotoxicant exposure. As with the FosBs and parkin, phosphorylated CREB and SRF increase early in the ARC and not the SN. CREB and SRF add an additional level to the potential regulation of parkin, allowing for some speculation on a parkin activation pathway in response to acute neurotoxicant exposure. Where one or more of the stresses caused by MPTP leads to the phosphorylation of CREB and SRF, which of these causes increased transcription of the *FosB* gene, FosB/ΔFosB proteins and parkin is not known. Identification of these pathways can be used as the basis of future experiments designed to discover which kinase or kinases are involved in MPTP-induced CREB and SRF phosphorylation, and whether both CREB and SRF are required for activation of FosB and parkin. Identification of the specific stress or combination of stresses caused by MPTP that are crucial to activate the FosB/parkin pathway in TIDA neurons could help explain why this pathway does not appear to function in the same way in NSDA neurons.

Whether the FosBs directly interact with the parkin promoter is not known. Chromatin immunoprecipitation (ChIP) followed by RTPCR would be the best approach to answer this question, but the *in vitro* model used in these experiments did not show a relationship between expression of the FosBs

and parkin. The MN9D cell model does not show MPP^+ induction of the FosBs or parkin, nor does PMA induced expression of the FosBs induce parkin expression. This is completely different than what is observed *in vivo,* so the best alternative option would be to use ChIP paired with RTPCR in the ARC. One issue, however, is that the ARC is a small brain region in mice that does not yield much protein. For an average Western blot, protein extracted from the ARC is on average 25 µg. Most protocols for ChIP analysis recommend that at least 1 mg of protein be used, which is not a problem in cell culture, but would require pooled ARC tissue from up to 40 mice. The use of such a large sample size of one is not financially practical. An alternative would be to find an in vitro cellular system that better models neurotoxicant induced activation of FosB and parkin expression in the ARC, possibly through one created by the fusion of TIDA neurons with a neuroblastoma cell line.

Chapter 7: General Discussion

Differences Between TIDA and NSDA Neurons

The differential expression of parkin is associated with the susceptibility of the NSDA neurons and the resilience of the TIDA neurons to neurotoxic insult (Benskey et al., 2012, 2015). Additional to how parkin regulation varies in these neurons, there are other inherent differences. The TIDA neurons are part of a circumventricular system within the brain that is not protected by the blood-brain barrier. The axons of the TIDA neurons terminate in the hypophyseal portal system and cell bodies are located along the third ventricle. Through their location, the TIDA neurons are exposed to blood in the ME and cerebrospinal fluid from the ventricular system of the brain. This compares to the NSDA neurons that are protected by the blood-brain barrier and are not directly exposed to substances carried in the blood. The difference in location of these neurons suggests that the TIDA neurons are more prone to exposure to stressors than the NSDA neurons. This is supported by the nearly 4 fold higher concentration of MPP^+ found in the ME as compared to the ST after MPTP as well as the higher basal levels of ROS via a DCF-DA assay that exist in the ME and ARC, as compared to the ST and SN (Benskey et al., 2012). It is possible that the TIDA neurons induce the increase in parkin as an adaptive mechanism acquired due to constant exposure to stress.

Additionally, the TIDA neurons have substantially shorter axons than the NSDA neurons. This could play a role in the signaling pathways that regulate parkin expression in response to acute MPTP exposure. Since MPP^+ is primarily thought to be taken into DA neurons via DAT located on axon terminals, the shorter axons in the TIDA neurons could facilitate a more rapid response, both in modifying gene expression in the cell bodies and delivery of cytoprotective proteins to the site of neurotoxicant insult in the axon terminals. As the axons of the NSDA neurons are significantly longer than the axons of the TIDA neurons, there may be an problem of stress responses present in the terminals signaling back to the cell bodies in the NSDA neurons. In addition, MPP^+ is known to destabilize microtubules, therefore vesicles and proteins transported via the microtubules would be expected to be hindered more in longer axons in the NSDA neurons as compared to the TIDA neurons (Cartelli et al., 2013; Cappelletti et al., 2005).

Another possible difference between the TIDA and NSDA neurons that could be a contributing factor is the presence of D2 autoreceptors at the axon terminals. The NSDA neurons have D2 autoreceptors that respond to synaptic DA and lead to a decrease in cAMP in presynaptic DA axon terminals (Kebabian and Greengard, 1971). Unlike the NSDA neurons, the presence of D2 autoreceptors on axon terminals of TIDA is not quite clear, with evidence both for and against (Timmerman et al., 1995; Berry and Gudelsky, 1991). Since DA from the TIDA neurons is released into the portal

blood, rather than a synapse, and is transported away from the presynaptic axon terminals it is likely that D2 autoreceptors (if present) do not have as robust a function as in the NSDA neurons.

D2 autoreceptors may factor into the differential response between these neurons by affecting the CREB pathway. MPTP has been shown to cause not only the depletion in DA stores, but an increase in DA release from NSDA neuron axon terminals in the ST (Ozaki et al., 1987; Serra et al., 2008). An increase in released DA in the ST would interact with the D2 autoreceptor, leading to the inhibition of adenylate cyclase and a subsequent decrease in cAMP and PKA activity. As a consequence, phosphorylation of CREB would be expected to decrease. This is consistent with the observed decrease in phosphorylated CREB (Ser133) in the SN after MPTP in the present studies. Assuming D2 autoreceptors do not have a strong control over the TIDA neurons, increased DA release would not be expected to effect cAMP or phosphorylation of CREB. Indeed, the present study shows that MPTP increases (rather than decreases) phosphorylated CREB in the ARC. This potential inherent difference between TIDA and NSDA neurons adds context to a potential activation pathway that results in increased parkin expression in response to acute neurotoxicant exposure.

Potential Pathway Involved in Parkin Regulation

Transcription factors and indices of oxidative and ER stress, mitochondrial damage, and proteasome impairment examined in the present series of experiments yield some insight into the stress response pathways following acute MPTP exposure. MPTP does not elicit effects on ATF4 or Nrf1, transcription factors known to respond to ER stress and proteasome impairment. Likewise, any damage caused to mitochondria at the times measured in these experiments, was not sufficiently robust to induce NRF1 in the mitochondrial biogenesis pathway. This is not to say these pathways are not involved in regulating parkin expression, but the results do not support the conclusion that the single MPTP exposure paradigm used in these studies engages these pathways. The only pathway that appears to be affected is the oxidative stress pathway, where ROS levels increase only in the ME at 6 h post-MPTP.

Oxidative stress can act through multiple pathways, two of which involve CREB and SRF, transcription factors of the *FosB* gene (Vialou et al., 2012). ROS can lead to an increase in intracellular Ca^{2+} as well as cAMP (Ermak and Davies 2002; Li et al., 2011). Ca^{2+} is a cofactor of calmodulin kinases and cAMP is a cofactor of PKA, both of which can phosphorylate CREB and SRF. Phosphorylation of CREB and SRF followed by increased FosB and ΔFosB expression and nuclear localization are consistent with the expectations of a parkin transcription factor (**Figure 7.1**).

High ΔFosB expression is also sufficient to drive parkin expression in both the ARC and SN. Based on the ability of ΔJunD to block the increased parkin expression after MPTP, it is likely that dimers containing a FosB protein directly interacts with the *Park2* promoter. If the FosBs do not directly interact with the protein, they are at least at a point where the CREB and SRF pathways converge. Additionally, CREB has been linked to neuron survival in response to ROS and loss of SRF increases the susceptibility of the NSDA neurons to MPTP (Lee et al., 2009; Rieker et al., 2012). This suggests that CREB and SRF are probably acting in other neuroprotective pathways, in addition to activating parkin through the FosBs. Another possibility is that CREB acts directly to regulate parkin, as it could interact with the known AP-1 site on the *Park2* promoter (Bouman et al., 2011).

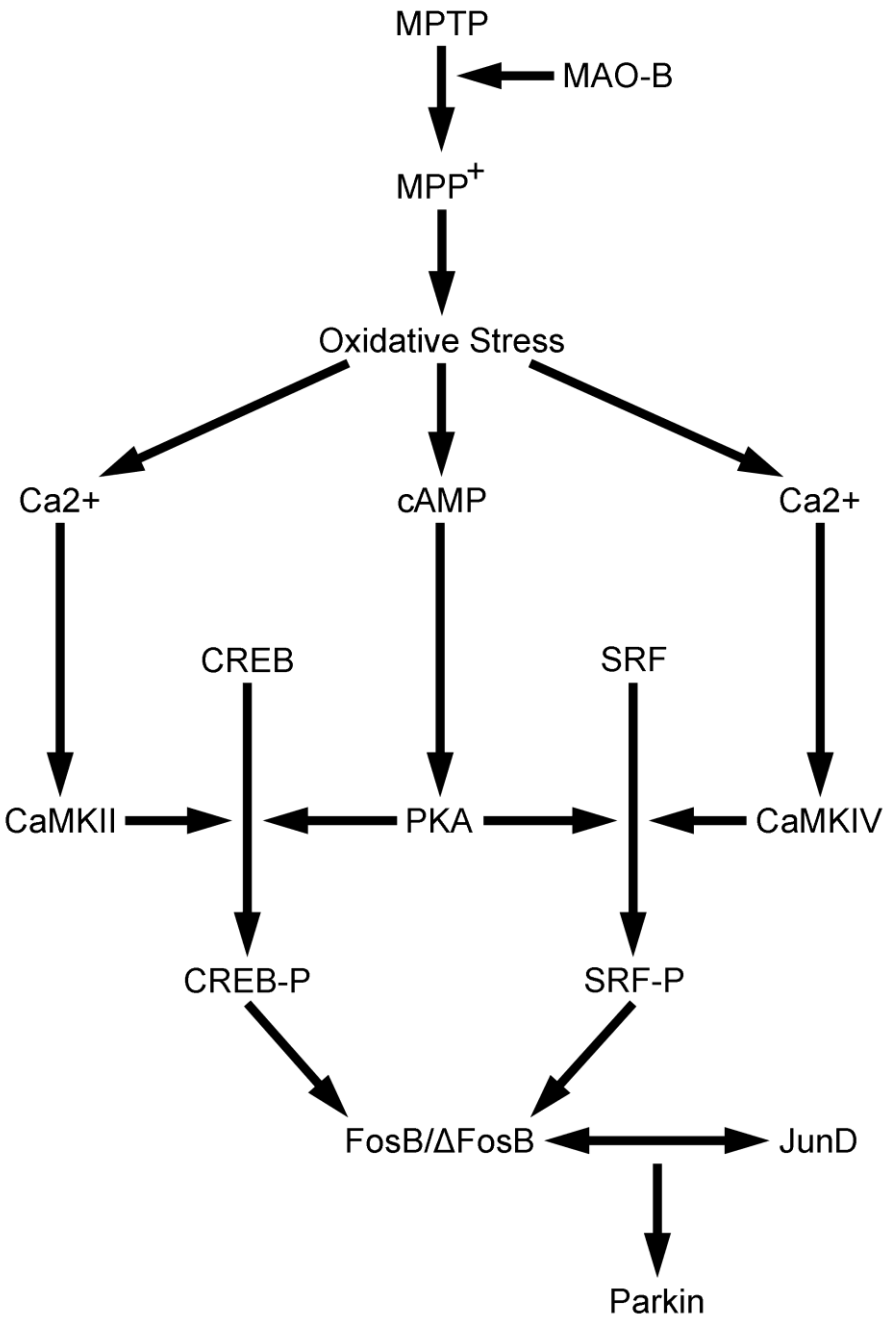

Figure 7.1 Predicted parkin regulatory pathway involved in the response to acute MPTP exposure. Oxidative stress caused by the effects of the metabolite of MPTP, MPP^+, causes increases in cAMP and Ca^{2+}. The intracellular Ca^{2+} acts as a cofactor for both CaMKII and CaMKIV, which can phosphorylate CREB and SRF, respectively. Likewise, cAMP would act as a cofactor of PKA and phosphorylate both CREB and SRF. The phosphorylated CREB and SRF act at the promoter of the *FosB* gene and increase expression of both FosB and ΔFosB, which dimerize with JunD and upregulate parkin expression.

Another potential transcription factor of parkin that was not examined or identified by predictive binding software is parkin. Parkin is already known to autoubiquitinate, but it may also regulate its own expression at the transcriptional level (Shimura et al., 2000; Zhang et al., 2000; Chaugule et al., 2011). The promoter region of *Park2* contains a perfect consensus binding sequence (GCCGGAG) of parkin -116 to -123 upstream of the transcriptional start site of parkin (Dupaln et al., 2013). Parkin has been shown to act as both a transcriptional activator of presenilin-1 and a repressor of presenilin-2 (Duplan et al., 2013). As these are the only known cases of parkin acting as a transcription factor, it is unclear whether parkin would act as an activator or repressor of itself. However, parkin acting as its own repressor would make the most sense as a mechanism to maintain parkin levels in the cells.

FosBs Beyond Parkin

AP-1 transcription factors, especially those with JunD containing dimers are present in neurons that survive brain injury (Pennypacker 1997, 1998, 2000). Increased expression of parkin in response to the FosBs is just one of the effects the FosBs may have in response to MPTP. ΔFosB has known roles in addiction and memory through altering synaptic plasticity. Indeed, known targets of ΔFosB are those that function in synaptic transmission (synaptotagmin 6, synaptogyrin 1, glutamate receptor 2, glutamate receptor

NMDA zeta 1, glutamate receptor AMPA 2 alpha 2, glutamic acid decarboxylase 2), cell signaling (adenylate cyclase activating peptide receptor, G-protein alpha o, protein kinase C beta, protein kinase II alpha, calmodulin 3), cell adhesion and motility (cadherin 2, kinesin family 1B and 5C, microtubule associated protein 2) and cellular stress responses (heat shock protein 40 and nuclear factor kappa-light chain-enhancer of activated B cells) (McClung and Nestler, 2003; Pitchers et al., 2013; Nestler et al., 2001; Nestler 2012, 2015).

At the cellular level, ΔFosB expression correlates with brain derived neurotrophic factor (BDNF) expression, induces the formation of dendritic spines, and alters the composition of neurotransmitter receptors (Robison et al., 2013; McClung and Nestler, 2003; Nestler et al., 2001; Nestler 2012, 2015; Nikulina et al., 2012; Krasnova et al., 2013; Wang et al., 2013). Changes in dendritic spines and receptors can alter how the neurons function, altering the sensitivity and reactivity of the neurons.

These alterations may be responsible for the hypothesized role of ΔFosB in L-DOPA-induced dyskinesia. ΔFosB has been found to be elevated in the ST of post-mortem PD patients with dyskinesia, overexpression of ΔFosB in the ST has been shown to produce dyskinesia in animals, and ΔJunD resets L-DOPA-induced dyskinesia in primates (Lindgren et al., 2011; Cao et al., 2010; Berton et al., 2009). This could cause increased activity of the MSN, resulting in the dyskinesia. In comparison to the apparent negative effects of

ΔFosB, increased BDNF appears to have neuroprotective benefits in response to 6-hydroxydopamine and MPTP induced axonal damage (Singh et al., 2006; Patil et al., 2014). Though there are some benefits to FosB and ΔFosB as a potential therapeutic target, the multiple downstream targets and effects make them unsuitable candidates for gene therapy.

Potential Future Directions

The link between the FosBs and regulation of parkin expression after MPTP is only part of a larger picture. MPTP can only be used to recapitulate some of the damage to DA neurons in PD. Other models examining the FosBs and parkin should be used to determine if the relationship between the two still holds true in other contexts. Two other procedures used to model features of PD are the overexpression of α-synuclein and the use of pre-formed α-synuclein fibrils. Both methods lead to the formation of Lewy bodies, a key pathology associated with PD that is lacking with the use of MPTP. In regards to parkin expression, whether there is the same differential expression of parkin between regions in α-synuclein based models is not known, let alone other proteins that may be neuroprotective. Additional to other models to induce effects similar to that observed in PD, potential regulators of parkin other than transcription factors should be examined.

One potential difference in responses between susceptible and resistant DA neurons could be the levels of microRNAs (miRNAs) present that can bind and suppress the expression of parkin mRNA. Algorithms from microrna.org and mirbase.org have shown 36 potential parkin mRNA binding miRNA candidates in mice and 49 in humans. In addition to examining miRNAs that are predicted to directly interact with parkin mRNA, some miRNAs, such as mir-34b and mir-34c have also been shown to regulate parkin expression (Minones-Moyano et al., 2011). Interestingly, PD brain

samples show concomitant decreases in mir-34b, mir-34c and parkin expression (Minones-Moyano et al., 2011). Since miRNAs only down-regulate expression, the decrease in both parkin and mir-34b and mir-34c; along with mir-34b and mir-34c not predicted to bind parkin mRNA, indicate that these miRNAs are most likely not functioning in the repression of parkin or binding parkin mRNA directly. Instead, these miRNAs may function in parkin activation by repressing an upstream transcription factor that is inhibitory to parkin expression.

Similar to the regulation of parkin via transcription factors, there could transcriptional coactivators involved. The histone acetyl transferase (HAT) p300 is one such transcriptional coactivator that has been shown to interact with members of the CREB family, the AP-1 family, HIF1, E2F, p53, MyoD, basal transcriptional machinery and others (Chan and La Thangue, 2001). There are five protein-binding domains on p300, as well as a bromodomain, which allows p300 to function as a HAT (Chan and La Thangue, 2001). Through acetylation of histone tails, the DNA becomes less tightly bound to the histones and the chromatin relaxes. This relaxation of the chromatin could be responsible for an increase in transcription and result in long-term changes in transcription.

In addition to acting as a HAT, p300 is also predicted to act as a bridge between transcription factors and basal transcriptional machinery, or as a scaffold recruiting other proteins that could modify transcription (Chan and

La Thangue, 2001). One of the ways that p300 is regulated is based on stability. Under normal conditions, p300 autoacetylates itself and can be destabilized by deacetylated via sirtuin 2 (dependent on the presence of NAD^+ as a cofactor) (Black et al., 2008). In the presence of oxidative stress and mitochondrial damage, p300 is not deacetylated and is a more stable protein and accumulates (Jain et al., 2012). As MPTP inhibits mitochondrial Complex I (which normally converts NADH to NAD^+), MPTP should decrease the amount of free NAD^+ present, decreasing SIRT2 activity and causing p300 accumulation. Since p300 has been shown via reported ChIP-Seq results on ENCODE to bind the *Park2* promoter and can be regulated by oxidative stress, it is an interesting potential avenue to explore.

Concluding Remarks

The differential susceptibility of the TIDA and NSDA neurons offers a unique tool to study how different populations of DA neurons react to stress in response to neurotoxic insult. The experiments in this dissertation have lead to the identification of potential transcriptional regulators involved in the differential regulation of parkin after acute MPTP exposure. Of these, only ΔFosB completely meets the expectations of a transcriptional activator of parkin, i.e. expression precedes parkin and is maintained as long as parkin, it is localized to the nuclei of DA neurons, and manipulations of the transcription factor or its actions produces corresponding alterations in

parkin expression. The experiments performed support the role of ΔFosB as a differentially expressed transcriptional activator of parkin. Furthermore, phosphorylated CREB and SRF, activators of the *FosB* gene, are consistent with activation of a FosB/ΔFosB mediated pathway for parkin activation following acute MPTP exposure. Though the small amount of protein each ARC sample yields makes it difficult to confirm ΔFosB directly interacts with the *PARK2* promoter via ChIP-RTPCR, results from AAV-mediated manipulations of ΔFosB and ΔJunD strongly suggest a close link between expression of ΔFosB and parkin. Though ΔFosB may not be the best therapeutic solution to make the NSDA neurons more like the TIDA neurons, it is a first step to at least examining how parkin may be regulated.

REFERENCES

REFERENCES

Agirre X, Roman-Gomez J, Vazquez I, Jimenez-Velasco A, Garate L, Montiel-Duarte C, Artieda P, Cordeu L, Lahortiga I, Calasanz MJ, Heiniger A, Torres A, Minna JD, Prosper F (2006) Abnormal methylation of the common PARK2 and PACRG promoter is associated with downregulation of gene expression in acute lymphoblastic leukemia and chronic myeloid leukemia. International journal of cancer 118:1945-1953.

Albin RL, Young AB, Penney JB (1989) The functional anatomy of basal ganglia disorders. Trends in neurosciences 12:366-375.

Alva-Murillo N, Medina-Estrada I, Baez-Magana M, Ochoa-Zarzosa A, Lopez-Meza JE (2015) The activation of the TLR2/p38 pathway by sodium butyrate in bovine mammary epithelial cells is involved in the reduction of Staphylococcus aureus internalization. Molecular immunology 68:445-455.

Andoh A, Fujiyama Y, Hata K, Araki Y, Takaya H, Shimada M, Bamba T (1999) Counter-regulatory effect of sodium butyrate on tumour necrosis factor-alpha (TNF-alpha)-induced complement C3 and factor B biosynthesis in human intestinal epithelial cells. Clinical and experimental immunology 118:23-29.

Apopa PL, He X, Ma Q (2008) Phosphorylation of Nrf2 in the transcription activation domain by casein kinase 2 (CK2) is critical for the nuclear translocation and transcription activation function of Nrf2 in IMR-32 neuroblastoma cells. Journal of biochemical and molecular toxicology 22:63-76.

Arnould T, Vankoningsloo S, Renard P, Houbion A, Ninane N, Demazy C, Remacle J, Raes M (2002) CREB activation induced by mitochondrial dysfunction is a new signaling pathway that impairs cell proliferation. The EMBO journal 21:53-63.

Asakawa S, Tsunematsu K, Takayanagi A, Sasaki T, Shimizu A, Shintani A, Kawasaki K, Mungall AJ, Beck S, Minoshima S, Shimizu N (2001) The genomic structure and promoter region of the human parkin gene. Biochemical and biophysical research communications 286:863-868.

Baguma-Nibasheka M, Fracassi A, Costain WJ, Moreno S, Kablar B (2016) Role of skeletal muscle in motor neuron development. Histology and histopathology 31:699-719.

Balasooriya IS, Wimalasena K (2007) Are SH-SY5Y and MN9D cells truly dopaminergic? Proceedings of the 3rd annual GRASP symposium: 25-26

Ballard PA, Tetrud JW, Langston JW (1985) Permanent human parkinsonism due to 1-methyl-4-phenyl-1,2,3,6-tetrahydropyridine (MPTP): seven cases. Neurology 35:949-956.

Bannister AJ, Kouzarides T (2011) Regulation of chromatin by histone modifications. Cell research 21:381-395.

Been LE, Hedges VL, Vialou V, Nestler EJ, Meisel RL (2013) DeltaJunD overexpression in the nucleus accumbens prevents sexual reward in female Syrian hamsters. Genes, brain, and behavior 12:666-672.

Behrouz B, Drolet RE, Sayed ZA, Lookingland KJ, Goudreau JL (2007) Unique responses to mitochondrial complex I inhibition in tuberoinfundibular dopamine neurons may impart resistance to toxic insult. Neuroscience 147:592-598.

Bellou V, Belbasis L, Tzoulaki I, Evangelou E, Ioannidis JP (2016) Environmental risk factors and Parkinson's disease: An umbrella review of meta-analyses. Parkinsonism & related disorders 23:1-9.

Benskey M, Behrouz B, Sunryd J, Pappas SS, Baek SH, Huebner M, Lookingland KJ, Goudreau JL (2012) Recovery of hypothalamic tuberoinfundibular dopamine neurons from acute toxicant exposure is dependent upon protein synthesis and associated with an increase in parkin and ubiquitin carboxy-terminal hydrolase-L1 expression. Neurotoxicology 33:321-331.

Benskey M, Lee KY, Parikh K, Lookingland KJ, Goudreau JL (2013) Sustained resistance to acute MPTP toxicity by hypothalamic dopamine neurons following chronic neurotoxicant exposure is associated with sustained up-regulation of parkin protein. Neurotoxicology 37:144-153.

Benskey MJ, Manfredsson FP, Lookingland KJ, Goudreau JL (2015) The role of parkin in the differential susceptibility of tuberoinfundibular and nigrostriatal dopamine neurons to acute toxicant exposure. Neurotoxicology 46:1-11.

Berry SA, Gudelsky GA (1991) Effect of D2 dopamine agonists on tuberoinfundibular dopamine neurons. Neuropharmacology 30:961-965.

Berton O, Guigoni C, Li Q, Bioulac BH, Aubert I, Gross CE, Dileone RJ, Nestler EJ, Bezard E (2009) Striatal overexpression of DeltaJunD resets L-DOPA-induced dyskinesia in a primate model of Parkinson disease. Biological psychiatry 66:554-561.

Bezard E, Imbert C, Gross CE (1998) Experimental models of Parkinson's disease: from the static to the dynamic. Reviews in the neurosciences 9:71-90.

Black JC, Mosley A, Kitada T, Washburn M, Carey M (2008) The SIRT2 deacetylase regulates autoacetylation of p300. Molecular cell 32:449-455.

Blaker AL, Taylor JM, Mack CP (2009) PKA-dependent phosphorylation of serum response factor inhibits smooth muscle-specific gene expression. Arteriosclerosis, thrombosis, and vascular biology 29:2153-2160.

Bohm M, Moellmann G, Cheng E, Alvarez-Franco M, Wagner S, Sassone-Corsi P, Halaban R (1995) Identification of p90RSK as the probable CREB-Ser133 kinase in human melanocytes. Cell growth & differentiation : the molecular biology journal of the American Association for Cancer Research 6:291-302.

Bostrom K, Wettesten M, Boren J, Bondjers G, Wiklund O, Olofsson SO (1986) Pulse-chase studies of the synthesis and intracellular transport of apolipoprotein B-100 in Hep G2 cells. The Journal of biological chemistry 261:13800-13806.

Bouman L, Schlierf A, Lutz AK, Shan J, Deinlein A, Kast J, Galehdar Z, Palmisano V, Patenge N, Berg D, Gasser T, Augustin R, Trumbach D, Irrcher I, Park DS, Wurst W, Kilberg MS, Tatzelt J, Winklhofer KF (2011) Parkin is transcriptionally regulated by ATF4: evidence for an interconnection between mitochondrial stress and ER stress. Cell death and differentiation 18:769-782.

Bradford ST, Wilhelm D, Koopman P (2007) Comparative analysis of anti-mouse SRY antibodies. Sexual development : genetics, molecular biology, evolution, endocrinology, embryology, and pathology of sex determination and differentiation 1:305-310.

Brown TP, Rumsby PC, Capleton AC, Rushton L, Levy LS (2006) Pesticides and Parkinson's disease--is there a link? Environmental health perspectives 114:156-164.

Buckingham M, Rigby PW (2014) Gene regulatory networks and transcriptional mechanisms that control myogenesis. Developmental cell 28:225-238.

Buhlman L, Damiano M, Bertolin G, Ferrando-Miguel R, Lombes A, Brice A, Corti O (2014) Functional interplay between Parkin and Drp1 in mitochondrial fission and clearance. Biochimica et biophysica acta 1843:2012-2026.

Cai M, Tian J, Zhao GH, Luo W, Zhang BR (2011) Study of methylation levels of parkin gene promoter in Parkinson's disease patients. The International journal of neuroscience 121:497-502.

Cao X, Yasuda T, Uthayathas S, Watts RL, Mouradian MM, Mochizuki H, Papa SM (2010) Striatal overexpression of DeltaFosB reproduces chronic levodopa-induced involuntary movements. The Journal of neuroscience : the official journal of the Society for Neuroscience 30:7335-7343.

Cappelletti G, Surrey T, Maci R (2005) The parkinsonism producing neurotoxin MPP+ affects microtubule dynamics by acting as a destabilising factor. FEBS letters 579:4781-4786.

Cartelli D, Casagrande F, Busceti CL, Bucci D, Molinaro G, Traficante A, Passarella D, Giavini E, Pezzoli G, Battaglia G, Cappelletti G (2013) Microtubule alterations occur early in experimental parkinsonism and the microtubule stabilizer epothilone D is neuroprotective. Scientific reports 3:1837.

Chae HD, Suh BC, Joh TH, Kim KT (1996) AP1-mediated transcriptional enhancement of the rat tyrosine hydroxylase gene by muscarinic stimulation. Journal of neurochemistry 66:1264-1272.

Chan HM, La Thangue NB (2001) p300/CBP proteins: HATs for transcriptional bridges and scaffolds. Journal of cell science 114:2363-2373.

Chan P, DeLanney LE, Irwin I, Langston JW, Di Monte D (1991) Rapid ATP loss caused by 1-methyl-4-phenyl-1,2,3,6-tetrahydropyridine in mouse brain. Journal of neurochemistry 57:348-351.

Chang CM, Chao CC (2013) Protein kinase CK2 enhances Mcl-1 gene expression through the serum response factor-mediated pathway in the rat hippocampus. Journal of neuroscience research 91:808-817.

Chaugule VK, Burchell L, Barber KR, Sidhu A, Leslie SJ, Shaw GS, Walden H (2011) Autoregulation of Parkin activity through its ubiquitin-like domain. The EMBO journal 30:2853-2867.

Chen H, Chan DC (2005) Emerging functions of mammalian mitochondrial fusion and fission. Human molecular genetics 14 Spec No. 2:R283-289.

Chen J, Kelz MB, Hope BT, Nakabeppu Y, Nestler EJ (1997) Chronic Fos-related antigens: stable variants of deltaFosB induced in brain by chronic treatments. The Journal of neuroscience : the official journal of the Society for Neuroscience 17:4933-4941.

Chen JY, Hsu PC, Hsu IL, Yeh GC (2001) Sequential up-regulation of the c-fos, c-jun and bax genes in the cortex, striatum and cerebellum induced by a single injection of a low dose of 1-methyl-4-phenyl-1,2,3,6-tetrahydropyridine (MPTP) in C57BL/6 mice. Neuroscience letters 314:49-52.

Chen PC, Vargas MR, Pani AK, Smeyne RJ, Johnson DA, Kan YW, Johnson JA (2009) Nrf2-mediated neuroprotection in the MPTP mouse model of Parkinson's disease: Critical role for the astrocyte. Proceedings of the National Academy of Sciences of the United States of America 106:2933-2938.

Chen T, Hou R, Li C, Wu C, Xu S (2015) MPTP/MPP+ suppresses activation of protein C in Parkinson's disease. Journal of Alzheimer's disease : JAD 43:133-142.

Choi HK, Won L, Roback JD, Wainer BH, Heller A (1992) Specific modulation of dopamine expression in neuronal hybrid cells by primary cells from different brain regions. Proceedings of the National Academy of Sciences of the United States of America 89:8943-8947.

Choi WS, Canzoniero LM, Sensi SL, O'Malley KL, Gwag BJ, Sohn S, Kim JE, Oh TH, Lee EB, Oh YJ (1999a) Characterization of MPP(+)-induced cell death in a dopaminergic neuronal cell line: role of macromolecule synthesis, cytosolic calcium, caspase, and Bcl-2-related proteins. Experimental neurology 159:274-282.

Choi WS, Yoon SY, Oh TH, Choi EJ, O'Malley KL, Oh YJ (1999b) Two distinct mechanisms are involved in 6-hydroxydopamine- and MPP+-induced dopaminergic neuronal cell death: role of caspases, ROS, and JNK. Journal of neuroscience research 57:86-94.

Clark IE, Dodson MW, Jiang C, Cao JH, Huh JR, Seol JH, Yoo SJ, Hay BA, Guo M (2006) Drosophila pink1 is required for mitochondrial function and interacts genetically with parkin. Nature 441:1162-1166.

Cookson MR (2009) alpha-Synuclein and neuronal cell death. Molecular neurodegeneration 4:9.

Cookson MR (2012) Parkinsonism due to mutations in PINK1, parkin, and DJ-1 and oxidative stress and mitochondrial pathways. Cold Spring Harbor perspectives in medicine 2:a009415.

Corre S, Galibert MD (2005) Upstream stimulating factors: highly versatile stress-responsive transcription factors. Pigment cell research / sponsored by the European Society for Pigment Cell Research and the International Pigment Cell Society 18:337-348.

Darzacq X, Shav-Tal Y, de Turris V, Brody Y, Shenoy SM, Phair RD, Singer RH (2007) In vivo dynamics of RNA polymerase II transcription. Nature structural & molecular biology 14:796-806.

Dauer W, Przedborski S (2003) Parkinson's disease: mechanisms and models. Neuron 39:889-909.

Delghandi MP, Johannessen M, Moens U (2005) The cAMP signalling pathway activates CREB through PKA, p38 and MSK1 in NIH 3T3 cells. Cellular signalling 17:1343-1351.

Deniaud A, Sharaf el dein O, Maillier E, Poncet D, Kroemer G, Lemaire C, Brenner C (2008) Endoplasmic reticulum stress induces calcium-dependent permeability transition, mitochondrial outer membrane permeabilization and apoptosis. Oncogene 27:285-299.

Dewing P, Chiang CW, Sinchak K, Sim H, Fernagut PO, Kelly S, Chesselet MF, Micevych PE, Albrecht KH, Harley VR, Vilain E (2006) Direct regulation of adult brain function by the male-specific factor SRY. Current biology : CB 16:415-420.

Digaleh H, Kiaei M, Khodagholi F (2013) Nrf2 and Nrf1 signaling and ER stress crosstalk: implication for proteasomal degradation and autophagy. Cellular and molecular life sciences : CMLS 70:4681-4694.

Du K, Montminy M (1998) CREB is a regulatory target for the protein kinase Akt/PKB. The Journal of biological chemistry 273:32377-32379.

Duchemin AM, Gudehithlu KP, Neff NH, Hadjiconstantinou M (1992) c-fos mRNA in mouse brain after MPTP treatment. Neurochemistry international 20:281-287.

Duplan E, Sevalle J, Viotti J, Goiran T, Bauer C, Renbaum P, Levy-Lahad E, Gautier CA, Corti O, Leroudier N, Checler F, da Costa CA (2013) Parkin differently regulates presenilin-1 and presenilin-2 functions by direct control of their promoter transcription. Journal of molecular cell biology 5:132-142.

Eagle AL, Gajewski PA, Yang M, Kechner ME, Al Masraf BS, Kennedy PJ, Wang H, Mazei-Robison MS, Robison AJ (2015) Experience-Dependent Induction of Hippocampal DeltaFosB Controls Learning. The Journal of neuroscience : the official journal of the Society for Neuroscience 35:13773-13783.

Ermak G, Davies KJ (2002) Calcium and oxidative stress: from cell signaling to cell death. Molecular immunology 38:713-721.

Escott-Price V, International Parkinson's Disease Genomics C, Nalls MA, Morris HR, Lubbe S, Brice A, Gasser T, Heutink P, Wood NW, Hardy J, Singleton AB, Williams NM, members Ic (2015) Polygenic risk of Parkinson disease is correlated with disease age at onset. Annals of neurology 77:582-591.

Fahn S (2003) Description of Parkinson's disease as a clinical syndrome. Annals of the New York Academy of Sciences 991:1-14.

Farre D, Roset R, Huerta M, Adsuara JE, Rosello L, Alba MM, Messeguer X (2003) Identification of patterns in biological sequences at the ALGGEN server: PROMO and MALGEN. Nucleic acids research 31:3651-3653.

Femino AM, Fay FS, Fogarty K, Singer RH (1998) Visualization of single RNA transcripts in situ. Science 280:585-590.

Fernstrom JD, Fernstrom MH (2007) Tyrosine, phenylalanine, and catecholamine synthesis and function in the brain. The Journal of nutrition 137:1539S-1547S; discussion 1548S.

Frigo DE, Tang Y, Beckman BS, Scandurro AB, Alam J, Burow ME, McLachlan JA (2004) Mechanism of AP-1-mediated gene expression by select organochlorines through the p38 MAPK pathway. Carcinogenesis 25:249-261.

Gavala ML, Hill LM, Lenertz LY, Karta MR, Bertics PJ (2010) Activation of the transcription factor FosB/activating protein-1 (AP-1) is a prominent downstream signal of the extracellular nucleotide receptor P2RX7 in monocytic and osteoblastic cells. The Journal of biological chemistry 285:34288-34298.

Geisler S, Holmstrom KM, Treis A, Skujat D, Weber SS, Fiesel FC, Kahle PJ, Springer W (2010) The PINK1/Parkin-mediated mitophagy is compromised by PD-associated mutations. Autophagy 6:871-878.

Gerfen CR, Surmeier DJ (2011) Modulation of striatal projection systems by dopamine. Annual review of neuroscience 34:441-466.

Ghee M, Baker H, Miller JC, Ziff EB (1998) AP-1, CREB and CBP transcription factors differentially regulate the tyrosine hydroxylase gene. Brain research Molecular brain research 55:101-114.

Gizang-Ginsberg E, Ziff EB (1994) Fos family members successively occupy the tyrosine hydroxylase gene AP-1 site after nerve growth factor or epidermal growth factor stimulation and can repress transcription. Molecular endocrinology 8:249-262.

Gregor PD, Sawadogo M, Roeder RG (1990) The adenovirus major late transcription factor USF is a member of the helix-loop-helix group of regulatory proteins and binds to DNA as a dimer. Genes & development 4:1730-1740.

Hafer G, Agarwal DP, Goedde HW (1987) Human brain aldehyde dehydrogenase: activity with DOPAL and isozyme distribution. Alcohol 4:413-418.

Hai T, Curran T (1991) Cross-family dimerization of transcription factors Fos/Jun and ATF/CREB alters DNA binding specificity. Proceedings of the National Academy of Sciences of the United States of America 88:3720-3724.

Hardy J (2010) Genetic analysis of pathways to Parkinson disease. Neuron 68:201-206.

Hayes JD, Chanas SA, Henderson CJ, McMahon M, Sun C, Moffat GJ, Wolf CR, Yamamoto M (2000) The Nrf2 transcription factor contributes both to the basal expression of glutathione S-transferases in mouse liver and to their induction by the chemopreventive synthetic antioxidants, butylated hydroxyanisole and ethoxyquin. Biochemical Society transactions 28:33-41.

He B, Wang M, Guo H, Jia Y, Yang X, Zhao R (2016) Effects of sodium butyrate supplementation on reproductive performance and colostrum composition in gilts. Animal : an international journal of animal bioscience 1-6.

Hedges VL, Chakravarty S, Nestler EJ, Meisel RL (2009) Delta FosB overexpression in the nucleus accumbens enhances sexual reward in female Syrian hamsters. Genes, brain, and behavior 8:442-449.

Heidenreich O, Neininger A, Schratt G, Zinck R, Cahill MA, Engel K, Kotlyarov A, Kraft R, Kostka S, Gaestel M, Nordheim A (1999) MAPKAP kinase 2 phosphorylates serum response factor in vitro and in vivo. The Journal of biological chemistry 274:14434-14443.

Heikkila RE, Hess A, Duvoisin RC (1984) Dopaminergic neurotoxicity of 1-methyl-4-phenyl-1,2,5,6-tetrahydropyridine in mice. Science 224:1451-1453.

Herdegen T, Kovary K, Buhl A, Bravo R, Zimmermann M, Gass P (1995) Basal expression of the inducible transcription factors c-Jun, JunB, JunD, c-Fos, FosB, and Krox-24 in the adult rat brain. The Journal of comparative neurology 354:39-56.

Hernandez DG, Reed X, Singleton AB (2016) Genetics in Parkinson disease: Mendelian versus non-Mendelian inheritance. Journal of neurochemistry 139 Suppl 1:59-74.

Hristova VA, Beasley SA, Rylett RJ, Shaw GS (2009) Identification of a novel Zn2+-binding domain in the autosomal recessive juvenile Parkinson-related E3 ligase parkin. The Journal of biological chemistry 284:14978-14986.

Hung HC, Lee EH (1998) MPTP produces differential oxidative stress and antioxidative responses in the nigrostriatal and mesolimbic dopaminergic pathways. Free radical biology & medicine 24:76-84.

Hung JJ, Wang YT, Chang WC (2006) Sp1 deacetylation induced by phorbol ester recruits p300 to activate 12(S)-lipoxygenase gene transcription. Molecular and cellular biology 26:1770-1785.

Hyun DH, Lee M, Hattori N, Kubo S, Mizuno Y, Halliwell B, Jenner P (2002) Effect of wild-type or mutant Parkin on oxidative damage, nitric oxide, antioxidant defenses, and the proteasome. The Journal of biological chemistry 277:28572-28577.

Imai Y, Soda M, Inoue H, Hattori N, Mizuno Y, Takahashi R (2001) An unfolded putative transmembrane polypeptide, which can lead to endoplasmic reticulum stress, is a substrate of Parkin. Cell 105:891-902.

Ingolia N (2011) Many paths to the same end: histone transcripts recruit canonical initiation factors through unconventional interactions. Molecular cell 41:133-135.

Itoh K, Tong KI, Yamamoto M (2004) Molecular mechanism activating Nrf2-Keap1 pathway in regulation of adaptive response to electrophiles. Free radical biology & medicine 36:1208-1213.

Itoh K, Wakabayashi N, Katoh Y, Ishii T, Igarashi K, Engel JD, Yamamoto M (1999) Keap1 represses nuclear activation of antioxidant responsive elements by Nrf2 through binding to the amino-terminal Neh2 domain. Genes & development 13:76-86.

Jain S, Wei J, Mitrani LR, Bishopric NH (2012) Auto-acetylation stabilizes p300 in cardiac myocytes during acute oxidative stress, promoting STAT3 accumulation and cell survival. Breast cancer research and treatment 135:103-114.

Jankovic J (2008) Parkinson's disease: clinical features and diagnosis. Journal of neurology, neurosurgery, and psychiatry 79:368-376.

Javitch JA, D'Amato RJ, Strittmatter SM, Snyder SH (1985) Parkinsonism-inducing neurotoxin, N-methyl-4-phenyl-1,2,3,6 -tetrahydropyridine: uptake of the metabolite N-methyl-4-phenylpyridine by dopamine neurons explains selective toxicity. Proceedings of the National Academy of Sciences of the United States of America 82:2173-2177.

Jorissen HJ, Ulery PG, Henry L, Gourneni S, Nestler EJ, Rudenko G (2007) Dimerization and DNA-binding properties of the transcription factor DeltaFosB. Biochemistry 46:8360-8372.

Kablar B (2004) MyoD-lacZ transgenes are early markers in the neural retina, but MyoD function appears to be inhibited in the developing retinal cells. International journal of developmental neuroscience : the official journal of the International Society for Developmental Neuroscience 22:215-224.

Karmodiya K, Krebs AR, Oulad-Abdelghani M, Kimura H, Tora L (2012) H3K9 and H3K14 acetylation co-occur at many gene regulatory elements, while H3K14ac marks a subset of inactive inducible promoters in mouse embryonic stem cells. BMC genomics 13:424.

Karunakaran S, Ravindranath V (2009) Activation of p38 MAPK in the substantia nigra leads to nuclear translocation of NF-kappaB in MPTP-treated mice: implication in Parkinson's disease. Journal of neurochemistry 109:1791-1799.

Kastner P, Dupuis A, Gaub MP, Herbrecht R, Lutz P, Chan S (2013) Function of Ikaros as a tumor suppressor in B cell acute lymphoblastic leukemia. American journal of blood research 3:1-13.

Kebabian JW, Greengard P (1971) Dopamine-sensitive adenyl cyclase: possible role in synaptic transmission. Science 174:1346-1349.

Kelz MB, Chen J, Carlezon WA, Jr., Whisler K, Gilden L, Beckmann AM, Steffen C, Zhang YJ, Marotti L, Self DW, Tkatch T, Baranauskas G, Surmeier DJ, Neve RL, Duman RS, Picciotto MR, Nestler EJ (1999) Expression of the transcription factor deltaFosB in the brain controls sensitivity to cocaine. Nature 401:272-276.

Kent WJ, Sugnet CW, Furey TS, Roskin KM, Pringle TH, Zahler AM, Haussler D (2002) The human genome browser at UCSC. Genome res. 12(6): 996-1006.

Kim KS, Park DH, Wessel TC, Song B, Wagner JA, Joh TH (1993) A dual role for the cAMP-dependent protein kinase in tyrosine hydroxylase gene expression. Proceedings of the National Academy of Sciences of the United States of America 90:3471-3475.

Kiryu-Seo S, Kato R, Ogawa T, Nakagomi S, Nagata K, Kiyama H (2008) Neuronal injury-inducible gene is synergistically regulated by ATF3, c-Jun,

and STAT3 through the interaction with Sp1 in damaged neurons. The Journal of biological chemistry 283:6988-6996.

Kitada T, Asakawa S, Hattori N, Matsumine H, Yamamura Y, Minoshima S, Yokochi M, Mizuno Y, Shimizu N (1998) Mutations in the parkin gene cause autosomal recessive juvenile parkinsonism. Nature 392:605-608.

Klein C, Westenberger A (2012) Genetics of Parkinson's disease. Cold Spring Harbor perspectives in medicine 2:a008888.

Kobayashi A, Kang MI, Okawa H, Ohtsuji M, Zenke Y, Chiba T, Igarashi K, Yamamoto M (2004) Oxidative stress sensor Keap1 functions as an adaptor for Cul3-based E3 ligase to regulate proteasomal degradation of Nrf2. Molecular and cellular biology 24:7130-7139.

Korner M, Rattner A, Mauxion F, Sen R, Citri Y (1989) A brain-specific transcription activator. Neuron 3:563-572.

Krasnova IN, Chiflikyan M, Justinova Z, McCoy MT, Ladenheim B, Jayanthi S, Quintero C, Brannock C, Barnes C, Adair JE, Lehrmann E, Kobeissy FH, Gold MS, Becker KG, Goldberg SR, Cadet JL (2013) CREB phosphorylation regulates striatal transcriptional responses in the self-administration model of methamphetamine addiction in the rat. Neurobiology of disease 58:132-143.

Kumar KR, Djarmati-Westenberger A, Grunewald A (2011) Genetics of Parkinson's disease. Seminars in neurology 31:433-440.

Kurosaki R, Muramatsu Y, Watanabe H, Michimata M, Matsubara M, Imai Y, Araki T (2003) Role of dopamine transporter against MPTP (1-methyl-4-phenyl-1,2,3,6-tetrahydropyridine) neurotoxicity in mice. Metabolic brain disease 18:139-146.

Langston JW, Forno LS, Tetrud J, Reeves AG, Kaplan JA, Karluk D (1999) Evidence of active nerve cell degeneration in the substantia nigra of humans years after 1-methyl-4-phenyl-1,2,3,6-tetrahydropyridine exposure. Annals of neurology 46:598-605.

Lee B, Cao R, Choi YS, Cho HY, Rhee AD, Hah CK, Hoyt KR, Obrietan K (2009) The CREB/CRE transcriptional pathway: protection against oxidative stress-mediated neuronal cell death. Journal of neurochemistry 108:1251-1265.

Lee J, Harley VR (2012) The male fight-flight response: a result of SRY regulation of catecholamines? BioEssays : news and reviews in molecular, cellular and developmental biology 34:454-457.

Lee TG, Park JB, Lee SD, Hong S, Kim JH, Kim Y, Yi KS, Bae S, Hannun YA, Obeid LM, Suh PG, Ryu SH (1997) Phorbol myristate acetate-dependent association of protein kinase C alpha with phospholipase D1 in intact cells. Biochimica et biophysica acta 1347:199-204.

Levitt M, Spector S, Sjoerdsma A, Udenfriend S (1965) Elucidation of the Rate-Limiting Step in Norepinephrine Biosynthesis in the Perfused Guinea-Pig Heart. The Journal of pharmacology and experimental therapeutics 148:1-8.

Li B, Du T, Li H, Gu L, Zhang H, Huang J, Hertz L, Peng L (2008) Signalling pathways for transactivation by dexmedetomidine of epidermal growth factor receptors in astrocytes and its paracrine effect on neurons. British journal of pharmacology 154:191-203.

Li X, Gehring K (2015) Structural studies of parkin and sacsin: Mitochondrial dynamics in neurodegenerative diseases. Movement disorders : official journal of the Movement Disorder Society 30:1610-1619.

Limb JK, Yoon S, Lee KE, Kim BH, Lee S, Bae YS, Jhon GJ, Kim J (2009) Regulation of megakaryocytic differentiation of K562 cells by FosB, a member of the Fos family of AP-1 transcription factors. Cellular and molecular life sciences : CMLS 66:1962-1973.

Lindgren HS, Rylander D, Iderberg H, Andersson M, O'Sullivan SS, Williams DR, Lees AJ, Cenci MA (2011) Putaminal upregulation of FosB/DeltaFosB-like immunoreactivity in Parkinson's disease patients with dyskinesia. Journal of Parkinson's disease 1:347-357.

Liu DX, Greene LA (2001) Regulation of neuronal survival and death by E2F-dependent gene repression and derepression. Neuron 32:425-438.

Liu Y, Peter D, Roghani A, Schuldiner S, Prive GG, Eisenberg D, Brecha N, Edwards RH (1992) A cDNA that suppresses MPP+ toxicity encodes a vesicular amine transporter. Cell 70:539-551.

Lohr KM, Chen M, Hoffman CA, McDaniel MJ, Stout KA, Dunn AR, Wang M, Bernstein AI, Miller GW (2016) Vesicular Monoamine Transporter 2 (VMAT2) Level Regulates MPTP Vulnerability and Clearance of Excess

Dopamine in Mouse Striatal Terminals. Toxicological sciences : an official journal of the Society of Toxicology 153:79-88.

Lookingland KJ, Moore KE (2005) Functional neuroanatomy of hypothalamic dopaminergic neuroendocrin ststems (Dunnet SB, Bentivoglio M, Bjorklund A, Hokfelt T). Handbook of chemical neuroanatomy 21: 433-521.

Lovenberg W, Weissbach H, Udenfriend S (1962) Aromatic L-amino acid decarboxylase. The Journal of biological chemistry 237:89-93.

Lutz AK, Exner N, Fett ME, Schlehe JS, Kloos K, Lammermann K, Brunner B, Kurz-Drexler A, Vogel F, Reichert AS, Bouman L, Vogt-Weisenhorn D, Wurst W, Tatzelt J, Haass C, Winklhofer KF (2009) Loss of parkin or PINK1 function increases Drp1-dependent mitochondrial fragmentation. The Journal of biological chemistry 284:22938-22951.

MacLeod D, Dowman J, Hammond R, Leete T, Inoue K, Abeliovich A (2006) The familial Parkinsonism gene LRRK2 regulates neurite process morphology. Neuron 52:587-593.

Maiuri P, Knezevich A, De Marco A, Mazza D, Kula A, McNally JG, Marcello A (2011) Fast transcription rates of RNA polymerase II in human cells. EMBO reports 12:1280-1285.

Marchitti SA, Deitrich RA, Vasiliou V (2007) Neurotoxicity and metabolism of the catecholamine-derived 3,4-dihydroxyphenylacetaldehyde and 3,4-dihydroxyphenylglycolaldehyde: the role of aldehyde dehydrogenase. Pharmacological reviews 59:125-150.

Markey SP, Johannessen JN, Chiueh CC, Burns RS, Herkenham MA (1984) Intraneuronal generation of a pyridinium metabolite may cause drug-induced parkinsonism. Nature 311:464-467.

Martin C, Zhang Y (2005) The diverse functions of histone lysine methylation. Nature reviews Molecular cell biology 6:838-849.

Matys V, Fricke E, Geffers R, Gossling E, Haubrock M, Hehl R, Hornischer K, Karas D, Kel AE, Kel-Margoulis OV, Kloos DU, Land S, Lewicki-Potapov B, Michael H, Munch R, Reuter I, Rotert S, Saxel H, Scheer M, Thiele S, Wingender E (2003) TRANSFAC: transcriptional regulation from patterns to profiles. Nucleic Acids Res 31: 374-378.

Matzuk MM, Saper CB (1985) Preservation of hypothalamic dopaminergic neurons in Parkinson's disease. Annals of neurology 18:552-555.

McClung CA, Nestler EJ (2003) Regulation of gene expression and cocaine reward by CREB and DeltaFosB. Nature neuroscience 6:1208-1215.

Merkenschlager M (2010) Ikaros in immune receptor signaling, lymphocyte differentiation, and function. FEBS letters 584:4910-4914.

Messeguer X, Escudero R, Farre D, Nunez O, Martinez J, Alba MM (2002) PROMO: detection of known transcription regulatory elements using species-tailored searches. Bioinformatics 18:333-334.

Milsted A, Serova L, Sabban EL, Dunphy G, Turner ME, Ely DL (2004) Regulation of tyrosine hydroxylase gene transcription by Sry. Neuroscience letters 369:203-207.

Minones-Moyano E, Porta S, Escaramis G, Rabionet R, Iraola S, Kagerbauer B, Espinosa-Parrilla Y, Ferrer I, Estivill X, Marti E (2011) MicroRNA profiling of Parkinson's disease brains identifies early downregulation of miR-34b/c which modulate mitochondrial function. Human molecular genetics 20:3067-3078.

Miranti CK, Ginty DD, Huang G, Chatila T, Greenberg ME (1995) Calcium activates serum response factor-dependent transcription by a Ras- and Elk-1-independent mechanism that involves a Ca2+/calmodulin-dependent kinase. Molecular and cellular biology 15:3672-3684.

Miras-Portugal MT, Diaz-Hernandez JI, Gomez-Villafuertes R, Diaz-Hernandez M, Artalejo AR, Gualix J (2015) Role of P2X7 and P2Y2 receptors on alpha-secretase-dependent APP processing: Control of amyloid plaques formation "in vivo" by P2X7 receptor. Computational and structural biotechnology journal 13:176-181.

Mitsui J, Tsuji S (2014) Genomic aspects of sporadic neurodegenerative diseases. Biochemical and biophysical research communications 452:221-225.

Morgan JI, Curran T (1995) Immediate-early genes: ten years on. Trends in neurosciences 18:66-67.

Mortimer JA, Borenstein AR, Nelson LM (2012) Associations of welding and manganese exposure with Parkinson disease: review and meta-analysis. Neurology 79:1174-1180.

Muller H, Helin K (2000) The E2F transcription factors: key regulators of cell proliferation. Biochimica et biophysica acta 1470:M1-12.

Muroyama A, Kobayashi S, Mitsumoto Y (2011) Loss of striatal dopaminergic terminals during the early stage in response to MPTP injection in C57BL/6 mice. Neuroscience research 69:352-355.

Nakabeppu Y, Nathans D (1991) A naturally occurring truncated form of FosB that inhibits Fos/Jun transcriptional activity. Cell 64:751-759.

Narendra D, Tanaka A, Suen DF, Youle RJ (2008) Parkin is recruited selectively to impaired mitochondria and promotes their autophagy. The Journal of cell biology 183:795-803.

Nestler EJ (2008) Review. Transcriptional mechanisms of addiction: role of DeltaFosB. Philosophical transactions of the Royal Society of London Series B, Biological sciences 363:3245-3255.

Nestler EJ (2012) Transcriptional mechanisms of drug addiction. Clinical psychopharmacology and neuroscience : the official scientific journal of the Korean College of Neuropsychopharmacology 10:136-143.

Nestler EJ (2015) FosB: a transcriptional regulator of stress and antidepressant responses. European journal of pharmacology 753:66-72.

Nestler EJ, Barrot M, Self DW (2001) DeltaFosB: a sustained molecular switch for addiction. Proceedings of the National Academy of Sciences of the United States of America 98:11042-11046.

Nikulina EM, Lacagnina MJ, Fanous S, Wang J, Hammer RP, Jr. (2012) Intermittent social defeat stress enhances mesocorticolimbic DeltaFosB/BDNF co-expression and persistently activates corticotegmental neurons: implication for vulnerability to psychostimulants. Neuroscience 212:38-48.

Nishi K (1997) Expression of c-Jun in dopaminergic neurons of the substantia nigra in 1-methyl-4-phenyl-1,2,3,6-tetrahydropyridine (MPTP)-treated mice. Brain research 771:133-141.

Nomaru H, Sakumi K, Katogi A, Ohnishi YN, Kajitani K, Tsuchimoto D, Nestler EJ, Nakabeppu Y (2014) Fosb gene products contribute to excitotoxic microglial activation by regulating the expression of complement C5a receptors in microglia. Glia 62:1284-1298.

Novotny V, Prieschl EE, Csonga R, Fabjani G, Baumruker T (1998) Nrf1 in a complex with fosB, c-jun, junD and ATF2 forms the AP1 component at the TNF alpha promoter in stimulated mast cells. Nucleic acids research 26:5480-5485.

Noyce AJ, Silveira-Moriyama L, Gilpin P, Ling H, Howard R, Lees AJ (2012) Severe dysphagia as a presentation of Parkinson's disease. Movement disorders : official journal of the Movement Disorder Society 27:457-458.

Nuytemans K, Theuns J, Cruts M, Van Broeckhoven C (2010) Genetic etiology of Parkinson disease associated with mutations in the SNCA, PARK2, PINK1, PARK7, and LRRK2 genes: a mutation update. Human mutation 31:763-780.

O'Carroll AM, Fowler CJ, Phillips JP, Tobbia I, Tipton KF (1983) The deamination of dopamine by human brain monoamine oxidase. Specificity for the two enzyme forms in seven brain regions. Naunyn-Schmiedeberg's archives of pharmacology 322:198-202.

Orekhova AS, Sverdlova PS, Spirin PV, Leonova OG, Popenko VI, Prasolov VS, Rubtsov PM (2011) [Novel bidirectional promoter from human genome]. Molekuliarnaia biologiia 45:486-495.

Ozaki N, Nakahara D, Kaneda N, Kiuchi K, Okada T, Kasahara Y, Nagatsu T (1987) Acute effects of 1-methyl-4-phenylpyridinium ion (MPP+) on dopamine and serotonin metabolism in rat striatum as assayed in vivo by a micro-dialysis technique. Journal of neural transmission 70:241-250.

Park J, Lee G, Chung J (2009) The PINK1-Parkin pathway is involved in the regulation of mitochondrial remodeling process. Biochemical and biophysical research communications 378:518-523.

Park J, Lee SB, Lee S, Kim Y, Song S, Kim S, Bae E, Kim J, Shong M, Kim JM, Chung J (2006) Mitochondrial dysfunction in Drosophila PINK1 mutants is complemented by parkin. Nature 441:1157-1161.

Patil SP, Jain PD, Ghumatkar PJ, Tambe R, Sathaye S (2014) Neuroprotective effect of metformin in MPTP-induced Parkinson's disease in mice. Neuroscience 277:747-754.

Pennypacker K (1997) Transcription factors in brain injury. Histology and histopathology 12:1125-1133.

Pennypacker K (1998) AP-1 transcription factors: short- and long-term modulators of gene expression in the brain. International review of neurobiology 42:169-197.

Pennypacker KR, Kassed CA, Eidizadeh S, O'Callaghan JP (2000) Brain injury: prolonged induction of transcription factors. Acta neurobiologiae experimentalis 60:515-530.

Perez-Otano I, Mandelzys A, Morgan JI (1998) MPTP-Parkinsonism is accompanied by persistent expression of a delta-FosB-like protein in dopaminergic pathways. Brain research Molecular brain research 53:41-52.

Pezzoli G, Cereda E (2013) Exposure to pesticides or solvents and risk of Parkinson disease. Neurology 80:2035-2041.

Pickart CM (2001) Mechanisms underlying ubiquitination. Annual review of biochemistry 70:503-533.

Pickrell AM, Huang CH, Kennedy SR, Ordureau A, Sideris DP, Hoekstra JG, Harper JW, Youle RJ (2015) Endogenous Parkin Preserves Dopaminergic Substantia Nigral Neurons following Mitochondrial DNA Mutagenic Stress. Neuron 87:371-381.

Pitchers KK, Vialou V, Nestler EJ, Laviolette SR, Lehman MN, Coolen LM (2013) Natural and drug rewards act on common neural plasticity mechanisms with DeltaFosB as a key mediator. The Journal of neuroscience : the official journal of the Society for Neuroscience 33:3434-3442.

Pons J, Evrard-Todeschi N, Bertho G, Gharbi-Benarous J, Benarous R, Girault JP (2007) Phosphorylation-dependent structure of ATF4 peptides derived from a human ATF4 protein, a member of the family of transcription factors. Peptides 28:2253-2267.

Poole AC, Thomas RE, Andrews LA, McBride HM, Whitworth AJ, Pallanck LJ (2008) The PINK1/Parkin pathway regulates mitochondrial morphology. Proceedings of the National Academy of Sciences of the United States of America 105:1638-1643.

Poole AC, Thomas RE, Yu S, Vincow ES, Pallanck L (2010) The mitochondrial fusion-promoting factor mitofusin is a substrate of the PINK1/parkin pathway. PloS one 5:e10054.

Potashkin JA, Kang UJ, Loomis PA, Jodelka FM, Ding Y, Meredith GE (2007) MPTP administration in mice changes the ratio of splice isoforms of fosB and rgs9. Brain research 1182:1-10.

Radhakrishnan SK, den Besten W, Deshaies RJ (2014) p97-dependent retrotranslocation and proteolytic processing govern formation of active Nrf1 upon proteasome inhibition. eLife 3:e01856.

Radhakrishnan SK, Lee CS, Young P, Beskow A, Chan JY, Deshaies RJ (2010) Transcription factor Nrf1 mediates the proteasome recovery pathway after proteasome inhibition in mammalian cells. Molecular cell 38:17-28.

Rath B, Pandey RS, Debata PR, Maruyama N, Supakar PC (2008) Molecular characterization of senescence marker protein-30 gene promoter: identification of repressor elements and functional nuclear factor binding sites. BMC molecular biology 9:43.

Raudino F (2012) The Parkinson disease before James Parkinson. Neurological sciences : official journal of the Italian Neurological Society and of the Italian Society of Clinical Neurophysiology 33:945-948.

Ren Y, Jiang H, Yang F, Nakaso K, Feng J (2009) Parkin protects dopaminergic neurons against microtubule-depolymerizing toxins by attenuating microtubule-associated protein kinase activation. The Journal of biological chemistry 284:4009-4017.

Ren Y, Zhao J, Feng J (2003) Parkin binds to alpha/beta tubulin and increases their ubiquitination and degradation. The Journal of neuroscience : the official journal of the Society for Neuroscience 23:3316-3324.

Rieker C, Schober A, Bilbao A, Schutz G, Parkitna JR (2012) Ablation of serum response factor in dopaminergic neurons exacerbates susceptibility towards MPTP-induced oxidative stress. The European journal of neuroscience 35:735-741.

Robison AJ, Vialou V, Sun HS, Labonte B, Golden SA, Dias C, Turecki G, Tamminga C, Russo S, Mazei-Robison M, Nestler EJ (2014) Fluoxetine epigenetically alters the CaMKIIalpha promoter in nucleus accumbens to regulate DeltaFosB binding and antidepressant effects. Neuropsychopharmacology : official publication of the American College of Neuropsychopharmacology 39:1178-1186.

Rosenbloom KR, Armstrong J, Barber GP, Casper J, Clawson H, Diekhans M, Dreszer TR, Fujita PA, Guruvadoo L, Haeussler M, Harte RA, Heitner S, Hickey G, Hinrichs AS, Hubley R, Karolchik D, Learned K, Lee BT, Li CH, Miga KH, Nguyen N, Paten B, Raney BJ, Smit AF, Speir ML, Zweig AS, Haussler D, Kuhn RM, Kent WJ (2015) The UCSC Genome Browser database: 2015 update. Nucleic acids res. 43: 670-681.

Rosenbloom KR, Sloan CA, Malladi VS, Dreszer TR, Leaned K, Kirkup VM, Wong MC, Maddren M, Fang R, Heitner SG, Lee BT, Barber GP, Harte RA, Diekhans M, Long JC, Wilder SP, Zweig AS, Karolchik D, Kuhn RM, Haussler D, Kent WJ (2013) ENCODE data in the UCSC Genome Browser: year 5 update. Nucleic acids res. (41): 56-63.

Russell LK, Mansfield CM, Lehman JJ, Kovacs A, Courtois M, Saffitz JE, Medeiros DM, Valencik ML, McDonald JA, Kelly DP (2004) Cardiac-specific induction of the transcriptional coactivator peroxisome proliferator-activated receptor gamma coactivator-1alpha promotes mitochondrial biogenesis and reversible cardiomyopathy in a developmental stage-dependent manner. Circulation research 94:525-533.

Sakata E, Yamaguchi Y, Kurimoto E, Kikuchi J, Yokoyama S, Yamada S, Kawahara H, Yokosawa H, Hattori N, Mizuno Y, Tanaka K, Kato K (2003) Parkin binds the Rpn10 subunit of 26S proteasomes through its ubiquitin-like domain. EMBO reports 4:301-306.

Sato S, Chiba T, Sakata E, Kato K, Mizuno Y, Hattori N, Tanaka K (2006) 14-3-3eta is a novel regulator of parkin ubiquitin ligase. The EMBO journal 25:211-221.

Satoh J, Kawana N, Yamamoto Y (2013) Pathway Analysis of ChIP-Seq-Based NRF1 Target Genes Suggests a Logical Hypothesis of their Involvement in the Pathogenesis of Neurodegenerative Diseases. Gene regulation and systems biology 7:139-152.

Serra PA, Pluchino S, Marchetti B, Desole MS, Miele E (2008) The MPTP mouse model: cues on DA release and neural stem cell restorative role. Parkinsonism & related disorders 14 Suppl 2:S189-193.

Shahbazian MD, Grunstein M (2007) Functions of site-specific histone acetylation and deacetylation. Annual review of biochemistry 76:75-100.

Shimada S, Kitayama S, Lin CL, Patel A, Nanthakumar E, Gregor P, Kuhar M, Uhl G (1991) Cloning and expression of a cocaine-sensitive dopamine transporter complementary DNA. Science 254:576-578.

Shimura H, Hattori N, Kubo S, Mizuno Y, Asakawa S, Minoshima S, Shimizu N, Iwai K, Chiba T, Tanaka K, Suzuki T (2000) Familial Parkinson disease gene product, parkin, is a ubiquitin-protein ligase. Nature genetics 25:302-305.

Shin JH, Ko HS, Kang H, Lee Y, Lee YI, Pletinkova O, Troconso JC, Dawson VL, Dawson TM (2011) PARIS (ZNF746) repression of PGC-1alpha contributes to neurodegeneration in Parkinson's disease. Cell 144:689-702.

Singh S, Ahmad R, Mathur D, Sagar RK, Krishana B (2006) Neuroprotective effect of BDNF in young and aged 6-OHDA treated rat model of Parkinson disease. Indian journal of experimental biology 44:699-704.

Sirito M, Lin Q, Maity T, Sawadogo M (1994) Ubiquitous expression of the 43- and 44-kDa forms of transcription factor USF in mammalian cells. Nucleic acids research 22:427-433.

Sirito M, Walker S, Lin Q, Kozlowski MT, Klein WH, Sawadogo M (1992) Members of the USF family of helix-loop-helix proteins bind DNA as homo- as well as heterodimers. Gene expression 2:231-240.

Struhl K (1988) The JUN oncoprotein, a vertebrate transcription factor, activates transcription in yeast. Nature 332:649-650.

Sun P, Enslen H, Myung PS, Maurer RA (1994) Differential activation of CREB by Ca2+/calmodulin-dependent protein kinases type II and type IV involves phosphorylation of a site that negatively regulates activity. Genes & development 8:2527-2539.

Sun X, Liu J, Crary JF, Malagelada C, Sulzer D, Greene LA, Levy OA (2013) ATF4 protects against neuronal death in cellular Parkinson's disease models by maintaining levels of parkin. The Journal of neuroscience : the official journal of the Society for Neuroscience 33:2398-2407.

Sveinbjornsdottir S (2016) The clinical symptoms of Parkinson's disease. Journal of neurochemistry.

Taguchi K, Motohashi H, Yamamoto M (2011) Molecular mechanisms of the Keap1-Nrf2 pathway in stress response and cancer evolution. Genes to cells : devoted to molecular & cellular mechanisms 16:123-140.

Tan NY, Khachigian LM (2009) Sp1 phosphorylation and its regulation of gene transcription. Molecular and cellular biology 29:2483-2488.

Thangasamy A, Rogge J, Krishnegowda NK, Freeman JW, Ammanamanchi S (2011) Novel function of transcription factor Nrf2 as an inhibitor of RON tyrosine kinase receptor-mediated cancer cell invasion. The Journal of biological chemistry 286:32115-32122.

Timmerman W, Deinum ME, Westerink BH, Schuiling GA (1995) Lack of evidence for dopamine autoreceptors in the mediobasal hypothalamus: a microdialysis study in awake rats. Neuroscience letters 195:113-116.

Trempe JF, Sauve V, Grenier K, Seirafi M, Tang MY, Menade M, Al-Abdul-Wahid S, Krett J, Wong K, Kozlov G, Nagar B, Fon EA, Gehring K (2013) Structure of parkin reveals mechanisms for ubiquitin ligase activation. Science 340:1451-1455.

Ulery PG, Nestler EJ (2007) Regulation of DeltaFosB transcriptional activity by Ser27 phosphorylation. The European journal of neuroscience 25:224-230.

Ulery PG, Rudenko G, Nestler EJ (2006) Regulation of DeltaFosB stability by phosphorylation. The Journal of neuroscience : the official journal of the Society for Neuroscience 26:5131-5142.

van der Mark M, Brouwer M, Kromhout H, Nijssen P, Huss A, Vermeulen R (2012) Is pesticide use related to Parkinson disease? Some clues to heterogeneity in study results. Environmental health perspectives 120:340-347.

Vattem KM, Wek RC (2004) Reinitiation involving upstream ORFs regulates ATF4 mRNA translation in mammalian cells. Proc Natl Acad Sci USA 101(31): 11269-11274.

Venugopal R, Jaiswal AK (1996) Nrf1 and Nrf2 positively and c-Fos and Fra1 negatively regulate the human antioxidant response element-mediated expression of NAD(P)H:quinone oxidoreductase1 gene. Proceedings of the National Academy of Sciences of the United States of America 93:14960-14965.

Vialou V, Feng J, Robison AJ, Ku SM, Ferguson D, Scobie KN, Mazei-Robison MS, Mouzon E, Nestler EJ (2012) Serum response factor and cAMP response element binding protein are both required for cocaine induction

of DeltaFosB. The Journal of neuroscience : the official journal of the Society for Neuroscience 32:7577-7584.

Vives-Bauza C, Zhou C, Huang Y, Cui M, de Vries RL, Kim J, May J, Tocilescu MA, Liu W, Ko HS, Magrane J, Moore DJ, Dawson VL, Grailhe R, Dawson TM, Li C, Tieu K, Przedborski S (2010) PINK1-dependent recruitment of Parkin to mitochondria in mitophagy. Proceedings of the National Academy of Sciences of the United States of America 107:378-383.

Waak J, Weber SS, Gorner K, Schall C, Ichijo H, Stehle T, Kahle PJ (2009) Oxidizable residues mediating protein stability and cytoprotective interaction of DJ-1 with apoptosis signal-regulating kinase 1. The Journal of biological chemistry 284:14245-14257.

Wang DB, Garden GA, Kinoshita C, Wyles C, Babazadeh N, Sopher B, Kinoshita Y, Morrison RS (2013) Declines in Drp1 and parkin expression underlie DNA damage-induced changes in mitochondrial length and neuronal death. The Journal of neuroscience : the official journal of the Society for Neuroscience 33:1357-1365.

Wang ZZ, Washabaugh CH, Yao Y, Wang JM, Zhang L, Ontell MP, Watkins SC, Rudnicki MA, Ontell M (2003) Aberrant development of motor axons and neuromuscular synapses in MyoD-null mice. The Journal of neuroscience : the official journal of the Society for Neuroscience 23:5161-5169.

Weihe E, Schafer MK, Erickson JD, Eiden LE (1994) Localization of vesicular monoamine transporter isoforms (VMAT1 and VMAT2) to endocrine cells and neurons in rat. Journal of molecular neuroscience : MN 5:149-164.

Wenzel DM, Lissounov A, Brzovic PS, Klevit RE (2011) UBCH7 reactivity profile reveals parkin and HHARI to be RING/HECT hybrids. Nature 474:105-108.

West AB, Kapatos G, O'Farrell C, Gonzalez-de-Chavez F, Chiu K, Farrer MJ, Maidment NT (2004) N-myc regulates parkin expression. The Journal of biological chemistry 279:28896-28902.

West AB, Lockhart PJ, O'Farell C, Farrer MJ (2003) Identification of a novel gene linked to parkin via a bi-directional promoter. Journal of molecular biology 326:11-19.

Wilson MA (2011) The role of cysteine oxidation in DJ-1 function and dysfunction. Antioxidants & redox signaling 15:111-122.

Wruck CJ, Claussen M, Fuhrmann G, Romer L, Schulz A, Pufe T, Waetzig V, Peipp M, Herdegen T, Gotz ME (2007) Luteolin protects rat PC12 and C6 cells against MPP+ induced toxicity via an ERK dependent Keap1-Nrf2-ARE pathway. Journal of neural transmission Supplementum 57-67.

Wu Z, Puigserver P, Andersson U, Zhang C, Adelmant G, Mootha V, Troy A, Cinti S, Lowell B, Scarpulla RC, Spiegelman BM (1999) Mechanisms controlling mitochondrial biogenesis and respiration through the thermogenic coactivator PGC-1. Cell 98:115-124.

Xie T, Belinsky M, Xu Y, Jaiswal AK (1995) ARE- and TRE-mediated regulation of gene expression. Response to xenobiotics and antioxidants. The Journal of biological chemistry 270:6894-6900.

Hu YC, XU Q, Guo JF, Ai SX, Song CY, Sun QY, Weng L, Zhou L, Jiang H, Shen L, Yan XX, Tang, BS (2015) Abnormal DNA methylation in substantia nigra region of MPTP-induced muse model of Parkinson's disease. Progress in biochemistry and biophysics 42(3): 277-285.

Yang F, Jiang Q, Zhao J, Ren Y, Sutton MD, Feng J (2005) Parkin stabilizes microtubules through strong binding mediated by three independent domains. The Journal of biological chemistry 280:17154-17162.

Yazgan O, Pfarr CM (2002) Regulation of two JunD isoforms by Jun N-terminal kinases. The Journal of biological chemistry 277:29710-29718.

Yoza BK, Brooks JW, Mizel SB (1992) Induction of AP-1 transcription factor components during T-cell activation by interleukin 1 and phorbol esters. Cell growth & differentiation : the molecular biology journal of the American Association for Cancer Research 3:677-684.

Yukimasa N, Isobe K, Nagai H, Takuwa Y, Nakai T (1999) Successive occupancy by immediate early transcriptional factors of the tyrosine hydroxylase gene TRE and CRE sites in PACAP-stimulated PC12 pheochromocytoma cells. Neuropeptides 33:475-482.

Zachariou V, Bolanos CA, Selley DE, Theobald D, Cassidy MP, Kelz MB, Shaw-Lutchman T, Berton O, Sim-Selley LJ, Dileone RJ, Kumar A, Nestler EJ (2006) An essential role for DeltaFosB in the nucleus accumbens in morphine action. Nature neuroscience 9:205-211.

Zhang C, Lee S, Peng Y, Bunker E, Giaime E, Shen J, Zhou Z, Liu X (2014) PINK1 triggers autocatalytic activation of Parkin to specify cell fate decisions. Current biology : CB 24:1854-1865.

Zhang Y, Gao J, Chung KK, Huang H, Dawson VL, Dawson TM (2000) Parkin functions as an E2-dependent ubiquitin- protein ligase and promotes the degradation of the synaptic vesicle-associated protein, CDCrel-1. Proceedings of the National Academy of Sciences of the United States of America 97:13354-13359.

Ziviani E, Tao RN, Whitworth AJ (2010) Drosophila parkin requires PINK1 for mitochondrial translocation and ubiquitinates mitofusin. Proceedings of the National Academy of Sciences of the United States of America 107:5018-5023.